
# MULTISCALE SIMULATION OF FREQUENCY DEPENDENT LINE MODELS AND NETWORK EQUIVALENTS

Felipe Camara Neto

Tese de Doutorado apresentada ao Programa de Pós-graduação em Engenharia Elétrica, COPPE, da Universidade Federal do Rio de Janeiro, como parte dos requisitos necessários à obtenção do título de Doutor em Engenharia Elétrica.

Orientador: Antonio Carlos Siqueira de Lima

Rio de Janeiro
Setembro de 2017

MULTISCALE SIMULATION OF FREQUENCY DEPENDENT LINE MODELS AND NETWORK EQUIVALENTS

Felipe Camara Neto

TESE SUBMETIDA AO CORPO DOCENTE DO INSTITUTO ALBERTO LUIZ COIMBRA DE PÓS-GRADUAÇÃO E PESQUISA DE ENGENHARIA (COPPE) DA UNIVERSIDADE FEDERAL DO RIO DE JANEIRO COMO PARTE DOS REQUISITOS NECESSÁRIOS PARA A OBTENÇÃO DO GRAU DE DOUTOR EM CIÊNCIAS EM ENGENHARIA ELÉTRICA.

Examinada por:

Prof. Antonio Carlos Siqueira de Lima, D.Sc.

Profa. Karen Caino de Oliveira Salim, D.Sc.

Prof. Sandoval Carneiro Jr., Ph.D.

Prof. Luiz Cera Zanetta Jr., D.Sc.

Prof. Fernando Augusto Moreira, Ph.D.

Prof. Washington Luiz Araujo Neves, Ph.D.

RIO DE JANEIRO, RJ – BRASIL
SETEMBRO DE 2017

Camara Neto, Felipe

Multiscale Simulation of Frequency Dependent Line Models and Network Equivalents /Felipe Camara Neto. – Rio de Janeiro: UFRJ/COPPE, 2017.

XV, 158 p.: il.; 29, 7cm.

Orientador: Antonio Carlos Siqueira de Lima

Tese (doutorado) – UFRJ/COPPE/Programa de Engenharia Elétrica, 2017.

Referências Bibliográficas: p. 133 – 151.

1. Electromagnetic transients. 2. Rational approximation. 3. Frequency dependent network equivalent. 4. Overhead lines. 5. Underground cables. 6. Dynamic phasors. 7. Multiscale simulation. 8. Hybrid simulation. I. Lima, Antonio Carlos Siqueira de. II. Universidade Federal do Rio de Janeiro, COPPE, Programa de Engenharia Elétrica. III. Título.

*This conquest is dedicated*
*to my wife Ruth and*
*my parents Adarlete & Paulo.*

*"How can I say thanks*
*For the things*
*You have done for me?*
*Things so undeserved*
*Yet You gave*
*To prove Your love for me*
*The voices of a million angels*
*Could not express my gratitude*
*All that I am and ever hope to be*
*I owe it all to Thee*
*To God, be the glory!"*
*(Andraé Crouch)*

# Acknowledgement

First of all, I would like to mention that this research was only made possible because I received an immeasurable support from my highly respected company, Furnas Centrais Elétricas, and all my managers during these past five years: Alcêo Mendes de Souza Junior, Cesar Ribeiro Zani, Christiano Lopes Rodrigues, Luiz Edmundo dos Santos Ferreira, Marco Antonio de Paiva Fontes, Mario Fernando Ellis and Victor Alexandre Belo França.

Words cannot express my gratitude to my advisor Prof. Antonio Carlos Siqueira de Lima. Only through his patience and dedication was this research feasible. To Prof. Kai Strunz, I would like to express my deepest appreciation for all his guidance. Accepting me as a visiting researcher at Technische Universität Berlin (TUB) really marked my life.

Since my first day in Germany I received an endless support from family Schmidt. To you, all my gratitude. You became part of my life. During my stay at TUB, two chinese colleagues became very special to me: Zhihui Li and Yu Liu. Thank you for sharing your time with me.

Several special people walked with me through this marathon and each one helped me with in a very unique way. To you Cynthia, Gecilda, João Paulo, Luziene and Trevor, all my gratitude.

Resumo da Tese apresentada à COPPE/UFRJ como parte dos requisitos necessários para a obtenção do grau de Doutor em Ciências (D.Sc.)

# SIMULAÇÃO MULTIESCALA DE LINHAS DE TRANSMISSÃO E EQUIVALENTES DE REDE VARIANTES NA FREQUÊNCIA

Felipe Camara Neto

Setembro/2017

Orientador: Antonio Carlos Siqueira de Lima

Programa: Engenharia Elétrica

A análise de sistemas elétricos engloba fenômenos com diferentes constantes de tempo, o que acarreta na utilização de diversas ferramentas de simulação. Como exemplo, transitórios rápidos envolvendo surtos de manobra demandam passos de integração na ordem de microssegundos enquanto para transitórios lentos, advindos da troca de energia entre geradores, adota-se passos de integração de milissegundos.

O presente trabalho investiga a utilização de modelos baseados em matrizes de admitância variantes na frequência para representação de linhas de transmissão aéreas, cabos submarinos e equivalentes de rede em coordenadas de fase para o desenvolvimento de algoritmos para simulação multiescala. Ao invés da utilização do Método das Características, a matriz de admitância nodal e duas decomposições alternativas são consideradas de modo a contornar a limitação do passo de integração em função do tempo de tráfego de linhas, a saber: o Folded Line Equivalent e a Decomposição Idempotente. O conceito de Latência será também investigado de modo a prover uma realização mais eficiente de modelos variantes na frequência.

As formulações desenvolvidas neste trabalho encontram aplicação imediata em programas para simulação de transitórios eletromagnéticos, tais como PSCAD, EMTP-RV e ATP dado que é mantida a representação através dos equivalentes de Norton. Por meio de fasores dinâmicos, torna-se viável a representação de fenômenos eletromagnéticos e eletromecânicos com o mesmo modelo computacional. Casos teste são empregados na avaliação do desempenho e precisão das formulações propostas. O Método das Características e a transformada numérica de Laplace são utilizados para fins de comparação. Com reduzido esforço computacional, resultados com excelente precisão são obtidos sem a presença de oscilações numéricas ou descontinuidades nas formas de onda.

Abstract of Thesis presented to COPPE/UFRJ as a partial fulfillment of the requirements for the degree of Doctor of Science (D.Sc.)

MULTISCALE SIMULATION OF FREQUENCY DEPENDENT LINE MODELS AND NETWORK EQUIVALENTS

Felipe Camara Neto

September/2017

Advisor: Antonio Carlos Siqueira de Lima

Department: Electrical Engineering

The evaluation of power systems encompasses phenomenon of distinct time-frames and so leads to the adoption of different simulation tools. For instance, fast transients related to switching maneuvers require time-steps of microseconds while slow transients, related to energy exchange between generators, demand time-steps of milliseconds. However, the need to assess conditions where slow frequency oscillations might be combined with fast transients is becoming more common.

This research evaluates the use of frequency dependent admittance-based models in the development of multiscale algorithms for phase-coordinate modeling of overhead lines, subsea cables and frequency dependent network equivalents. Unlike the modeling with the Method of Characteristics, the direct fitting of the nodal admittance matrix and two alternative schemes are considered to cope with the trade-off between time-step and traveling times, namely: the Folded Line Equivalent and Idempotent Decomposition. The concept of Latency is also addressed in a distinct way to provide more efficient realization frequency dependent models to allow the so-called multirate simulation.

The major advantage of the designed models is the straightforward implementation in EMTP-like programs such as PSCAD, EMTP-RV and ATP since they attain the same Norton-type structure. In addition, dynamic phasors allowed the unification of electromagnetic and electromechanical modeling into a single model. Both numerical performance and accuracy of the proposed schemes are evaluated through several test cases. The Method of Characteristics and the Numerical Laplace Transform are used for comparison. The computational burden is considerably reduced without significant loss of accuracy and with no numerical oscillations or discontinuities in the waveforms.

# Contents

# List of Figures

# List of Tables

# Chapter 1

# Introduction

## 1.1 Initial Considerations

Actual power systems are becoming even more complex due to high penetration of renewable sources and an increasing usage of power electronics devices. Thus, a detailed representation of such large networks can become very time-consuming. To face this issue, significant efforts have been made on the development of new transient models and solution techniques during the last decades in order to develop faster simulation tools.

The transient analysis of electrical power systems is commonly performed considering slow and fast phenomenon independently. The transient stability (TS) analysis which encompasses slow phenomena assumes the network in quasi-steady-state and balanced conditions. As a consequence, phasorial representation can be applied. On the other hand, the fast phenomena commonly known as electromagnetic transients (EMT) requires a time-domain representation of all elements involved. While for TS analysis a long-term representation of electric machines and load is sought, in an EMT analysis the frequency dependence is of paramount importance.

Traditionally, simulation tools for power system analysis are based on fixed time-step techniques. Hence, only phenomena within the same time frame can be evaluated. In the case of EMT, the main feature is a detailed three-phase representation using real or instantaneous variables with time-steps in the order of microseconds. Conversely, for electromechanical or TS evaluations, the quasi-steady-state assumption allows the adoption of single phase representation by means of phasors with time-steps in the range of milliseconds. In general, these are the reasons why it is prohibitive both formulations in order to allow an evaluation involving either fast and slow transients.

Emerging trends have been making headway in the search for a unique simulation tool to bridge EMT and TS simulations. Putting together the advantage of both formulations continues to be the much-desired goal. The first attempts in the 1980s [1] resulted in the so-called hybrid simulator in which electromagnetic and electromechanical solvers alternate in order to provide a coupled solution. However, integrating these two types of simulators brings up some issues, for instance, communication protocols between algorithms, exchanging data timings, waveform-to-phasor conversions and conversely.

In the early 1990s, the concept of time-varying or dynamic phasors was introduced by Venkatasubramanian [2]. He extended the phasor-based notation to accommodate fast electromagnetic transients. One of the benefits of such representation is that more physical insight can be gained since the notion of phasors directly identifies the variation of a given quantity unlike instantaneous values. This formulation was then incorporated to power system modeling and stated as Shifted Frequency Analysis (SFA) [3–7].

Later, a distinguished method named Frequency-Adaptive Simulation of Transients (FAST) [8–14] extended the application of dynamic phasors in order to allow variable time-step simulations as opposed to interfacing two distinct programs. Therefore, if electromagnetic phenomenon are involved, one can adopt time-steps of microseconds and when the transients vanish the time-step can be increased to values in the range of milliseconds. This novel formulation presents an ultimate feature since it allows the integrative modeling of EMT and TS phenomenon within the same environment.

## 1.2 Historical Review

### 1.2.1 Overview on Simulation Techniques

In the matter of network solution techniques, the classical nodal analysis was introduced in the very first versions of Electromagnetic Transients Program (EMTP) [15] for the solution of circuit equations. Nevertheless, it has some limitations including the inability to process ungrounded voltage sources and to obtain branch currents in a simple and efficient manner. In 1975, a set of modifications to the nodal method were proposed and the resultant formulation was then called modified nodal analysis (MNA) [16]. A general-purpose solution technique was then provided with more flexibility to model voltage and current sources and switches. More recently, a commercial version of EMTP, the so-called EMTP-RV [17] was implemented using an augmented version of the MNA and later it was modified to directly include state-space elements [18]. Despite

the limitation, the EMTP formulation is the basis of other transient programs such as PSCAD/EMTDC and the ATP/EMTP (Alternative Transient Program). According to the Brazilian Grid Code, the latter is the only program accepted in the analysis of electromagnetic transients for the Brazilian Independent System Operator (ONS – Operador Nacional do Sistema Elétrico Brasileiro).

In order to efficiently perform all computations, the decomposition of a given network into small and isolated portions was the ultimate technique to optimize the number of algebraic multiplications. The re-ordering scheme and exploitation of sparsity was extremely important because it reduced storage requirements and solution times tremendously [19]. Moreover, the solution time was drastically reduced if the iteration and factorization process was confined to only those nodes which contain components with nonlinear characteristic [15]. It is worth mentioning the use of network equivalents to gain computational efficiency with an acceptable degree of accuracy. Partition techniques initially exploited the advantage of multiprocessor machines and parallel computations originated from the decoupling effects introduced by transmission lines once an uncoupled nodal admittance matrix was commonly established [20–22]. On the ground of network partitioning, multirate simulation of networks exhibiting a wide variety of time constants decreases the simulation run times by exploiting the property of circuit latency [23, 24] using, for instance, the Multi-Area Thévenin Equivalents (MATE) technique [25–34]. The fundamental idea is to use different time-steps for each subsystem. For the sake of knowledge, MATE formulated the main ideas of Diakoptics [35–38] in a conceptually and computationally efficient solution framework to subdivide a complex network into independent subnetworks interconnected with as many links as desired and evaluated independently with the overall solution integrated at the level of the links. Despite the advantages of Diakoptics, introduced by Kron in the 1950s, it did not fulfill its potential of becoming a universal tool for the study of large and complex power systems especially due to the success of sparsity techniques. While sparsity techniques take advantage of the very sparse nature of the admittance matrix, Diakoptics splits the network into dense subsystems connected by a few links.

The earliest attempt to interface EMT and TS simulations was carried out in [1]. In this groundwork, the computation of converter and stability transients was performed simultaneously by two different solvers with periodic coordination of the results. This concept resulted in the so-called hybrid simulation [39–42] by splitting the original network into two parts, a detailed and an external system. For instance, the detailed system is a small one evaluated by an electromagnetic solver since accurate results are needed while the external system is larger and evaluated by an electromechanical solver. A method for linking diverse simulation techniques such

as waveform-type, phasor-type and algebraic-type models as well as a combination of separate solvers was presented in [43]. Additionally, the computational advantages of partitioning and parallelism computations could be also incorporated.

The research for new techniques revealed new alternatives to accelerate simulations without sacrificing accuracy on the ground of a unique algorithm gathering both EMT and TS formulations. The concept of dynamic phasors [2] introduced a complex form notation and it was extended to the so-called Shifted Frequency Analysis (SFA) [3–7]. However, as highlighted in [13], the SFA method is efficient for power system slow dynamic studies and also capable of simulating fast transients. The simulation of either slow or fast transients should be determined prior to the beginning of the simulation. Thus, the SFA method presents an inherent limitation for simulating both phenomena within the same simulation run. As shown in [8–14], the so-called Frequency-Adaptive Simulation of Transients (FAST) method can be understood as a modification of the original SFA approach to allow variable time-step simulations. Hence, one can use small time-steps when fast transients are involved and large time-steps when low frequency transients are to be observed.

Afterwards, an implicitly-coupled solution approach was proposed as a combination of EMT and TS equations [44, 45]. The algorithm solves the equations simultaneously enabling the adoption of different time-steps. Alternatively, like the dynamic phasors approach, in [46] a time-domain transformation method was applied and all development was based on the concept of differential networks in order to bridge the gap between EMT and TS simulation tools.

### 1.2.2 Overview on Network Equivalents

In the matter of EMT evaluations, the full representation of a power system is not feasible in terms of the required computation efforts. As a consequence, a small part of the system is modeled in detail and the remaining equipment is represented by an appropriate equivalent. Although the system may be considered predominantly inductive at power frequency, at higher frequencies the reactance changes from inductive to capacitive and vice versa, giving a number of resonance peaks at which the system is purely resistive. Therefore, it is desirable to represent the system by an equivalent network having the same frequency behavior.

The use of frequency dependent network equivalents (FDNE) in power systems goes as far back as the late 1960s and early 1970s with the pioneering work in this area conducted by Hingorani and Burbery [47]. They outlined an approach to take into account the frequency dependency of an equivalent network to be used in HVDC design for filter specification and voltage distortion evaluation at converter stations.

In the 1970s, another research carried out by Clerici and Marzio [48] looked for

a way to mix the use of digital computation to assess network equivalents followed by TNA validation for rightly representation of FDNE through the synthesis of a Foster-based equivalent circuit. Firstly, the method ignores the losses in order to determine the L and C values for the required resonant frequencies and so an optimization procedure is necessary to improve the fit.

Notably registered in Electra magazine in 1979, the CIGRE Working Group 13.05 [49] addressed necessary improvements in the representation and calculation techniques capable of dealing with an enlarged frequency bandwidth for the determination of switching transients. It was pointed out in this work that the commonly two neighboring buses representation technique may not guarantee accurate results. This issue holds for both analogical and digital simulations.

Even though several further published approaches dealt with a new way to improve the equivalent fitting, almost all proposed variations of the RLC equivalent network formerly proposed by Hingorani and Burbery [50–59]. The use of a limited number of RLC branches gives good matches at the selected frequency peaks but their response at other frequencies is less accurate. For a fixed number of branches, the error increases with a larger frequency range. Therefore the accuracy of a FDNE can always be improved by increasing the number of branches, although at a cost of greater complexity or could even be computationally prohibitive [60].

Frequency-domain simulations have important advantages for its accuracy and simplicity since no approximation or fitting is necessary, e.g., the field phenomena in the ground and inside the conductor of transmission lines. Hence, as opposed to previous works, Semlyen and Iravani [61] presented an approach for the direct integration of an external system modeled by its frequency-domain equivalent with a study zone rather than by fitting a RLC network or by introducing an extended interface to reduce the complexity of the external system. This hybrid tool matched up both frequency- and time-domain advantages since the time-domain simulation of switchings and nonlinear behavior is done in a straightforward way.

An alternative approach to the synthesis of RLC branches is the network fitting by rational functions that can be carried out either in the $s$-domain or in the $z$-domain. Typically, the $s$-domain fitting is independent of the simulation time-step while in the $z$-domain the parameters are functions of the simulation time-step [60]. It is noteworthy that rational function approximations were first proposed by Semlyen and Abdel-Rahman [62] to represent frequency dependent effects in transmission line transients which opened the possibility of using state equations for the network solution.

Traditionally, FDNEs are established in the frequency-domain using an admittance-based formulation. The very first approximation of a given FDNE impedance using a $s$-domain rational function was addressed in [63]. A robust pole

relocation algorithm widely known as *Vector Fitting* (VF) routine was proposed in [64] and later refined in [65–67], allowing an efficient realization of rational approximations of frequency-domain responses. Afterwards, VF was subsequently applied to FDNE identification [68–76]. Given its facility of use together with a free distribution of a MATLAB-routine containing the VF algorithm, it has been used in a wide range of electromagnetic transient evaluations [66, 77–89]. Other formulations in the $s$-domain have also been proposed in technical literature such as the Frequency-Partitioning Fitting (FPF) [90–92], Dominant Poles [93, 94], evolutionary algorithms [95] and Levenberg–Marquardt [96–102]. Alternatively, one may use a $z$-domain approach for the approximation of response in either frequency- or time-domain [103–107]. Henriksen [108] gives a discussion of accuracy aspects regarding $z$-domain implementations in EMTP-like programs. The so-called IARMA (Interpolated Auto-Regressive Moving Average) is a full frequency dependent line model proposed in [109, 110] based on a two-sided recursion formulation [111]. The $z$-domain was also used for the identification of FDNE, such as in [103, 112–119]. Some comparisons of the adequacy of $z$-domain approaches for FDNE were carried out in [120, 121], including a direct fitting of time-domain responses using the time-domain *Vector Fitting* routine proposed in [117].

Some hybrid approaches seeking to pursue advantages of different methods have been proposed. The Two-Layer Network Equivalent technique [122, 123] is an approach that aims to attach $s$-based rational fitted models to the standard RLC synthesis in order to correct the frequency response. This hybrid tool is more efficient than lumped parameters because much of the fitting burden of the network to be synthesized is removed. In [124] both VF and Frequency-Partitioning Fitting techniques are applied looking for a low-order model. The Matrix Pencil Method (MPM), first introduced by Sarkar [125, 126], is a time-domain technique to model transient response and afterwards was enhanced as a new frequency-domain version developed and applied for rational approximation [127–129]. The most attracting feature of the MPM is its general mathematical foundation which permits both frequency and time-domain fitting of FDNEs. Finally, [130] uses both VF and time-domain techniques in order to efficiently identify the approximation order.

### 1.2.3 Overview on Transmission Line Modeling

Traveling wave problems were already studied with graphical methods in the 1920s and 1930s, long before digital computers became available. Basically two techniques evolved, namely, Bewley's lattice diagram technique [131] and the Bergeron's method. In the former, a record is kept of the transmitted and reflected waves and their apportionment is computed from reflection and refraction

coefficients. The Bergeron's method, also known as Method of Characteristics (MoC), was probably used first by Löwy [132] and Schnyder [133] for hydraulic surges. Bergeron applied it to a wide variety of problems [134] and strongly advocated its use. It does not need reflection and refraction coefficients. Instead, it uses linear relationships between current and voltage, the so-called characteristics, which are invariant when seen by a fictitious observer who travels with the wave. Therefore, it is often called Bergeron's method today. Both techniques for solving traveling wave problems were adopted in computer programs [135, 136] but Bergeron's method was best suited for digital solutions. It is noteworthy that these methods are efficient only for lossless and distortionless lines and it is well known that propagation in transmission lines is far from distortionless. Better approximations for losses had to be found. Reasonable accuracy was obtained by lumping resistance at one or more points along the line [15]. This alternative is generally acceptable if the resistance is constant and small compared to the surge impedance. But resistance of the ground path is highly dependent on frequency and some programs have been modified so as to handle this frequency dependence.

Actually, the most common mathematical models for simulating transmission lines are based on the Method of Characteristics (MoC), also known as the traveling-wave method. The solution of line equations resembles a decoupled Norton-type model at each end but retaining the relationship between them. The decoupling signifies that what happens at one end takes the line traveling time $\tau$ to be reproduced at the opposite end.

The techniques to solve frequency dependent models in order to allow a time-domain simulation can be classified into two main categories: modal domain or time-domain techniques. Modal domain models rely on the use of modal decomposition assuming a real and constant modal transformation matrix calculated at a user-specified frequency [137–144]. This type of modeling has an advantage since it simplifies the passage from modal coordinates to phase-coordinates and reduces the number of convolutions. The drawback is that the results are accurate only for symmetric and transposed configurations. Further improvements addressed the inclusion of frequency dependent transformation matrices for better representation of untransposed parallel lines [77, 145, 146]. Phase-domain models have no constraints due to the line configuration such as parallel circuits, non-symmetric disposal of phase conductors and diverse cable arrangements. Since the modeling is directly formulated in the phase-domain, inaccuracies concerned with modal transformations are avoided [79, 80, 91, 92, 109–111, 147–157].

For multiscale simulations, a frequency dependent line model based on FAST concept was introduced in [14]. A real and constant transformation matrix is assumed. The MoC is adopted if the time-step is smaller than the slowest modal

traveling time, otherwise, an equivalent $\pi$–circuit is used instead. It is not a general approach as it cannot deal with underground/submarine cables which present a heavy frequency dependent transformation matrix and cannot consider the case of a full frequency dependent line model for large time-steps.

## 1.3 Motivation

Nowadays, there is an ever-growing number of applications where overhead lines, underground and submarine cable systems may experience a complex environment, full of harmonics together with power/voltage oscillations, such as wind-farms both on or offshore, HVDC links or even in scenarios with a heavy load of communications and control actions associated as in the so-called smart-grids. These systems can pose a huge challenge for time-domain simulations as phenomenon with large frequency spectrums may be seen in either steady or transient states. This situation is rather distinct from the one typically found in present studies performed in the design and pre-operational stages. For instance, using conventional tools such as an EMTP-type of software in the transient analysis of HVDC converters demand a long initialization time before the actual transient simulation takes place. If transient stability studies are to be performed, the converter modeling is then very crude and simple and cannot include negative sequence components due to small differences between converter transformer, or the detail impact of the converter transformer saturation in the overall transient performance when small frequencies phenomena (typically in the range of a few or a fraction of hertz) are to be considered.

An important aspect to be mentioned is the size of practical systems when a detailed three-phase representation is mandatory. Through available techniques for reducing large systems into small network equivalents, the challenge takes into account the frequency dependence of parameters. Otherwise, the equivalent behavior matches only at the fundamental frequency. The recommended approach comprises the adoption of the so-called FDNE in which the system behavior on a wide frequency range can be included in electromagnetic transient evaluations. An example of a straightforward application is the interaction between HVDC converters. Conventional EMTP-type of software uses only fixed time-steps and at several times the simulation run may become very time-consuming. Therefore, an alternative to reduce the computational burden is the possibility to design a multiscale formulation suitable to allow a variable time-step feature.

Typically, combined EMT and TS analyses are performed in a rather simplistic manner. The reduced network used for EMT analysis is simulated considering a long observation time which leads to a rather inaccurate simulation, as the machine models can present several simplifications of the mechanical shaft torsional

interaction. Furthermore, some load dynamics cannot easily be implemented in EMT analysis without a detailed characterization of the load itself. Thus, fast simulation tools play an important role in order to face actual complex systems without compromising accuracy.

## 1.4 Objectives

The objective of this research is to investigate the representation of frequency dependent models considering a variable time-step framework. The development maintains the well known Norton-type companion networks adopted by existing EMTP-like programs. This approach permits integration with existing EMTP-like software or the development of a new simulation program.

In this research, frequency dependent line models are based on a rational approximation of the nodal admittance matrix. Thus, they are not hampered by limitations of simulation time-step length due to modal traveling times. Typically, frequency dependent line models in time-domain simulations demand that the time-step must be smaller than the largest modal traveling time. The usage of a rational approximation of a nodal admittance matrix allows the modeling of frequency dependent network equivalents (FDNE) to be included in the frame-work as well. The rational approximation of the nodal admittance matrix considers three possible approaches, namely: direct fitting of the nodal admittance matrix, usage of a Folded Line Equivalent or Idempotent Decomposition. These three approaches will be discussed in detail in Chapter 2.

The inclusion of a variable time-step length is sought using mainly two distinct approaches: one based on real variables and the other which relies on a complex domain formulation of voltages and currents. The latter is known in technical literature as FAST (Frequency-Adaptive Simulation of Transients). This framework allows phasor-based simulations to be included and can be understood as a dynamic phasor based approach. It is worth mentioning that when using FAST it is possible, with small modifications in the expressions, to attain the same structure of actual companion networks in EMTP-like programs.

To improve the numerical performance in the rational modeling of frequency dependent models, the concept of latency exploitation will be addressed to perform multirate simulations. The idea of latency is to use different time-steps for distinct poles, i.e., fast poles are solved using a small time-step while slower poles may be solved using larger time-steps. For the separation of slow and fast dynamics, a novel technique named Multiple Companion Networks (MCN) is going to be introduced.

## 1.5 Organization

This thesis is organized in 5 chapters as follows:

- Chapter 1 presents the introduction and a historical background of the technical literature related to this research.
- Chapter 2 presents the current practices in the modeling of frequency dependent network equivalents (FDNE) and transmission lines based on real or instantaneous variables. Next, it proposes a reinitialization approach to allow a unique intermediate step to provide the usage of multiple time-steps. The novel multiscale approach is validated in time-domain simulations through three alternative line models and a FDNE describing a 34 kV distribution network.
- Chapter 3 introduces the FAST approach on the ground of complex variables or dynamic phasors. The same reinitialization approach is applied with the advantage that synchronous machine models commonly used in TS analysis can be interfaced. Moreover, there is no constraint when the time-step is increased since the phasor-based mode simulation can be exploited. For the sake of clarity, each test case considered in Chapter 2 is repeated in order to validate the proposed multiscale formulation.
- Chapter 4 investigates the applicability of the latency concept in the rational modeling of FDNE and full frequency dependent transmission lines with a new technique named Multiple Companion Networks (MCN). The main idea of latency is to use different time-steps for distinct poles, i.e., fast poles are solved using a small time-step while slower poles may be solved using larger time-steps.
- Chapter 5 summarizes the main results of this research and proposes some topics for future investigation.

# Chapter 2

# Modeling Using Real Variables

In this chapter, a Multiple Time-Step (MTS) approach is presented. It is a novel multiscale formulation for admittance-based models for time-domain simulations. It assumes that all the models involved are to be represented via a rational approximation. Thus, it can consider phase-coordinate frequency dependent line models and frequency dependent network equivalents (FDNE) with multiple changes in time-step along the simulation run. Three possible approaches are considered in the rational approximation of transmission lines, namely: direct fitting of the nodal admittance matrix, Folded Line Equivalent (FLE) and Idempotent Decomposition. A case of a FDNE of a network comprising overhead lines and underground cable is also considered. To achieve the equivalent a full-frequency dependent line model, the so-called ULM, is applied to both overhead lines and underground cables.

Time-domain responses obtained with the so-called Multiple Time-Step (MTS) approach are compared with those calculated using a computer code implemented with *Mathematica* or PSCAD. Six test cases are considered to demonstrate that the multiscale modeling using real variables attains the same accuracy as fixed time-step simulations. Regardless of the change in time-step length, the proposed formulation allows smooth transitions without numerical oscillations or discontinuities in the waveform

The greatest feature of the novel admittance-based multiscale approach is the straightforward implementation since it retains the same structure adopted by EMTP-like programs. However, the major issue associated with the modeling based on real or instantaneous variables is that it poses a limitation due to the maximum time-step size associated with the sampling rate of the fundamental frequency.

## 2.1 Introduction

The precise calculation of electromagnetic transients (EMT) in time-domain simulations of electric power systems requires the inclusion of frequency dependence. There are a number of scenarios where, for a precise evaluation of electromagnetic transients (EMT), one cannot deal with lumped and frequency independent components [142]. To take into account, for instance, the frequency dependence in distributed elements/networks, it is mandatory the synthesis of a given frequency response to allow the interface with EMTP-like programs [19].

Several efforts have been reported in the search for more flexible solution algorithms like decomposition of the network into small and isolated portions to optimize the number of algebraic multiplications [15] and partition techniques for parallel computations [20–22]. It is noteworthy that the reduction of portions of the original system into small network equivalents results in a reduced amount of equations to be solved and therefore contributing to a faster simulation. This network tearing formulation has been proposed by Kron in his Diakoptics book [37]. The so-called Multi-Area Thevenin Equivalents (MATE) [27–34], which can also include the idea of latency exploitation [23, 24, 158], is essentially a direct application of Diakoptics approach.

Until the present, all EMTP-like programs do not feature variable time-step and, as a consequence, the simulation run may become very time-consuming in some scenarios. With the increasing complexity of power systems there might be some scenarios where a small time-step length is needed in the first instant of the simulation while a more coarse one can be used in the remainder of the evaluation. Consider, for instance, switching or reclosing analysis covering several runs of a transmission line maneuver where the system dynamics might be of interest. If the simulation time-step can be changed throughout the run a less dense data set can be obtained in the analysis of system performance. Another possible area of interest is in the assessment of networks with a substantial presence of power electronic converters as those related to the integration of renewable sources or involved in the development of FACTS devices. Thus, the development of a multiscale formulation for admittance-based models is intended for a direct implementation in EMTP-like programs in order to allow simulations with multiple time-steps.

## 2.2 Lumped Elements

This section aims to establish the discretization of differential equations to describe the behavior of lumped elements. Companion networks in the form of Norton-type equivalents are intended to perform time-domain simulations.

### 2.2.1 Inductor

The behavior of an inductor $L$ expressed by means of real variables can be described through the following differential equation

$$\frac{di_L(t)}{dt} = \frac{v_L(t)}{L} \tag{2.1}$$

Applying the trapezoidal integration rule to (2.1) yields

$$i_L(t) - i_L(t - \Delta t) = \frac{\Delta t}{2L}(v_L(t) + v_L(t - \Delta t)) \tag{2.2}$$

Collecting like terms and casting in the form of companion networks, the resulting time discrete model can expressed by

$$i_L(t) = G_L \; v_L(t) + his_L(t) \tag{2.3}$$

where

$$\begin{aligned} G_L &= \frac{\Delta t}{2L} \\ his_L(t) &= i_L(t - \Delta t) + G_L \; v_L(t - \Delta t) \end{aligned} \tag{2.4}$$

and the numerical implementation of this time equivalent circuit is illustrated in Figure 2.1.

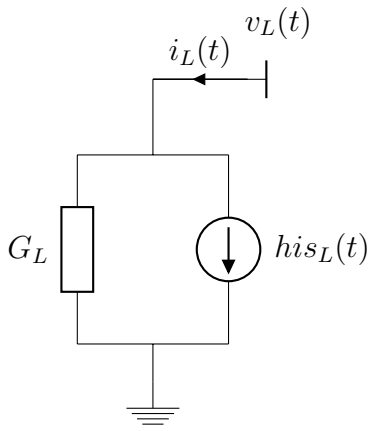


Figure 2.1: Companion model for $L$

### 2.2.2 Capacitor

The behavior of a capacitor $C$ expressed by means of real variables can be described through the following differential equation

$$\frac{dv_c(t)}{dt} = \frac{i_c(t)}{C} \tag{2.5}$$

Applying the trapezoidal integration rule to (2.5) yields

$$v_c(t) - v_c(t - \Delta t) = \frac{\Delta t}{2C}(i_c(t) + i_c(t - \Delta t)) \tag{2.6}$$

Collecting like terms and casting in the form of companion networks, the resulting time discrete model can be expressed by

$$i_c(t) = G_c \; v_c(t) - his_c(t) \tag{2.7}$$

where

$$\begin{aligned} G_C &= \frac{2C}{\Delta t} \\ his_c(t) &= i_c(t - \Delta t) + G_c \; v_c(t - \Delta t) \end{aligned} \tag{2.8}$$

and the numerical implementation of this time equivalent circuit is illustrated in Figure 2.2.

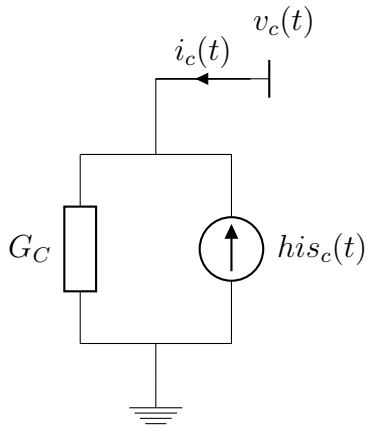


Figure 2.2: Companion model for $C$

## 2.3 Overhead Lines and Cables

### 2.3.1 Method of Characteristics

The most common mathematical model for simulating overhead transmission lines or underground cables, hereafter referred just as line, are based on the Method of Characteristics (MoC), also known as the traveling-wave method. It consists the full representation of the distributed nature of transmission line impedances together with the skin effect in conductors and earth return path.

The general solution of the line equations resembles a decoupled Norton-type model at each end. It means that a line can be represented by an admittance in parallel with a current source at each terminal and what happens at one end takes the traveling time $\tau$ to be reproduced at the opposite end. The formulation int the frequency-domain is given as follows [159]

$$\mathbf{I}_k = \mathbf{Y}_c\mathbf{V}_k - \mathbf{H}\left[\mathbf{Y}_c\mathbf{V}_m + \mathbf{I}_m\right] \tag{2.9a}$$

$$\mathbf{I}_m = \mathbf{Y}_c\mathbf{V}_m - \mathbf{H}\left[\mathbf{Y}_c\mathbf{V}_k + \mathbf{I}_k\right] \tag{2.9b}$$

where $\mathbf{Y}_c$ is the characteristic admittance and $\mathbf{H}$ is the propagation function given by

$$\begin{aligned} \mathbf{Y}_c &= \mathbf{Z}^{-1}\sqrt{\mathbf{ZY}} \\ \mathbf{H} &= \exp\left(-\ell\sqrt{\mathbf{YZ}}\right) \end{aligned} \tag{2.10}$$

in which $\mathbf{Z}$ and $\mathbf{Y}$ are the series impedance and shunt admittance matrices per unit length and $\ell$ is the line length. The time-domain counterparts obtained by means of convolutions are given by

$$\mathbf{i}_k = \mathbf{y}_c * \mathbf{v}_k - \mathbf{h} * \left[\mathbf{y}_c * \mathbf{v}_m + \mathbf{i}_m\right] \tag{2.11a}$$

$$\mathbf{i}_m = \mathbf{y}_c * \mathbf{v}_m - \mathbf{h} * \left[\mathbf{y}_c * \mathbf{v}_k + \mathbf{i}_k\right] \tag{2.11b}$$

as $\mathbf{y}_c$ and $\mathbf{h}$ are the unit impulse responses of $\mathbf{Y}_c$ and $\mathbf{H}$, $\mathbf{v}_k$, $\mathbf{v}_m$, $\mathbf{i}_k$ and $\mathbf{i}_m$ are the terminal voltages and injected currents and the symbol $*$ indicates convolution. The implementation of the time equivalent circuit is illustrated in Fig. 2.3

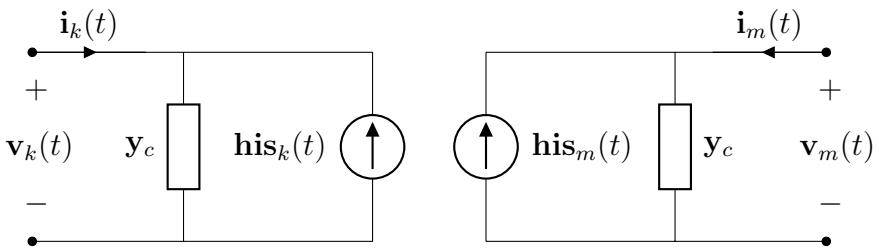


Figure 2.3: Time-domain line equivalent

with

$$\mathbf{his}_k = \mathbf{h} * [\mathbf{y}_c * \mathbf{v}_m + \mathbf{i}_m] \tag{2.12a}$$

$$\mathbf{his}_m = \mathbf{h} * [\mathbf{y}_c * \mathbf{v}_k + \mathbf{i}_k] \tag{2.12b}$$

For underground cables the procedure is basically the same, only the frequency-domain behavior of the per-unit-length parameters will be different.

The techniques to solve frequency dependent models in order to allow time-domain simulations can be classified into two main categories: modal domain and phase-domain techniques. Modal domain models rely on the use of modal decomposition assuming a real and constant modal transformation matrix calculated at a user-specified frequency [137–144]. This kind of modeling has an advantage since it simplifies the passage from the modal coordinates to phase-coordinates and reduces the number of convolutions. The drawback is that the results are accurate only for symmetric and transposed configurations. Further improvements were addressed for the inclusion of frequency dependent transformation matrices for better representation of untransposed parallel lines [77, 145, 146]. Phase-domain models have no constraint due to the line configuration such as parallel circuits, non-symmetric disposal of phase conductors and diverse cable arrangements. Since the modeling is directly formulated in the phase domain, inaccuracies concerned with modal transformations are avoided [79, 80, 91, 92, 109–111, 147–157].

Simulation of electromagnetic transients with the MoC requires the characteristic admittance $\mathbf{Y}_c$ and the propagation function $\mathbf{H}$ matrices to be subjected to rational approximations as it allows an efficient integration with time-domain solvers. The *Vector Fitting* (VF) routine [64, 65, 67, 68] will be used in this research as the identification tool for frequency-domain responses. The rational representation of $\mathbf{Y}_c$ has the form

$$\mathbf{Y_c}(s) \approx \sum_{m=1}^{M} \frac{\mathbf{R}_m}{s - p_m} + \mathbf{D} \tag{2.13}$$

where $p_m$ is a set of common poles obtained from the rational fitting of the trace

of the characteristic admittance [88], either real or complex conjugate, $\mathbf{R}_m$ is the residue matrices and $\mathbf{D}$ is the real part of $\mathbf{Y_c}$ at infinite frequency. On the base of ULM [80] approach, the fitting of $\mathbf{H}$ is distinct since its elements may contain contributions from different time delays. Firstly, the modes of $\mathbf{H}$ are fitted in order to extract the delay $\tau_i$ for each mode and the set of poles $p_i$ [84]. Next, the modes with nearly equal delays are collapsed as one delay group with $\tau_g$. After identifying each delay $\tau_i$, the elements of $\mathbf{H}$ are fitted in the phase-domain using the poles from the modes and can be written as

$$\mathbf{H}(s) \approx \sum_{n=1}^{N} \left( \sum_{m=1}^{M} \frac{\mathbf{R}_{m,n}}{s - p_{m,n}} \right) \exp(-\mathrm{s}\ \tau_{\mathrm{n}}) \tag{2.14}$$

where $N$ denotes the number of modes, $M$ is the number of poles, $\tau_n$ is the time delay, $p_{m,n}$ is the set of poles and $\mathbf{R}_{m,n}$ is the residue matrices associated with the $n^{th}$ mode. Alternatively, other identification methods such as the Frequency-Partitioning Fitting (FPF) [90–92] and the Matrix Pencil Method (MPM) [125, 126, 128, 129] could be used for phase-domain modeling instead. On the other hand, the Levenberg–Marquardt scheme [96–102] and the Dominant Poles method [93, 94] were applied in modal domain modeling.

Even though the achieved approximation for $\mathbf{Y}_c$ and $\mathbf{H}$ correspond to a passive rational model within a user-defined band, the simulation using the ULM formulation sometimes gives unstable results due to out-of-band passivity violations. This issue was addressed in [160]. Another bottleneck in the ULM formulation may present numerical instability related to the occurrence of large ratios between residues and poles. This problem also leads to unstable time-domain simulations due to interpolation errors resulted from the contributions of distinct modes and further details can be found in [161, 162]. Some countermeasures were introduces to avoid such issues and reference [157] proposed the Idempotent Decomposition as an alternative to the ULM approach for phase-coordinates modeling since it provides an easier way to extract the delays in the identification of the propagation function $\mathbf{H}$. The decomposition of $\mathbf{H}$ into the sum of products of idempotent matrices allows the grouping of modes and revealed a suitable approach to avoid the stability problems related to large residue-pole ratios.

For time-domain simulations, the MoC modeling of overhead transmission lines and cables implies the adoption of a time-step smaller than the traveling time. In practice, the presence of short or nonideally transposed lines requires the explicit representation of each section and so results in a large computational burden. In order to cope this issue for short lines, alternative models were proposed in [89, 163, 164].

### 2.3.2 Nodal Admittance Matrix

The application of a MoC-based line model requires a time-step adopted by the simulation solver smaller than the traveling time delay. Hence, it creates a dilemma in the modeling of a system that includes long and short lines. As short lines require a very small time step, it increases substantially the computation burden. Some efforts addressed the modeling of short lines to overcome the limitation of using a time step not larger than the time delay [89, 163, 164] but this problem has been traditionally coped by cascading $\pi$-sections which in practice makes it difficult to include frequency dependent effects [19].

One alternative approach to $\pi$-sections is the modeling through the line nodal admittance matrix $\mathbf{Y}_n$ in the frequency domain. As a more compact form, $\mathbf{Y}_n$ is computed based on the line parameters and then subjected to a rational approximation. In this research, the *Vector Fitting* routine [64, 65, 67, 68] was adopted although other identification methods such as the Frequency-Partitioning Fitting or the Matrix Pencil Method could be used instead. Hence, $\mathbf{Y}_n$ presents the following form

$$\mathbf{Y_n}(s) \approx \sum_{m=1}^{M} \frac{\mathbf{R}_m}{s - p_m} + \mathbf{D} \tag{2.15}$$

where $p_m$ is a set of common poles, either real or complex conjugate, $\mathbf{R}_m$ is the residue matrix and $\mathbf{D}$ is the real part of of $\mathbf{Y_n}$ at infinite frequency.

For a transmission line with $n$ phases, the nodal admittance matrix $\mathbf{Y_n}$ relating the injected currents and the node voltages is given by

$$\mathbf{Y_n}(s) = \begin{bmatrix} \mathbf{Y}_s & \mathbf{Y}_m \\ \mathbf{Y}_m & \mathbf{Y}_s \end{bmatrix} \tag{2.16}$$

where $\mathbf{Y}_s$ and $\mathbf{Y}_m$ are $n \times n$ block matrices defined by

$$\mathbf{Y}_s = \mathbf{Y}_c \left(\mathbf{I} + \mathbf{H}^2\right) \left(\mathbf{I} - \mathbf{H}^2\right)^{-1} \tag{2.17a}$$

$$\mathbf{Y}_m = -2\ \mathbf{Y}_c\ \mathbf{H} \left(\mathbf{I} - \mathbf{H}^2\right)^{-1} \tag{2.17b}$$

and $\mathbf{I}$ is an $n \times n$ identity matrix.

The issue associated with this approach is that the resulting model is often inaccurate with high-impedance terminations since it is characterized by a large eigenvalue ratio and low observability of small eigenvalues at low frequencies. The accuracy problem can be overcome with the Modal Vector Fitting (MVF) method [165] even though the computation time can be substantial. Alternatively, the Mode-Revealing Transformation (MRT) [76] scheme can be used.

### 2.3.3 Folded Line Equivalent

The representation of frequency dependent lines is commonly based on traveling waves models and the inherent time delay has to be taken into account for accurate evaluations. As a consequence, an issue rises in simulations comprising long and short lines since the later require a time-step small enough to track the transient behavior.

In order to overcome time-step constraints concerned with line lengths, the modeling from its nodal admittance matrix $\mathbf{Y}_n$ in the frequency domain seems to be a suitable approach. Unfortunately, one challenge faced by admittance-based models has to do with large eigenvalue ratios and inaccurate observability of small eigenvalues at low frequencies which result in error magnifications in time-domain simulations with high-impedance terminations. In other words, it means that diagonalizing $\mathbf{Y}_n$ and carrying out the matrix inversion shows that the small eigenvalues of $\mathbf{Y}_n$ become the large eigenvalues of $\mathbf{Z}_n$.

Seeking to face this challenge, the Folded Line Equivalent (FLE) approach [89] allows one to fit the matrix elements retaining a high accuracy of the small eigenvalues. The methodology consists in decomposing $\mathbf{Y}_n$ into an open-circuit and short-circuit counterparts, namely $\mathbf{Y}_{oc}$ and $\mathbf{Y}_{sc}$, respectively. The modeling is done directly in the phase-domain, thereby being applicable to both overhead lines (transposed and untransposed) and underground cables.

Given the definition for $\mathbf{Y_n}$ in (2.16), the equivalent nodal admittance matrix is given by

$$\mathbf{Y}_{FLE}(s) = \mathbf{K}^{-1} \cdot \mathbf{Y}_n \cdot \mathbf{K} = \begin{bmatrix} \mathbf{Y}_{oc} & \mathbf{0} \\ \mathbf{0} & \mathbf{Y}_{sc} \end{bmatrix} \tag{2.18}$$

where

$$\begin{aligned} \mathbf{K} &= \begin{bmatrix} \mathbf{I} & \mathbf{I} \\ \mathbf{I} & -\mathbf{I} \end{bmatrix} \\ \mathbf{Y}_{oc} &= \mathbf{Y}_s + \mathbf{Y}_m \\ \mathbf{Y}_{sc} &= \mathbf{Y}_s - \mathbf{Y}_m \end{aligned} \tag{2.19}$$

and I is an identity matrix. K in (2.19) is also known as the media and anti-media transformation matrix and it has been used for modal-domain analysis of transmission lines [166].

A great feature of FLE is that the matrices to be fitted have half the dimension of the original admittance matrix, i.e., $\mathbf{Y}_n$ has a dimension $2n \times 2n$ while both $\mathbf{Y}_{oc}$ and $\mathbf{Y}_{sc}$ are $n \times n$ matrices. Furthermore, the ratio between the largest and smallest

eigenvalues in both $\mathbf{Y}_{oc}$ and $\mathbf{Y}_{sc}$ reduces considerably when compared with the ones found in $\mathbf{Y}_n$.

The rational approximation of $\mathbf{Y}_{oc}$ and $\mathbf{Y}_{sc}$ is based on the VF routine and carried out independently. It is required that both tend to the characteristic admittance in the high frequency range, i.e., both models must be asymptotically correct. Hence, the fitting is carried out using (2.20),

$$\begin{aligned}\overline{\mathbf{Y}}_{oc}(s) &= \mathbf{Y}_{oc}(s) - \mathbf{Y}_c(\infty) \approx \sum_{n=1}^{N} \frac{\mathbf{R}_{oc_n}}{s - p_{oc_n}} \\ \overline{\mathbf{Y}}_{sc}(s) &= \mathbf{Y}_{sc}(s) - \mathbf{Y}_c(\infty) \approx \sum_{m=1}^{M} \frac{\mathbf{R}_{sc_m}}{s - p_{sc_m}}\end{aligned} \tag{2.20}$$

where $\mathbf{Y}_c(\infty) = \mathbf{G}(\infty)$, i.e, the real part of the characteristic admittance matrix at infinite frequency. It is assumed that both functions to be fitted, i.e., $\overline{\mathbf{Y}}_{oc}$ and $\overline{\mathbf{Y}}_{sc}$, are strictly proper and there is no a priori relationship between the number of poles used in fitting either function. The FLE realization can be transformed back into the original phase-coordinates via the transformation

$$\mathbf{Y}_n(s) = \mathbf{K} \cdot \begin{bmatrix} \mathbf{Y}_{oc} & \mathbf{0} \\ \mathbf{0} & \mathbf{Y}_{sc} \end{bmatrix} \cdot \mathbf{K}^{-1} \tag{2.21}$$

The FLE model is recommended to be embedded into EMTP-like programs aiming to replace the MoC-based model when the selected time-step is larger than the line travel time. To interface the FLE model with a time-domain solver, the node voltages are transformed into and $\mathbf{v}_{oc}$ and $\mathbf{v}_{sc}$ by the transformation (2.22) for the convolution computations and the history current source in phase-domain is obtained from the one containing the open-circuit and short-circuit counterparts by

$$\mathbf{v} = \mathbf{K} \cdot \begin{bmatrix} \mathbf{v}_{oc} \\ \mathbf{v}_{sc} \end{bmatrix} \tag{2.22}$$

$$\mathbf{his} = \mathbf{K} \cdot \begin{bmatrix} \mathbf{i}_{oc} \\ \mathbf{I}_{sc} \end{bmatrix} \tag{2.23}$$

in which $\mathbf{i}_{oc}$ and $\mathbf{i}_{sc}$ are updated in accordance with (A.3).

### 2.3.4 Idempotent Decomposition

The Idempotent Decomposition was firstly addressed to the rational approximation of $\mathbf{H}$ in [167] for the modeling of overhead lines in phase-coordinates. Contrary to the modal domain approach, it represents a linear transformation based on idempotents instead of eigenvectors [152, 153]. Later, reference [157] investigated the possibility of applying idempotents for a full frequency dependent Idempotent line model (Id-Line) suitable for the analysis of underground cables and overhead lines using the MoC. However, it was found that the accuracy is dependent on the number of phases involved. As the number of phases involved increases there is a decrease in the quality of the rational approximation of $\mathbf{H}$.

In this research, an investigation based on idempotents will be carried out on the rational approximation of $\mathbf{Y}_n$ as an alternative to the FLE model. The rational approximation of $\mathbf{Y}_n$ is accomplished by an eigendecomposition into modal propagation parameters, resulting in the product of a frequency dependent transformation matrix $\mathbf{T}$, a diagonal matrix of modes $\mathbf{Y_m}$ and the inverse matrix of $\mathbf{T}$ given by

$$\mathbf{Y}_n(s) = \mathbf{T} \cdot \mathbf{Y_m} \cdot \mathbf{T}^{-1} \tag{2.24}$$

Writing the transformation matrices $\mathbf{T}$ and $\mathbf{T}^{-1}$ in terms of their respective rows $\mathbf{r}_i$ and columns $\mathbf{c}_i$

$$\begin{aligned} \mathbf{Y}_n(s) &= \begin{bmatrix} \mathbf{c}_1 & \dots & \mathbf{c}_n \end{bmatrix} \begin{bmatrix} y_1 & & \\ & \ddots & \\ & & y_n \end{bmatrix} \begin{bmatrix} \mathbf{r}_1 \\ \vdots \\ \mathbf{r}_n \end{bmatrix} \\ \mathbf{Y}_n(s) &= [\mathbf{c}_1\mathbf{r}_1]\ y_1 + \cdots + [\mathbf{c}_n\mathbf{r}_n]\ y_n \\ \mathbf{Y}_n(s) &= \sum_{i=1}^{n} \mathbf{M}_i\ \mathbf{y}_i \end{aligned} \tag{2.25}$$

where $n$ is the number of modes and $\mathbf{M}_i$ are the idempotent matrices to be subjected to rational approximation. Aiming the reduction in the order of the rational functions, the proposition to group idempotent matrices with close eigenvalues, as adopted in [157], will be employed in a similar fashion like the grouping routine used in the ULM approach.

For the time-domain implementation of the Idempotent model, the history current source should be represented as a set of parallel current sources associated with each idempotent matrix $\mathbf{M}_i$ since $\mathbf{Y}_n$ is now a sum of several independent matrices, as depicted in Fig. 2.4.

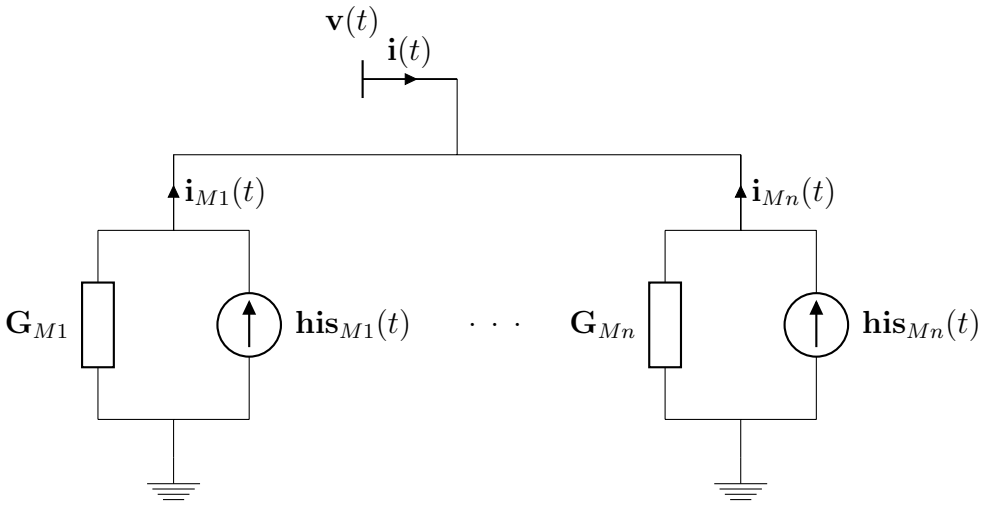


Figure 2.4: Time-domain implementation of the Idempotent model

## 2.4 Frequency Dependent Network Equivalents

A key issue in electromagnetic transient simulations is how to deal with large networks as there are several cases where one is only interested in the transient response of part of this network. A suitable solution is to replace a large portion of a given network by a frequency dependent network equivalent (FDNE). It consists in a black-box equivalent emulating the behavior of the actual network as seen at a set of ports.

The research involving FDNE dates back to 70s and the very first techniques were based on the synthesis of RLC branches [47, 50–59] but the drawback of this procedure is that it gives good matches at selected frequencies but the response at other frequencies is less accurate.

A number of methods based on rational approximations of a given frequency response have been proposed in the last two decades using either the VF algorithm, the MPM method or the FPF technique. This kind of representation allows the achievement of very accurate results in a wide frequency range and enables one the direct interface of rational models with EMTP-type programs by means of trapezoidal integration rule [90, 168] or recursive convolution [139].

The modeling of a given frequency dependent model is performed through its nodal admittance matrix $\mathbf{Y}_n$ with respect to the sending and receiving ends. The structure, concerned with the input-output relation between the terminals in a wide frequency range, is shown in (2.26) and is assumed the same notation like in [169].

$$\mathbf{Y}_n(s) = \begin{bmatrix} \mathbf{Y}_{SS} & \mathbf{Y}_{SR} \\ \mathbf{Y}_{RS} & \mathbf{Y}_{RR} \end{bmatrix} \tag{2.26}$$

Since $\mathbf{Y}_n$ represents a passive symmetric element, so $\mathbf{Y}_{SR} = \mathbf{Y}_{SR}^T$ and unlike a homogeneous line section $\mathbf{Y}_{SS} \neq \mathbf{Y}_{RR}$.

The $\mathbf{Y}_n$ matrix can be obtained via direct computations or by a detailed representation of an actual system followed by a frequency sweep in EMTP-ATP, PSCAD/EMTDC or EMTP-RV. The calculated or extracted frequency response is to be subjected to a rational approximation with the *Vector Fitting* routine resulting in the following pole-residue model

$$\mathbf{Y_n}(s) \approx \sum_{m=1}^{M} \frac{\mathbf{R}_m}{s - p_m} + \mathbf{D} \tag{2.27}$$

where $p_m$ is a set of common poles, either real or complex conjugate, $\mathbf{R}_m$ is the residue matrix and $\mathbf{D}$ is the real part of $\mathbf{Y_n}$ at infinite frequency.

A great feature of the modeling based on the nodal admittance matrix is that it

enables the modeling of nonhomogeneous system (NhS) [169–171]. Nonhomogeneous transmission systems occur in several practical configurations such as cascade of slightly different lines, nonideally transposed overhead lines, cross-bonded cables and river crossings. It also includes the corona effect, which is a source of attenuation and distortion of surges and overvoltages in overhead lines [172]. Once the time-domain representation of a NhS demands the explicit representation of each homogeneous section, i.e., each untransposed line or cable segment, thereby not being an efficient solution, this approach allows to exploiting a NhS as a particular case of a FDNE. It requires the derivation of an input-output relation between the systems terminals and, from this, obtain an equivalent nodal admittance matrix [173].

## 2.5 Multiscale Approach

### 2.5.1 Introduction

The novel approach designed in this research aims to enable simulations with variable time-step featuring the same Norton-type structure adopted by EMTP-like programs. With little effort, it allows evaluations with multiple time-steps in a simple and straightforward way without modifications in actual companion models. Besides keeping the accuracy of the original time-step invariant approach, the proposed multiscale approach provides a sensible gain in the overall computation time and also a smooth transition regardless of the change in time-step length.

### 2.5.2 Reinitialization Approach

To illustrate the modification to be carried out in companion networks, consider a scalar case of the well-known discrete time equivalent of an inductance $L$ given by

$$\begin{aligned} his_1(t) &= i_1(t-\Delta t_1) + g_1\, v(t-\Delta t_1) \\ g_1 &= \frac{\Delta t_1}{2L} \end{aligned} \tag{2.28}$$

where $g_1$ is a conductance, $his_1(t)$ is a history current source, $v(t)$ is the terminal voltage and $\Delta t_1$ is the time-step.

At a given instant $t$ when the time-step size is changed to $\Delta t_2$, the node current and voltage should not change due to the modification of the time-step. Thus, to ensure this condition, the history current source has to be re-calculated on the base of the new conductance $g_2$ related with the new time-step length $\Delta t_2$ by

$$\begin{aligned} his_1(t) + g_1\, v(t) &= his_2(t) + g_2\, v(t) \\ his_2(t) &= his_1(t) + (g_1 - g_2)\, v(t) \end{aligned} \tag{2.29}$$

After the transition, the companion network slightly changes with the updated current source given by

$$\begin{aligned} his_2(t) &= i_2(t-\Delta t_2) + g_2\, v(t-\Delta t_2) \\ g_2 &= \frac{\Delta t_2}{2L} \end{aligned} \tag{2.30}$$

The whole process is depicted in Fig. 2.5.

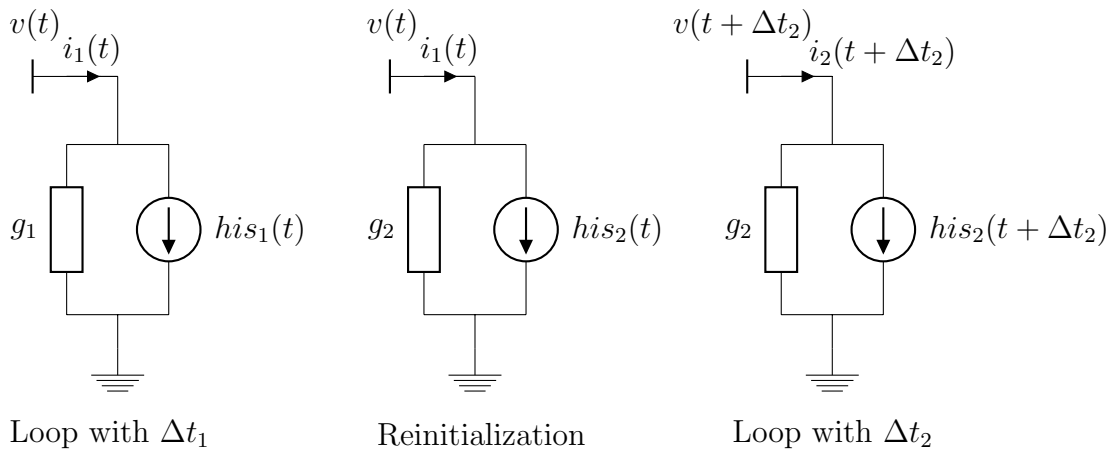


Figure 2.5: Sketch for time-step transition

The following pseudo-code can be used to compute the time response. Based on the modified-augmented nodal analysis (MANA) [17], which is an extension of the formulation presented in [16], $RHS$ stands for the vector of known quantities in MANA, $Sys1$ is the system matrix when $\Delta t_1$ and $Sys2$ is the one related to time-step $\Delta t_2$.

```
*** Loop with delta_t 1 ***
for n = 2:100
his(n) = i(n-1)+ g1*v(n-1)
output(n) = inverse(Sys1)*RHS
end

*** update current source ***
his(n) = his(n) + (g1-g2)*v(n)

*** Loop with delta_t 2 ***
for n = 101:150
his(n) = i(n-1)+ g2*v(n-1)
output(n) = inverse(Sys2)*RHS
end
```

A general case which consists in more than one element in the assembling of the equivalent conductance is considered: a discrete time conductance $g_1^i$ associated with pole $i$ using $\Delta t_1$ and $g_2^i$ the conductance for the same pole but using $\Delta t_2$ instead. Then, at the instant of the time-step transition, the equivalent current source must

be updated as

$$his_2(t) = \sum_{i=1}^{N} his_2^i(t) = \sum_{i=1}^{N} his_1^i(t) + \sum_{i=1}^{N} (g_1^i - g_2^i)\, v(t) \tag{2.31}$$

where $his_k^i$ (with $k = 1, 2$) is the history current source associated with the $i^{\text{th}}$ pole and $v(t)$ is the terminal voltage. It should be remarked that in the updating stage all branches have to be individually reinitialized and then gathered into one equivalent current source as highlighted in Fig. 2.6.

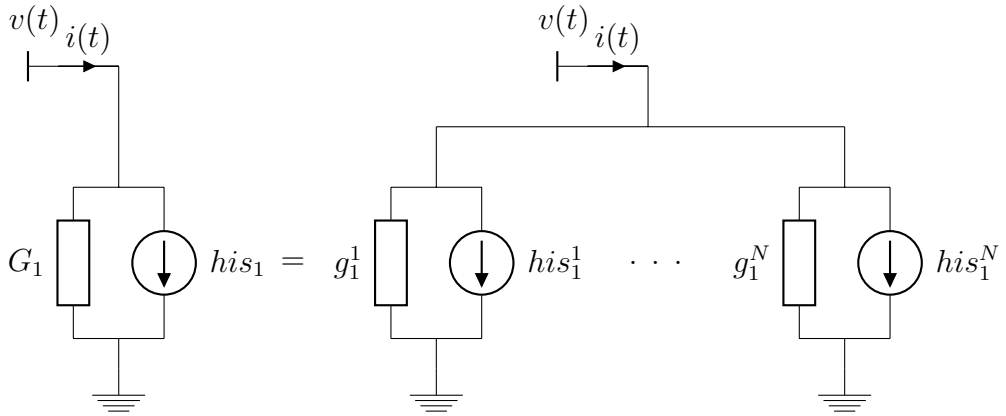


(a) Companion network for $\Delta t_1$

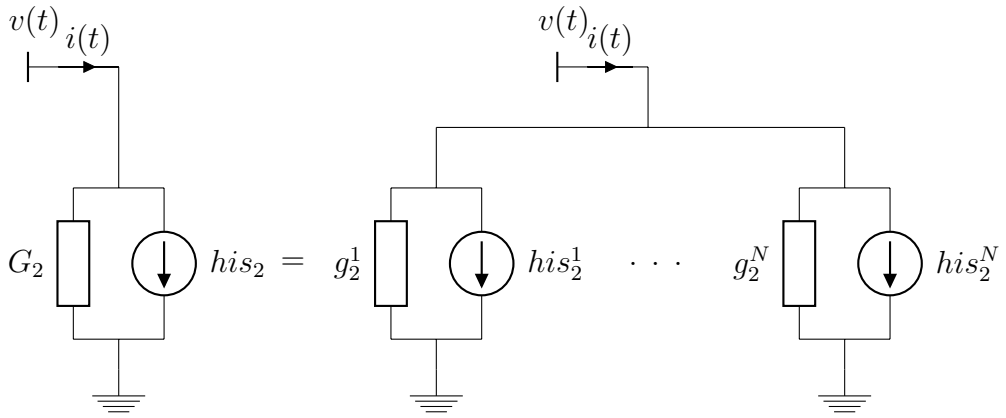


(b) Companion network for $\Delta t_2$

Figure 2.6: Sketch for time step transition

The extension to the multi-phase case is straightforward, see [168] for details. Although only a single change in the time-step was depicted, this procedure can be applied for multiple changes along the simulation run in the same fashion in accordance with the reinitialization steps.

## 2.6 Test cases

For the assessment of the accuracy and numerical performance of the proposed Multiple Time-Step (MTS) approach, a set of six test cases is going to be evaluated, namely:

1. #1: a RLC circuit
2. #2: a FDNE describing a 34 kV distribution network
3. #3: a 132-kV, 10 km long overhead line (Yn-Line)
4. #4: a 132-kV, 10 km long overhead line (FLE-Line)
5. #5: a 132-kV, 10 km long overhead line (Id-Line)
6. #6: a single-core armoured HVDC subsea cable, 2.5 km length (FLE-Line)

A PSCAD simulation will provide the reference for test cases #1 and #2. Despite the apparent similarity of cases #3 to #5, each multiscale simulation will be performed through the following formulations presented in Section 2.3, namely: nodal admittance matrix (Yn-Line), Folded Line Equivalent (FLE-Line) and Idempotent Decomposition (Id-Line). A a fixed time-step simulation with the universal line model (ULM) [80] will be adopted for validation of the test cases involving the overhead line. For the HVDC subsea cable, another simulation method using a frequency-domain algorithm based on the Numerical Laplace Transform (NLT) [174–176] will be applied.

It is worth mentioning that for all test cases the instant for the time-step transition is defined prior the simulation starts as well as the new time-step value. The developed computer codes with *Mathematica* [177] for time-domain simulations adopted the Modified Nodal Analysis (MNA) formulation to solve the circuit equations [16] in a similar fashion like MatEMTP [178]. A conventional laptop was used for the calculations with a 2.9 GHz, Core i7 computer with 8 GB of RAM.

### 2.6.1 Case #1: RLC

To exemplify the first application of a multiscale simulation with the novel MTS approach, consider the very simple RLC circuit shown in Fig. 2.7. The parameters for this evaluation are given by

$$V_s = \cos\,(2\,\pi\,50\,t)$$
$$R = 100\ \Omega \qquad L = 110\ \mathsf{mH} \qquad C = 0.25\ \mu\mathsf{F}$$
$$i_L(0) = 0\ \mathsf{A} \qquad v_C(0) = 0\ \mathsf{V}$$

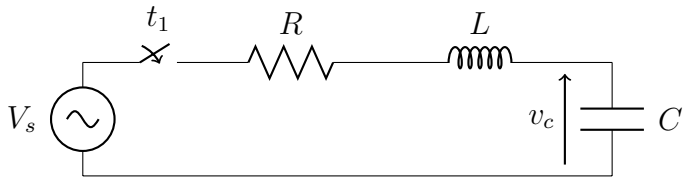


Figure 2.7: Case #1: RLC circuit

As initially stated, the initial conditions of $v_c$ and $i_L$ are zero. The simulation concerns with the switching at $t_1 = 0$ s, i.e., the instant at which the input voltage is in its maximum value. Initially, the circuit is simulated considering an initial time-step $\Delta t_1 = 10\ \mu$s and when the circuit reaches the steady-state the time-step is increased to $\Delta t_2 = 500\ \mu$s.

The first variable of interest is the capacitor voltage and its transient behavior is shown in Fig. 2.8. The validation of the achieved result is done with same circuit simulated with PSCAD which is a fixed time-step solver. An excellent match can be observed and there are no numerical oscillations or discontinuity in the waveform due to the change in the time-step.

To highlight that in the proposed approach there is no discontinuity issues during the time-step transition, Fig. 2.9 depicts the capacitor voltage at the instant near the time-step switch. A smooth waveform due to the time-step transition can be observed. The current waveform attains the same accuracy as depicted in Fig. 2.10 as can be seen and as the current response has no mismatches between the current calculated using only a single time-step and the one using the proposed formulation.

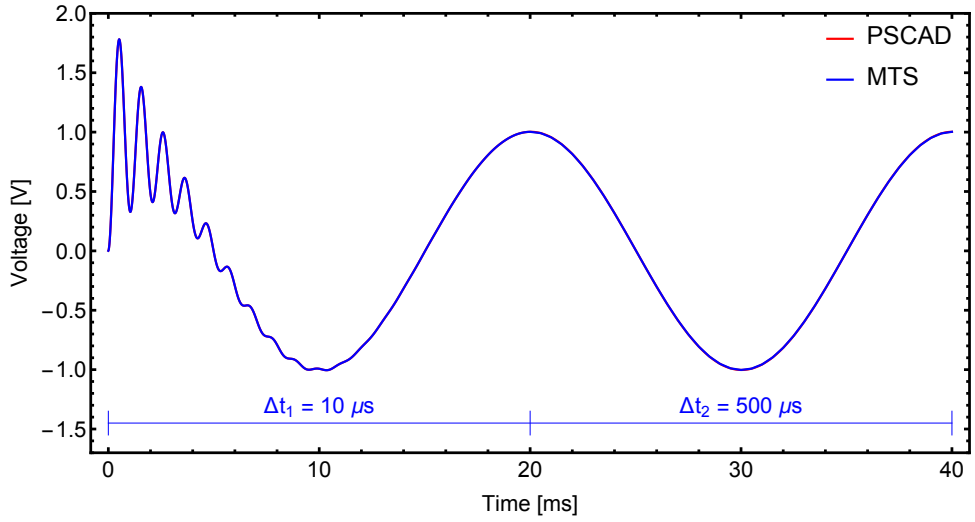


Figure 2.8: Case #1: Simulated capacitor voltage

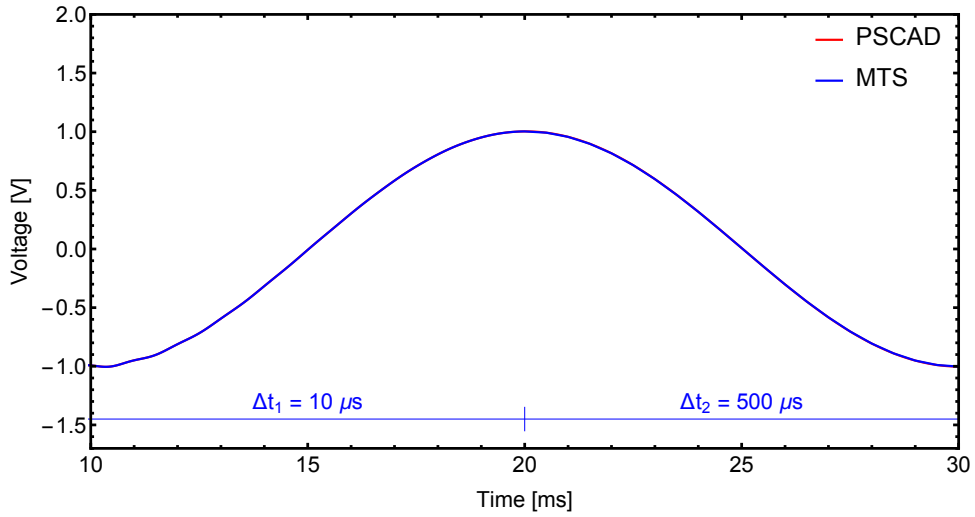


Figure 2.9: Case #1: Simulated capacitor voltage (detail)

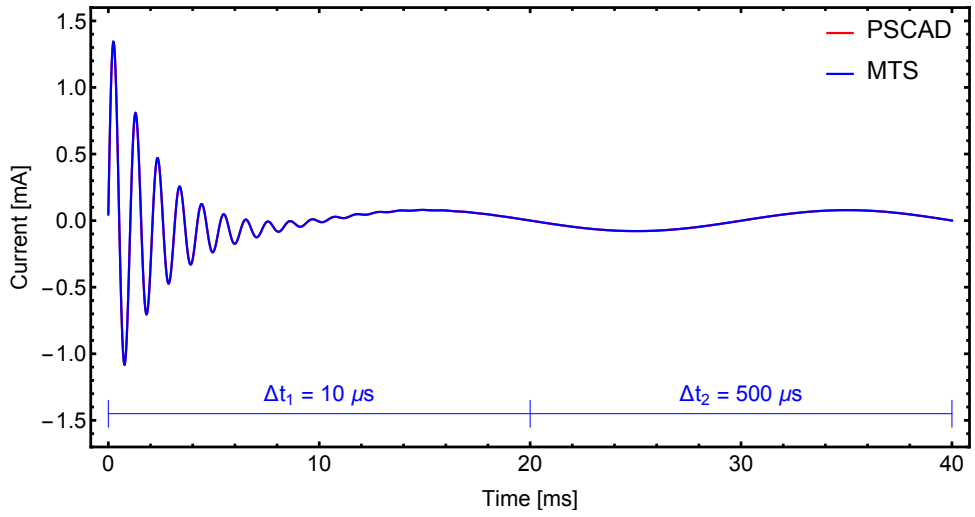


Figure 2.10: Case #1: Simulated current

### 2.6.2 Case #2: FDNE

This test case is intended to model a frequency dependent network equivalent (FDNE) in phase-coordinates for time-domain simulations. The system describes a 24 kV rural distribution network adopted in [66, 121] and depicted in Figure 2.11. The length of each circuit in km and the details of the network configuration can be found in Figure 2.11. The system is assumed to be unloaded. The overhead line data and underground cable arrangement are depicted in Figure 2.12. The data for each single-core cable is presented in Table 2.1.

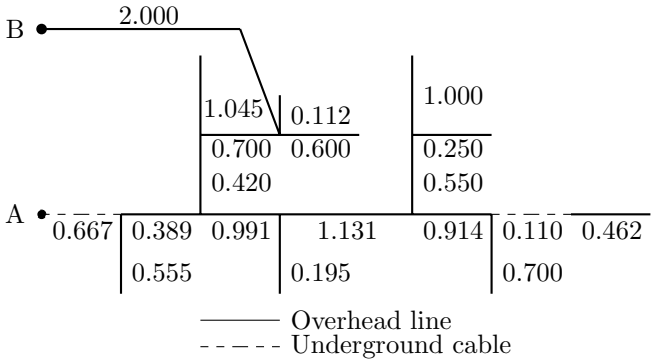


Figure 2.11: Case #2: Power system distribution network

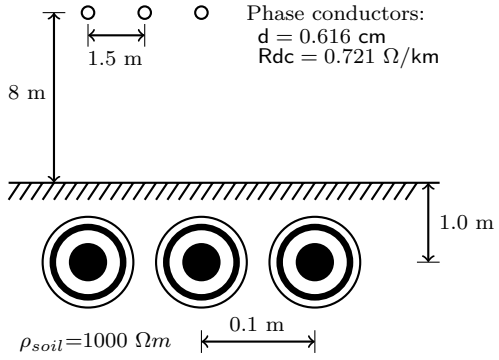


Figure 2.12: Case #2: Overhead line and underground cable configuration

Table 2.1: Case #2: Single core cable data

| | | |
|---|---|---|
| core conductor | radius=5.325 mm | $\rho_c = 4.179 \cdot 10^{-8}\,\Omega$.m |
| first insulation layer | thickness=5.5 mm | $\varepsilon_1 = 2.3$ |
| sheath | thickness=0.35 mm | $\rho_s = 1.724 \cdot 10^{-8}\,\Omega$.m |
| jacket | thickness=4 mm | $\varepsilon_2 = 2.30$ |

The complete system considering a full phase-domain line model was implemented in PSCAD/EMTDC. A frequency sweep with logarithmically spaced samples in the frequency range between 1 Hz – 100 kHz as seen from the three-phase buses $A$ and $B$ was carried out in order to obtain an equivalent $6 \times 6$ nodal

admittance matrix $\mathbf{Y}_n$ to be subject to a rational approximation using the *Vector Fitting* routine. The rational approximation considering 64 poles is shown in Figure 2.13a. A very good match was attained in all frequency range. The fitted eigenvalues as well as the ones from the original equivalent admittance matrix are depicted in Figure 2.13b.

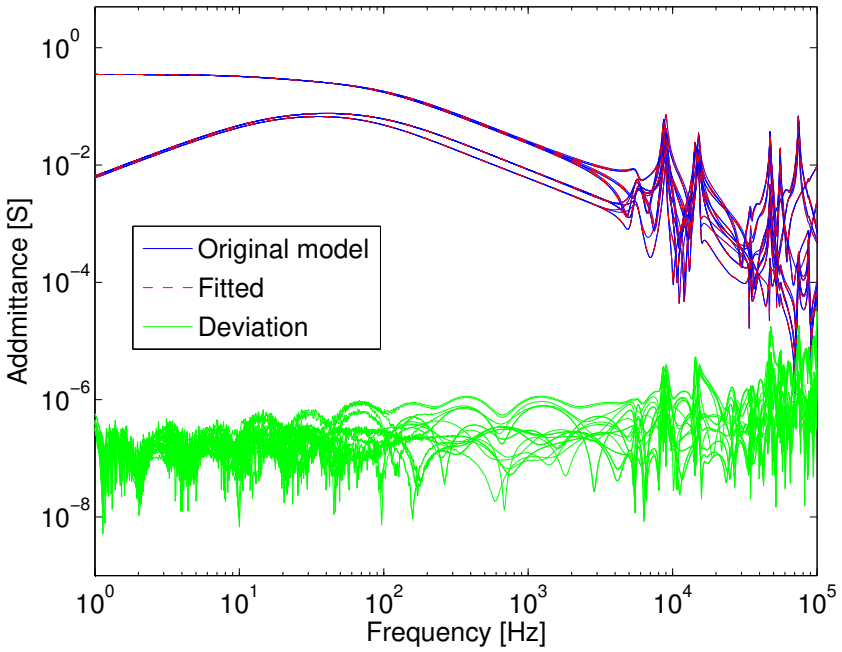


(a) Fitting of $\mathbf{Y}_n$

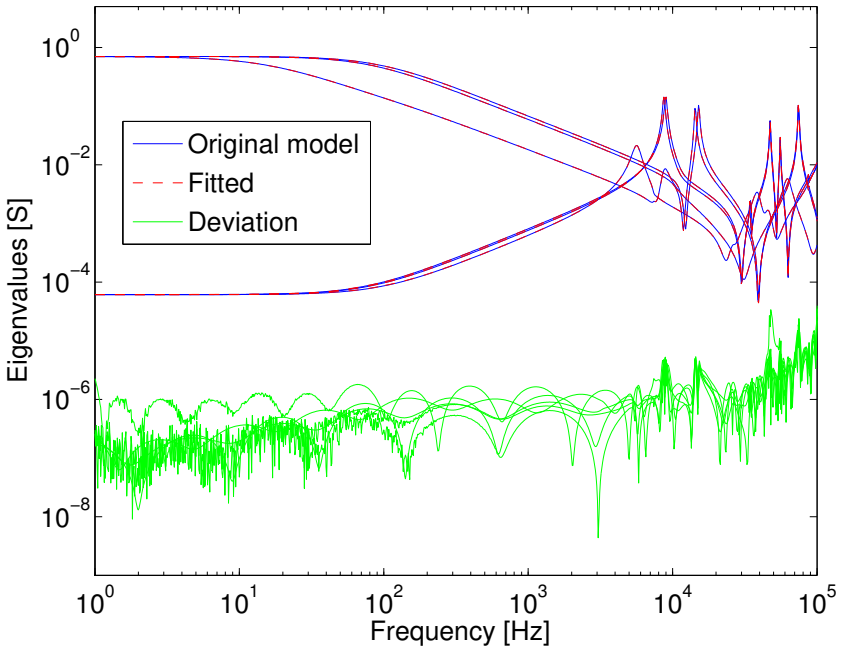


(b) Eigenvalues of $\mathbf{Y}_n$

Figure 2.13: Case #2: Fitting results (FDNE)

To ensure the accuracy of the fitted small eigenvalues at the lower frequency range, the Mode-Revealing Transformation (MRT) [76] approach was used. MRT aims to improve the observability of these small eigenvalues by choosing a suitable real transformation matrix that preserves the physical properties of symmetry, realness, stability, causality and passivity. It can be understood as an alternative to the Modal Vector Fitting presented in [165, 179].

To illustrate the performance of the proposed methodology, consider a single-phase energization as depicted in Figure 2.14 where the switch closes in $t_1 = 0$ s. Initially, a time-step $\Delta t_1 = 0.5\,\mu$s is used and after 4 ms it is increased to $\Delta t_2 = 500\,\mu$s. The complete network was also simulated using PSCAD with a time-step $\Delta t = 0.5\,\mu$s.

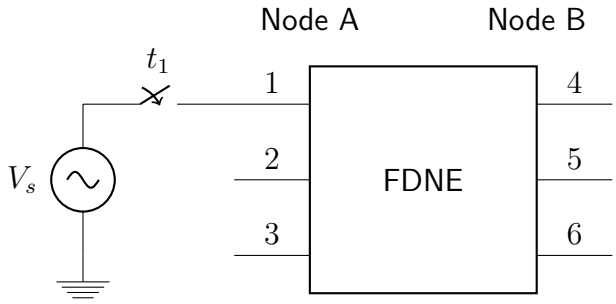


Figure 2.14: Case #2: Circuit for time-domain simulation

The transient voltage at terminal #4, i.e., the first phase in node B, is depicted in Fig. 2.15 considering both approaches. An excellent match can be observed and there are no oscillations or discrepancies due to the change in the time-step.

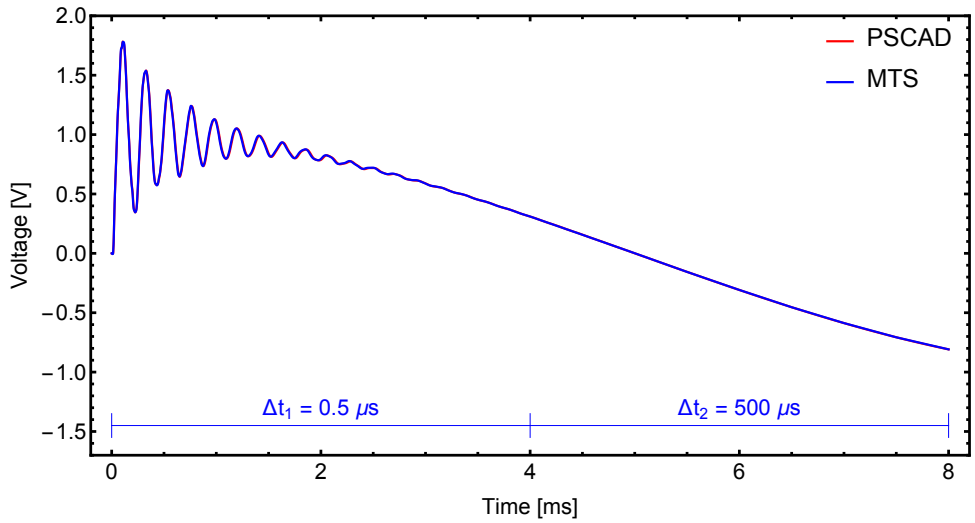


Figure 2.15: Case #2: Simulated voltage at terminal # 4

To emphasize that in the proposed approach there is no discontinuity issues during the time-step transition, Fig. 2.16 depicts the voltage at terminal #4 at the instant near the time-step switch. A smooth waveform can be observed with no numerical oscillation due to the time-step transition.

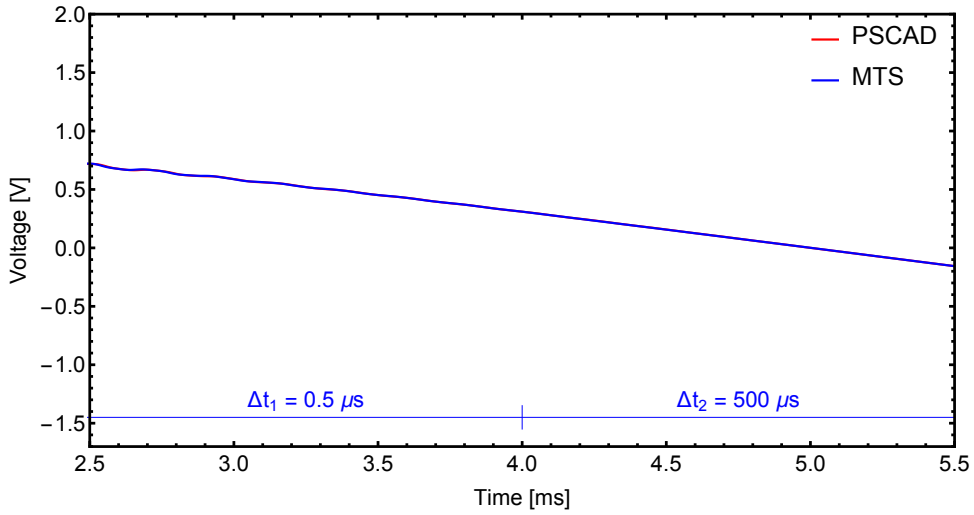


Figure 2.16: Case #2: Simulated voltage at terminal # 4 (detail)

Now consider the same network as before where a first switch closes at $t_1 = 0$ s and now a second switch closes at $t_2 = 10$ ms. The circuit is depicted in Fig. 2.17 where $R = 100\ \Omega$. The same initial time-step as in the previous case was considered, i.e., $\Delta t_1 = 0.5\ \mu$s, and again after 4 ms it changes to $\Delta t_2 = 500\ \mu$s until 10 ms. Next, a short-circuit is applied and the time-step changes back to $\Delta t = 0.5\ \mu$s.

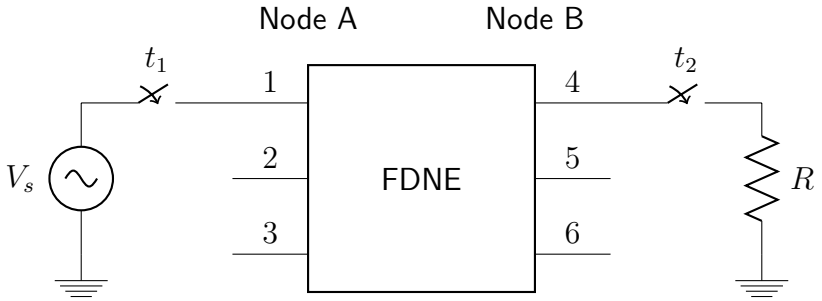


Figure 2.17: Case #2: Circuit for time-domain simulation

Figure 2.18a depicts the voltage behavior at terminal #4 for this second test. There is a very good agreement between these two results. Some small discrepancies can be seen in the first instants after the second switching as shown in Fig. 2.18b. These differences are due to the upper limit of 100 kHz in the FDNE fitting. The line model used in PSCAD considered a frequency range from 1 Hz up to 1 MHz for the fitting of the characteristic admittance and propagation function.

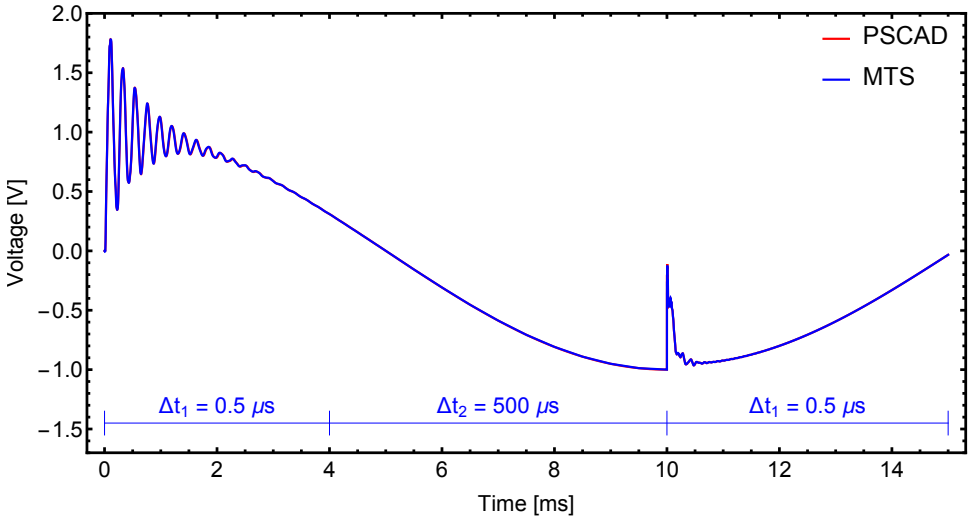


(a) Simulated voltage at terminal # 4

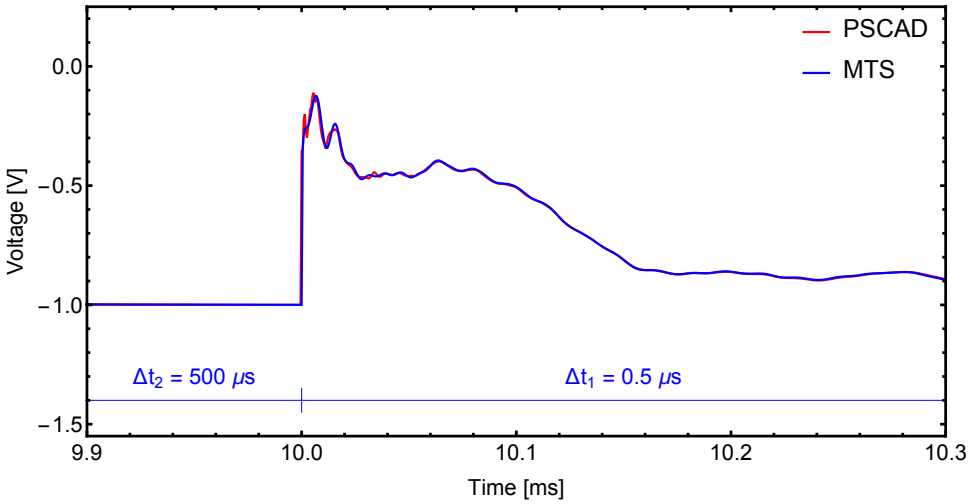


(b) Simulated voltage at terminal # 4 (detail)

Figure 2.18: Case #2: Time-domain simulation

The current injection at terminal #1 is depicted in Fig. 2.19 and again a very good agreement can be seen. As the current response has a lower frequency content, there are no substantial mismatches between the current calculated using only a single time-step and the one using the proposed formulation.

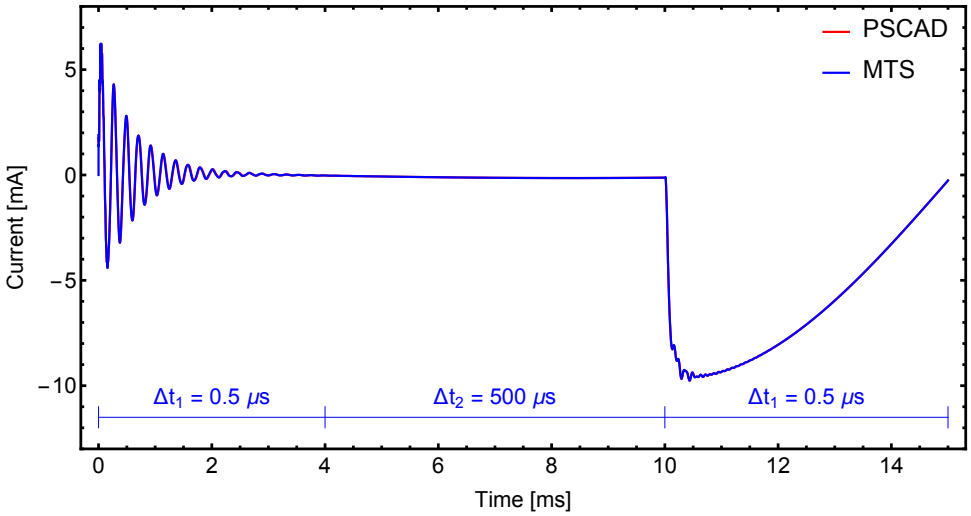


(a) Simulated current at terminal # 1

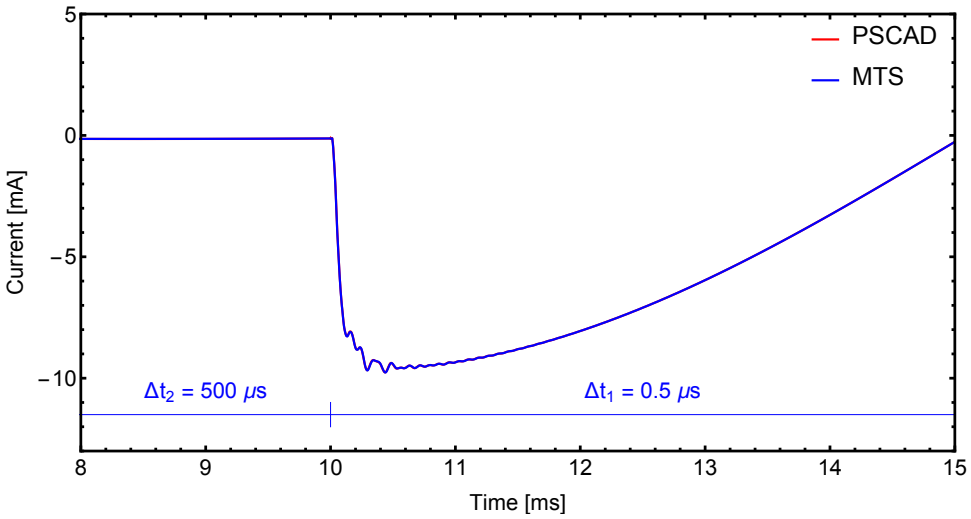


(b) Simulated current at terminal # 1 (detail)

Figure 2.19: Case #2: Time-domain simulation

### 2.6.3 Case #3: Overhead Line (Yn-Line)

This test case aims to demonstrate the applicability of the MTS approach in the simulation of a nodal admittance-based line model (**Y**n–Line). Fig. 2.20 shows the 132 kV overhead line to be considered. It consists of a 10 km long untransposed flat configuration with ground wires continuously grounded [180].

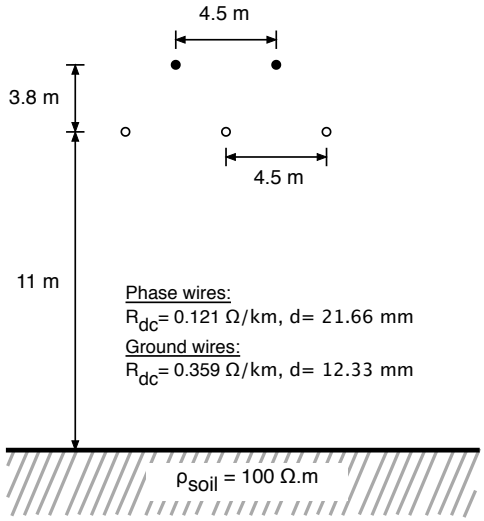


Figure 2.20: Case #3: 132-kV transmission line geometry

The modeling is based on the equivalent nodal admittance matrix $\mathbf{Y}_n$, according to Section 2.3.2, that relates the voltages and currents at the terminals in the frequency domain. A six-terminal frequency dependent model is able to take into account the inherent propagation phenomena of overhead lines and underground cables for time-domain evaluations. In order to obtain the admittance matrix $\mathbf{Y}_n$ with respect to the sending and receiving ends, a computer code was developed with *Mathematica* to obtain the line parameters using a combination of linearly and logarithmically spaced samples in the frequency range between 1 Hz – 150 kHz. The calculated frequency response was then subjected to a rational approximation by means of the *Vector Fitting* routine which resulted in a pole-residue model with 88 poles. Fig. 2.21 shows the elements and the eigenvalues of $\mathbf{Y}_n$ with the respective deviations.

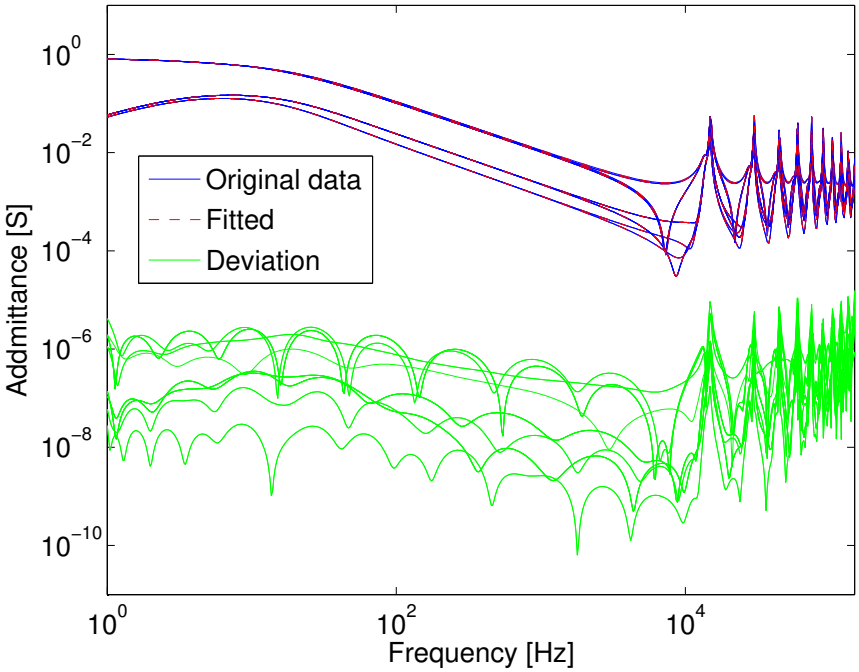


(a) Fitting of $\mathbf{Y_n}$

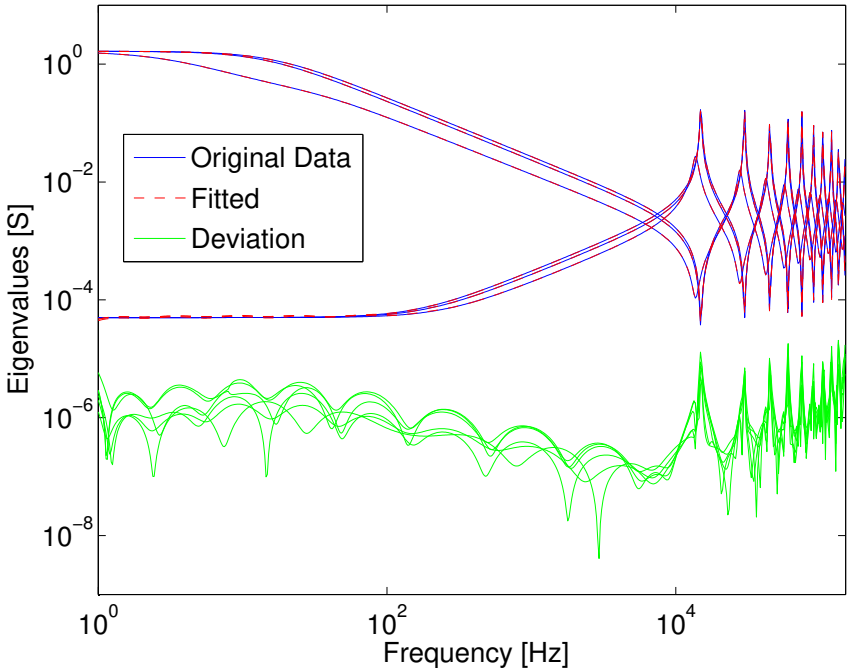


(b) Eigenvalues of $\mathbf{Y}_n$

Figure 2.21: Case #3: Fitting results (Yn-Line)

For the given rational model a time-domain simulation was performed in order to evaluate the multiscale line model. Fig. 2.22 depicts the system to be evaluated, i.e., a single-phase energization by a unit sinusoidal voltage source followed by a capacitor bank energization. The short-circuit reactance is considered by means of an inductance $L = 110$ mH.

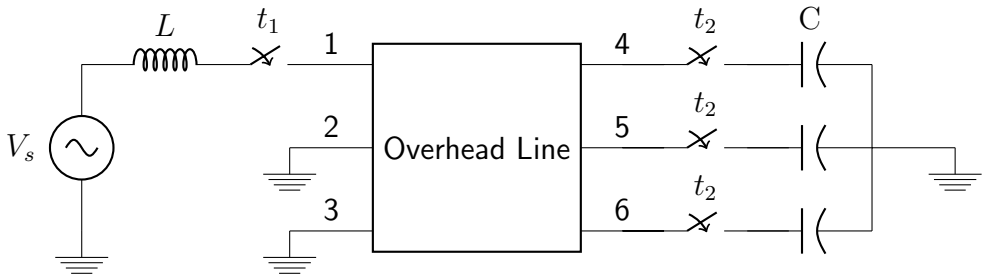


Figure 2.22: Case #3: Circuit for time-domain simulation

The first maneuver to be performed is a single phase energization at $t_1 = 0$ s and Fig. 2.23 shows the simulated voltage at terminal #4 with an initial time-step $\Delta t_1 = 1$ $\mu$s. After 20 ms, when all transients have decayed and the voltage reaches its peak value, the time-step is increased to $\Delta t_2 = 500$ $\mu$s. A comparison with the voltage response with the ULM model highlights that a very accurate result is attained. Furthermore, no discontinuity at the transition instant is observed.

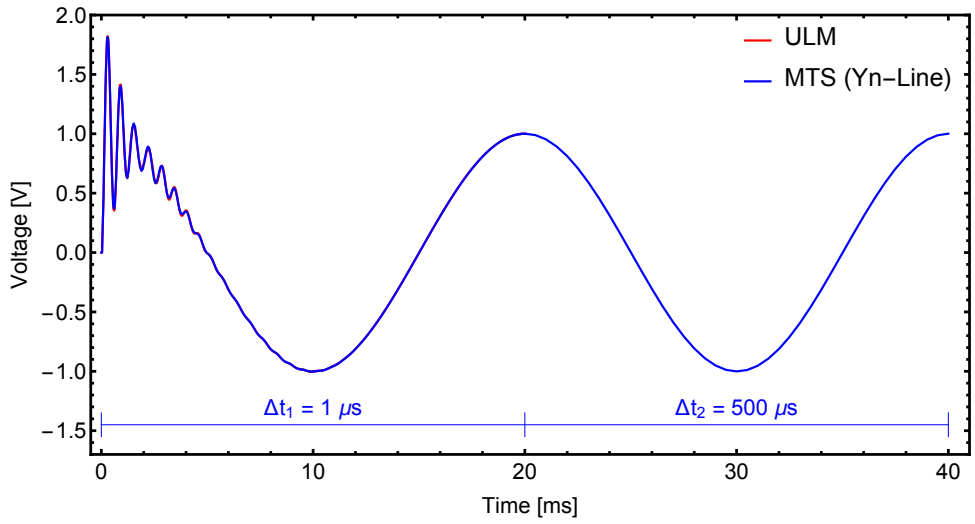


Figure 2.23: Case #3: Simulated voltage at terminal # 4

In order to verify the versatility of the novel technique, a second switch closes at $t_2 = 40$ ms to energize the capacitor bank where $C = 0.1$ $\mu$F, see Fig. 2.24. The switching occurs when the voltage at terminal #4 is at its maximum. At this same instant, the time-step length is reduced to the initial value $\Delta t_1 = 1$ $\mu$s. In Fig. 2.25 is shown the overall simulation for this test case.

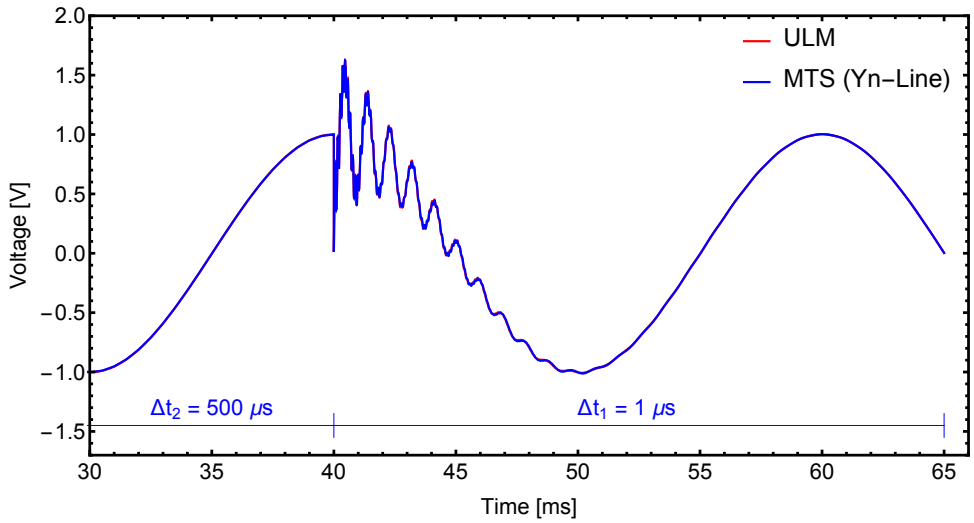


Figure 2.24: Case #3: Simulated voltage at terminal # 4

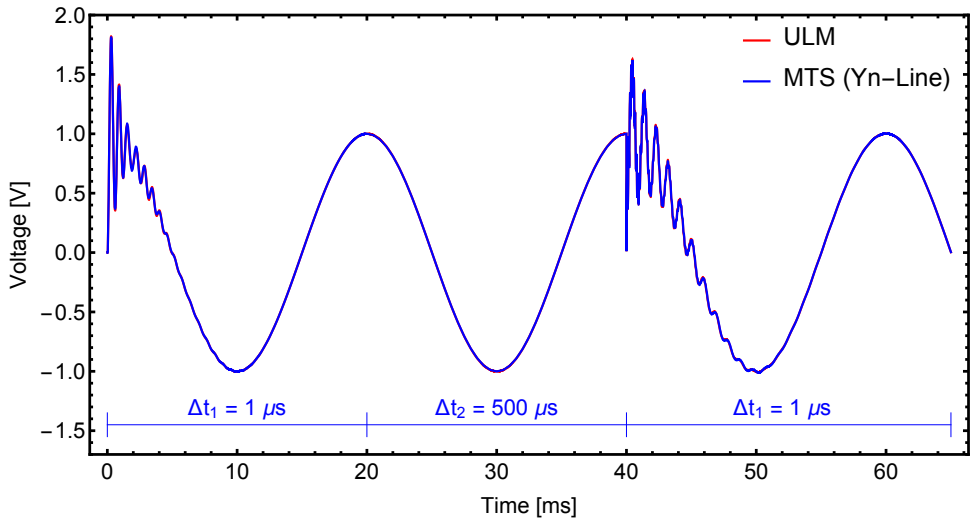


Figure 2.25: Case #3: Simulated voltage at terminal # 4

The current injected at terminal #1 is presented in Fig. 2.26. Again a very good agreement can be seen as there are no substantial mismatches between the current calculated using only a single time-step and the one using the proposed formulation.

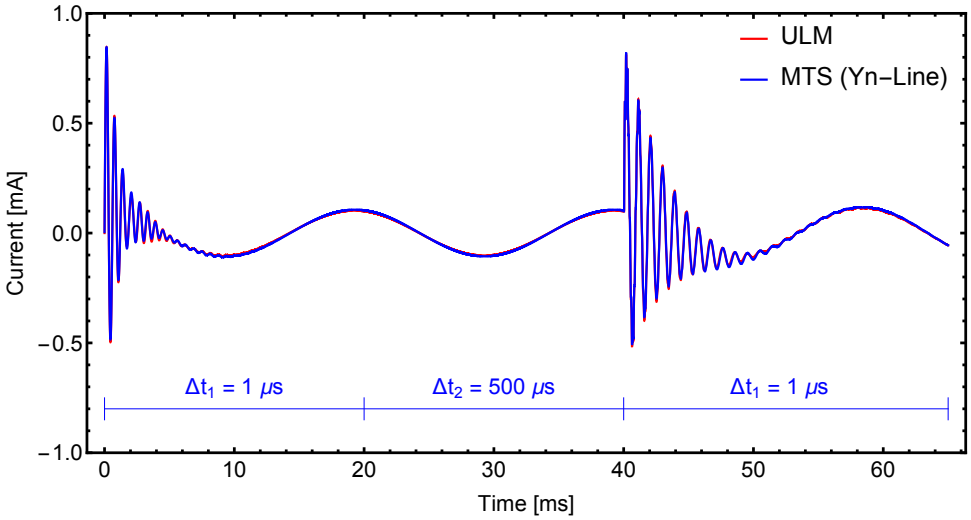


(a) Current at terminal # 1

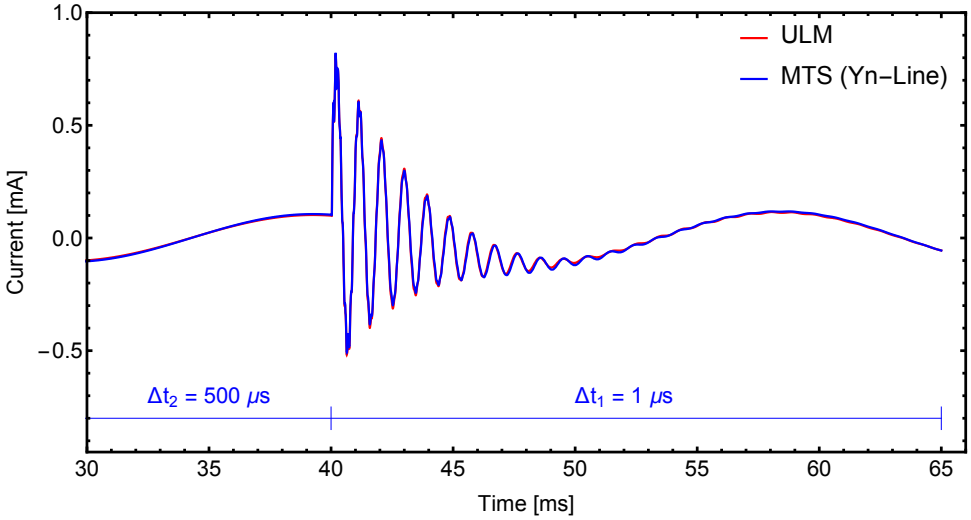


(b) Detailed view

Figure 2.26: Case #3: Time-domain simulation

It is worth mentioning that when the system under evaluation reaches the steady-state there is no constraint for the new time-step length. If one desires a larger time-step, for instance, $\Delta t > 1$ ms, a phasor-based formulation is required. In Chapter 3, the concept of dynamic phasors is introduced to enable the integrated simulation of electromagnetic and electromechanical transients. As a consequence, synchronous machine models can be interfaced with the multiscale line model.

### 2.6.4 Case #4: Overhead Line (FLE-Line)

This test case aims to demonstrate the applicability of the new MTS approach for line simulations based on the Folded Line Equivalent (FLE–Line) model [89]. The overhead line is the same as the previous one, see Fig. 2.20. The modeling is based on the same nodal admittance matrix $\mathbf{Y}_n$ as in case #3. As discussed in Section 2.3.3, the methodology consists in decomposing $\mathbf{Y}_n$ into an open-circuit and short-circuit counterparts, namely $\mathbf{Y}_{oc}$ and $\mathbf{Y}_{sc}$, respectively.

The calculated $\mathbf{Y}_n$ in the frequency range between 0.01 Hz – 150 kHz was then converted into $\mathbf{Y}_{oc}$ and $\mathbf{Y}_{sc}$ matrices and subjected to a rational approximation with the *Vector Fitting* routine. Fig. 2.27 shows the fitting results for $\mathbf{Y}_{oc}$ and $\mathbf{Y}_{sc}$ and 50 poles were used in the fitting for both $\mathbf{Y}_{oc}$ and $\mathbf{Y}_{sc}$. The fitted eigenvalues are shown in Fig. 2.28

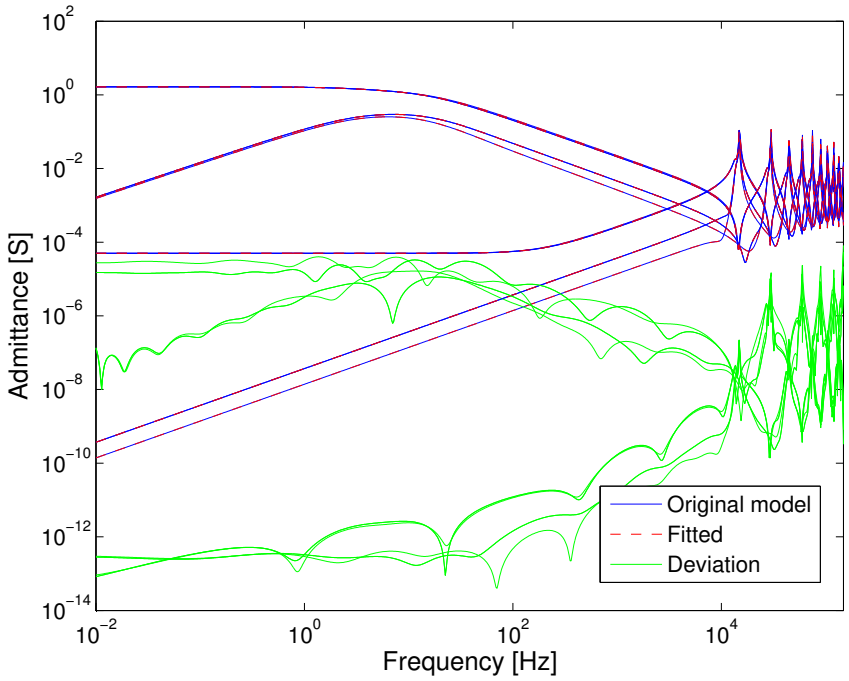


Figure 2.27: Case #4: Fitting of $\mathbf{Y}_{oc}$ and $\mathbf{Y}_{sc}$ (FLE-Line)

The great feature of the FLE model is that the eigenvalues are accurately fitted in the low frequency range and particularly suitable to the situation when the time-step is larger than the line travel time. This situation occurs frequently in practice as power systems often have long and short lines.

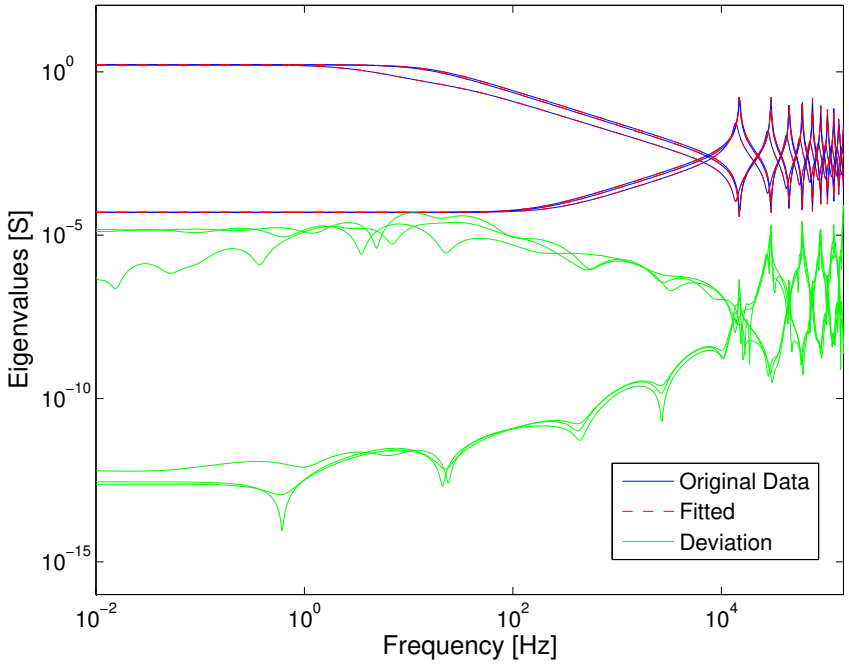


Figure 2.28: Case #4: Eigenvalues of $\mathbf{Y}_{oc}$ and $\mathbf{Y}_{sc}$ (FLE-Line)

In order to evaluate this alternative multiscale line model, the same time-domain simulation performed in the previous section is considered. As aforementioned, the simulation starts with time-step $\Delta t_1 = 1$ $\mu$s and after 20 ms the time-step is increased to $\Delta t_2 = 500$ $\mu$s. Next, at the same instant that the capacitor bank is energized, the time-step changes back to $\Delta t_1 = 1$ $\mu$s. For the sake of clarity, the circuit to be simulated is shown in Fig. 2.29.

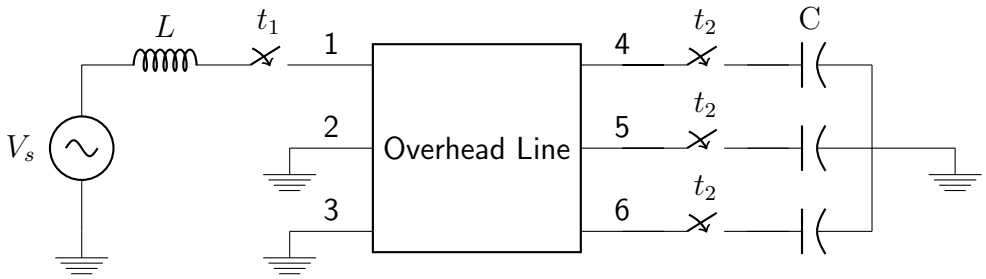


Figure 2.29: Case #4: Circuit for time-domain simulation

The simulated voltage at terminal #4 is shown in Fig. 2.30 and no discontinuity in the waveform is observed when the time-step is changed. A comparison with the results obtained with the ULM model highlights that a very accurate result is attained.

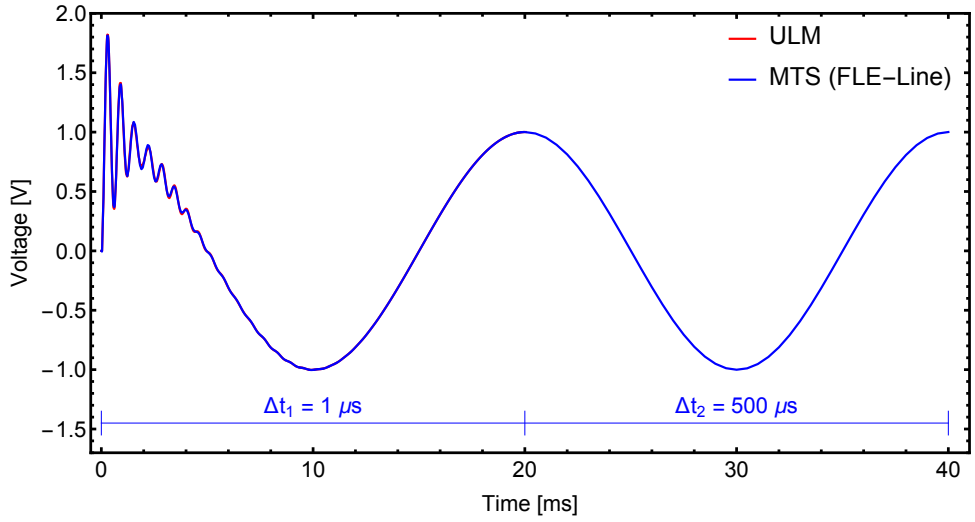


Figure 2.30: Case #4: Simulated voltage at terminal # 4

The voltage at terminal #4 can be visualized in Fig. 2.31 when the capacitor bank is inserted. Like in the previous test case, the waveform has a good match with the ULM curve and the MTS approach proves its versatility with distinguished accuracy. The voltage profile along the overall simulation is shown in Fig. 2.32.

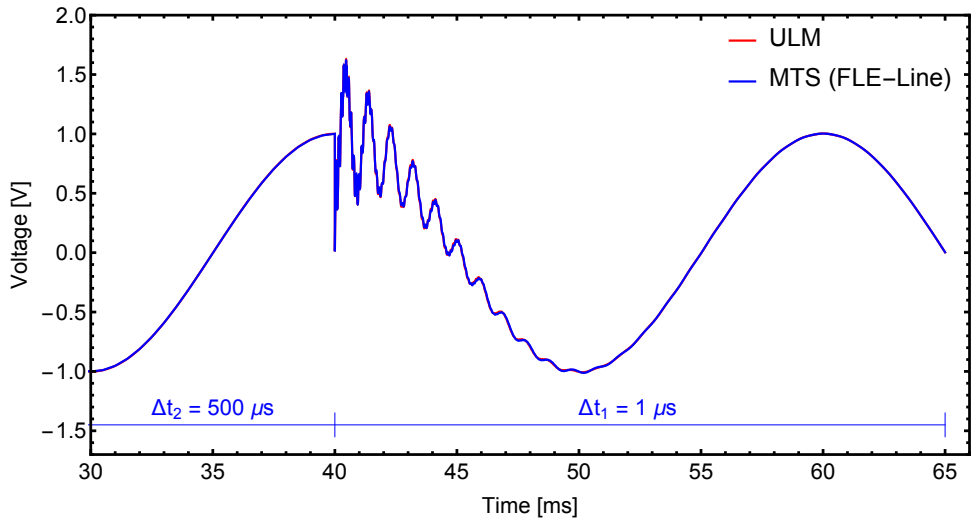


Figure 2.31: Case #4: Simulated voltage at terminal # 4

The current injection at terminal #1 is presented in Fig. 2.33. Again a very good agreement can be seen as there are no substantial mismatches between the current calculated using only a single time-step and the one using the proposed formulation.

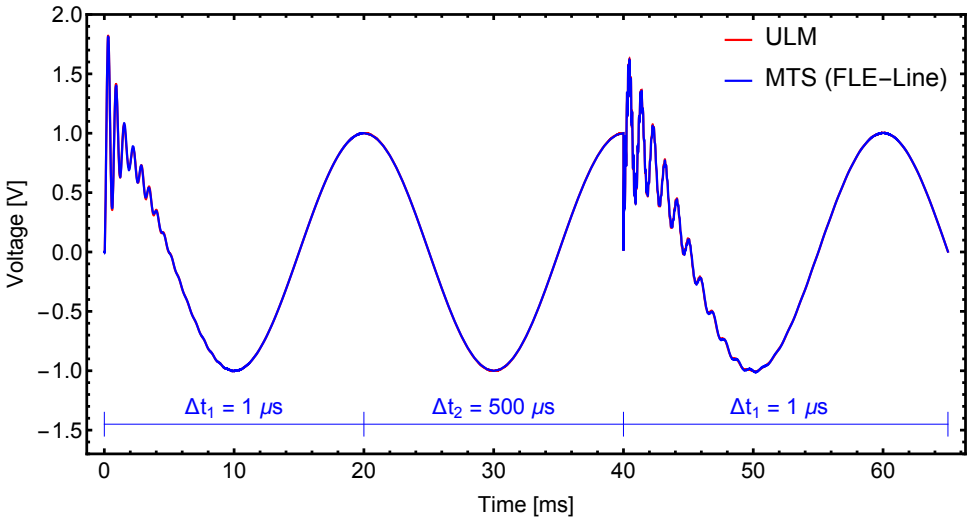


Figure 2.32: Case #4: Simulated voltage at terminal # 4

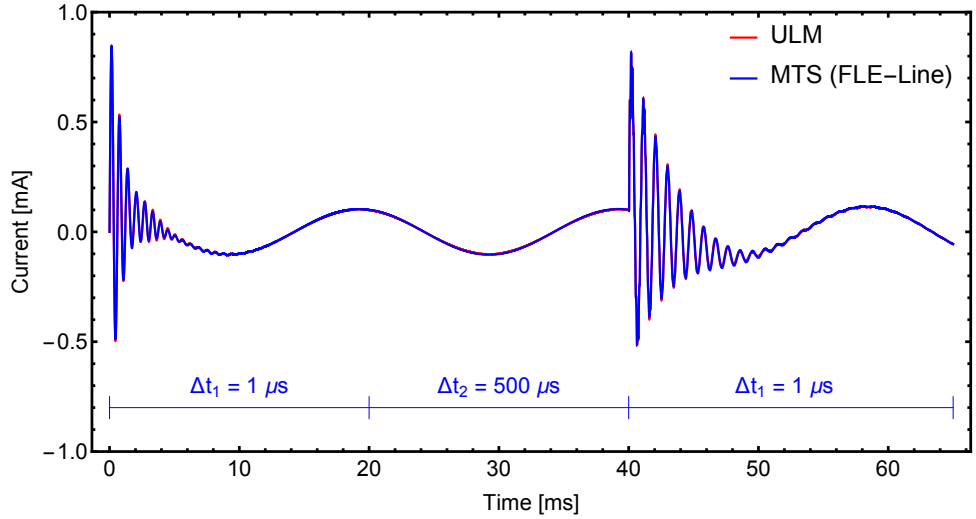


(a) Case #4: Simulated current at terminal # 1

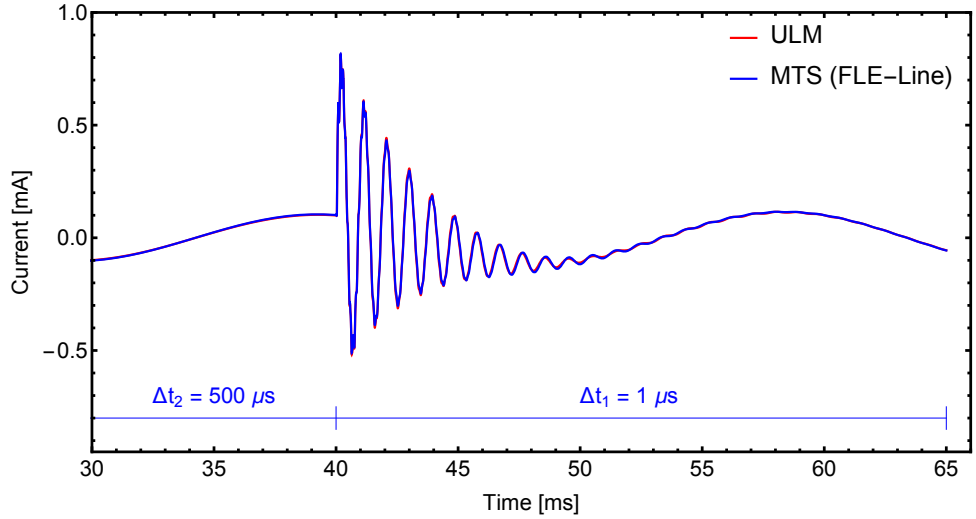


(b) ase #4: Simulated current at terminal # 1 (detail)

Figure 2.33: Case #4: Time-domain simulation

### 2.6.5 Case #5: Overhead Line (Id-Line)

This test case aims to evaluate the Idempotent Decomposition in the rational approximation of $\mathbf{Y}_n$ and demonstrate the multiscale MTS approach for simulations based on the Idempotent Line (Id–Line) model, in accordance with Section 2.3.4. For the overhead line configuration, see Fig. 2.20.

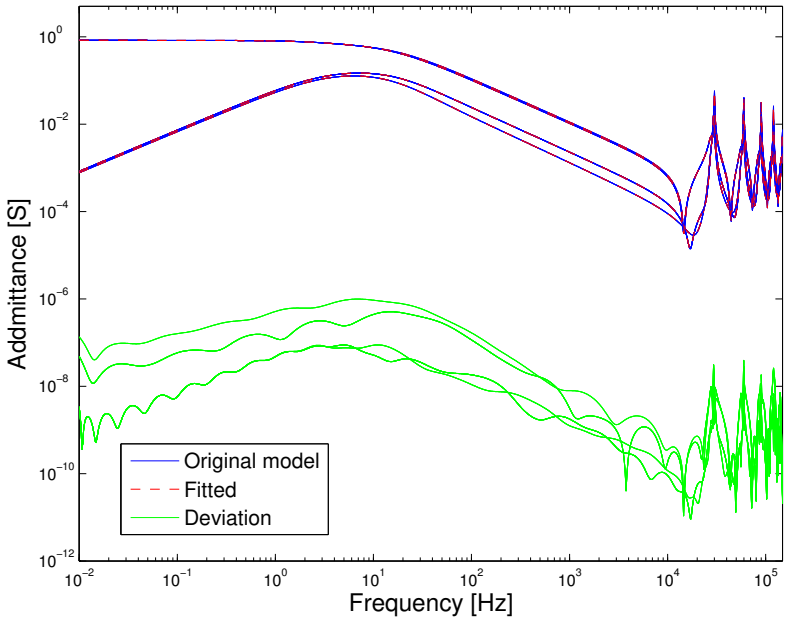


(a) Fitting of $\mathbf{M}_1$

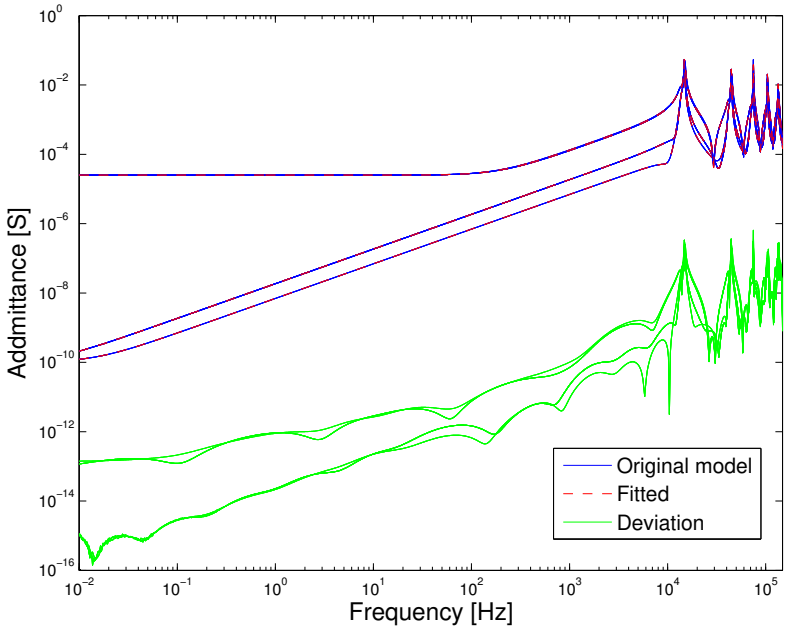


(b) Fitting of $\mathbf{M}_2$

Figure 2.34: Case #5: Fitting results (Id-Line)

In a similar fashion as adopted in [157], the grouping scheme of modes with close eigenvalues resulted in two idempotent matrices, namely, $\mathbf{M}_1$ and $\mathbf{M}_2$. The rational fitting of $\mathbf{M}_1$ and $\mathbf{M}_2$ with 60 and 50 poles, respectively, in the frequency range between 0.01 Hz – 150 kHz is shown in Fig. 2.34.

In order to evaluate this alternative multiscale line model, a single-phase energization is performed followed by a capacitor bank energization, like in the previous section. As aforementioned, the simulation starts with $\Delta t_1 = 1$ $\mu$s and after 20 ms the time-step is increased to $\Delta t_2 = 500$ $\mu$s. Next, at the same instant that the capacitor bank is energized, the time-step changes back to $\Delta t_1 = 1$ $\mu$s. For the sake of clarity, the circuit to be simulated is shown in Fig. 2.35.

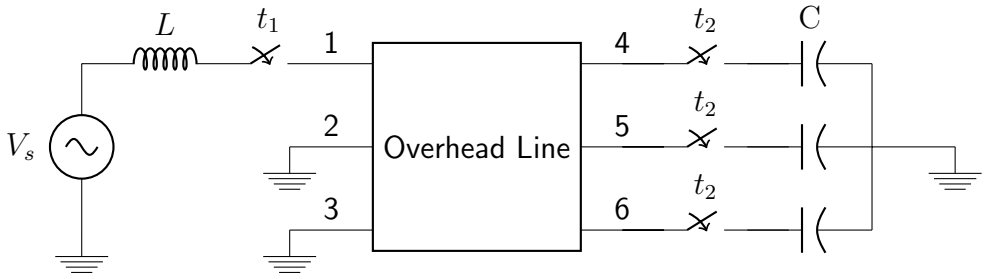


Figure 2.35: Case #5: Circuit for time-domain simulation

The simulated voltage at terminal #4 presents very accurate result in comparison with the ULM model, as demonstrated in Fig. 2.36. Like in the previous case, the waveform has a good match with the ULM curve. It could be demonstrated that MTS approach holds its versatility with a different line model maintaining a high accuracy level. The effect of the capacitor maneuver in the voltage profile at terminal #4 can be visualized in Fig. 2.37 and the overall simulation for this test case is shown in Fig. 2.38.

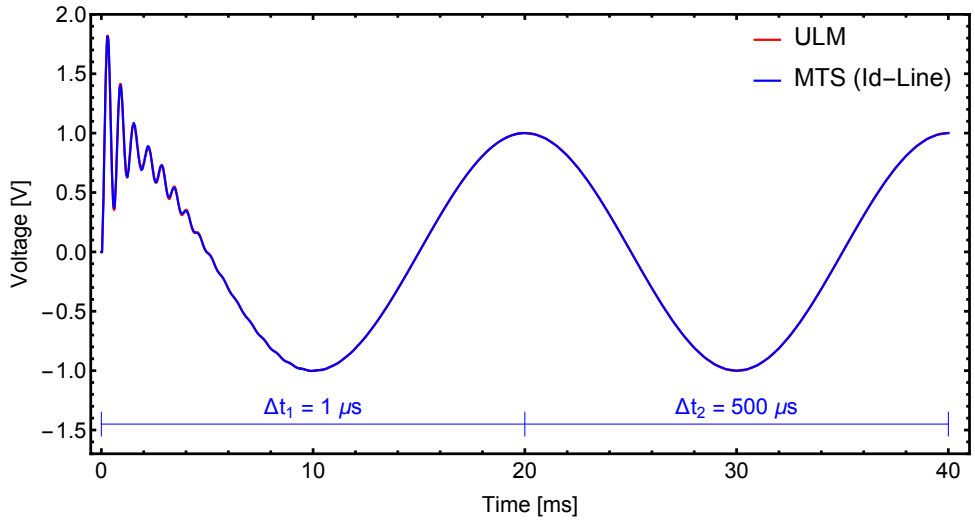


Figure 2.36: Case #5: Simulated voltage at terminal # 4

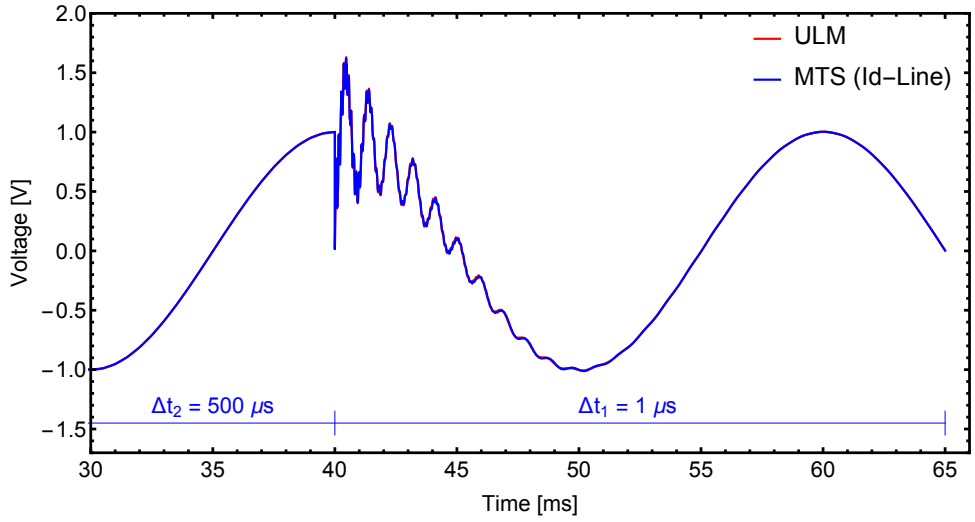


Figure 2.37: Case #5: Simulated voltage at terminal # 4

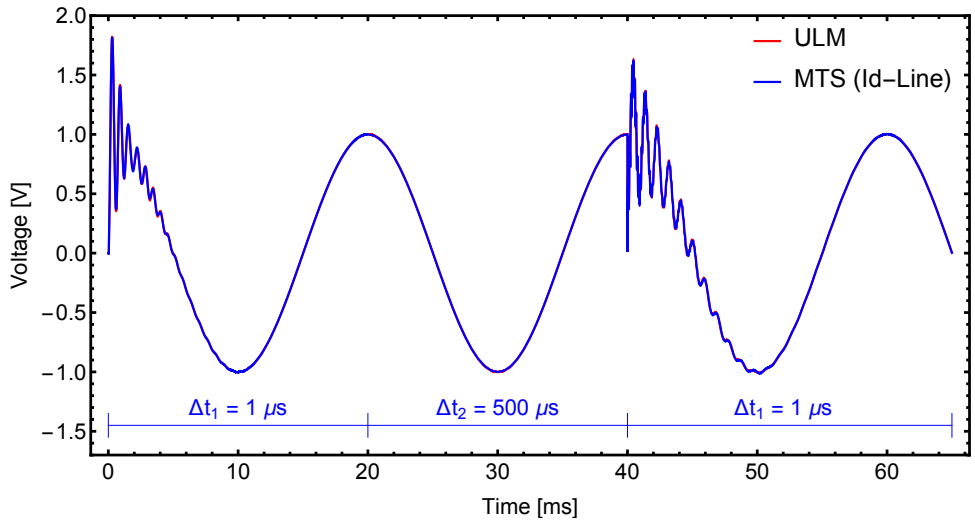


Figure 2.38: Case #5: Simulated voltage at terminal # 4

The current injection at terminal #1 is presented in Fig. 2.39. Again a very good agreement can be seen as there are no substantial mismatches between the current calculated using only a single time-step and the one using the proposed formulation.

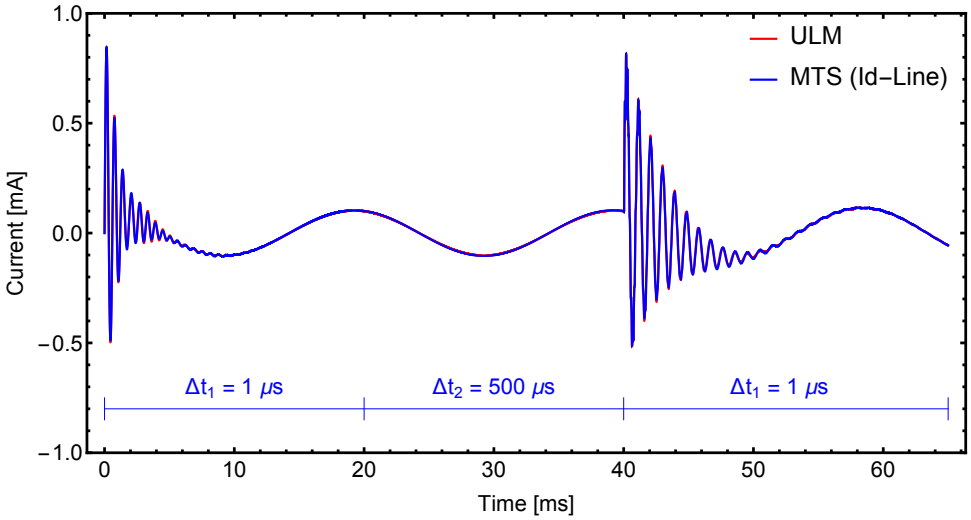


(a) Simulated current at terminal # 1

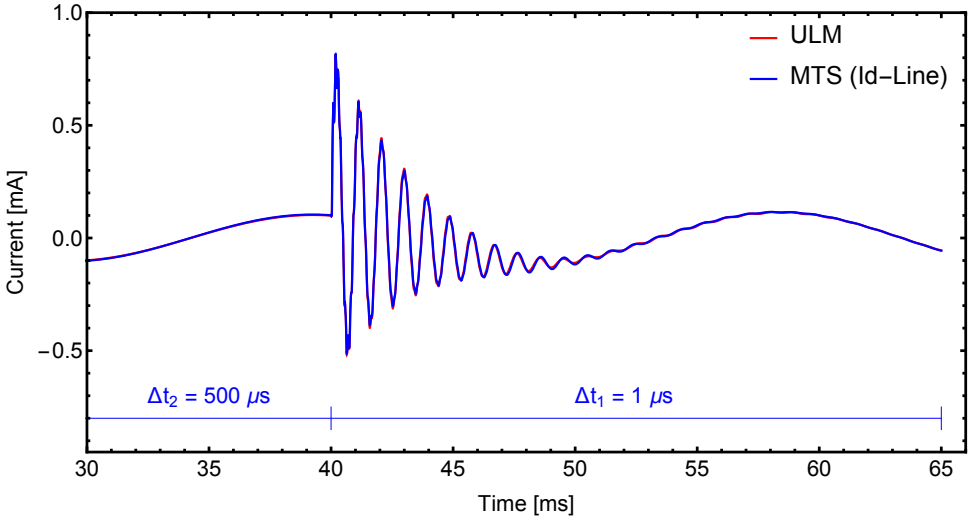


(b) Simulated current at terminal # 1 (detail)

Figure 2.39: Case #5: Time-domain simulation

### 2.6.6 Case #6: HVDC Cable (FLE-Cable)

Nowadays, there is an increasing number of applications where subsea power cables are employed. Just to name a few, connection of offshore wind farms with the main grid or interconnection between islands through HVDC converters are some examples. The advancements in the filed of voltage-source converters (VSC) renewed the interest in applications using direct current (DC) cables since it overcomes some disadvantages associated with conventional HVDC transmission systems.

In order to address such recent trend, this test case considers a single core (SC) armoured subsea cable which is the same used in a VSC–HVDC application [181]. The cable configuration is depicted in Fig. 2.40 and the main data are given in Table 2.2. In some of these applications, the cables are buried just below the seabed, with depths varying from 1 to 2 m. Here, the burial depth is 1.5 m below the seabed [182] and a length of 2.5 km is considered.

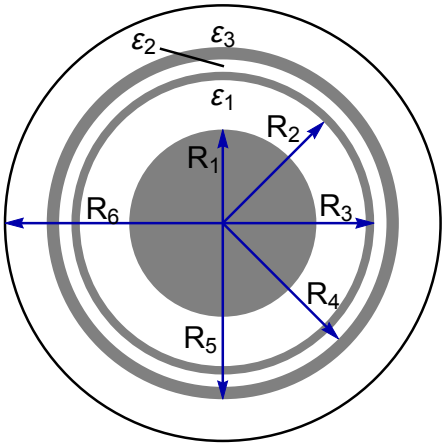


Figure 2.40: Case #6: 75 kV HVDC subsea cable configuration

Table 2.2: Case #6: Subsea cable data

| | | |
|---|---|---|
| Core conductor | $R_1 = 18.95$ mm | $\rho_c = 1.723 \times 10^{-8}\,\Omega$.m |
| First insulation layer | $R_2 = 28.95$ mm | $\varepsilon_1 = 2.5$ |
| Sheath | $R_3 = 30.65$ mm | $\rho_s = 22 \times 10^{-8}\,\Omega$.m |
| Second insulation layer | $R_4 = 33.15$ mm | $\varepsilon_2 = 2.5$ |
| Armour | $R_5 = 35.65$ mm | $\rho_a = 11 \times 10^{-8}\,\Omega$.m, $\mu_a = 90$ |
| Armour insulation | $R_6 = 44.10$ mm | $\varepsilon_3 = 2.5$ |

The evaluation is going to be restricted to the FLE model which encompass the nodal admittance matrix $\mathbf{Y}_n$ that relates the terminal voltage and current in the frequency domain. As depicted in Section 2.3.3, the methodology consists in decomposing $\mathbf{Y}_n$ into an open-circuit and short-circuit counterparts, namely $\mathbf{Y}_{oc}$ and $\mathbf{Y}_{sc}$, respectively. The calculated $\mathbf{Y}_n$ in the frequency range 0.1 Hz – 100 kHz was then converted into $\mathbf{Y}_{oc}$ and $\mathbf{Y}_{sc}$ counterparts and subjected to rational approximation

with the *Vector Fitting* routine. Fig. 2.41 shows the fitting results for $\mathbf{Y}_{oc}$, $\mathbf{Y}_{sc}$ and their eigenvalues. The passive model was achieved with 25 poles for $\mathbf{Y}_{oc}$ and 30 poles for $\mathbf{Y}_{sc}$.

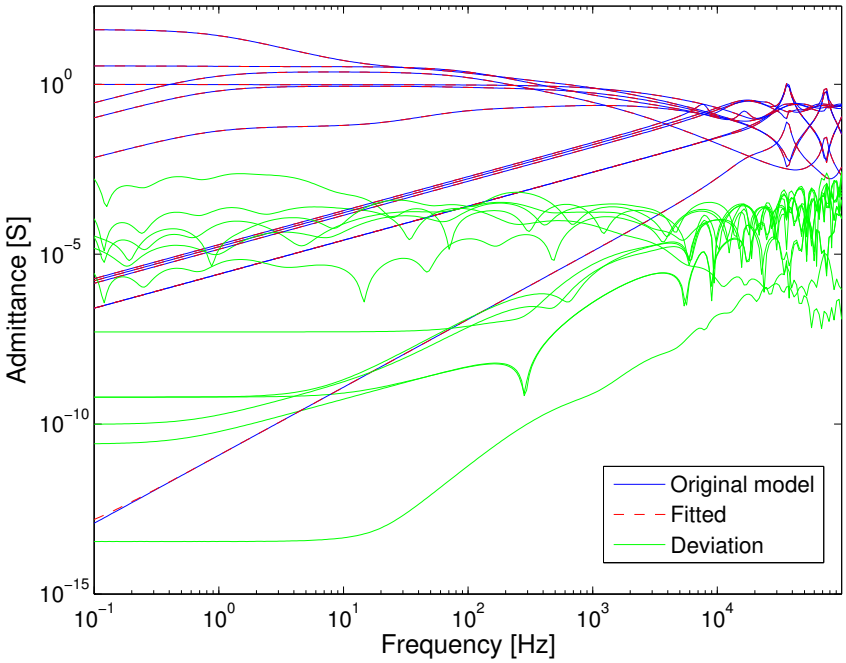


(a) Fitting of $\mathbf{Y}_{oc}$ and $\mathbf{Y}_{sc}$

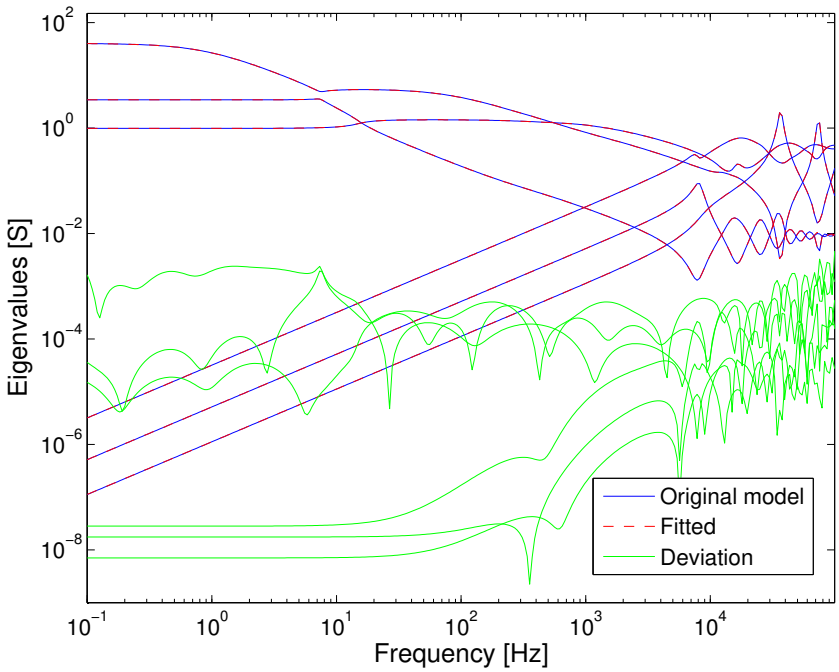


(b) Eigenvalues of $\mathbf{Y}_{oc}$ and $\mathbf{Y}_{sc}$

Figure 2.41: Case #6: Fitting results (75 kV submarine cable)

For assessment of the multiscale time-domain response, consider the scheme depicted in Fig. 2.42. A voltage source which is ramped up linearly to 1 V in 50 $\mu$s is applied in the core conductor. The sheath and armour are bolted together as this is typically the practical scenario. An initial time-step $\Delta t_1 = 0.05$ $\mu$s is assumed and later it is increased to $\Delta t_2 = 5$ $\mu$s.

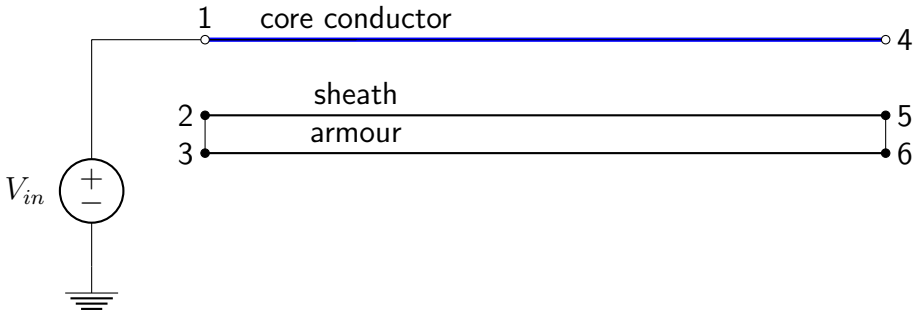


Figure 2.42: Case #6: Circuit for time-domain simulation

The simulated core and sheath voltages at the receiving end are depicted in Fig. 2.43 and the validation is done with the results obtained with the NLT [174–176] algorithm which is an analytic approach that provides the exact solution. In a similar fashion, the current in the core conductor is shown in Fig. 2.44 and again a very accurate match is attained. It can be verified that in this special case involving a subsea cable the proposed multiscale approach is able to reproduce the voltage profile even with an increase of 100 times in the time-step before the variables reached their steady-state value.

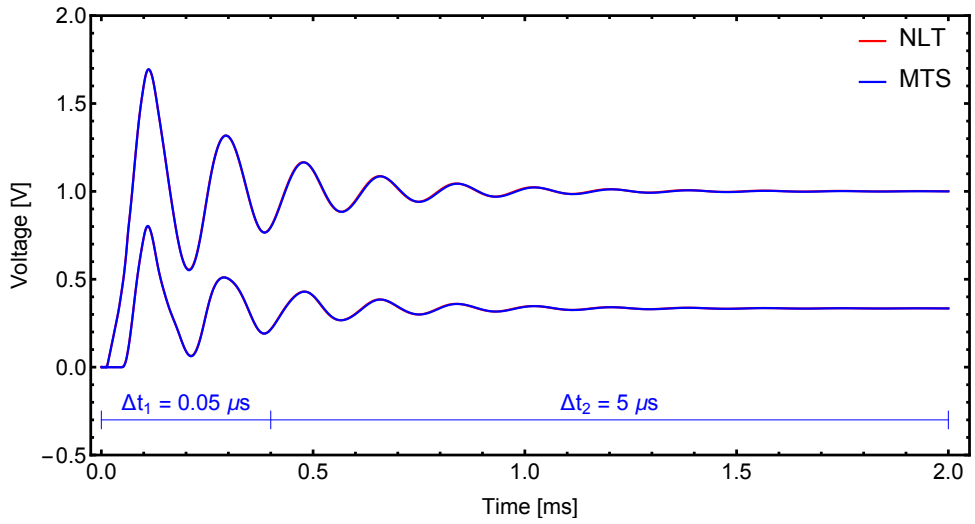


Figure 2.43: Case #6: Simulated core and sheath voltages

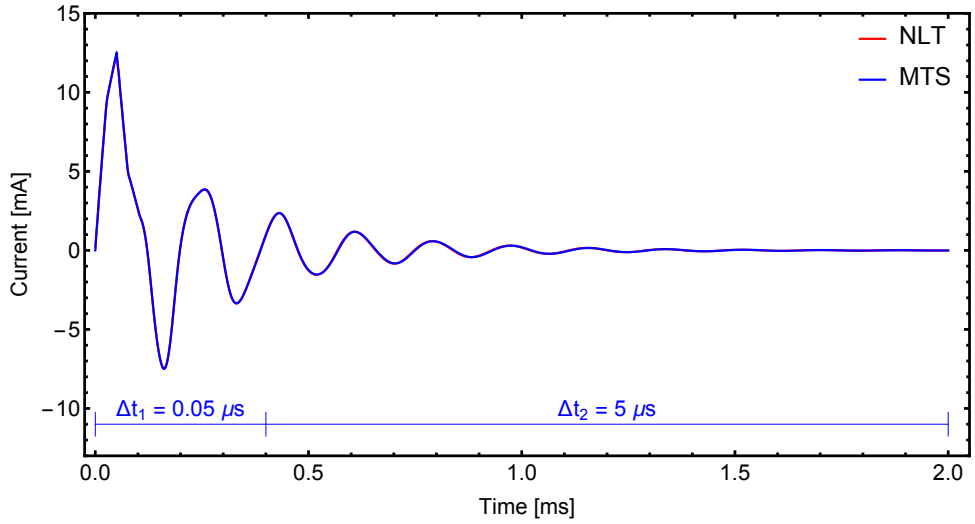


Figure 2.44: Case #6: Simulated current at terminal #1

It is noteworthy that the FLE model is best suited for situations where the time-step is larger than the line travel time [89] due to its fully-coupled nodal admittance matrix. In practice, it occurs in systems comprising both long and short lines. This feature enables to circumvent the constraint associated with the MoC-based models. Here a larger initial time-step could be used instead. However, the evaluation aimed to demonstrate how flexible and efficient the novel MTS approach can be without restriction to the new time-step.

## 2.7 Numerical Efficiency

As will be shown in Table 2.3, in the matter of computational performance, there are a number of scenarios where an admittance-based formulation, comprised of a fully-coupled admittance matrix, showed to be more efficient than the MoC-based model. Besides the possibility of adopting time-steps larger than with the MoC, mainly in evaluations with short lines [89], the drawback of ULM formulation is that it requires high computational efforts to execute the convolutions involving $\mathbf{Y}_c$ and $\mathbf{H}$ and interpolations of historic current vectors.

For validation of test cases #1 and #2, the simulation with PSCAD was considered as the reference. In test cases #3 to #5, which comprise an OHL, an user-defined algorithm was developed to implement the ULM model. Finally, a frequency-domain algorithm based on NLT was adopted for test case #6. Since the ULM code is not a compiled version, the computation time would be definitely much smaller.

The numerical efficiency of the novel MTS approach is highlighted in Table 2.3. It lists the machine time needed for each test case, comparing the standard fixed time-step computation with the proposed variable time-step algorithm. For test cases #3 to #5, the processing time required bt the ULM code and PSCAD is also reported. It can be seen that besides providing a simulation without substantial loss of accuracy, the proposed algorithm considerably reduces the computational burden.

Table 2.3: Computation time with MTS

| | PSCAD | ULM | Standard* | MTS | Reduction |
|---|---|---|---|---|---|
| Case #1 (RLC) | – | – | 0.195 s | 0.101 s | 48% |
| Case #2 (FDNE) | 30.69 s | – | 2.66 s | 1.72 s | 35% |
| Case #3 ($Y_n$–Line) | 1.65 s | 88 min | 9.90 s | 6.95 s | 30% |
| Case #4 (FLE–Line) | 1.65 s | 88 min | 11.46 s | 7.65 s | 33% |
| Case #5 (Id–Line) | 1.65 s | 88 min | 11.91 s | 8.36 s | 30% |
| Case #6 (FLE–Cable) | – | – | 15.74s | 3.13 s | 80% |

* fixed time-step

In the rational fitting of the admittance matrices of all investigated models, it was not the intention to achieve an order as low as possible to minimize the computation time. For the sake of comparison, the number of poles in the rational model of each matrix for the 132 kV overhead line (OHL) considered in test cases #3 to #5 is presented in Table 2.4. Even though the admittance-based models required more poles in the rational approximation than ULM, the timing results demonstrate substantial reduction in comparison with the MoC-based simulation with ULM. When applying the novel MTS approach, the overall computation time is significantly reduced. It is worth mentioning that a concrete quantitative prediction of timings cannot be realistic due to the evaluated system and the observation time.

Table 2.4: OHL fitting

| ULM | | $Y_n$ | FLE | | Id | |
|---|---|---|---|---|---|---|
| H | $Y_c$ | - | $Y_{oc}$ | $Y_{sc}$ | $M_1$ | $M_2$ |
| 30 | 10 | 88 | 50 | 50 | 60 | 50 |

Valuable information taken from Table 2.3 is the computation time achieved with Id–Line. Even with a higher number of poles, it can be seen that the overall time is slightly higher if compared with FLE–Line and $Y_n$–Line simulations. This evidence encourages further investigations on Idempotent Decomposition as an alternative technique to the direct fitting of $\mathbf{Y}_n$ due to the inherent inaccurate observability of small eigenvalues in the low frequency range.

For the sake of comparison, Fig. 2.45 presents the simulated voltage considering all three distinct formulations employed in the modeling of the OHL. The error of each formulation is shown in Fig. 2.46 from the results obtained using the ULM.

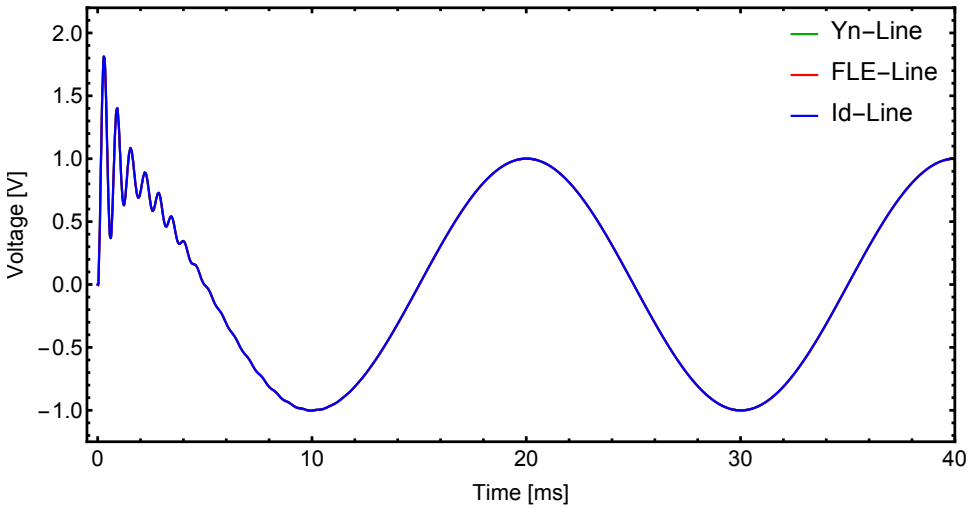


(a) Transmission line energization

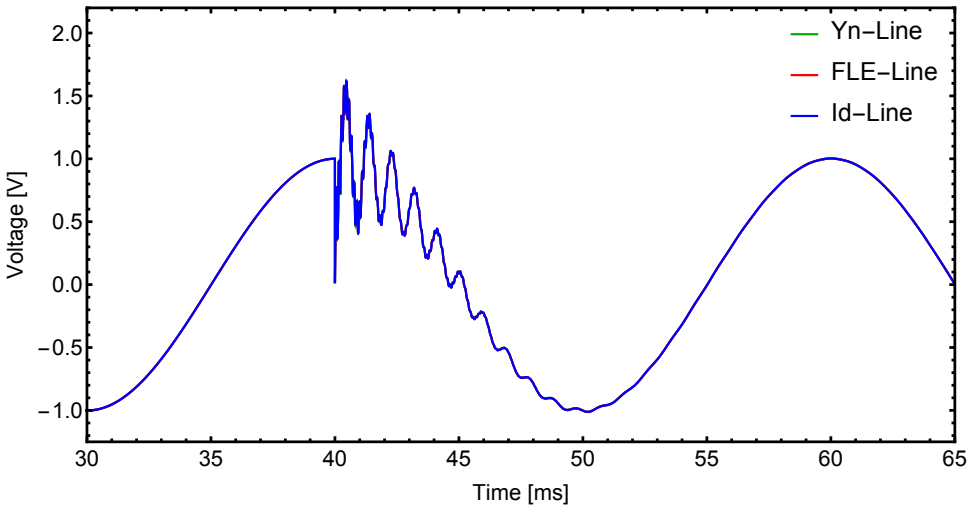


(b) Capaccitor bank energization

Figure 2.45: Comparison of simulated voltage at terminal #4 (OHL)

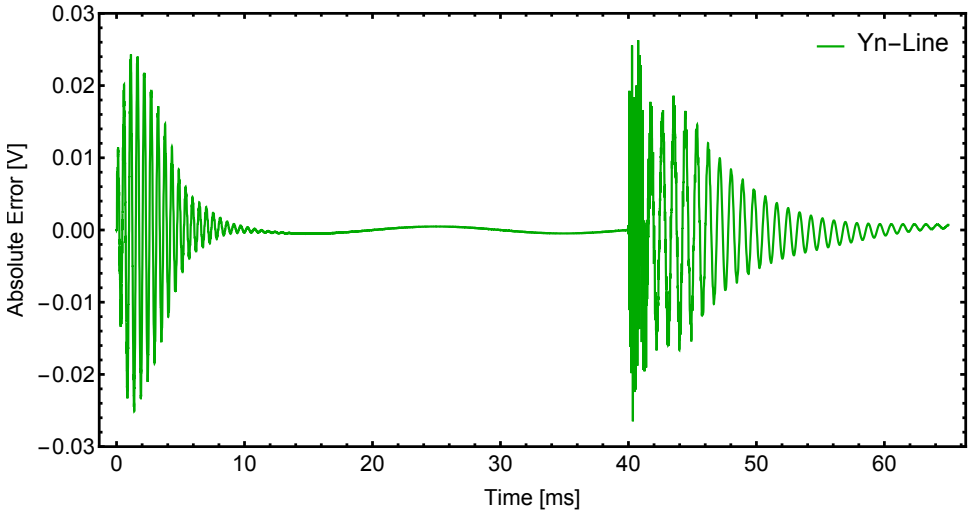


(a) Simulated voltage at terminal # 4

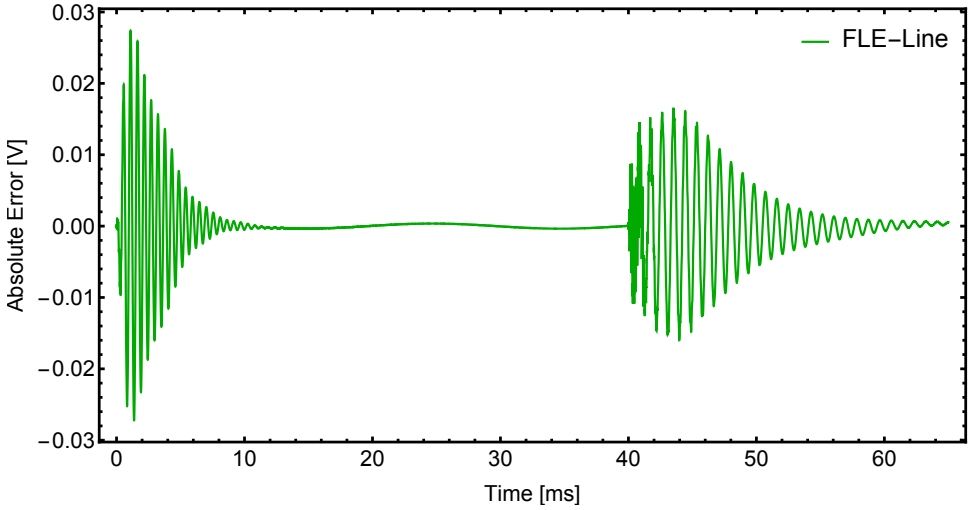


(b) Simulated voltage at terminal # 4

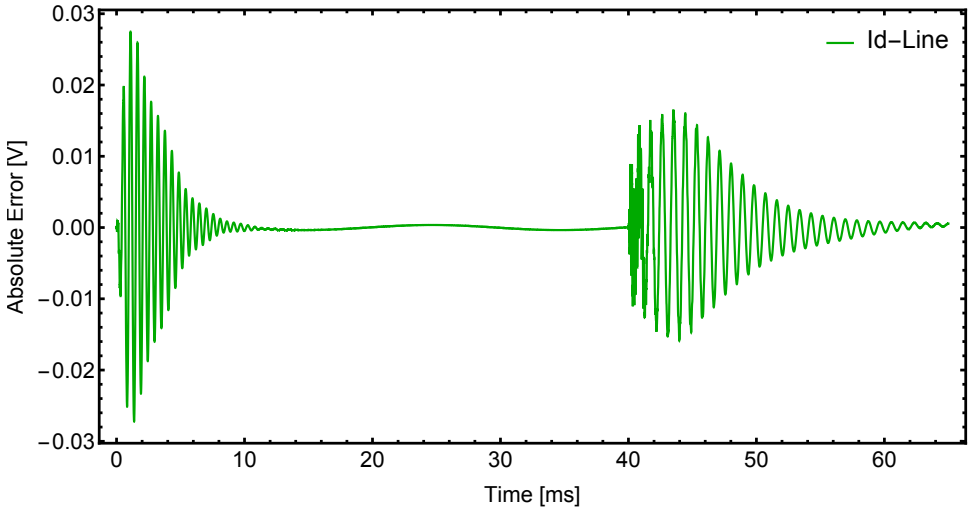


(c) Simulated voltage at terminal # 4

Figure 2.46: MTS approach: deviation from ULM simulation

## 2.8 Discussion

The application of the novel Multiple Time-Step (MTS) approach for time-domain simulation of frequency dependent line models and network equivalents was evaluated. Test cases comprised lumped elements, a frequency dependent network equivalent (FDNE), an overhead line (OHL) and a single-core armoured subsea cable were considered.

The FDNE modeling demonstrated the accuracy and usefulness of frequency dependent equivalents for EMT evaluations. Time-domain results achieved with the reduced network matched precisely with the detailed simulation with PSCAD comprising the complete system represented with a full phase-domain line model.

Special attention was directed to the OHL modeling with computations performed through its nodal admittance matrix and two distinct decompositions, namely: the Folded Line Equivalent (FLE) and the Idempotent Decomposition. In the modeling of the subsea cable, just the FLE formulation was applied. The test cases comprised of OHL closely matched the results from the ULM which considered a fitting of $\mathbf{Y}_c$ and $\mathbf{H}$ up to 1 MHz. The results indicate that besides keeping the accuracy of fixed time-step simulations, the new Id–Line model provided similar numerical performance in comparison with $Y_n$–Line and FLE–Line models. In the matter of accuracy, the same conclusion holds for the subsea cable simulation in which the frequency-domain NLT algorithm was adopted for validation.

As a contribution to the renewed interest on the Idempotent Decomposition, the viability of grouping Idempotent matrices with similar eigenvalues was evaluated with success. Additional investigations are recommended to be done with Idempotent Decomposition as an alternative technique to the direct fitting of frequency dependent lines and network equivalents.

The greatest feature of admittance-based formulations addressed in this work is that a fully-coupled admittance matrix does not require a topological modifications on the network matrix if the time-step is larger than the slowest modal traveling time. It can be applied in a straightforward way since it retains the same structure used in EMTP-like programs. The proposed multiscale formulation allowed a more efficient realization of rational approximations of frequency dependent models as the computational burden is considerably reduced without a significant loss of accuracy. The inclusion of a single intermediate step is enough to allow the usage of multiple time-steps along the simulation run.

Passivity enforcement is the major bottleneck in the field of rational macromodeling once unstable simulations can be verified, even though the elements of a given matrix $\mathbf{Y}_n$ have been fitted using only stable poles. The requirement of a passive model entails a post-processing scheme based on residue perturbation

to ensure passivity [183]. Even though the elements of $\mathbf{Y}_n$ were accurately fitted, the small eigenvalues can be corrupted in the lower frequency range [89], and the direct fitting of $\mathbf{Y}_n$ fails in this requirement. For this reason, the lowest frequency 1 Hz was chosen in the rational approximation of the $Y_n$–Line. Fortunately, the FLE circumvents the problem that occurs with the direct fitting of the nodal admittance matrix demonstrating a suitable alternative for retaining the accuracy of the eigenvalues of $\mathbf{Y}_n$. Even though a passive model via the FLE was reached for the OHL, it was not the case for the system of single-core cables. An accurate fitting for $\mathbf{Y}_{oc}$ and $\mathbf{Y}_{sc}$ was achieved without a good observability of all eigenvalues. Hence, a single-core armoured subsea cable was employed.

It is worth mentioning some issues regarding with the modeling based on the Method of Characteristics (MoC) and the ones associated with the nodal admittance matrix. The former can present unstable time-domain simulations [161, 162] while the latter can face the appearance of Gibbs phenomena [121]. In the case of MoC-based approach, the major drawback appears when short lines are evaluated with long lines, thus requiring very small time-steps. Contrarily, admittance-based formulations overcome such constraint allowing one to adopt time-steps greater than the travel time. To face this challenge, the FLE model is recommended since it can take into account the frequency dependent effects of the line as opposed to the common practice to employ $\pi$-sections. Time-domain simulations based on real or instantaneous variables have an inherent limitation regarding the maximum time-step size due to the sampling rate of the fundamental frequency. Thus, there is a trade-off between precision and computational performance.

In order to generalize the MTS approach, an extension of this formulation is presented in Chapter 3 aiming to cope with time-steps in the order of milliseconds, namely, the Frequency-Adaptive Simulation of Transients (FAST) concept. This multiscale approach enables the integrated simulation of EMT and TS with an inherent feature to process either instantaneous or phasor-based variables and it allows the integration of synchronous or induction machine models. Alternatively to the averaging method [184], FAST can be used to bridge evaluations with power electronic converters.

In Chapter 4, a new Multiple Companion Networks (MCN) technique is proposed to improve the numerical efficiency in the rational modeling of frequency dependent transmission lines. Resorting to latency exploitation, different time-steps are adopted for the poles associated with fast and slow dynamics. This new formulation seeks to overcome the high computational burden in the commonly fixed time-step modeling based on real variables.

# Chapter 3

# Modeling Using Complex Variables

In the previous chapter, the Multiple Time-Step (MTS) approach was found to be a feasible alternative for time-domain simulations of frequency dependent line models and network equivalents in EMTP-like programs. Nonetheless, its application for larger time-steps, for instance, greater than 1 ms, still merits further research work related on how to circumvent such constraint.

In the present chapter, the Frequency-Adaptive Simulation of Transients (FAST) concept is addressed regarding admittance-based models. FAST can be understood as a generalization of the dynamic phasors concept and provides the advantage of tracking either instantaneous or envelope waveforms. Furthermore, it allows multiple changes in time-step with smooth transitions without numerical oscillations or discontinuities in the waveform regardless of the change in time-step.

The same test cases considered in the previous chapter will be adopted here. Time-domain responses based on the full phase-domain Universal Line Model (ULM) will be used to verify the accuracy of the test cases comprising an overhead line (OHL) and frequency dependent network equivalent (FDNE). For the HVDC subsea cable, an alternative simulation method using a frequency-domain algorithm based on the Numerical Laplace Transform (NLT) will be considered. For this simulation NLT was used because there is no accurate model for a subsea cable in EMTP-type of software.

Results indicate that the modeling using either real or complex variables attain the same accuracy within the same time scale. When encompassing large time-steps in steady state analysis, e.g., 10 ms, the FAST approach should be used instead as it can handle phasor-based representation.

## 3.1 Introduction

The research on new techniques to incorporate the slow frequency transients, typically in the range of a few or a fraction of hertz into electromagnetic transients (EMT) evaluations, revealed some alternatives to bridge EMT and transient stability (TS) analysis. Stated as hybrid simulators [40], they enable one to deal with different time frames in the same simulation run alternating electromagnetic and electromechanical solvers in order to provide a coupled solution [39, 41, 42]. The former processes instantaneous variables with time-steps in the order of microseconds while the latter deals with phasors using time-steps in the order of milliseconds

The unification of electromagnetic and electromechanical modeling into a single formulation became possible with the advent of the dynamic or time-varying phasors concept reported in the groundwork developed in [2]. With the aid of analytic signals or complex variables, commonly used in communication theory [185], and the Hilbert transform [186] it became possible to process and trace either the envelope or the instantaneous time-domain waveforms of a given variable. The first application of dynamic phasors in power systems considered a transmission line with distributed parameters and a detailed synchronous machine model was presented in [3]. Named as shifted frequency analysis (SFA), this formulation was also applied in the modeling of induction motors and power transformers [4–7]. As highlighted in [13], the SFA method is efficient for power system slow dynamic studies and also capable of simulating fast transients. Nevertheless, the simulation of either slow or fast transients should be determined prior to the simulation start. Thus, the method presents an inherent limitation for simulating both phenomenon within the same simulation run

The so-called Frequency-Adaptive Simulation of Transients (FAST) concept was latter introduced to allow the change in the time-step applied in the modeling of transformers, synchronous machines and transmission lines [8–14]. Hence, one can use small time-steps when fast transients are involved and larger time-steps when low frequency transients are to be observed

In the present Chapter, the Multiple Time-Step (MTS) formulation will be extended in order to enhance the available admittance-based frequency dependent models for overhead lines, cables and network equivalents using FAST. Resorting to the feature of a fully-coupled admittance matrix, the multiscale approach based on FAST will be implemented in a straightforward way, aiming to retain the same structure used in EMTP-type programs

## 3.2 Dynamic Phasors

The complex transformation by means of Hilbert transforms has been properly established in a way to find an unique analytic function whose real part is the same as the original one. This groundwork is sufficient to established a novel reference frame to gather both electromagnetic and electromechanical modeling with the aid of dynamic phasors.

### 3.2.1 Analytic Signals

The dynamic phasor concept rely on the application of analytic or complex signals $\mathcal{A}[\cdot]$ as adopted in frequency modulation for radio transmission [187]. Basically, it express a real signal $s(t)$ in a complex form where the imaginary part $\sigma(t)$ is obtained by the Hilbert transform of the original signal, as shown in (3.1).

$$\mathcal{A}[s(t)] = \underline{s}(t) = s(t) + j\mathcal{H}[s(t)] = s(t) + j\sigma(t) \tag{3.1}$$

Real signals typically have its spectrum centered at the fundamental frequency $f_s$ and, as a consequence of this transformation, analytical signals maintain only its positive content with the magnitude multiplied by two, see Fig. 3.1.

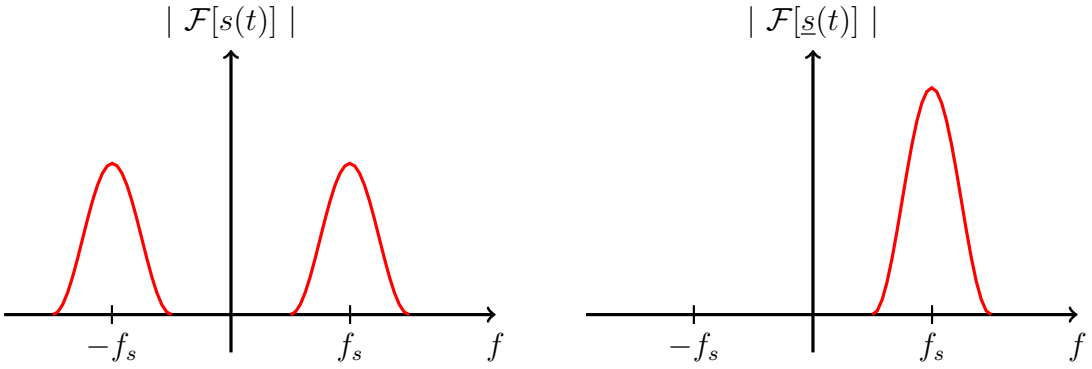


(a) Real signal $s(t)$ (b) Analytic signal $\underline{s}(t)$

Figure 3.1: Fourier spectra

### 3.2.2 Frequency Shifting

Multiplying the analytic signal by $e^{-j\omega_s t}$ degenerates the so-called dynamic phasor $\mathcal{D}[\cdot]$ and the related frequency spectra is then shifted to the origin, as illustrated in Fig. 3.2. In practice, this shifting approach converts a bandpass signal into a low-pass one that corresponds to the complex envelope of the real signal $s(t)$.

$$\mathcal{D}[\underline{s}(t)] = \underline{s}(t)\ e^{-j\omega_s t} \tag{3.2}$$

The key advantage of such representation lies in the requirement of much less samples to accurately represent dynamic phasors in comparison with instantaneous signals. This process, stated as the Shifted Frequency Analysis (SFA), filters out the power frequency and only deviations from this frequency are observed. Hence, in steady-state and electromechanical analysis, where the signals are close to the fundamental frequency, the application of dynamic phasors allows one to use large time-steps without sacrificing accuracy.

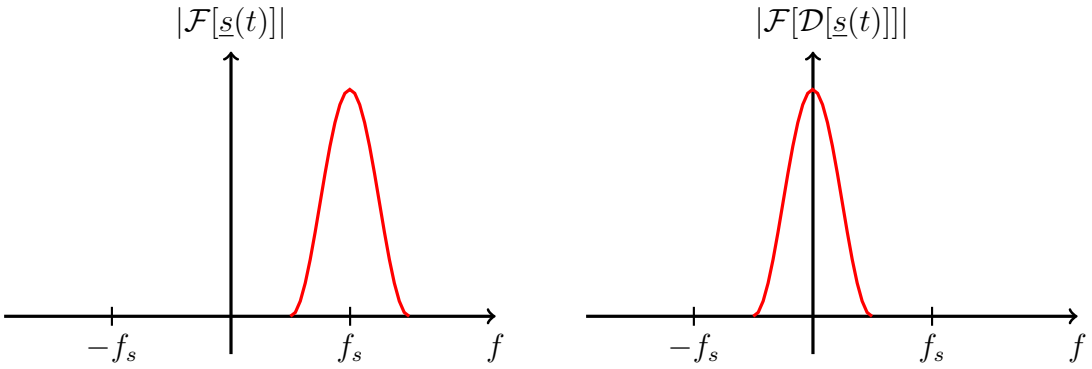


(a) Analytic signal $\underline{s}(t)$ (b) Dynamic phasor $\mathcal{D}\underline{s}(t)$

Figure 3.2: Fourier spectra

### 3.2.3 On the Analytic Signals

A kind of graph employed in audio engineering is used to plot a three-dimensional version of analytic functions. Fig. 3.3 shows the analytic signal curves when both parts of the function are plotted against time. The projections show the real and the imaginary parts as functions of time [188]. The rear projection plane shows the analytic function plotted on the complex plane. Such curve is referred as Heyser spirals or Heyser corkscrew used initially by Richard Heyser to analyze loudspeaker performance [189].

Consider the real function $\cos\omega t$. The complex extension of $\cos\omega t$, i.e, with its Hilbert transformed counterpart, is given by

$$e^{j\omega t} = \cos\omega t + j\sin\omega t \tag{3.3}$$

The magnitude of $\cos\omega t$ varies from -1 to +1 and at times it is zero. However, one may feel that its envelope is constant and this intuition is satisfied defining the envelope to be the magnitude of the full complex function $e^{j\omega t}$. In a Heyser corkscrew, this magnitude appears as the radial distance of the central figure to the time axis and from Fig. 3.3 it is clear the the envelope of $\cos\omega t$ is always 1.

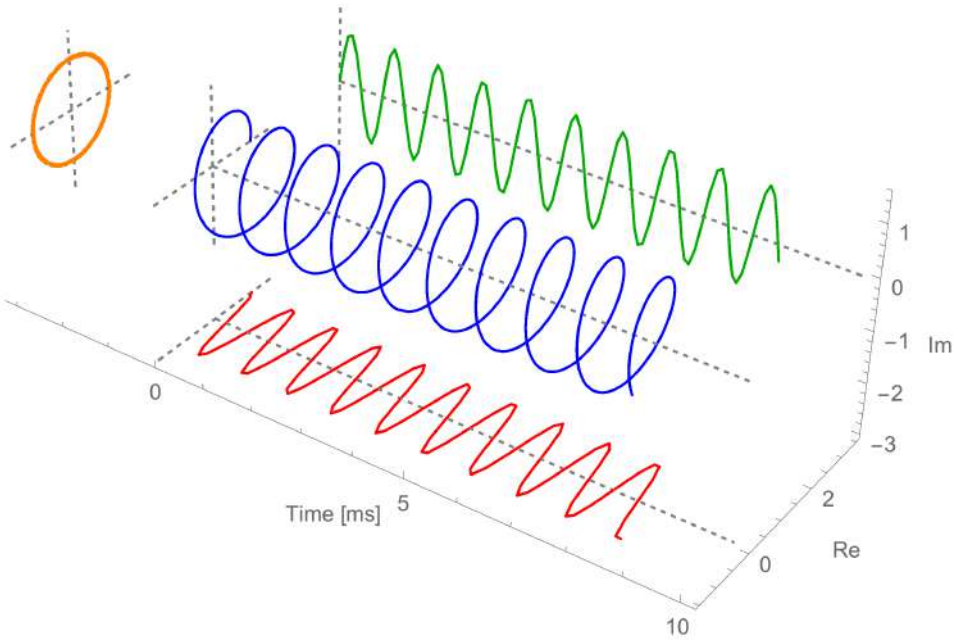


Figure 3.3: Analytic signal $\mathcal{A}[\cdot]$

It is worth emphasizing that the connection between the real and imaginary parts is the so-called Hilbert transform. The connection between the real part and the whole, i.e., the analytic function, is best illustrated by examining the relation

$$\cos \omega t = \frac{e^{j\omega t} + e^{-j\omega t}}{2} \tag{3.4}$$

which is an inversion of the standard definition $e^{j\omega t} = \cos \omega t + j \sin \omega t$. As aforementioned, to get the complex extension of $\cos \omega t$ one should express it in its exponential form, suppress the negative frequency term $e^{-j\omega t}$ and double the frequency part. After some basic manipulation, it can be seen that $\cos \omega t = \mathrm{Re}[e^{j\omega t}]$.

## 3.3 Lumped Elements

This section aims to establish the discretization of differential equations to describe the behavior of lumped elements by means of analytic signals. Companion networks in the form of Norton-type equivalents are intended to perform time-domain simulations.

### 3.3.1 Inductor

Expressing the voltage and current variables as analytic signals, i.e, in the complex form, the behavior of an inductor L is described through the following differential equation:

$$\frac{d\underline{i}_L(t)}{dt} = \frac{\underline{v}_L(t)}{L} \tag{3.5}$$

Inserting the definition of shifted analytic signals (3.2) into (3.5)

$$\frac{d(\mathcal{D}[\underline{i}_L(t)]e^{j\omega_s t})}{dt} = \frac{\underline{v}_L(t)}{L} \tag{3.6}$$

and performing the derivative term, yield

$$\begin{aligned}\frac{d\mathcal{D}[\underline{i}_L(t)]}{dt} =& e^{-j\omega_s t}\left(-j\omega_s \underline{i}_L(t) + \frac{\underline{v}_L(t)}{L}\right) \\ =& -j\omega_s \mathcal{D}[\underline{i}_L(t)] + \frac{\mathcal{D}[\underline{v}_L(t)]}{L}\end{aligned} \tag{3.7}$$

Applying the trapezoidal integration rule to (3.7) gives

$$\begin{aligned}\mathcal{D}[\underline{i}_L(t)] - \mathcal{D}[\underline{i}_L(t-\Delta t)] =& -j\omega_s \frac{\Delta t}{2}(\mathcal{D}[\underline{i}_L(t)] + \mathcal{D}[\underline{i}_L(t-\Delta t)]) \\ &+ \frac{\Delta t}{2L}(\mathcal{D}[\underline{v}_L(t)] + \mathcal{D}[\underline{v}_L(t-\Delta t)])\end{aligned} \tag{3.8}$$

Backsubstitution into the analytic form notation, gives

$$\begin{aligned}\underline{i}_L(t) - e^{j\omega_s \Delta t}\underline{i}_L(t-\Delta t) =& -j\omega_s \frac{\Delta t}{2}(\underline{i}_L(t) + e^{j\omega_s \Delta t}\underline{i}_L(t-\Delta t)) \\ &+ \frac{\Delta t}{2L}(\underline{v}_L(t) + e^{j\omega_s \Delta t}\underline{v}_L(t-\Delta t))\end{aligned} \tag{3.9}$$

Collecting like terms, yields

$$\underline{i}_L(t) = \underline{G}_L\ \underline{v}_L(t) + e^{j\omega_s \Delta t}\ [\underline{\mu}\ \underline{i}_L(t-\Delta t) + \underline{G}_L\ \underline{v}_L(t-\Delta t)] \tag{3.10}$$

and casting in the form of a companion network, the resulting discrete model can

be expressed by

$$\underline{i}_L(t) = \underline{G}_L \ \underline{v}_L(t) + \underline{h}_L(t) \tag{3.11}$$

where

$$\begin{aligned} \underline{G}_L &= \frac{\Delta t/2L}{1 + j\omega_s \Delta t/2} \qquad \underline{\mu} = \frac{1 - j\omega_s \Delta t/2}{1 + j\omega_s \Delta t/2} \\ \underline{h}_L(t) &= e^{j\omega_s \Delta t} \ [\underline{\mu} \ \underline{i}_L(t - \Delta t) + \underline{G}_L \ \underline{v}_L(t - \Delta t)] \end{aligned} \tag{3.12}$$

It is noteworthy that the obtained model retains the common structure of EMTP-like programs [19] when handling only with real values, i.e., in the case where the frequency shifting equals $\omega_s = 0$ rad/s.

### 3.3.2 Capacitor

On the basis of analytic signals representation, the behavior of a capacitor C is described through the following differential equation:

$$\frac{d\underline{v}_C(t)}{dt} = \frac{\underline{i}_C(t)}{C} \tag{3.13}$$

Inserting the definition of shifted analytic signals (3.2) into (3.13)

$$\frac{d(\mathcal{D}[\underline{v}_C(t)]e^{j\omega_s t})}{dt} = \frac{\underline{i}_C(t)}{C} \tag{3.14}$$

and performing the derivative term, yields

$$\begin{aligned} \frac{d\mathcal{D}[\underline{v}_C(t)]}{dt} =& e^{-j\omega_s t} \left( -j\omega_s \underline{v}_C(t) + \frac{\underline{i}_C(t)}{C} \right) \\ =& - j\omega_s \mathcal{D}[\underline{v}_C(t)] + \frac{\mathcal{D}[\underline{i}_C(t)]}{C} \end{aligned} \tag{3.15}$$

Applying the trapezoidal integration rule to (3.15) gives

$$\begin{aligned} \mathcal{D}[\underline{v}_C(t)] - \mathcal{D}[\underline{v}_C(t - \Delta t)] =& - j\omega_s \frac{\Delta t}{2} (\mathcal{D}[\underline{v}_C(t)] + \mathcal{D}[\underline{v}_C(t - \Delta t)]) \\ &+ \frac{\Delta t}{2C} (\mathcal{D}[\underline{i}_C(t)] + \mathcal{D}[\underline{i}_C(t - \Delta t)]) \end{aligned} \tag{3.16}$$

Backsubstitution into the analytic form notation, gives

$$\begin{aligned} \underline{v}_C(t) - e^{j\omega_s \Delta t} \underline{v}_C(t - \Delta t) =& - j\omega_s \frac{\Delta t}{2} (\underline{v}_C(t) + e^{j\omega_s \Delta t} \underline{v}_C(t - \Delta t)) \\ &+ \frac{\Delta t}{2C} (\underline{i}_C(t) + e^{j\omega_s \Delta t} \underline{i}_C(t - \Delta t)) \end{aligned} \tag{3.17}$$

Collecting like terms, yields

$$\underline{i}_C(t) = \underline{G}_C \; \underline{v}_C(t) - e^{j\omega_s \Delta t} \; [\underline{i}_C(t - \Delta t) + \underline{G}_C \; \underline{v}_C(t - \Delta t)] \tag{3.18}$$

and casting in the form of a companion network, the resulting discrete model can expressed by

$$\underline{i}_C(t) = \underline{G}_C \; \underline{v}_C(t) - \underline{h}_C(t) \tag{3.19}$$

where

$$\begin{aligned} \underline{G}_C &= \frac{1 + j\omega_s \Delta t/2}{\Delta t/2C} \\ \underline{h}_C(t) &= e^{j\omega_s \Delta t} \; [\underline{i}_C(t - \Delta t) + \underline{G}_C \; \underline{v}_C(t - \Delta t)] \end{aligned} \tag{3.20}$$

It is noteworthy that the obtained model retains the common structure of EMTP-like programs [19] when handling only with real values, i.e., in the case where the frequency shifting equals $\omega_s = 0$ rad/s.

## 3.4 Rational Models

Frequency dependent models usually are described by rational approximations of a given frequency response, commonly in the form of an admittance matrix relating terminal voltages and currents. In order to perform a time-domain realization of a pole-residue or state-space model, e.g., in the form of (3.21), one can resort either to trapezoidal integration [90, 168] or recursive convolution [139] approaches

$$\mathbf{Y}(s) \approx \sum_{m=1}^{N} \frac{\mathbf{R}_m}{s - p_m} + \mathbf{D} \tag{3.21}$$

where $p_m$ is a set of common poles, either real or complex conjugate, $\mathbf{R}_m$ is the residue matrix and $\mathbf{D}$ is a real-based matrix associated with the behavior of $\mathbf{Y}(s)$ at an infinite frequency.

This section intends to extend the existing formulae in order to process analytic signals, which corresponds with the proposal of this thesis.

### 3.4.1 Trapezoidal Integration Rule

Assume a first order pole-residue model in the form of (3.21). In the time-domain, it can be rewritten as

$$\frac{d\underline{x}(t)}{dt} = p\,\underline{x}(t) + r\,\underline{v}(t) \tag{3.22}$$

Resorting to the definition of dynamic phasors, i.e., insertion of (3.2) in (3.22)

$$\frac{d[\mathcal{D}[\underline{x}(t)]\,e^{j\omega_s t}]}{dt} = p\,\underline{x}(t) + r\,\underline{v}(t) \tag{3.23}$$

Evaluating the derivative term gives

$$j\omega_s\,\mathcal{D}[\underline{x}(t)]\,e^{j\omega_s t} + e^{j\omega_s t}\,\frac{d\mathcal{D}[\underline{x}(t)]}{dt} = p\,\underline{x}(t) + r\,\underline{v}(t) \tag{3.24}$$

Collecting like terms yields

$$\begin{aligned} \frac{d\mathcal{D}[\underline{x}(t)]}{dt} &= e^{-j\omega_s t}\,[(p - j\omega)\,\underline{x}(t) + r\,\underline{v}(t)] \\ &= (p - j\omega)\,\mathcal{D}[\underline{x}(t)] + r\,\mathcal{D}[\underline{v}(t)] \end{aligned} \tag{3.25}$$

Performing the discretization by means of trapezoidal integration rule, (3.25) is

expanded as follows

$$\begin{aligned}\mathcal{D}[\underline{x}(t)] - \mathcal{D}[\underline{x}(t-\Delta t)] =& (p - j\omega)\,\frac{\Delta t}{2}(\mathcal{D}[\underline{x}(t)] + \mathcal{D}[\underline{x}(t-\Delta t)]) \\ &+ r\,\frac{\Delta t}{2}(\mathcal{D}[\underline{v}(t)] + \mathcal{D}[\underline{v}(t-\Delta t)])\end{aligned} \tag{3.26}$$

Back substitution into the the analytic signal notation, yields

$$\begin{aligned}\underline{x}(t) - \underline{x}(t-\Delta t)\,e^{j\omega_s \Delta t} =& (p - j\omega)\,\frac{\Delta t}{2}(\underline{x}(t) + \underline{x}(t-\Delta t)\,e^{j\omega_s \Delta t}) \\ &+ r\,\frac{\Delta t}{2}(\underline{v}(t) + \underline{v}(t-\Delta t)\,e^{j\omega_s \Delta t})\end{aligned} \tag{3.27}$$

Finally, after some manipulation, (3.27) can be simplified as

$$\begin{aligned}\underline{x}(t) &= \underline{\alpha}\,\underline{x}(t-\Delta t) + \underline{\lambda}\,\underline{v}(t) + \underline{\mu}\,\underline{v}(t-\Delta t) \\ \underline{i}(t) &= \underline{x}(t) + d\,\underline{v}(t)\end{aligned} \tag{3.28}$$

where

$$\begin{aligned}&\underline{p} = p - j\omega_s \\ &\underline{\alpha} = e^{j\omega_s \Delta t}\left(\frac{2 + \underline{p}\,\Delta t}{2 - \underline{p}\,\Delta t}\right) \qquad \underline{\lambda} = \frac{r\,\Delta t}{2 - \underline{p}\,\Delta t} \qquad \underline{\mu} = e^{j\omega_s \Delta t}\left(\frac{r\,\Delta t}{2 - \underline{p}\,\Delta t}\right)\end{aligned} \tag{3.29}$$

As the state variable $\underline{x}(t)$ in (3.28) depends on the input voltage at the same instant, it cannot be implemented in this form. By modification of the state variable and scaling the input like in [81]

$$\hat{\underline{x}}(t) = \underline{x}(t) - \underline{\lambda}\,\underline{v}(t) \tag{3.30}$$

(3.28) attains the same structure as defined in Appendix A

$$\begin{aligned}\underline{x}(t) &= \underline{\alpha}\,\underline{x}(t-\Delta t) + (\underline{\alpha}\,\underline{\lambda} + \underline{\mu})\,\underline{v}(t-\Delta t) \\ \underline{i}(t) &= \underline{x}(t) + (d + \underline{\lambda})\,\underline{v}(t)\end{aligned} \tag{3.31}$$

### 3.4.2 Recursive Convolution

Let an input-output in the frequency domain given by

$$I(s) = Y(s)\, V(s) \tag{3.32}$$

The time-domain counterpart is obtained by the convolution

$$i(t) = \int_0^{\infty} Y(u)\, v(t-u)\, du \tag{3.33}$$

It is known that (3.33) can be solved based on the preceding time-step [139, 190], as follows

$$i(t) = e^{p\Delta t}\, i(t-\Delta t) + \int_0^{\Delta t} Y(u)\, v(t-u)\, du \tag{3.34}$$

Assuming that the impulse response $y(t)$ is approximated by an exponential function or a sum of then, like in (3.21), (3.34) takes the following form

$$i(t) = e^{p\Delta t}\, i(t-\Delta t) + r \int_0^{\Delta t} e^{pu}\, v(t-u)\, du \tag{3.35}$$

Substituting the real variables $i$ and $v$ in (3.35) by their analytic counterparts and resorting to the definition of dynamic phasors

$$\begin{aligned} \underline{i}(t) &= e^{p\Delta t}\, \underline{i}(t-\Delta t) + r \int_0^{\Delta t} e^{pu}\, e^{j\omega_s(t-u)}\, \mathcal{D}[\underline{v}(t-u)]\, du \\ &= e^{p\Delta t}\, \underline{i}(t-\Delta t) + r\, e^{j\omega_s t} \int_0^{\Delta t} e^{(p-j\omega_s)u}\, \mathcal{D}[\underline{v}(t-u)]\, du \end{aligned} \tag{3.36}$$

By means of linear interpolation $\mathcal{D}[\underline{v}(t-u)]$ can be expanded as

$$\begin{aligned} e^{j\omega_s t}\int_0^{\Delta t} &= e^{j\omega_s t}\int_0^{\Delta t} e^{(p-j\omega_s)u}\left[\underline{v}(t)-\left(\frac{\underline{v}(t)-\underline{v}(t-\Delta t)}{\Delta t}\right)u\right]du \\ &= e^{j\omega_s t}\int_0^{\Delta t} e^{(p-j\omega_s)u}\,\underline{v}(t)\,du + e^{j\omega_s t}\int_0^{\Delta t} e^{(p-j\omega_s)u}\left(\frac{\underline{v}(t)-\underline{v}(t-\Delta t)}{\Delta t}\right)u\,du \\ &= e^{j\omega_s t}\,\underline{v}(t)\int_0^{\Delta t} e^{(p-j\omega_s)u}\,du + e^{j\omega_s t}\left(\frac{\bar{v}(t)-\underline{v}(t-\Delta t)}{\Delta t}\right)\int_0^{\Delta t} e^{(p-j\omega_s)u}\,u\,du \end{aligned} \tag{3.37}$$

Back substitution with analytic signals

$$= \underline{v}(t)\int_0^{\Delta t} e^{(p-j\omega_s)u}\,du + \left(\frac{\underline{v}(t)-e^{j\omega\Delta t}\underline{v}(t-\Delta t)}{\Delta t}\right)\int_0^{\Delta t} e^{(p-j\omega)u}\,u\,du \tag{3.38}$$

Solving the integrals and collecting like terms yields

$$\underline{i}(t) = \underline{\alpha}\,i(t-\Delta t) + \underline{\lambda}\,\underline{v}(t) + \underline{\mu}\,\underline{v}(t-\Delta t) \tag{3.39}$$

where

$$\begin{aligned} \underline{p} &= p - j\omega_s \\ \underline{\alpha} &= e^{\underline{p}\Delta t} \\ \underline{\lambda} &= -\frac{r}{\underline{p}}\left(1+\frac{1-e^{\underline{p}\Delta t}}{\underline{p}}\right) \\ \underline{\mu} &= -\frac{r}{\underline{p}}\left(\alpha-\frac{1-e^{\underline{p}\Delta t}}{\underline{p}\Delta t}\right)e^{j\omega\Delta t} \end{aligned} \tag{3.40}$$

## 3.5 Multiscale Approach

### 3.5.1 Introduction

The novel Multiple Time-Step (MTS) approach designed in the previous Chapter for real-based variables has a remarkable feature that no modification is necessary in actual companion networks adopted by EMTP-like programs. With little effort, it allows evaluations with variable time-steps in a simple and straightforward way.

In this chapter, it is intended the generalization of MTS aiming to cope with larger time-steps in the order of milliseconds. On the ground of dynamic phasors, the FAST formulation is extended to the modeling of frequency dependent lines and network equivalents. To achieve such feature, the shift frequency is introduced as an additional parameter depending on the phenomena to be observed. This multiscale approach enables the integrated simulation of EMT and TS with an inherent feature to process either instantaneous- ou phasor-based variables. It allows the integration of synchronous or induction machine models and is intended to bridge evaluations with power electronics converters alternatively to the averaging method [184].

### 3.5.2 Reinitialization Approach

In Section 2.5.2 an innovative procedure was introduced to make feasible the modification on the time-step resulting in no discontinuity issues after the transition. As aforementioned, the simulation with real or instantaneous variables poses a limitation related with the maximum time-step size due to the sampling rate of the fundamental frequency. The modeling based on dynamic phasors is able to circumvent such constraint.

In a similar fashion, the reinitialization approach also encompasses simulations involving complex variables. At a given instant $t$ when the time-step size is changed from $\Delta t_1$ to $\Delta t_2$, the current and voltage at the node should not change due to the modification of the time-step. Thus, to ensure this condition, the history current source has to be re-calculated on the base of the new conductance $\underline{g}_2$ related with the new time-step length $\Delta t_2$.

To illustrate the modification to be carried out in the companion network comprising N elements in parallel, the voltage and history current sources in (3.41) are now complex variables, in accordance with (3.1).

$$\underline{his}_2(t) = \sum_{i=1}^{N} \underline{his}_2^i(t) = \sum_{i=1}^{N} \underline{his}_1^i(t) + \sum_{i=1}^{N} (\underline{g}_1^i - \underline{g}_2^i)\, \underline{v}(t) \tag{3.41}$$

where $\underline{his}_k^i$ (with $k = 1, 2$) is the history current source associated with the $i^{\text{th}}$ pole

and $\underline{v}(t)$ is the terminal voltage.

It should be remarked that in the updating stage all the branches have to be individually reinitialized and then gathered into one equivalent current source. This procedure is highlighted in Fig. 3.4.

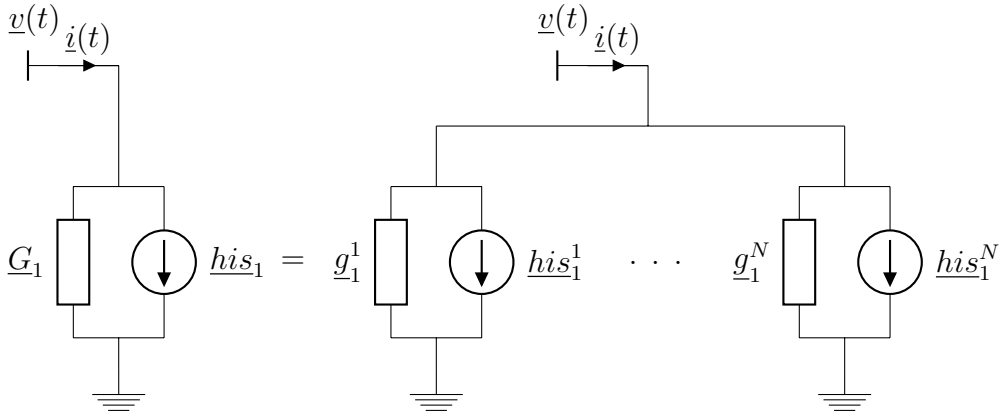


(a) Companion network for $\Delta t_1$

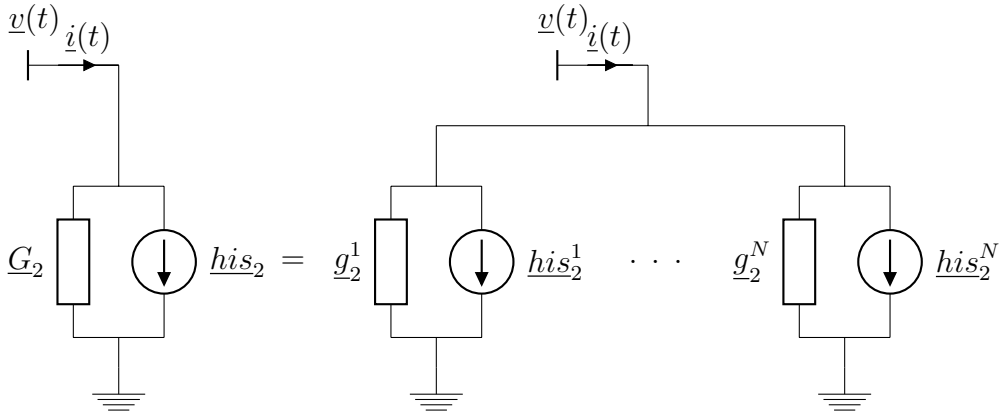


(b) Companion network for $\Delta t_2$

Figure 3.4: Sketch for time step transition

In addition, if a phasor-based evaluation is desired, i.e, with time-steps in the order of milliseconds, the shift frequency has to be adjusted. For the simulation of electromagnetic transients, no frequency shifting is required. However, if the simulation of electromechanical transients is considered, then $\omega_s = \omega$.

For convenience, a pseudo-code is re-introduced to be used to compute the time-domain response, based on the modified-augmented nodal analysis (MANA) [17] which is an extension of the formulation presented in [16]. In the pseudo-code $RHS$ stands for the vector of known quantities in MANA, $Sys1$ is the system matrix when $\Delta t_1$ and $Sys2$ is the one related to time-step $\Delta t_2$.

```
*** Loop with delta 1 ***
for n = 2:100
ws = 0
his(n) = i(n-1) + g1*v(n-1)
output(n) = inverse(Sys1)*RHS
end

*** update current source ***
his(n) = his(n) + (g1-g2)*v(n)

*** Loop with delta 2 ***
ws = 2*pi*f
for n = 101:150
his(n) = i(n-1) + g2*v(n-1)
output(n) = inverse(Sys2)*RHS
end
```

Although only a single change in the time-step was depicted, this procedure can be applied for multiple changes in the simulation time-step in the same fashion in accordance with the reinitialization steps. The extension to the multi-phase case is straightforward, see [168] for details.

## 3.6 Test cases

The same evaluations performed in Chapter 2 will be considered in order to assess the accuracy and numerical performance of the Frequency-Adaptive Simulation of Transients (FAST) approach in the modeling of frequency dependent admittance-based models. For the sake of clarity, a set of six test cases is going to be evaluated, namely:

1. #1: a RLC circuit
2. #2: a FDNE describing a 34 kV distribution network
3. #3: a 132-kV, 10 km long overhead line (Yn-Line)
4. #4: a 132-kV, 10 km long overhead line (FLE-Line)
5. #5: a 132-kV, 10 km long overhead line (Id-Line)
6. #6: a single-core armoured HVDC submarine cable, 2.5 km length (FLE-Line)

A PSCAD simulation will provide the reference for test cases #1 and #2. Despite the apparent similarity of cases #3 to #5, each multi-scale simulation will be performed through the following formulations presented in Section 2.3, namely: nodal admittance matrix (Yn-Line), Folded Line Equivalent (FLE-Line) and Idempotent Decomposition (Id-Line). A a fixed time-step simulation with the universal line model (ULM) [80] will be adopted for validation of the test cases involving the overhead line. For the HVDC subsea cable, another simulation method using a frequency-domain algorithm based on the Numerical Laplace Transform (NLT) [174–176] will be applied.

It is worth mentioning that for all test cases the instant for the time-step transition is defined prior the simulation starts as well as the new time-step value. The developed computer codes with *Mathematica* [177] for time-domain simulations adopted the Modified Nodal Analysis (MNA) formulation to solve the circuit equations [16] in a similar fashion like MatEMTP [178]. A conventional laptop was used for the calculations with a 2.9 GHz, Core i7 computer with 8 GB of RAM.

### 3.6.1 Case #1: RLC

To exemplify the first application of a multiscale simulation with the FAST, let the very simple RLC circuit shown in Fig. 3.5. The parameters for this evaluation are given by

$$V_s = \cos\,(2\,\pi\,50\,t)$$
$$R = 100\ \Omega \qquad L = 110\ \text{mH} \qquad C = 0.25\ \mu\text{F}$$
$$i_L(0) = 0\ \text{A} \qquad v_C(0) = 0\ \text{V}$$

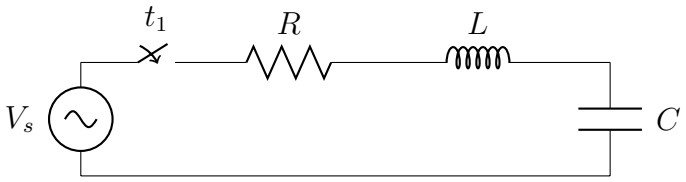


Figure 3.5: Case #1: RLC circuit

The simulation is concerned with a switch closing at $t_1 = 0$ s, i.e., the instant at which the input voltage is in its maximum value. Initially, the circuit is evaluated considering an initial time-step $\Delta t_1 = 10\ \mu$s and it is increased to $\Delta t_2 = 500\ \mu$s after the circuit reaches the steady-state. A comparison between the real part of the simulated capacitor voltage with the PSCAD curve presents a smooth transition due to the change in the time-step, see Fig. 3.6. An excellent match can be observed in the instantaneous waveform.

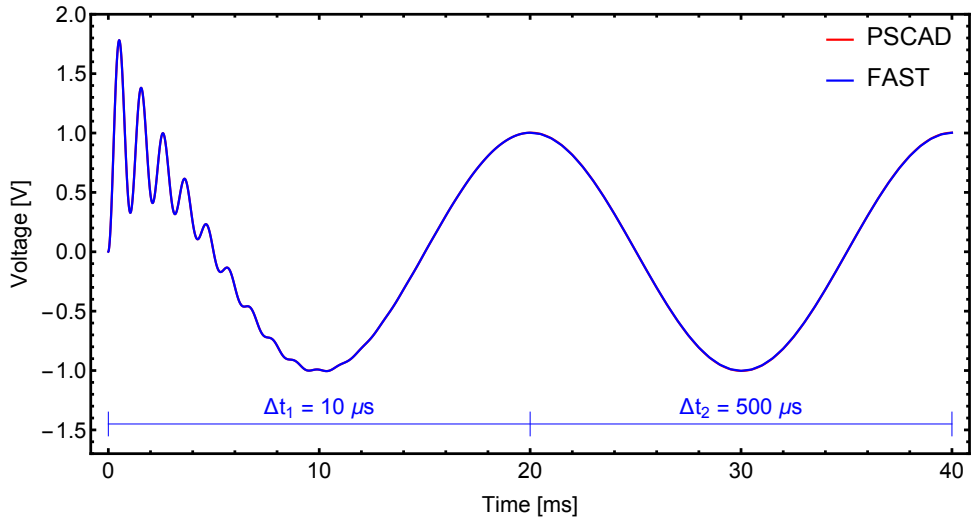


Figure 3.6: Case #1: Simulated capacitor voltage

One great feature of FAST is that it allows the extraction of both instantaneous and envelope waveforms, see Fig. 3.7, and one can decide which waveform to trace depending on the type of phenomena to be observed. For instance, the real part or the instantaneous waveform of a given complex variable is of prime interest following any disturbance and if the system is under steady-state the envelope or the absolute part may be preferred.

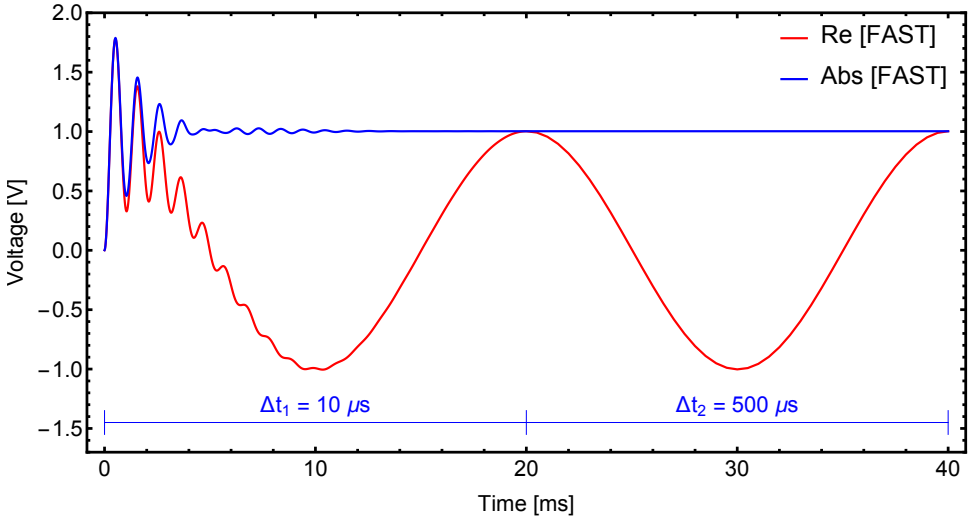


(a) Instantaneous and envelope waveforms

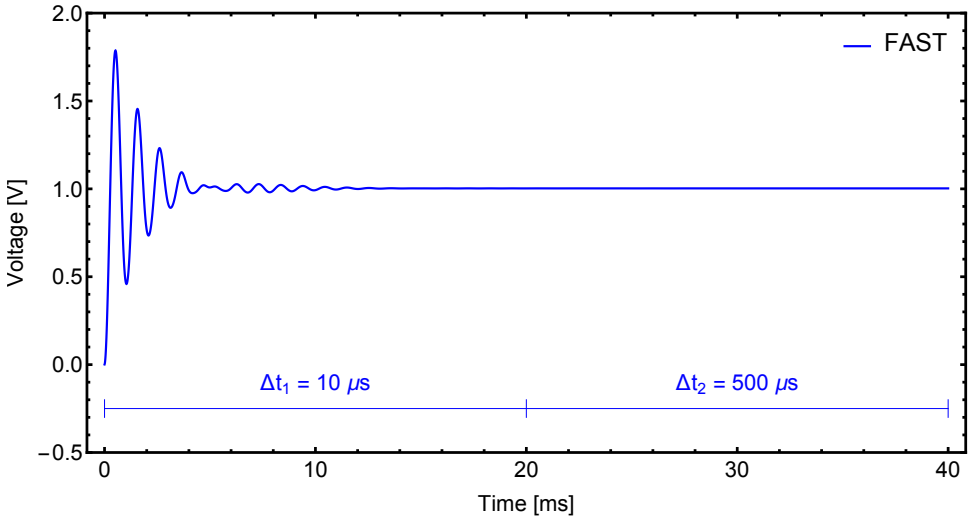


(b) Envelope waveform

Figure 3.7: Case #1: Simulated capacitor voltage

The simulated current is presented in Fig. 3.8 and a very good agreement is observed between the current profile using a single time-step and the one using the novel formulation For a better visualization, Fig. 3.8b shows only the envelope waveform.

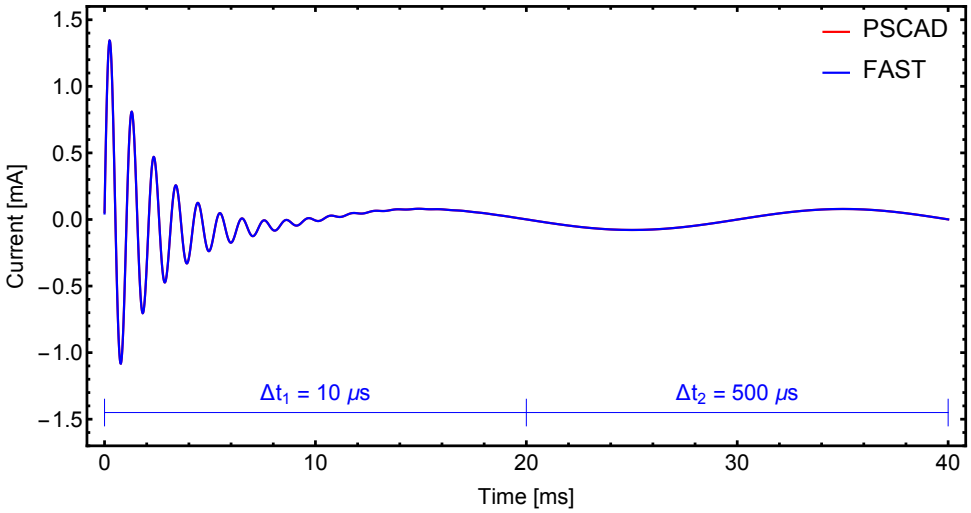


(a) Instantaneous waveform

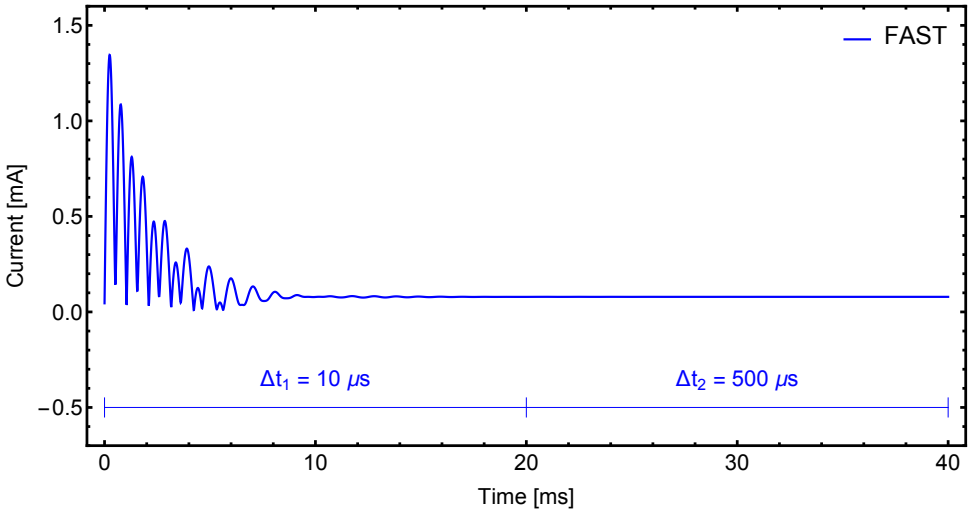


(b) Envelope waveform

Figure 3.8: Case #1: Simulated current

It is worth mentioning that when the system under evaluation reaches the steady-state there is no constraint for the new time-step. If one desires a time-step larger than, for instance, $\Delta t_2 > 2$ ms, in order to accelerate the simulation, the phasor-based formulation must be employed. This is achieved by setting the shift frequency $f_s = 50$ Hz, contrary at the beginning of the simulation when the shift frequency is $f_s = 0$ Hz for an EMTP-type simulation. The versatility of the multiscale technique can be seen in Fig. 3.9 which shows the transition between instantaneous and envelope waveforms when the time-step is changed to $\Delta t_1 = 10$ $\mu$s or $\Delta t_2 = 10$ ms.

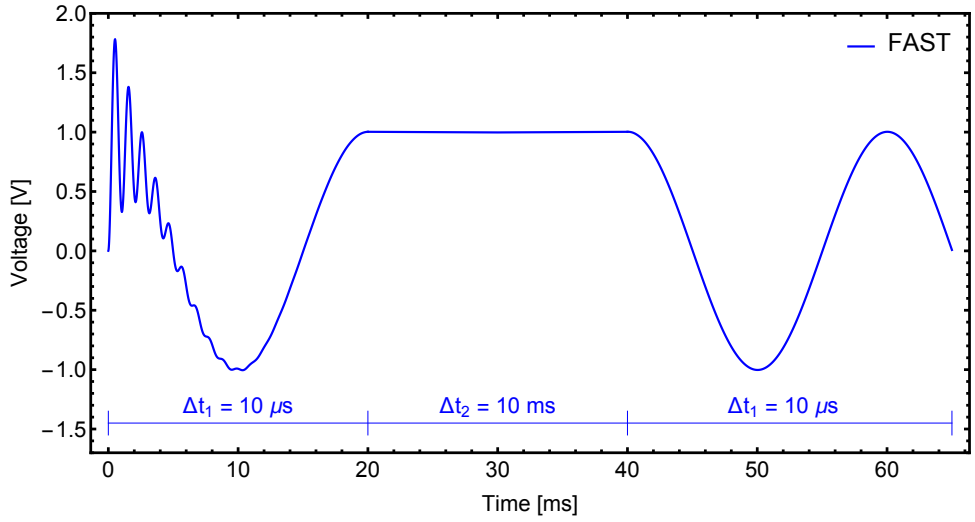


Figure 3.9: Case #1: Simulated capacitor voltage

### 3.6.2 Case #2: FDNE

This test case aims to demonstrate the multiscale methodology in the modeling of an admittance-based model representing a frequency dependent network equivalent (FDNE) in phase-coordinates. The system describes a 24 kV rural distribution network and its details can be reviewed in Section. 2.6.2. The rational approximation is shown in Fig. 2.13.

For the sake of clarity, the same evaluation performed in Section. 2.6.2 is sketched in Figure 3.10, i.e., a single-phase energization by a unit sinusoidal voltage source at $t_1 = 0$ s followed by a short-circuit after 10 ms. An initial time-step $\Delta t_1 = 0.5\,\mu$s is adopted and after 4 ms, when all transients vanished, it is increased to $\Delta t_2 = 500\,\mu$s. Next, the time-step is reduced to $\Delta t_1 = 0.5\,\mu$s in order to simulate the fault.

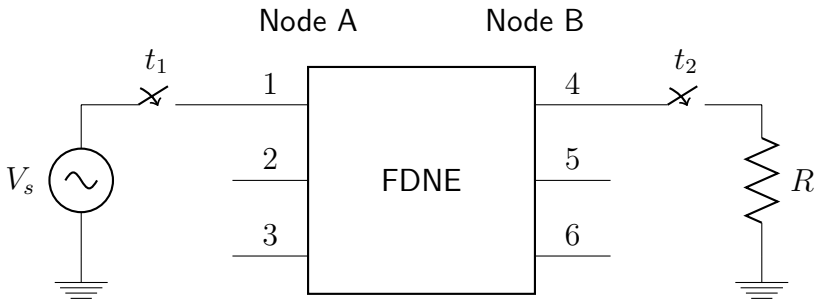


Figure 3.10: Case #2: Circuit for time-domain simulation

In order to verify the accuracy of FAST, the simulated voltage at terminal #4 is compared with PSCAD curve using a fixed time-step $\Delta t = 0.5\,\mu$s, as can be seen in Fig. 3.11. An excellent match is attained and no numerical oscillations are observed when the time-step is changed. Since the complex formulation allows the extraction of the instantaneous and envelope waveforms, Fig. 3.12 depicts the real and absolute waveforms of the voltage profile at terminal #4.

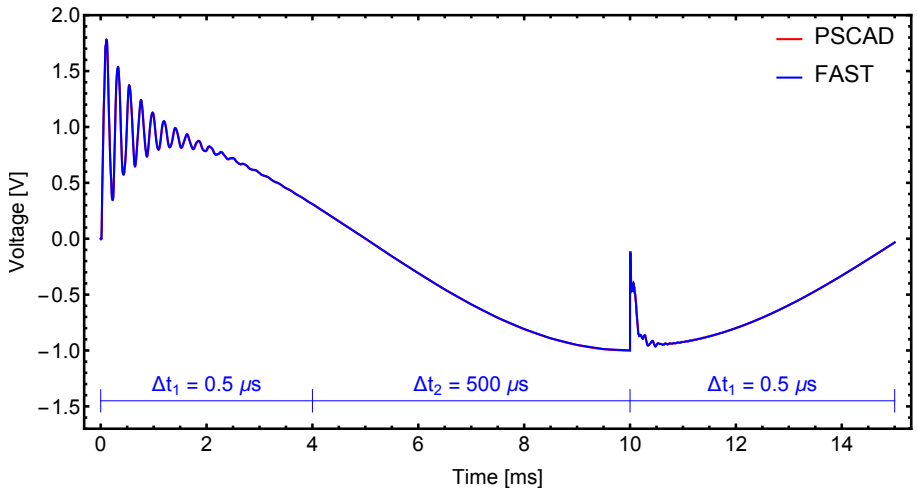


Figure 3.11: Case #2: Simulated voltage at terminal # 4

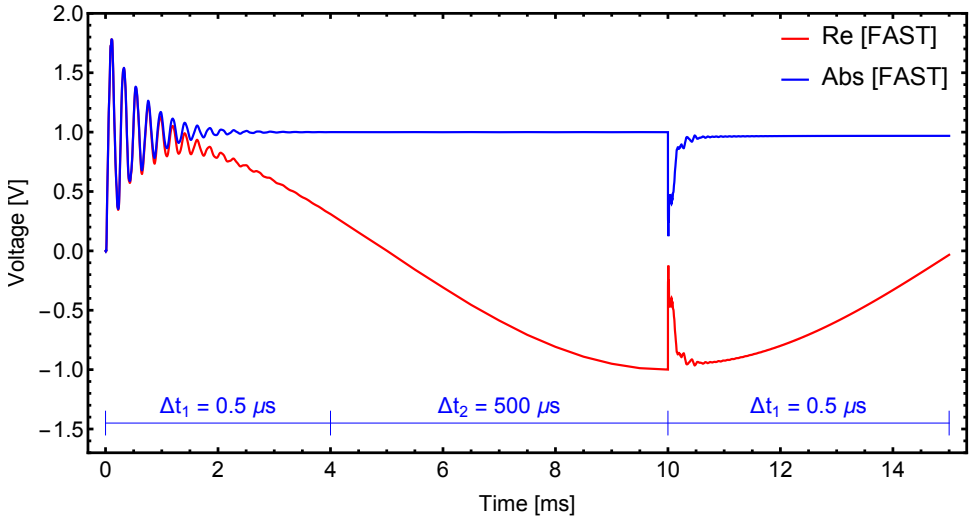


(a) Instantaneous and envelope waveforms

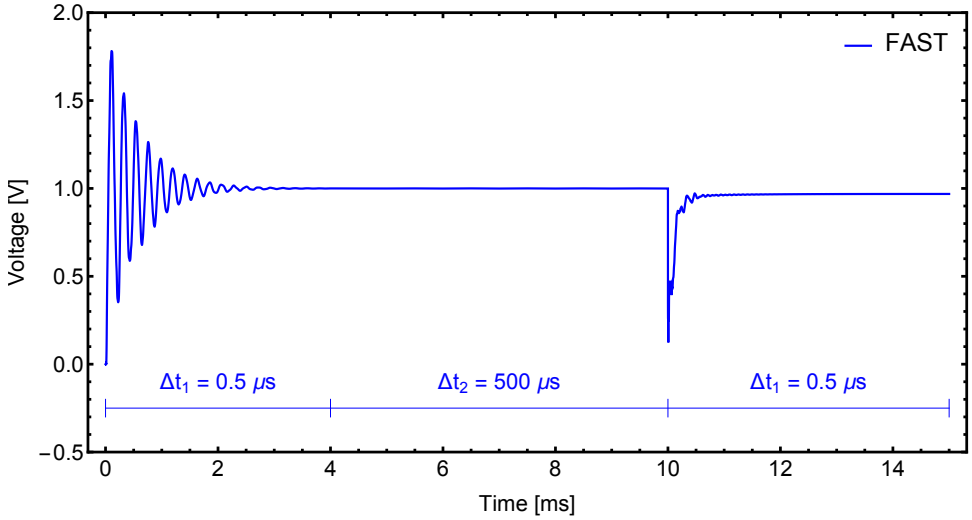


(b) Envelope waveform

Figure 3.12: Case #2: Simulated voltage at terminal #4

A very good agreement can be seen in the simulated current at terminal #1 with the novel formulation, as presented in Fig. 3.13, since any apparent mismatches is observed in comparison with the simulated current using a single time-step. For a better visualization, Fig. 3.13b shows only the envelope waveform.

Using FAST the phasor-mode formulation must be employed if one desires a time-step larger than, for instance, $\Delta t_2 > 2$ ms. To demonstrate this versatility, the transition between instantaneous and envelope waveforms is shown in Fig. 3.14 when the time-step is changed from $\Delta t_1 = 0.5$ $\mu$s to $\Delta t_2 = 10$ ms. This is achieved by setting the shift frequency $f_s = 50$ Hz.

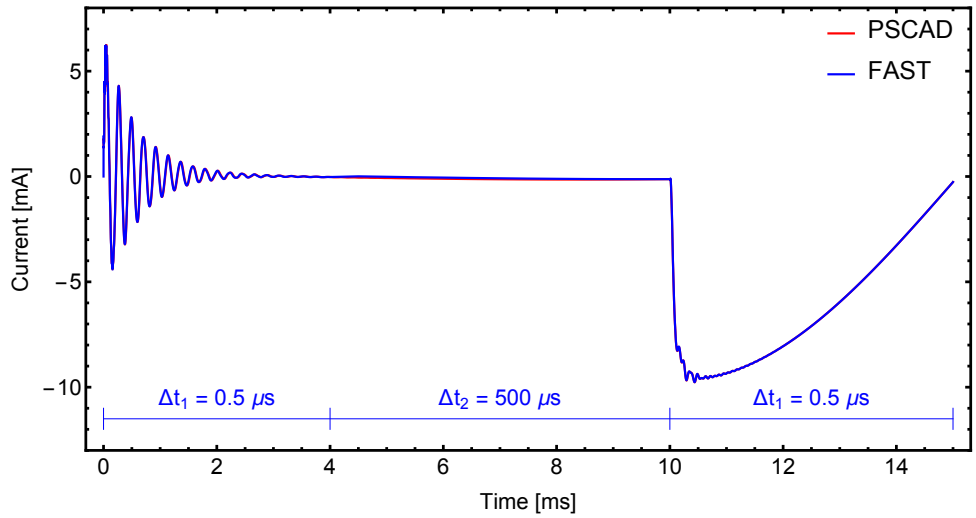


(a) Instantaneous and envelope waveform

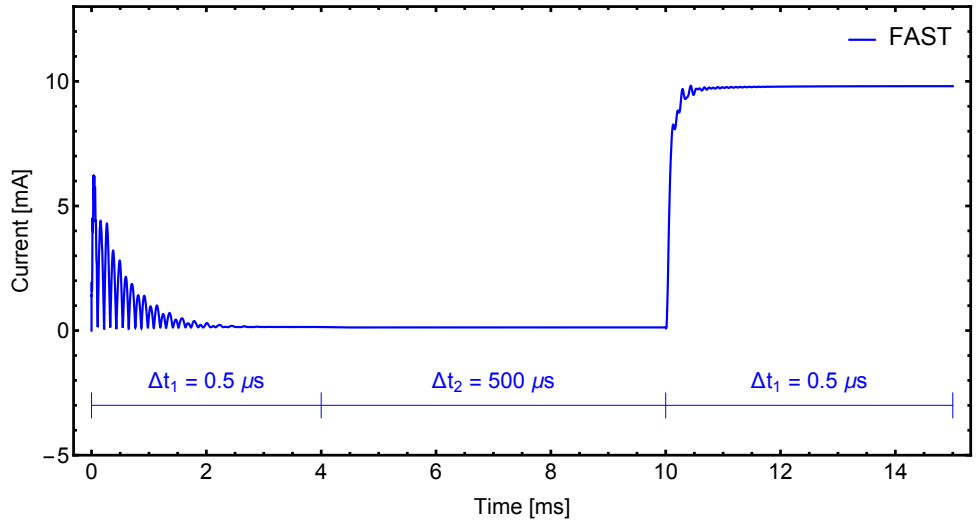


(b) Envelope waveform

Figure 3.13: Case #2: Simulated current at terminal #1

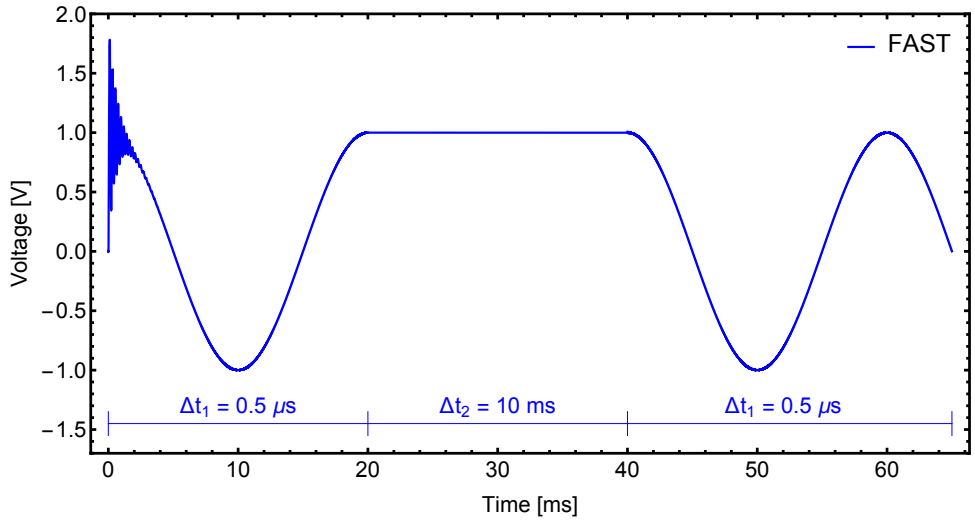


Figure 3.14: Case #2: Simulated voltage at terminal #4

### 3.6.3 Case #3: Overhead Line (Yn-Line)

This test case aims to demonstrate the multiscale simulation of a nodal admittance-based line (**Y**n–Line) using FAST. For the sake of clarity, the 132 kV overhead line depicted in Fig. 3.15 is the same as the one considered in Section 2.6.3 and the rational approximation of $\mathbf{Y}_n$ matrix is shown in Fig. 2.21.

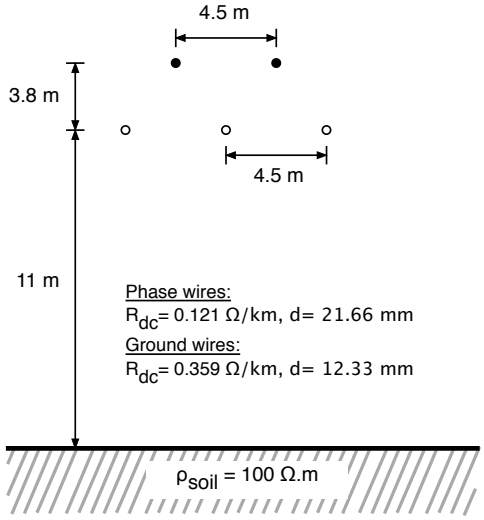


Figure 3.15: Case #3: 132-kV transmission line geometry

The evaluation to be performed considers a single-phase energization at $t_1 = 0$ s by a unit sinusoidal voltage source followed by a capacitor bank energization, as depicted in Fig. 3.16. The short-circuit reactance is considered by means of an inductance $L = 110$ mH and the capacitor bank is given by $C = 0.1$ $\mu$F

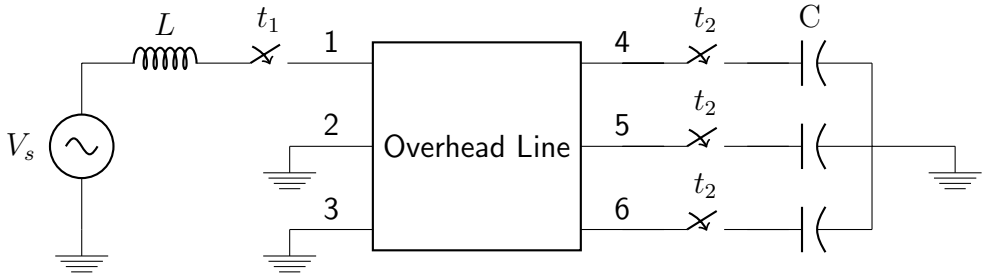


Figure 3.16: Case #3: Circuit for time-domain simulation

The simulation starts with $\Delta t_1 = 1$ $\mu$s in order to track the transient behavior and it is increased to $\Delta t_2 = 500$ $\mu$s as soon as the system reaches the steady-state. It was chosen the instant at which the voltage is in its maximum value. Once the simulation run reached 40 ms, the time-step is reduced to $\Delta t_1 = 1$ $\mu$s for a capacitor bank energization, like the evaluation performed in Section 2.6.3. Fig. 3.17a presents the simulated voltage at terminal #4 and a detailed view instants prior to the capacitor insertion is highlighted in Fig. 3.17b. The accuracy and versatility of this multiscale

approach is proved through the very accurate match with ULM curve along the overall simulation run.

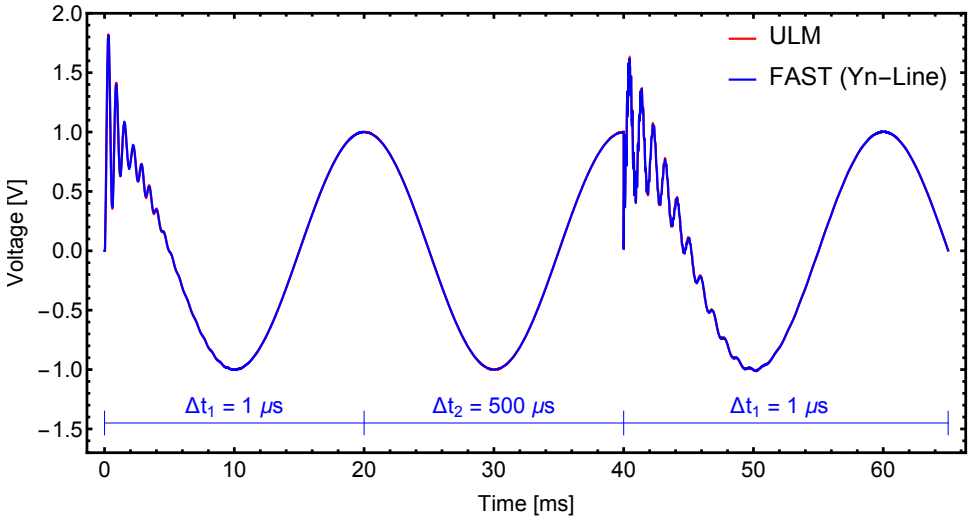


(a) Overall simulation

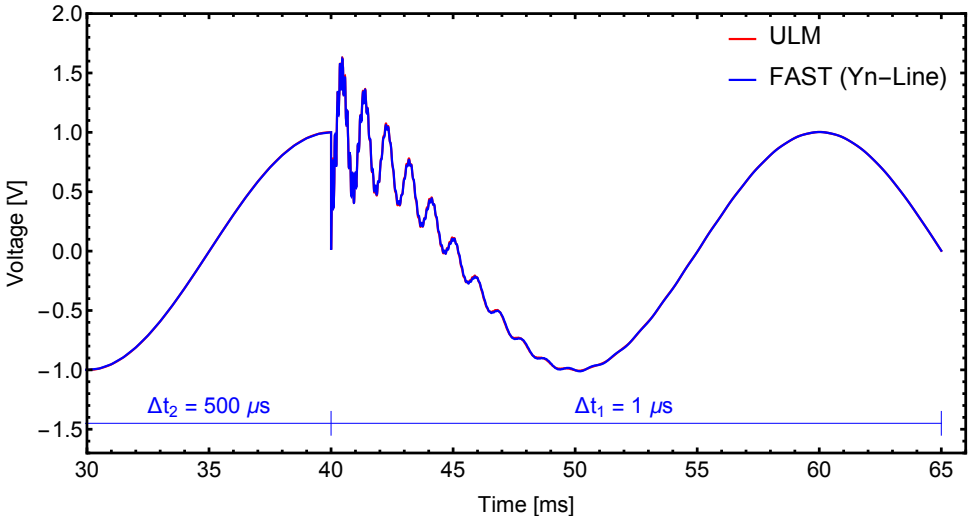


(b) Capacitor bank energization

Figure 3.17: Case #3: Simulated voltage at terminal #4

Since the complex formulation allows the extraction of the instantaneous and envelope waveforms, Fig. 3.18 repeats latter figure but only with the instantaneous and envelope waveforms obtained with FAST. Evidence of the added value achieved with the envelope waveform and its usefulness can be observed in Fig. 3.19 where the curve for the whole simulation run is shown.

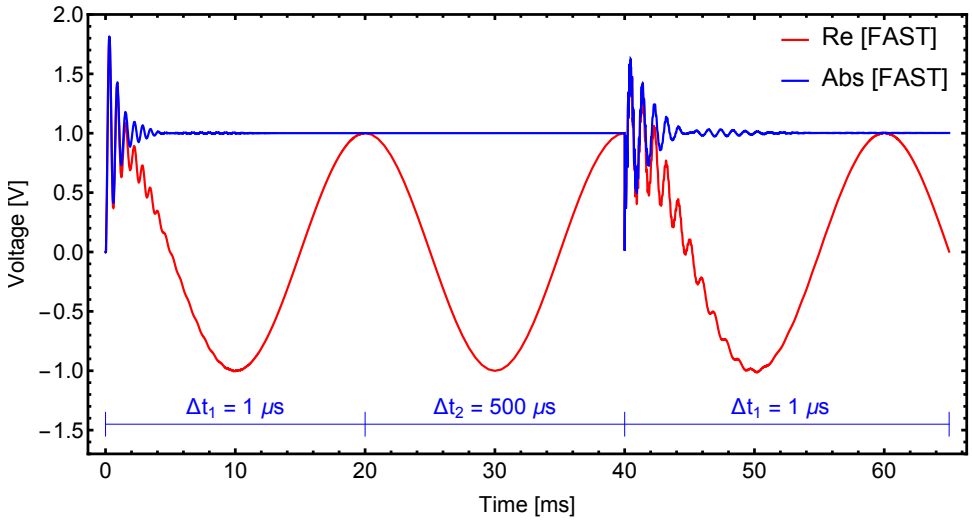


(a) Overall simulation

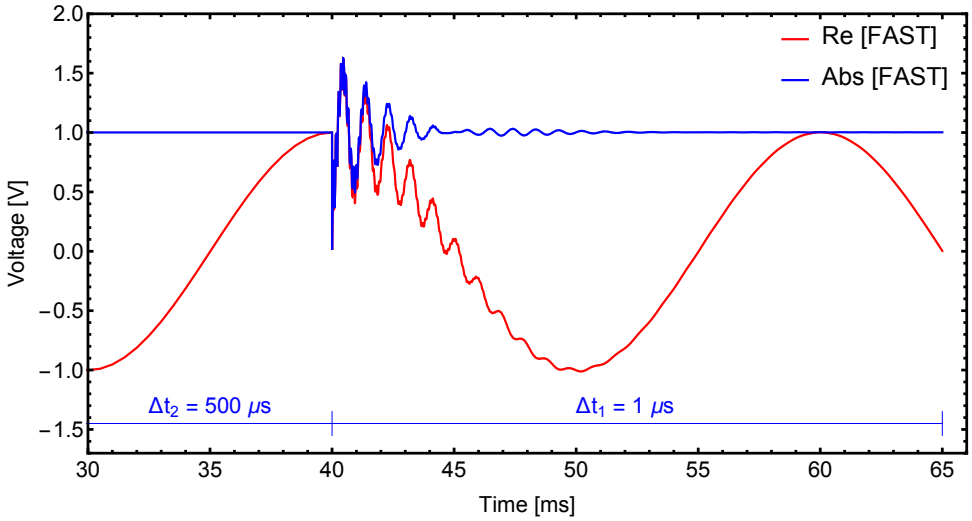


(b) Capacitor bank energization

Figure 3.18: Case #3: Simulated voltage at terminal #4

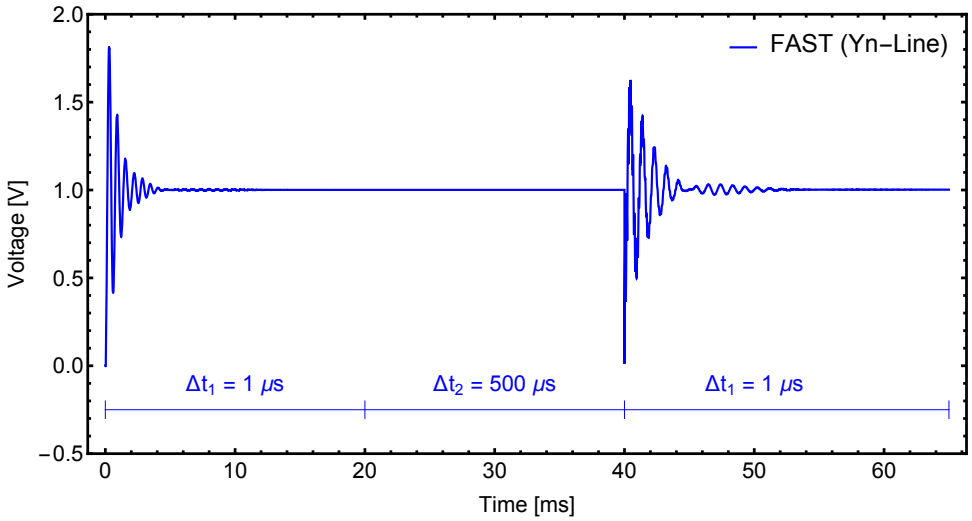


Figure 3.19: Case #3: Envelope of the simulated voltage at terminal # 4

The simulated current at terminal #1 is presented in Fig. 3.20 and a very good agreement can be seen between the simulated current using a single time-step and the one using the novel formulation. Besides providing a simulation without significant loss of accuracy, the proposed methodology reduces considerably the computational burden. For a better visualization, Fig. 3.20b shows only the envelope waveform.

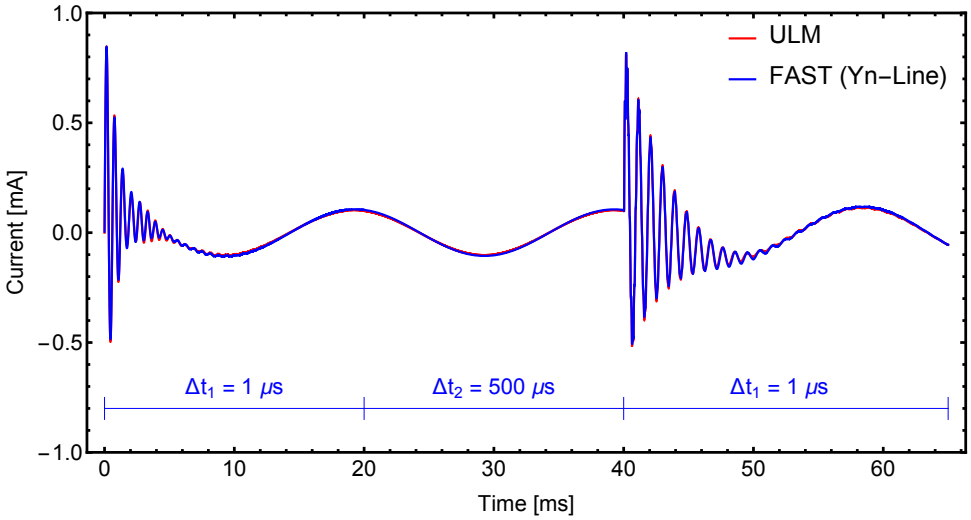


(a) Instantaneous waveform

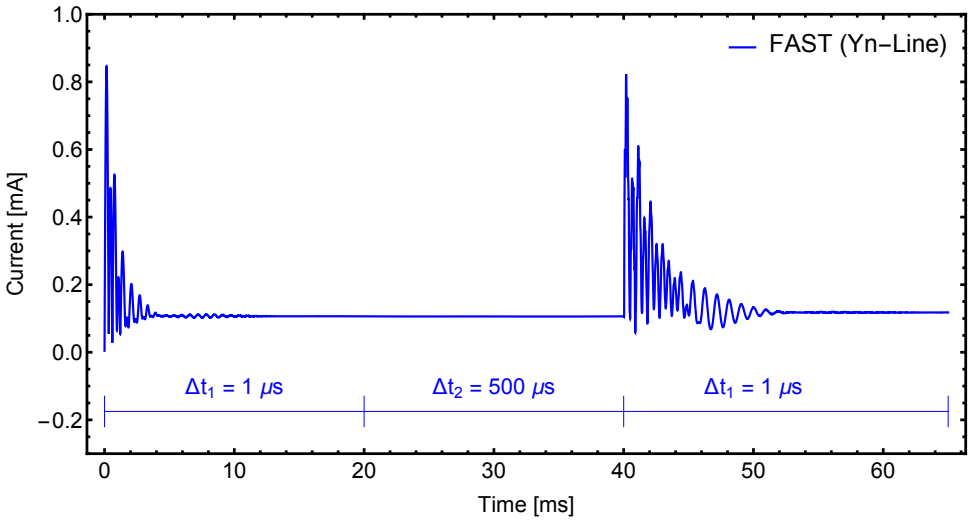


(b) Envelope waveform

Figure 3.20: Case #3: Simulated current at terminal #1

As aforementioned, there is no constraint for the new time-step length when the system under evaluation reaches the steady-state. Hence, a time-step in the order of milliseconds can be employed in order to accelerate the evaluation run by means of the phasor-mode simulation. The transition between instantaneous and envelope waveforms when the time-step is changed to $\Delta t_1 = 1$ $\mu$s or $\Delta t_2 = 10$ ms is shown in Fig. 3.21.

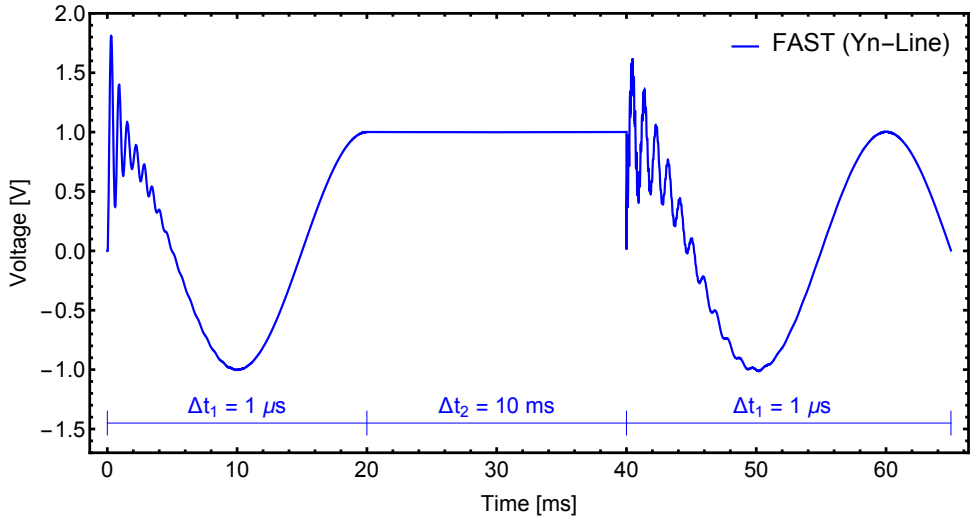


Figure 3.21: Case #3: Simulated voltage at terminal # 4

### 3.6.4 Case #4: Overhead Line (FLE-Line)

This test case aims to demonstrate the applicability of FAST in the modeling of transmission lines based on the FLE formulation (FLE–Line). The admittance-based model designed for multiscale simulations considered the line configuration depicted in Fig. 3.15 with the rational fitting of $\mathbf{Y}_{oc}$ and $\mathbf{Y}_{sc}$ matrices presented in Fig. 2.27. Further details can be seen in Section 2.6.4.

For the sake of clarity, the circuit in Fig. 3.22 depicts the system to be evaluated, i.e., a single-phase energization at $t_1 = 0$ s followed by a capacitor bank energization at $t_1 = 40$ ms. The short-circuit reactance is considered by means of an inductance $L = 110$ mH and the capacitor bank is given by $C = 0.1$ $\mu$F.

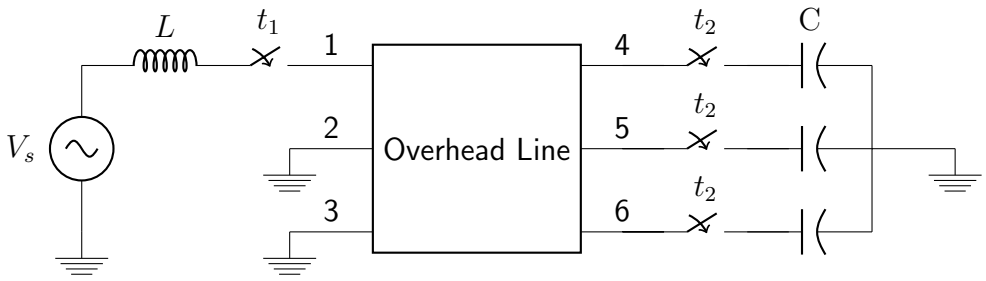


Figure 3.22: Case #4: Circuit for time-domain simulation

In accordance with the evaluation performed in Section 2.6.4, the simulation starts with an initial time-step $\Delta t_1 = 1$ $\mu$s in order to track the transient behavior. Once the system reached the steady-state, it is increased to $\Delta t_2 = 500$ $\mu$s. Having the simulation run elapsed 40 ms, the time-step is reduced to $\Delta t_1 = 1$ $\mu$s to perform the capacitor bank energization.

The simulated instantaneous voltage at terminal #4 is presented in Fig. 3.23a and Fig. 3.23b shows some instants prior to the capacitor bank energization to highlight the accuracy and versatility of this novel multiscale line model. It can be seen a very accurate match with ULM curve along the overall simulation run.

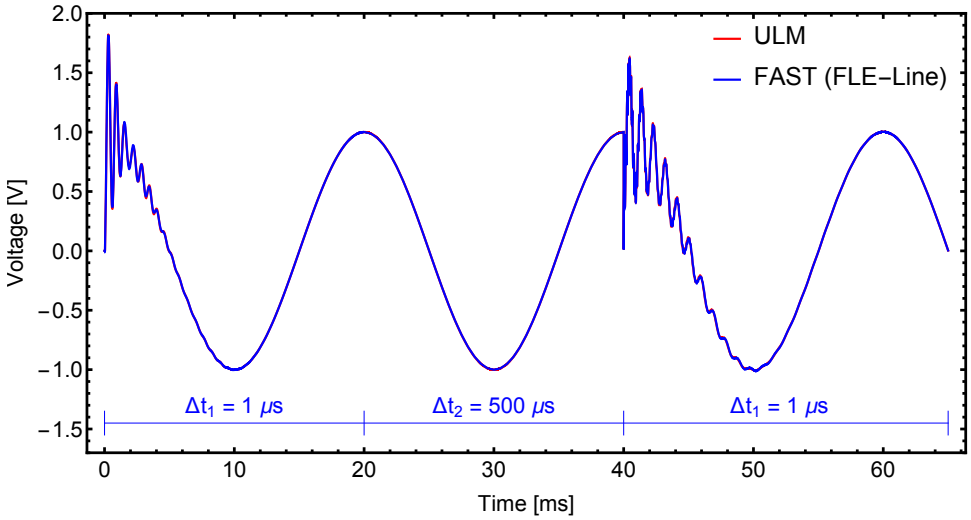


(a) Overall simulation

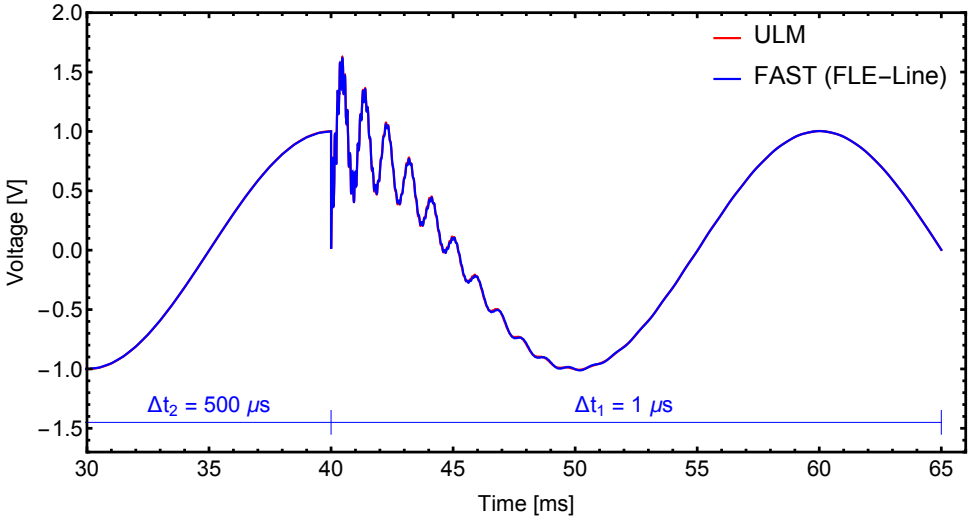


(b) Capacitor bank energization

Figure 3.23: Case #4: Simulated voltage at terminal #4

The added value achieved with the complex formulation adopted by FAST is the possibility to extract either the instantaneous or envelope waveforms. Here, Fig. 3.24 repeats latter figure but only with the instantaneous and envelope waveforms and Fig. 3.25 shows the envelope waveform for the whole simulation run.

The simulated current at terminal #1 using FAST is presented in Fig. 3.26 and compared with the ULM curve obtained using a single time-step. It can be seen a good match between them without substantial loss of accuracy. For a better visualization, Fig. 3.26b shows only the envelope waveform.

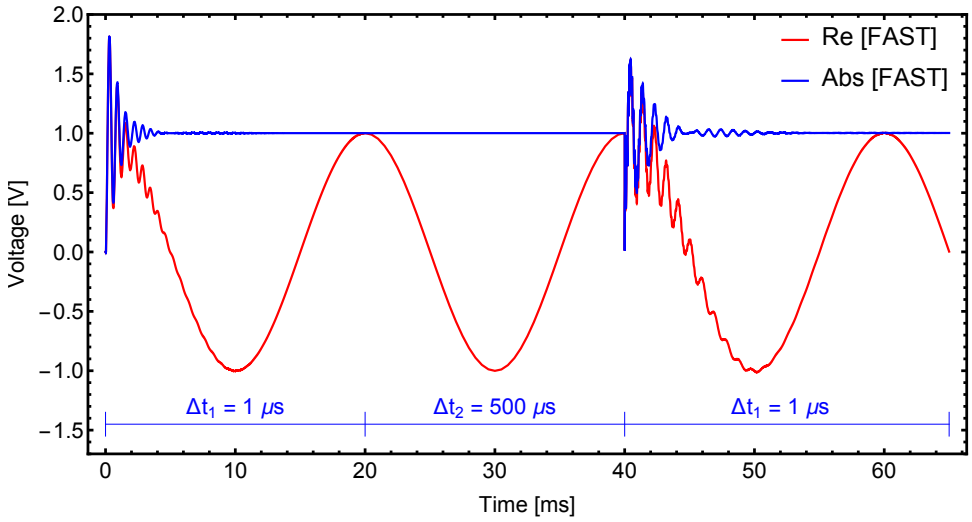


(a) Overall simulation

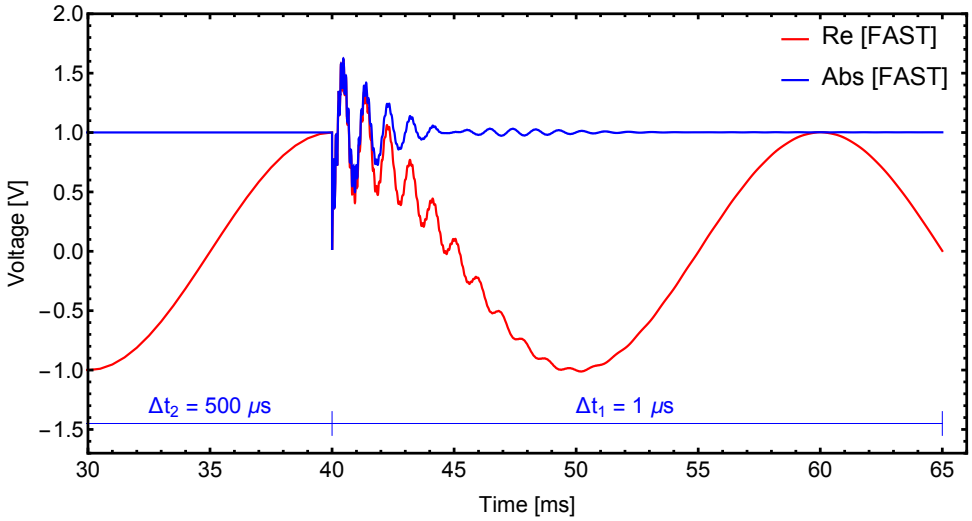


(b) Capacitor bank energization

Figure 3.24: Case #4: Simulated voltage at terminal #4

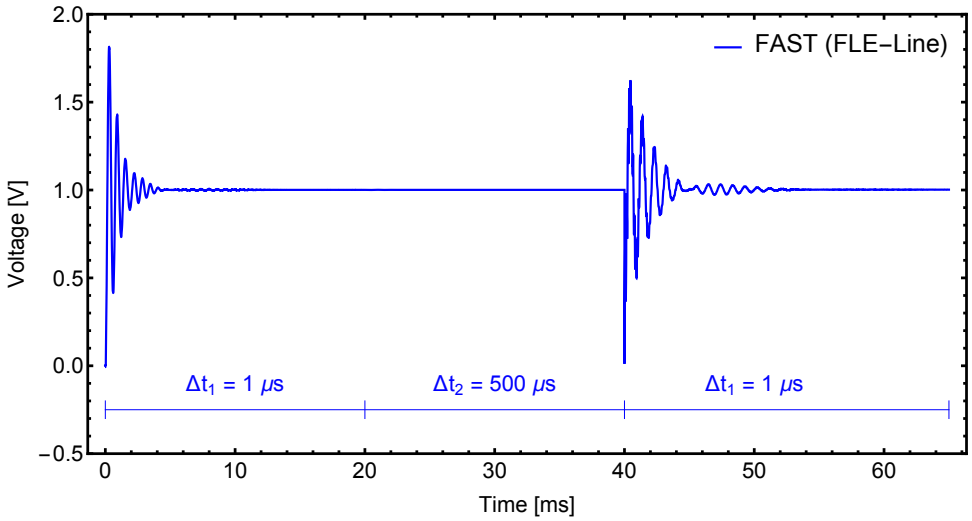


Figure 3.25: Case #4: Envelope of the simulated voltage at terminal # 4

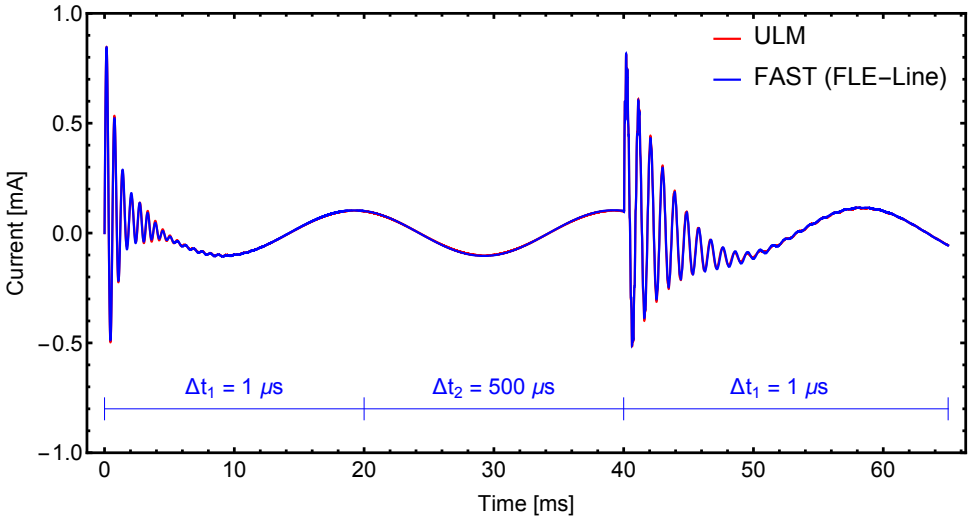


(a) Overall simulation

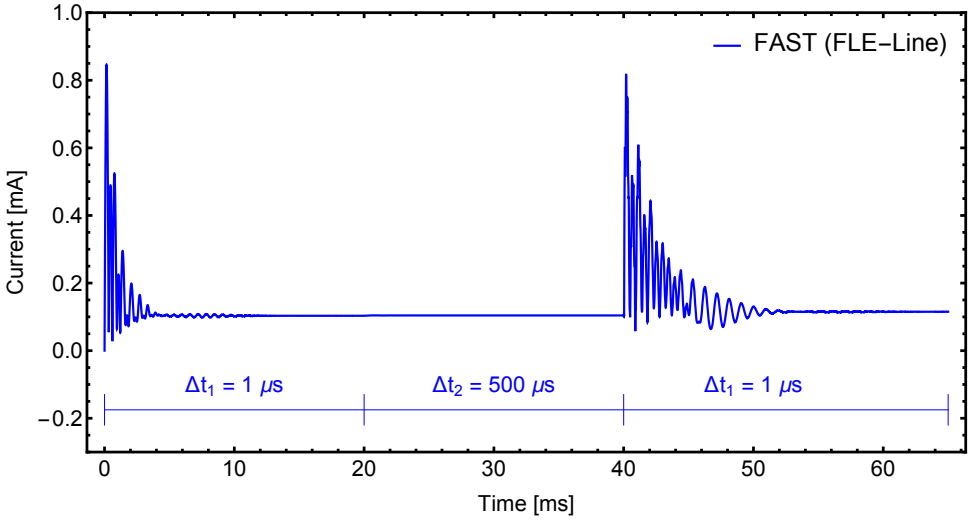


(b) Capacitor bank energization

Figure 3.26: Case #4: Simulated current at terminal # 1

By setting the shift frequency $f_s = 50$ Hz, it is allowed a phasor-based simulation which enables the adoption of time-steps larger than, for instance, $\Delta t_2 > 2$ ms. The transition between the real and phasor-based representations in shown Fig. 3.27 when the time-step is changed from $\Delta t_1 = 1$ $\mu$s to $\Delta t_2 = 10$ ms and vice versa.

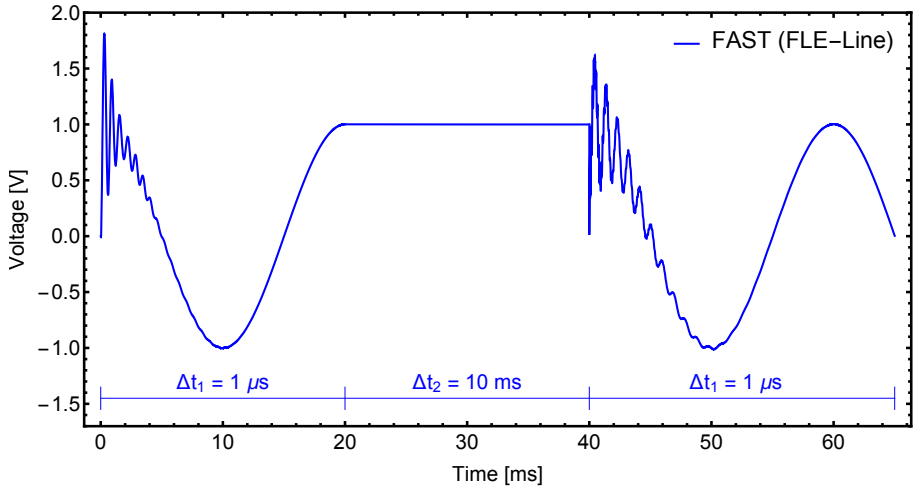


Figure 3.27: Case #4: Simulated voltage at terminal # 4

### 3.6.5 Case #5: Overhead Line (Id-Line)

This test case aims to evaluate an admittance-based line model based on the Idempotent Decomposition (Id–Line). In order to demonstrate a multiscale simulation with FAST, the same overhead line configuration depicted in Fig. 3.15 will be considered. For the rational fitting of the idempotent matrices, see Fig. 2.34 in Section 2.6.5.

For the sake of clarity, the circuit in Fig. 3.28 depicts the system to be evaluated, i.e., a single-phase energization at $t_1 = 0$ s followed by a capacitor bank energization at $t_1 = 40$ ms. The short-circuit reactance is considered by means of an inductance $L = 110$ mH and the capacitor bank is given by $C = 0.1$ $\mu$F.

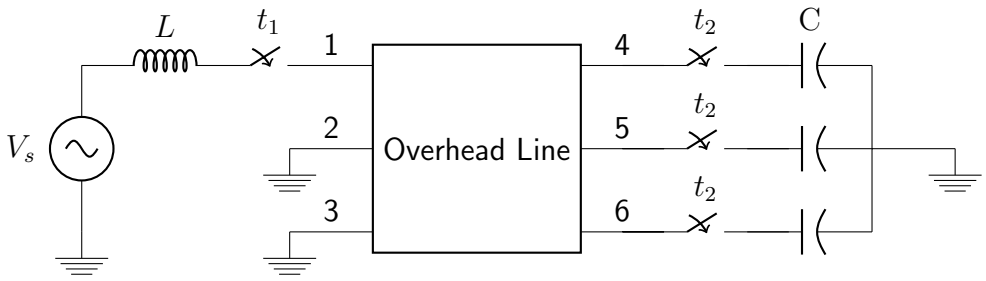


Figure 3.28: Case #5: Circuit for time-domain simulation

In accordance with the evaluation performed in Section 2.6.5, the simulation starts with $\Delta t_1 = 1$ $\mu$s to track the transient behavior. Once the system reached the steady-state, the time-step is increased to $\Delta t_2 = 500$ ms at the instant the voltage is in its maximum value. Having the simulation run elapsed 40 ms, the time-step is changed to $\Delta t_1 = 1$ $\mu$s for the capacitor bank insertion.

In the same way as in the previous transmission line evaluations, a very accurate match is achieved with the Id–Line model. Fig. 3.29a presents the simulated voltage at terminal #4 and Fig. 3.29b depicts some instants prior to the capacitor energization. The instantaneous and envelope waveforms obtained with FAST are shown in Fig. 3.30 while only the envelope is presented in Fig. 3.31.

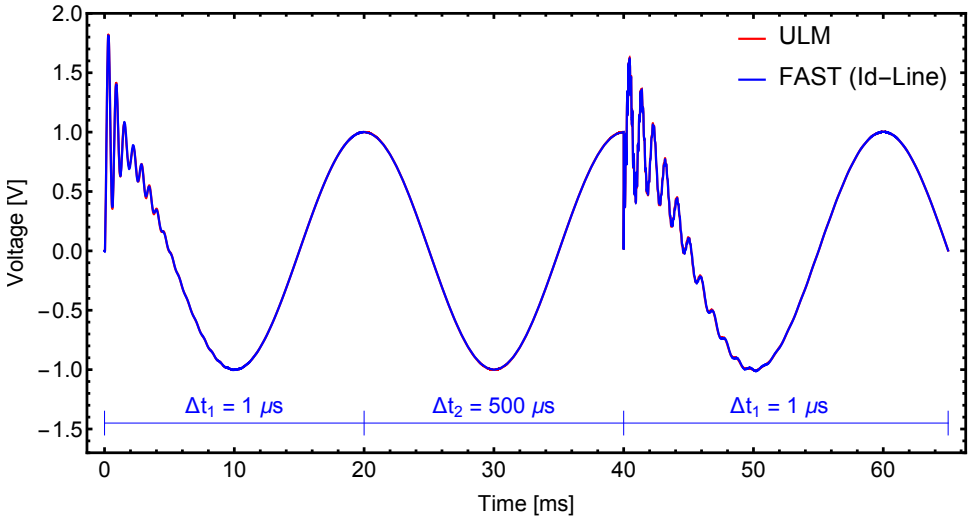


(a) Overall simulation

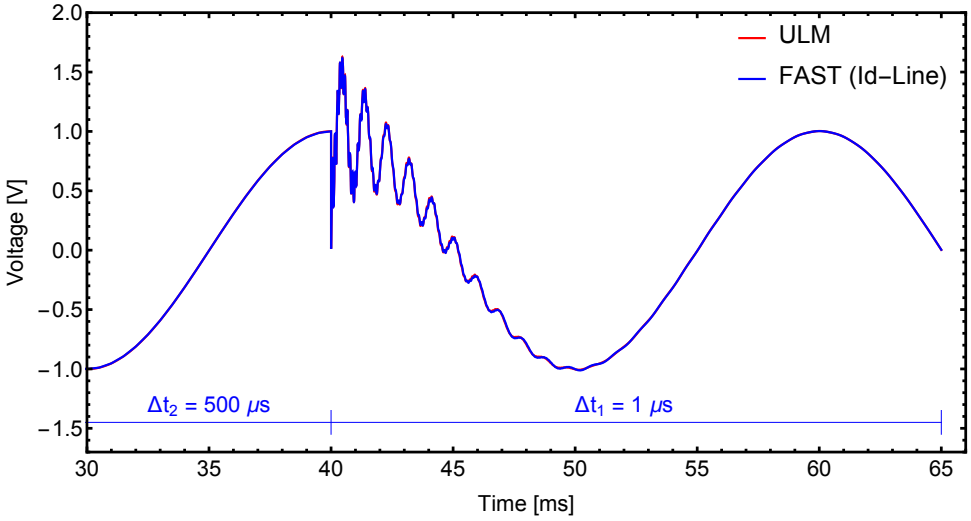


(b) Capacitor bank energization

Figure 3.29: Case #5: Simulated voltage at terminal #4

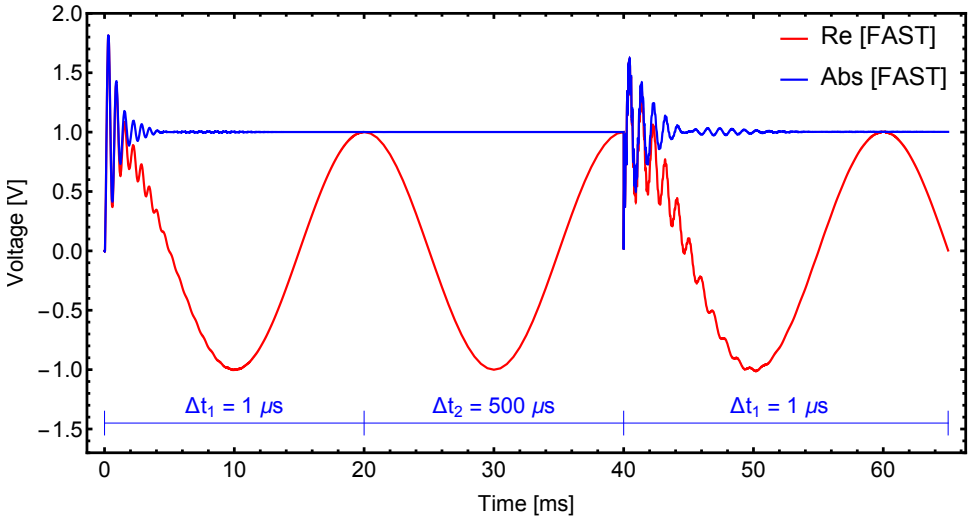


(a) Overall simulation

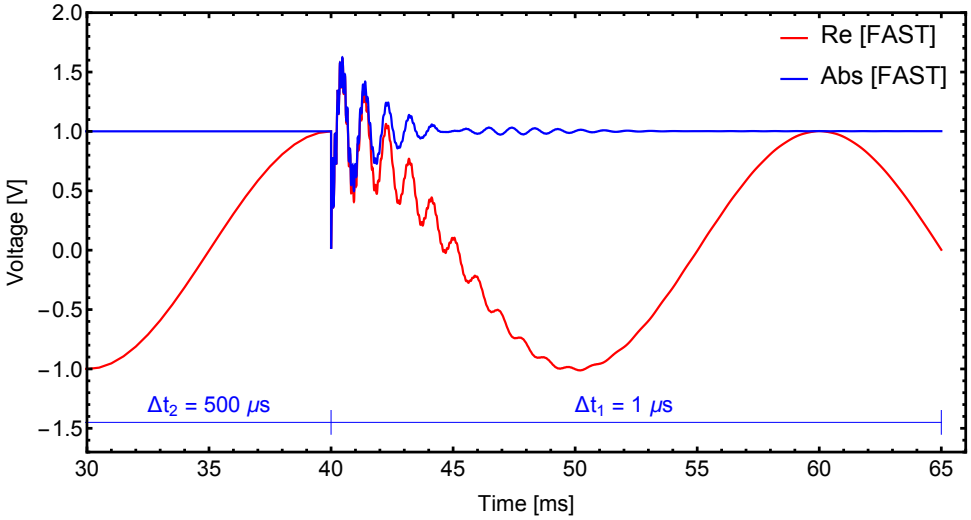


(b) Capacitor bank energization

Figure 3.30: Case #5: Simulated voltage at terminal #4

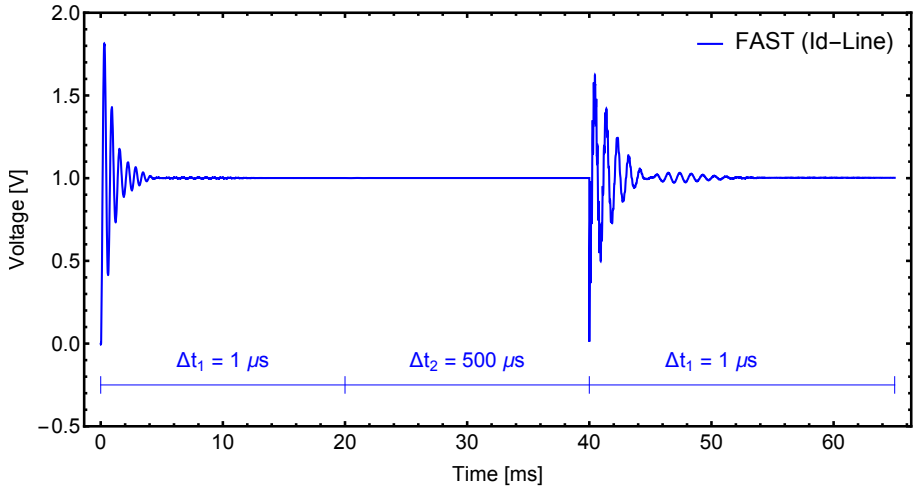


Figure 3.31: Case #5: Envelope of the simulated voltage at terminal # 4

The simulated current at terminal #1 is presented in Fig. 3.32. Again a very good agreement can be seen as there are no mismatches between the simulated current using a single time-step and the one using the novel formulation. For a better visualization, Fig. 3.32b shows only the envelope waveform.

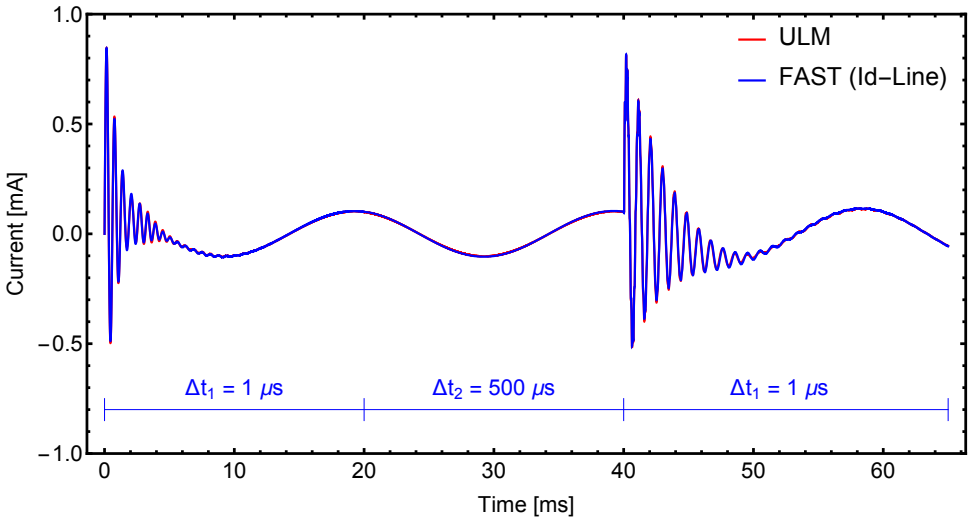


(a) Overall simulation

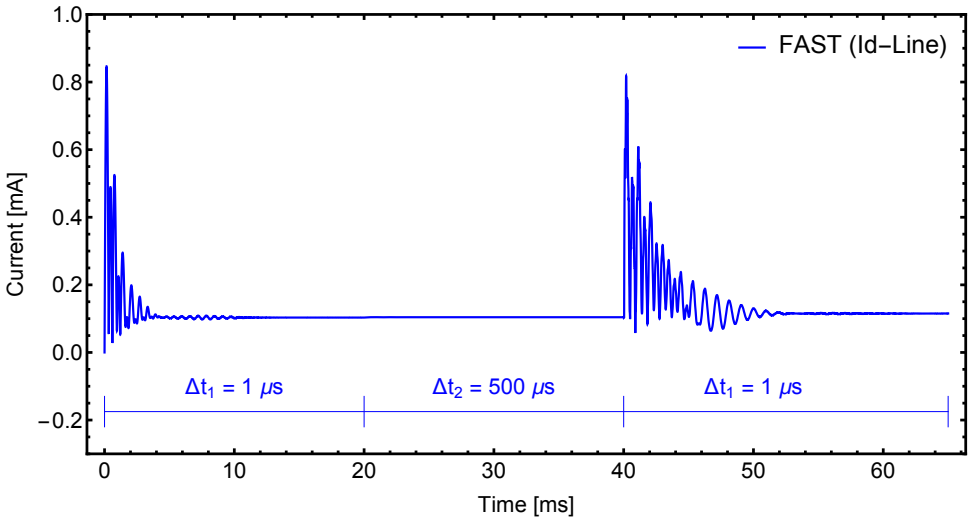


(b) Capacitor bank energization

Figure 3.32: Case #5: Simulated current at terminal # 1

The versatility of FAST technique, i.e., the transition between electromagnetic and electromechanical modes, allows one to change the time-step without any constraint regarding the new value. For instance, Fig. 3.33 shows an application in which the time-step varies from $\Delta t_1 = 1$ $\mu$s to $\Delta t_2 = 10$ ms and vice versa.

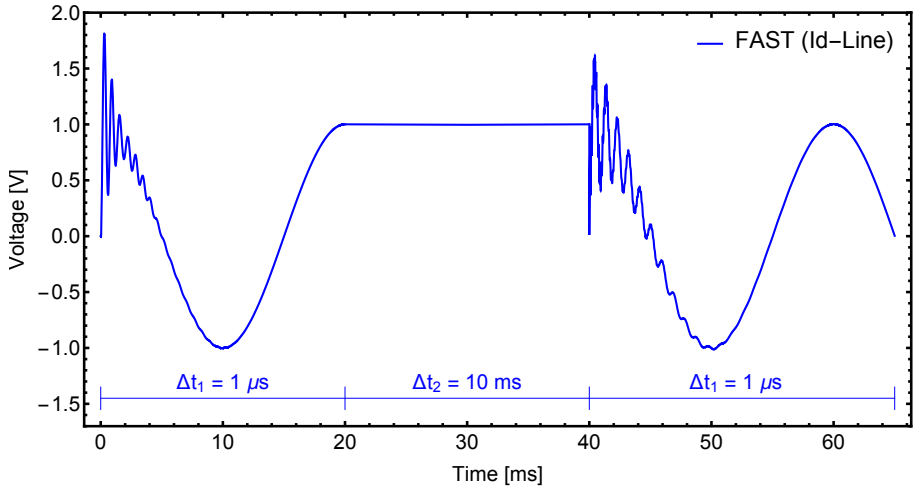


Figure 3.33: Case #5: Simulated voltage at terminal # 4

### 3.6.6 Case #6: HVDC Cable (FLE-Cable)

This test case aims to demonstrate the applicability of FAST for multiscale simulation of an admittance-based line model based on the FLE formulation (FLE–Cable). For the sake of clarity, the 2.5 km length 75 kV subsea cable configuration is depicted in Fig. 2.40. Further detail regarding the rational approximation of $\mathbf{Y}_{oc}$ and $\mathbf{Y}_{sc}$ matrices can be found in Fig. 2.41 of Section 2.6.6.

As already introduced in Section 2.6.6, the circuit of Fig. 3.34 depicts the system to be evaluated, i.e., a voltage source which is ramped up linearly to 1 V in 50 $\mu$s applied to the core conductor. The sheath and armour are bolted together as this is typically the practical scenario. An initial time-step $\Delta t_1 = 0.05$ $\mu$s is assumed and later it is increased to $\Delta t_2 = 5$ $\mu$s.

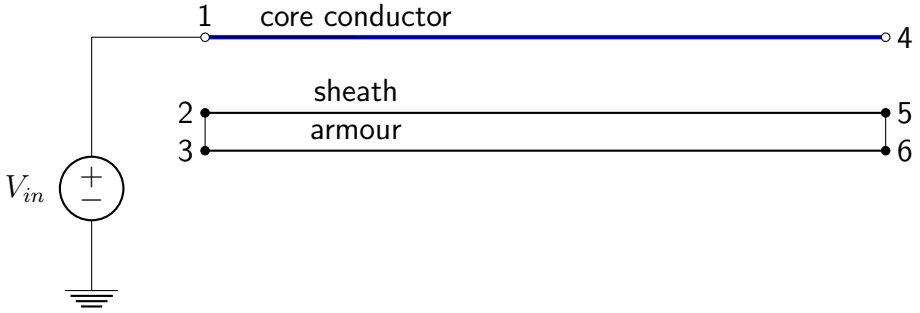


Figure 3.34: Case #6: Circuit for time-domain simulation

The simulated core and sheath voltages at the receiving end are depicted in Fig. 3.35 and the validation is done with the results obtained with the NLT algorithm which is an analytical approach that provides the exact solution. In a similar fashion, the current in the core conductor is shown in Fig. 3.36.

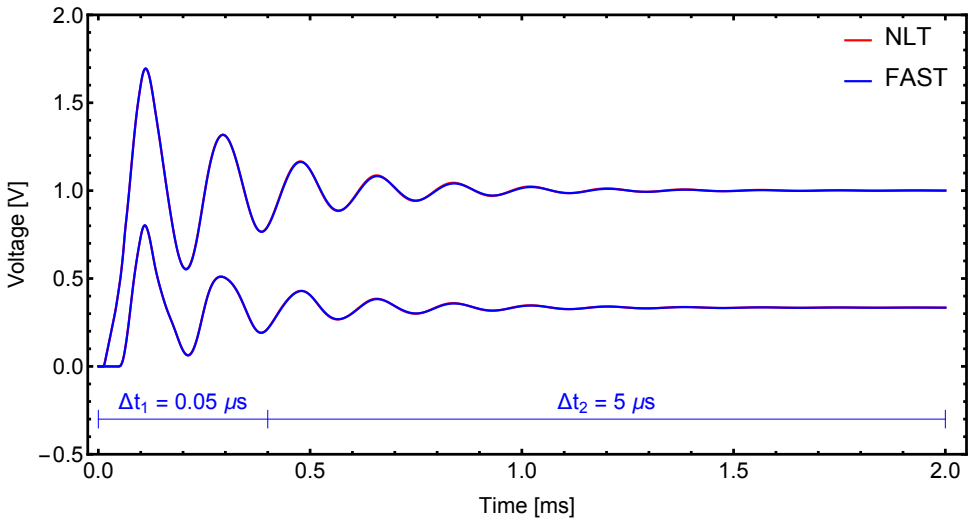


Figure 3.35: Case #6: Simulated core and sheath voltages

It can be verified in this special case involving a subsea cable that the proposed multiscale approach was able to reproduce the voltage and current profiles even with an increase of 100 times in the time-step before the variables reached their steady-state value without any discontinuity in the waveform. Here a larger initial time-step could be used instead. However, the evaluation aimed to demonstrate how flexible and efficient the novel reinitialization approach can be without restriction regarding the new time-step length.

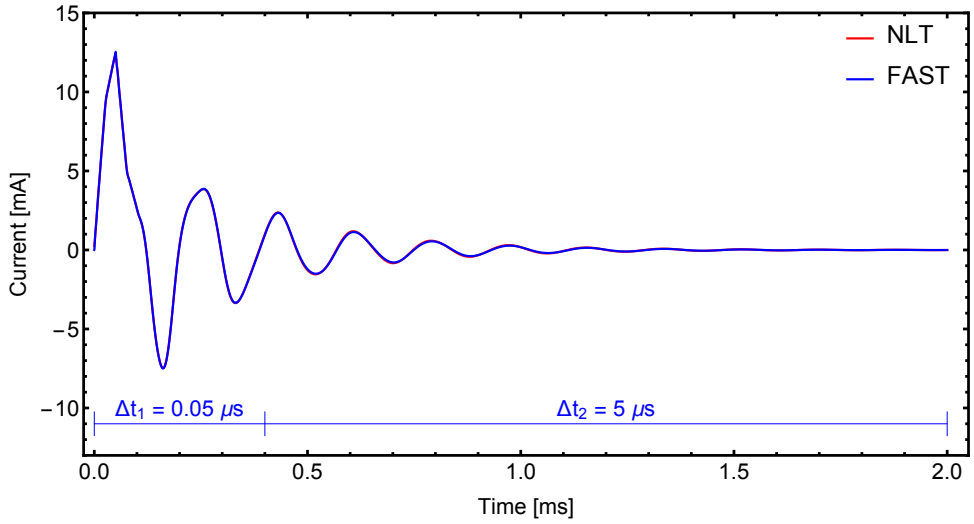


Figure 3.36: Case #6: Simulated current at terminal #1

In order to accelerate even more the simulation run, Fig. 3.37 and Fig. 3.38 show the versatility of the novel technique when the time-step is changed from $\Delta t_1 = 0.05$ $\mu$s to $\Delta t_2 = 2$ ms. Having the simulation run elapsed 8 ms, the time-step is reduced to 50 $\mu$s in order to simulate the transient behavior when the voltage source is ramped down to 0 V.

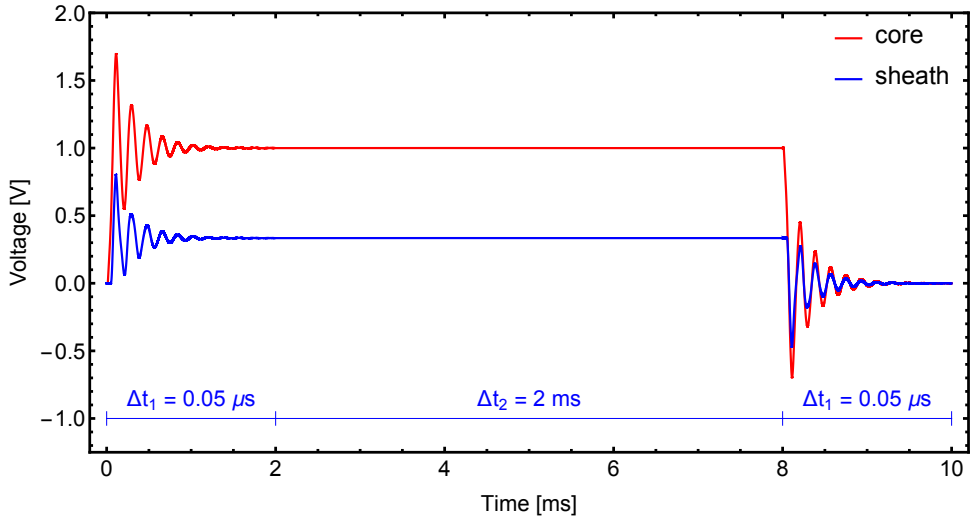


Figure 3.37: Case #6: Simulated core and sheath voltages

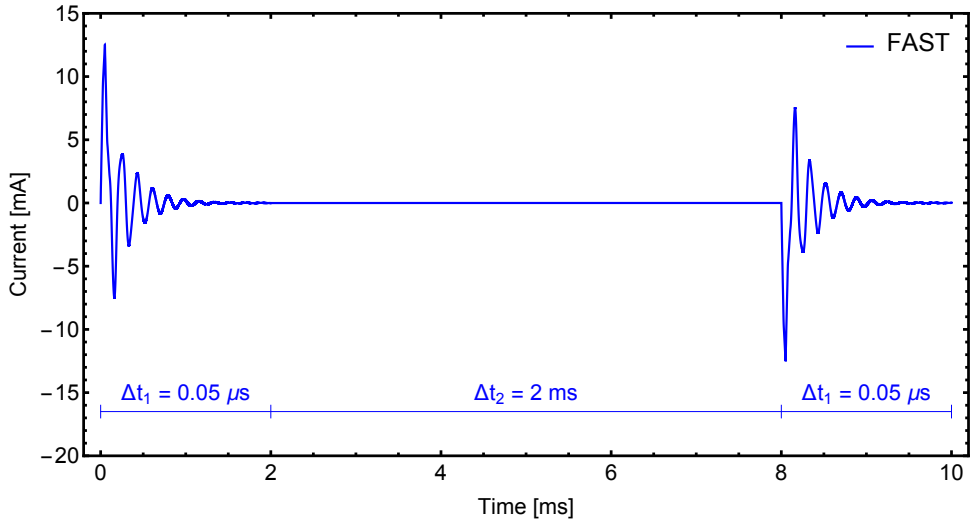


Figure 3.38: Case #6: Simulated current at terminal #1

## 3.7 Numerical Efficiency

The same finds highlighted in Section 2.7 in the modeling based on real variables apply in this complex framework stated as FAST. Besides the computation gains achieved with the multiscale simulation, it is noteworthy to mention the success in the development of frequency dependent models to be incorporated into transient stability simulations.

In a similar way, Table 3.1 depicts the computation time required in each test case regarding the computations performed with FAST. It can be noticed that the computation times with FAST is in general slightly higher than with the Multiple Time-Step (MTS) approach. The reason for such difference is explained by the fact that MTS deals with real variables while FAST handles complex variables.

Table 3.1: Computation time with FAST

| | PSCAD | ULM | Standard* | FAST | Reduction |
|---|---|---|---|---|---|
| Case #1 (RLC) | – | – | 0.235 s | 0.121 s | 48% |
| Case #2 (FDNE) | 30.69 s | – | 2.96 s | 1.82 s | 38% |
| Case #3 ($Y_n$–Line) | 1.65 s | 88 min | 10.43 s | 7.18 s | 31% |
| Case #4 (FLE–Line) | 1.65 s | 88 min | 10.86 s | 7.51 s | 31% |
| Case #5 (Id–Line) | 1.65 s | 88 min | 12.10 s | 8.61 s | 32% |
| Case #6 (FLE–Cable) | – | – | 17.05 s | 3.37 s | 80% |

* fixed time-step

For the sake of comparison, Fig. 3.39 presents the simulated voltage considering all three distinct formulations employed in the modeling of the OHL using FAST. The error of each formulation is shown in Fig. 3.40 from the results obtained using the ULM.

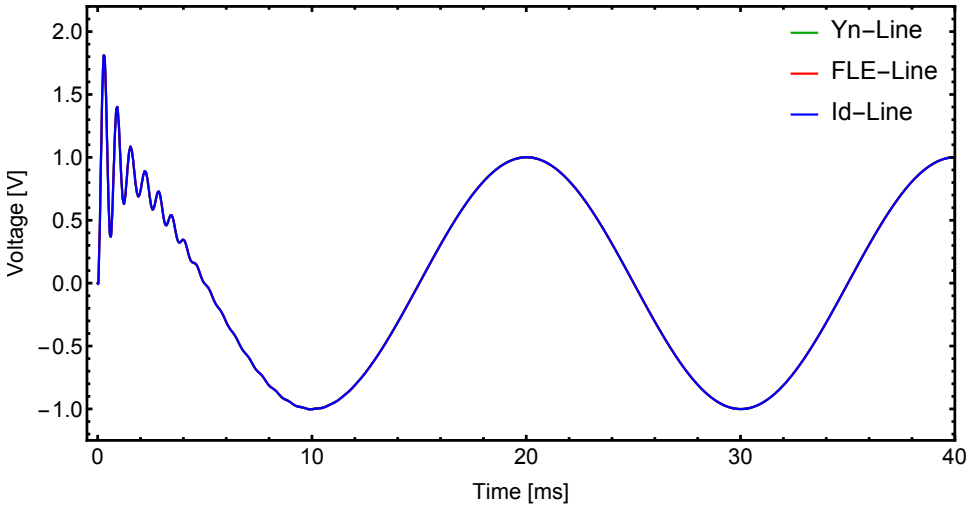


(a) Transmission line energization

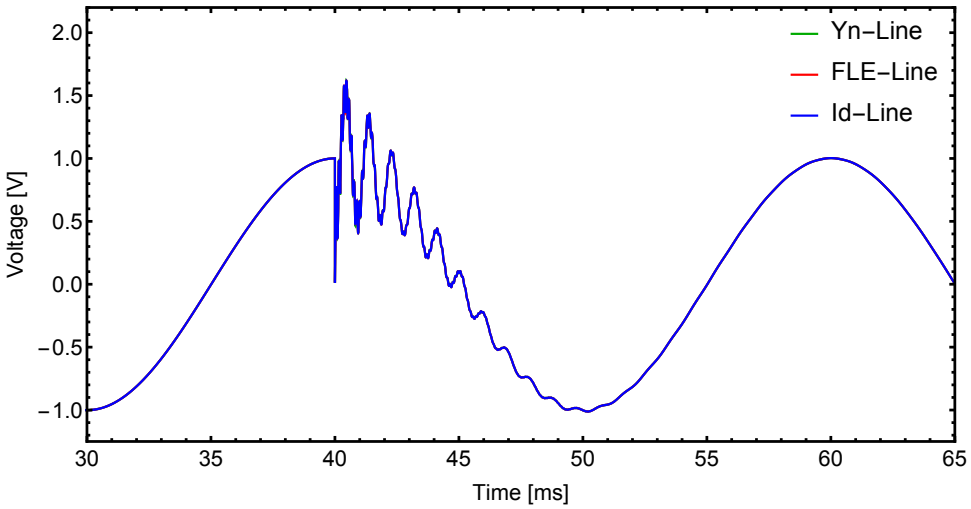


(b) Capaccitor bank energization

Figure 3.39: Comparison of the simulated voltage at terminal # 4 (OHL)

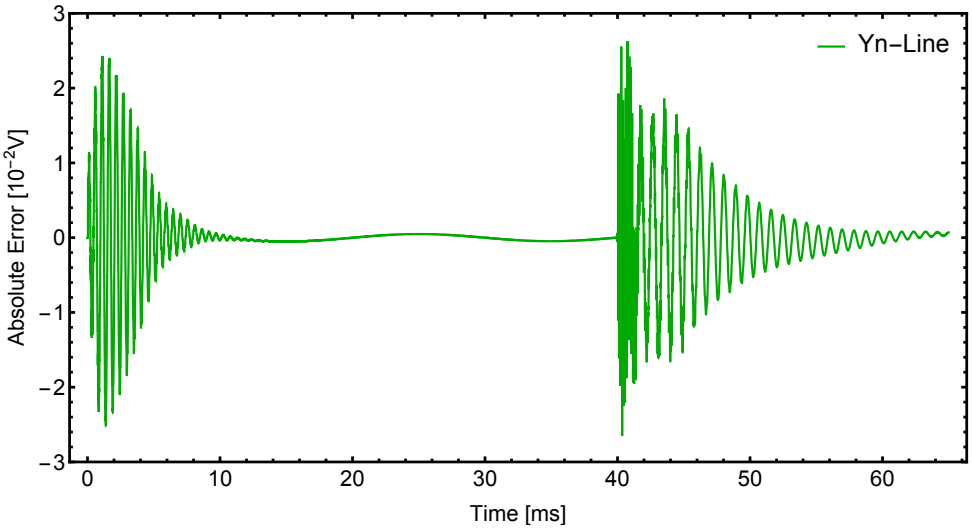


(a) Simulated voltage at terminal # 4

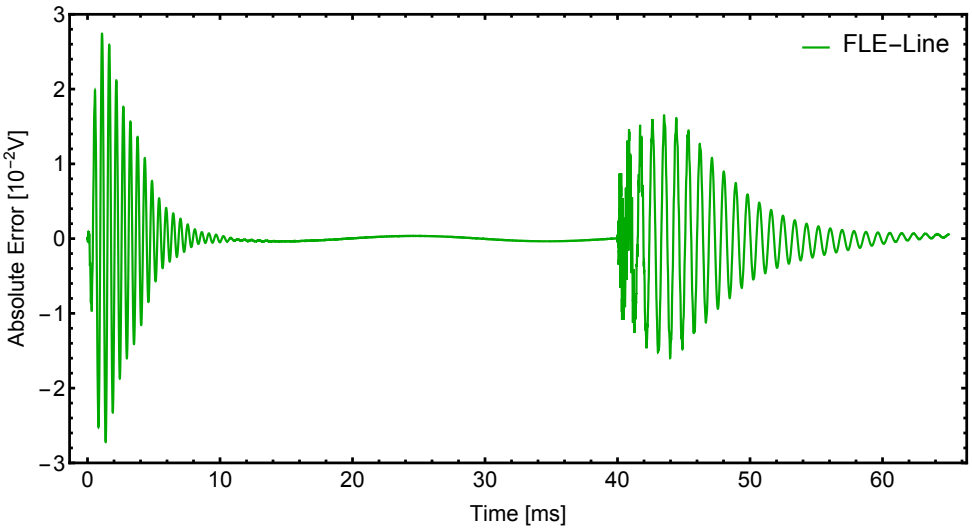


(b) Simulated voltage at terminal # 4

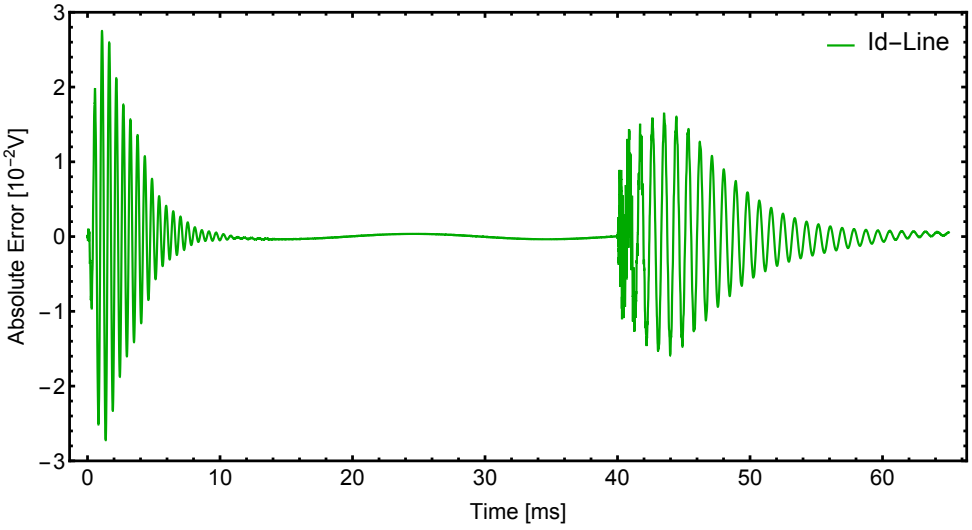


(c) Simulated voltage at terminal # 4

Figure 3.40: FAST approach: deviation from ULM simulation

## 3.8 Discussion

In this Chapter, the modeling of frequency dependent models using FAST concept was addressed. The designed reinitialization approach in Chapter 2 to face the time-step transition regarding the modeling using real variables was modified to include the frequency shifting in the trapezoidal integration rule and recursive convolution expressions. The novel intermediate step was introduced to maintain unchanged the state variables at the moment when the time-step is modified resulting in a rather distinct network admittance matrix, i.e., if one desires to perform EMT evaluations the network matrix is real; otherwise, for TS evaluations, it is complex. The designed companion network for time-domain simulations attained the same structure of the well-known Norton-type models used in EMTP-like programs just with small modifications to accommodate the frequency shifting.

The frequency dependent admittance-based models employed in this Chapter aimed to extend the contribution in the field of transmission lines with FAST started in [14] with a multiscale MoC-based model. However, the designed MoC line model is not a general approach as it cannot deal with underground/submarine cables which present a heavy frequency dependent transformation matrix and cannot consider the case of a full frequency dependent line model for large time-steps. Conversely, the fully-coupled admittance-based structure addressed in this research does not require a topological modification on the network matrix and hence holds the full frequency dependent feature for large time-steps

In the same way as the simulations performed for validation of the Multiple Time-Step (MTS) formulation in Chapter 2, the results achieved with FAST provided a sensible gain in the overall computation time. Regardless of the change in time-step length a smooth transition was achieved without a significant loss of accuracy. The major difference between MTS and FAST is that the former is confined to the analysis based on instantaneous variables and limited in the sense of the maximum time-step while the latter is able to process phasor-based variables without restriction for new time-steps. This feature highlights the versatility of this ultimate approach. The numerical accuracy of FAST and the issues concerned with passivity enforcement and time-domain simulations are the same as aforementioned in Section 2.8 of Chapter 2.

The employment of dynamic phasors, in the sense of a complex representation, seems to be a feasible solution for evaluations with power electronic converters. Contrary to the well-known averaging method [184], FAST can be used to provide a more accurate solution instead of approximations based on time-varying windows

# Chapter 4

# Multirate Simulation

One main characteristic of current EMTP-like programs is the usage of a single time-step in the solution of the whole network. This often leads to an unnecessary large simulation time compared with a scheme in which a small part of the network could be solved using a small time-step and the remaining network could be solved with a larger time-step. Stated as Latency concept, the idea of an implicit decoupling or partitioning of a given network exhibiting a wide variety of time constants is evaluated to perform multirate simulations.

In the present Chapter, the so-called multirate simulation is addressed to exploit latency in the modeling of frequency dependent admittance-based models. The resulting Norton-type companion network is assembled in a distinct way in accordance with a novel concept defined as Multiple Companion Networks (MCN). By relaxing some coefficients used in the discrete time equivalent with the aid of a model decomposition using the Folded Line Equivalent (FLE), a relaxed version of MCNR rearranges how latency is exploited in the MCN in order to overcome the limitation found in the earlier approach.

Time-domain evaluations performed with frequency dependent admittance-based models for transmission line modeling demonstrate that the improvements introduced with the novel MCN approach provides a more efficient realization with substantial gains in the overall computation time without significant loss of accuracy.

## 4.1 Introduction

Electromagnetic transient programs allowed for a rapid and wide development of time-domain models for linear, nonlinear and frequency dependent devices. One alternative technique to improve the numerical performance of fixed time-step simulation tools and to overcome the unnecessary computation time is to rely on the concept of latency exploitation. In latency [23, 24, 158] the network is divided into at least two sub-networks. The first one associated with the fastest time-constants is solved using a small time-step while a larger time-step is used to solve the other part of the network. Naturally, the number of network subdivisions can increase leading to several sub-networks, each being solved with a given time-step. For this reason, latency exploitation may also be called multirate simulation.

To avoid the drawbacks of frequency dependent models which are based on the method of characteristics (MoC), as highlighted in Section 2.3.1, the rational approximation of the nodal admittance matrix $\mathbf{Y}_n$ in phase-coordinates can be employed in the modeling of transmission lines and network equivalents. However, as pointed out in [89], the direct fitting of $\mathbf{Y}_n$ is not so general and suitable for admittance-based models since the smallest eigenvalues at the low-frequency range may not be properly fitted leading to rather inaccurate time-domain responses. This limitation can be overcome with the use of the folded line equivalent (FLE) model introduced in [89].

Alternatively to the so-called Multi-Area Thevenin Equivalents (MATE) [27–34], that adopts the network tearing formulation in a similar fashion to Diakoptics [37], two distinct approaches based on Norton-type companion networks are introduced. Stated as Multiple Companion Networks (MCN) and Relaxed Multiple Companion Networks (MCNR) formulations, they provide the development of accurate and efficient methods for the rational approximation of frequency dependent models to be incorporated into EMTP-like programs in a simple and straightforward way.

## 4.2 Multiple Companion Networks

A distinct scheme for time-domain simulations of frequency dependent admittance-based models is proposed using the concept defined as Multiple Companion Networks (MCN). As it is based on companion networks, i.e., Norton equivalents, it does not require a series link to connect the "fast"part of the network with the one with "slow"dynamics like in MATE concept. It can deal with networks without "tearing"it in parts.

The idea behind MCN can be understood as a dual implementation of MATE without demanding a link to interconnect the fast and slow parts of the network. In MATE the structure is essentially the one shown in Fig. 4.1. A series element is needed to connect both networks and interpolation of the historic voltage source may be needed.

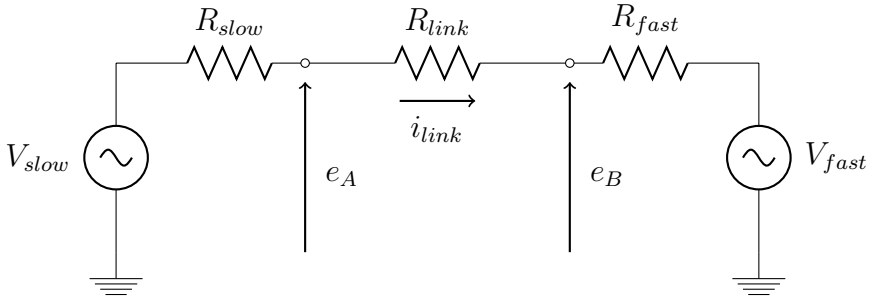


Figure 4.1: Basic structure of MATE algorithm

In MCN the advantage of the companion network realization of convolution-based models is contemplated. The rational model of $\mathbf{Y}_n$ is divided in two parts each being implemented as an independent Norton equivalent as in (4.1), hence the name MCN. Using recursive convolution or trapezoidal integration allows the model to be connected to any EMTP-type program equivalent [68, 90, 139].

$$\mathbf{Y}_n \approx \sum_{n=1}^{N_{fast}} \frac{\mathbf{R}^n_{fast}}{s - p^n_{fast}} + \sum_{n=1}^{N_{slow}} \frac{\mathbf{R}^n_{slow}}{s - p^n_{slow}} + \mathbf{Y}_c(\infty) \tag{4.1}$$

where $p^n$ is a set of common poles, either real or complex conjugate, $\mathbf{R}^n$ is the residue matrices and $\mathbf{Y}_c(\infty) = \mathbf{G}(\infty)$, i.e., the real part of the characteristic admittance matrix at infinite frequency.

In the discretization process both fast and slow subnetworks will create an equivalent conductance that can be directly inserted in the system nodal admittance matrix before entering the time-step loop. The current source associated with the slow poles is only updated every $k^{th}$ time-step while the one associated with the fast mode is updated every time-step, with $k$ being a natural number, as depicted in Fig. 4.2.

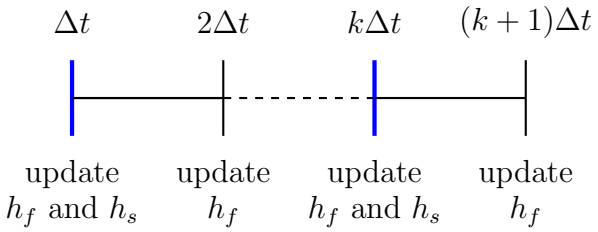


Figure 4.2: Time-line for updating current sources in MCN

To illustrate this procedure consider a simple $RL$ parallel circuit as shown in Fig. 4.3a, where $R_f$, $L_f$ stands for the branch with the fast dynamics, i.e., small time-constant to be solved using a small time-step $\Delta t_1$ and $R_s$, $L_s$ is the branch with the slow dynamics, i.e., larger time-constant which can be solved with a time-step $\Delta t_2 = k\,\Delta t_1$ with $k > 1$ and $k \in \mathbb{N}$.

Using MCN leads to the discrete time equivalent shown in Fig. 4.3b, where $G_f$ is the equivalent conductance obtained using the smaller time-step $\Delta t_1$ and the same can be said about the history current source $h_f(t)$, $G_s$ and $h_s(t)$ are the elements of the discrete circuit obtained using $\Delta t_2$. Both $G_s$ and $G_f$ are added to the system nodal conductance matrix. The updating of the history current sources is distinct though. The one associated with the smaller time-step, i.e., $h_f(t)$, is updated at every time-step while $h_s(t)$ is updated only every $k^{th}$ time-step.

For instance, suppose that for the $RL$-parallel circuit shown in Fig. 4.3a the "fast branch" has a time-constant of 100 $\mu$s, thus being solved with $\Delta t_1 = 10\,\mu$s, while the "slow branch" has a time-constant of 10 ms, which could be solved with $\Delta t_2 = 1\,$ms, i.e., $k = 100$.

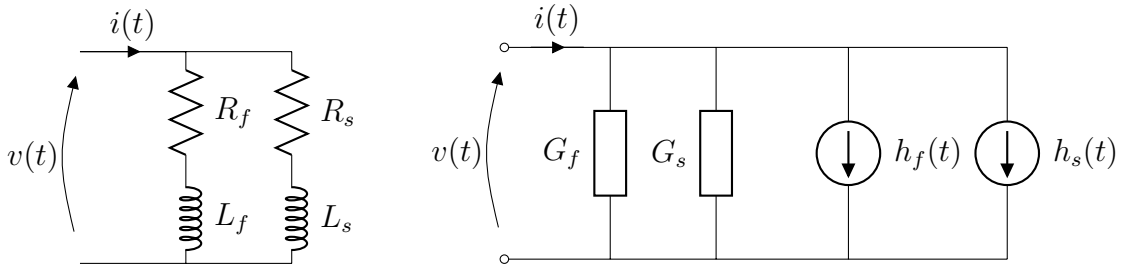


(a) actual circuit (b) discrete-time equivalent

Figure 4.3: Parallel $RL$ circuit to illustrate latency exploitation

## 4.3 Relaxed Multiple Companion Networks

To overcome the limitation in the original scheme of MCN for $k \geq 10$, as it will be shown in Section 4.4.1, a modified version is proposed, i.e, MCNM, which is suitable to overcome the small $k$ limitation without significant loss of accuracy. To explain this in further details, the implementation of convolution-based models must be considered.

Let a pole-residue model in which the set of differential equations resembles the $RL$-parallel circuit shown in Fig. 4.3a. In the time discrete equivalent by means of recursive convolution or trapezoidal integration, the history current sources are updated as

$$\begin{aligned} h_f(t) &= \alpha_f\, h_f(t-\Delta t) + c_f\, v(t-\Delta t) \\ h_s(t) &= \alpha_s\, h_s(t-\Delta t) + c_s\, v(t-\Delta t) \end{aligned} \tag{4.2}$$

where the coefficients $\alpha_f$, $\alpha_s$, $c_f$ and $c_s$ are the same as defined in Appendix A. In its original formulation, $h_f(t)$ is discretized using $\Delta t_1$ while $h_s(t)$ is updated using $\Delta t_2 = k\,\Delta t_1$ every $k^{th}$ time-step, as depicted in Fig. 4.2. In the modified approach, both $h_f$ and $h_s$ are discretized using the same time-step $\Delta t_1$. At every $k^{th}$ time-step, $h_f$ and $h_s$ are updated using (4.2) otherwise $h_s$ is updated by (4.3)

$$h_s(t) = h_s(t-\Delta t) + c_s\, v(t-\Delta t) \tag{4.3}$$

The following pseudo-code illustrates this procedure and Fig. 4.4 highlights the updating process for the current sources in the modified version of MCN.

```
= = = = = = = Modified MCN = = = = = = =
for n = 2:k:100
    hf(n) = alpha_f*hf(n-1) + c*v(n-1)
    hs(n) = alpha_s*hs(n-1) + c*v(n-1)
    htotal(n) = hf(n) + hs(n)
    // update right hand side //
    RHS = [htotal(n) Sv]
    sol(n) = solve(Yaugmented,RHS)
for n = n+1:n+k-1
    hf(n) = alpha_f*hf(n-1) + c*v(n-1)
    hs(n) = hs(n-1) + c*v(n-1)
    htotal(n) = hf(n) + hs(n)
    // update right hand side //
    RHS = [htotal(n) Sv]
    sol(n) = solve(Yaugmented,RHS)
```

```
end
end
```

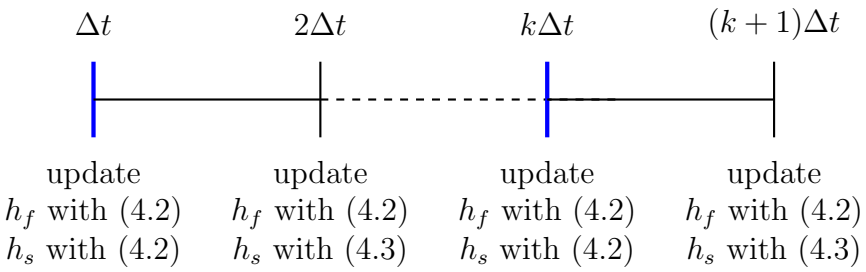


Figure 4.4: Time-line for updating current sources in MCNM

In the original approach, the slow poles were assumed to be the real ones. When implementing the modified approach to MCN, it was found that mostly slow current history sources were associated with alpha close to unity. Thus, the criteria for assignment of the slow poles was enhanced to a threshold value of $\alpha \geq 0.99$. This led to the relaxed version of the MCN, i.e., MCNR, in which $h_s$ uses (4.3) at every time-step. The following pseudo-code illustrates this procedure and Fig. 4.5 illustrates the updating process for the current sources in the relaxed version of MCN.

```
= = = = = = = Relaxed MCN = = = = = = =
for n = 2:100
    hf(n) = alpha_f*hf(n-1) + c*v(n-1)
    hs(n) = hs(n-1) + c*v(n-1)
    htotal(n) = hf(n) + hs(n)
    // update right hand side //
    RHS = [htotal(n) Sv]
    sol(n) = solve(Yaugmented,RHS)
end
```

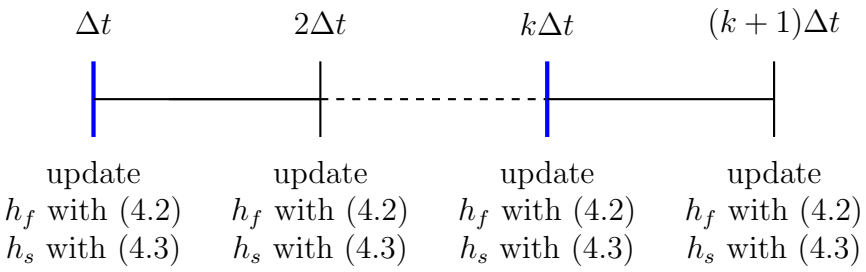


Figure 4.5: Time-line for updating current sources in MCNR

To illustrate the numerical performance of both approaches, consider again the simple circuit in Fig. 4.3a, assuming that a step voltage is applied at $t = 0$ s and the modified version of MCN is used to obtain the injected current. The slow branch is represented by the following admittances,

$$y_s(s) = \frac{10}{s + 100} \tag{4.4}$$

while the fast branch has

$$y_f(s) = \frac{400}{s + 10^4} \tag{4.5}$$

The faster time-step is $\Delta t_1 = 10\,\mu$s and the slow one is $\Delta t_2 = 500\,\Delta t_1$. The result is depicted in Fig. 4.6, considering both approaches of MCN, i.e., the modified and relaxed MCN. It can be noticed that all results are in very close agreement despite the large difference between the time-steps.

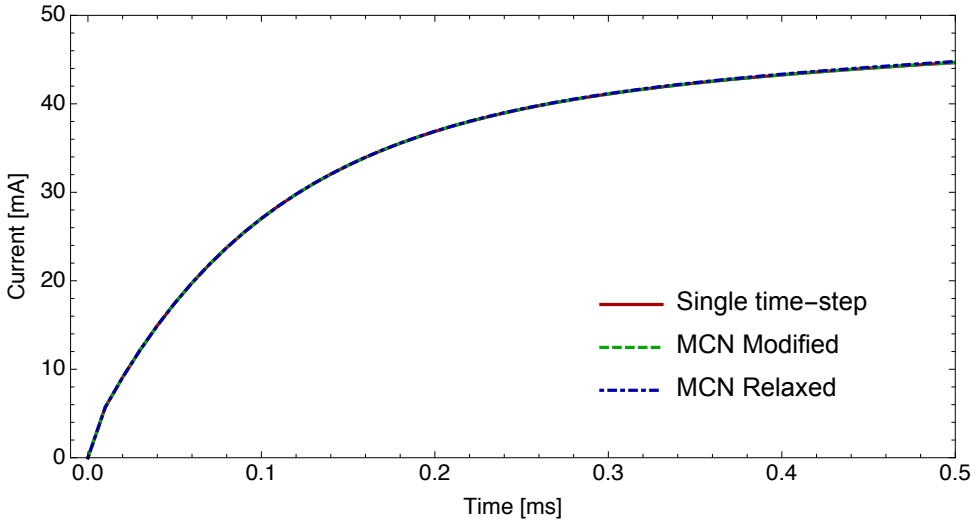


Figure 4.6: Injected current in a RL parallel circuit

As pointed out in [89], the direct fitting of the nodal admittance matrix is not suitable for a general transmission line model as the smallest eigenvalues at the low-frequency range may not be properly fitted leading to inaccurate responses. The limitation associated with the direct fitting can be overcome with the use of the Folded Line Equivalent (FLE) model, in accordance with Section 2.3.3.

## 4.4 Test Cases

For the assessment of the accuracy and numerical performance of MCN and MCNR modeling, a set of test cases has been considered, namely:

1. #1: a 230 kV, 10 km long overhead line (MCN).
2. #2: a 132 kV, 300 m long overhead line (MCNR).
3. #3: a 132 kV, 10 km long overhead line (MCNR).
4. #4: a 500 kV, 50 km long double-circuit overhead line (MCNR).

The geometry of the above transmission lines is shown in Fig. 4.7 along with the conductors data. All configurations assumed ground wires to be continuously grounded and hence eliminated by means of Kron reduction.

In test case #1 the MCN approach is to be addressed in order to verify the accuracy and validation range of ratio $k$ in the modeling of a FDNE described from the frequency response of an untransposed overhead line. Next, the enhancement of MCN, i.e., MCNR, is investigated using one example taken from the original FLE paper [89] in test case #2. Test case #3 considers the same line geometry with a different length instead. Finally, test case #4 investigates the feasibility of the proposed formulation for a highly coupled configuration.

The time-domain simulations were carried out with *Mathematica* using the modified nodal analysis as in [157], based on the approach of the MatEMTP [178]. Furthermore, the conventional MCN, the FLE and the MCNR approach considered the order reduction scheme proposed in [90], which in the case of a complex conjugate pair, only one is used with the associated residue being multiplied by a factor of 2 and the imaginary part of the response associated with the pole being disregarded. This gives a close to 50% reduction in computation time for models with mainly complex poles [191].

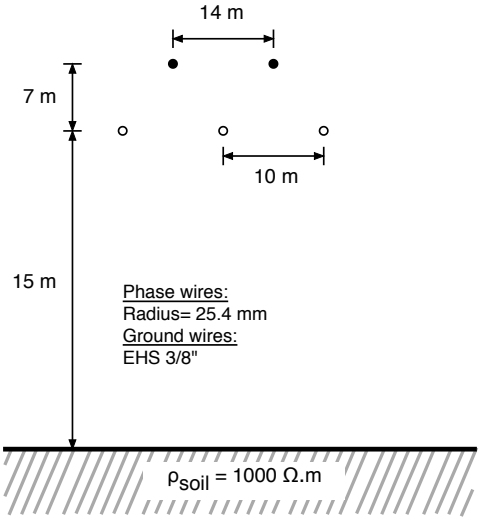


(a) 230 kV transmission line geometry

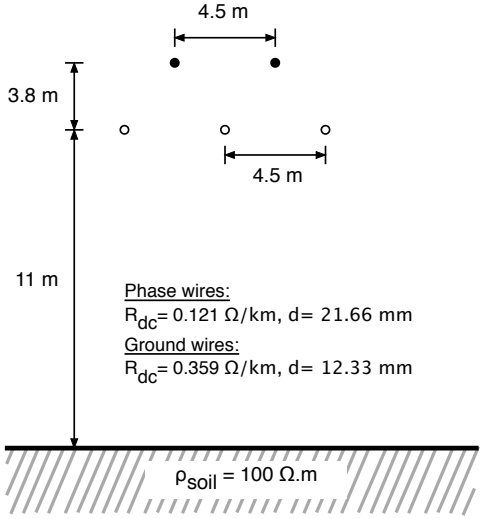


(b) 132 kV transmission line geometry

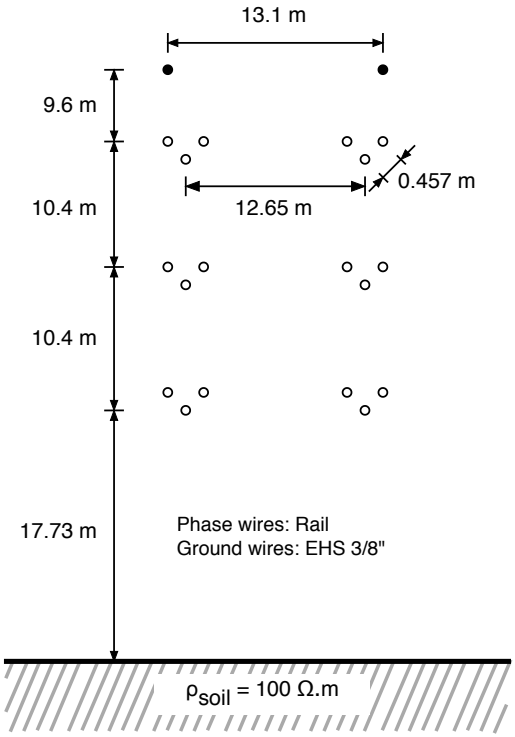


(c) 500 kV transmission line geometry

Figure 4.7: System geometry

### 4.4.1 Case #1: LT 230 kV - 10 km (MCN)

The MCN approach is going to be applied in this test case comprising a 230 kV overhead line with a length of 10 km. The geometry is shown in Fig. 4.7a and it consists in an untransposed flat configuration with ground wires continuously grounded.

The nodal admittance of a transmission line is obtained in a similar fashion shown in Section 2.3.2 and, as in the case of a uniform line, the structure of $\mathbf{Y}_n$ is symmetric and resembles the description of a FDNE. Using a combination of linearly and logarithmically spaced samples between 1 Hz and 50 kHz, an accurate fitting with VF routine was obtained using 54 poles, with 20 poles being real.

One key point in latency exploitation is the definition of the slow and fast parts of the network. A discussion of some of this issue is found in [29]. When rational modeling is considered, the division of the network is essentially straightforward. As real and complex poles are involved, it was postulated that the slow part of the network may only deal with real poles. The tests carried out indicate that the real poles can be realized with a higher time-step. It was assumed that fast poles present high frequency components thus requiring complex conjugate poles.

For a time-domain evaluation, consider the case of an open circuit test. A step voltage is applied at one of the phases at the sending end while the other phases are grounded via a very small resistance. All phases are open at the receiving end. The transmission line is modeled as a black-box model as shown in Fig. 4.8.

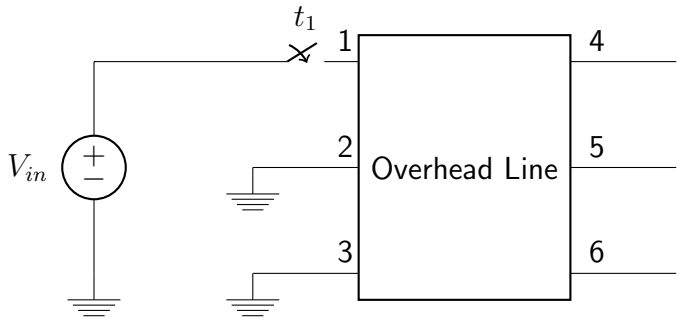


Figure 4.8: Case #1: Circuit for time-domain simulation

In Fig. 4.9 the voltage at terminals 4, 5 and 6 are shown when the FDNE is modeled as a single companion network like the common procedure adopted in EMTP-like programs. Due to the finite frequency band of the FDNE, the time-domain responses are prone to Gibbs oscillation. To avoid these oscillations, one may resort to a filter as shown in [121].

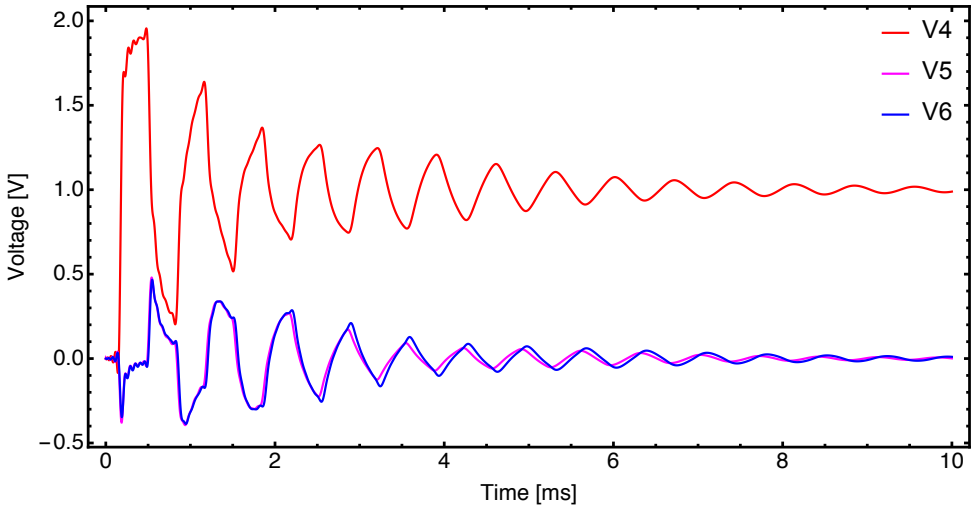


Figure 4.9: Case #1: Simulated voltage at receiving end terminals

In this research, the MCN approach was used to investigate the maximum number of poles associated with the slow subnetwork as well as the maximum ratio $k$ between the slow and fast time-steps. The absolute value of the largest mismatch as a function of the number of poles in the slow part of the network was found for diverse values of $k$ and the number of poles as part of the slow subnetwork either real or complex. It was possible to note that the error is basically monotonically increasing whenever only real poles are considered. If complex poles are considered in the slow part of the network a decrease in the mismatch is found. This result seems to indicate that it is possible to mix real and complex poles in the slow part of the network. Probably a distinct division of the network using only a few real poles and the low frequency complex poles might give an accurate response as well. It could be seen that the mismatch is not heavily affected by this change in $k$. However, as $k$ increases, there is a significant change in the maximum error found. Fig. 4.10 summarizes these findings where it can be seen that as the number of poles in the slow part of the network increases there is a considerable rise in the maximum error for $k \geq 10$.

Table 4.1 summarizes the numerical performance of the MCN considering different number of slow poles and for $k = 5$ and $k = 10$. Despite the increase in the error, with a higher number of poles in the slow part of the network there is also an increment in the numerical performance of the MCN. There is a clear tradeoff between accuracy and the number of poles in the slow part of the network and the ratio between the time-steps of the slow and fast parts of the network. For an accurate modeling of the network the computational gain was around 15%.

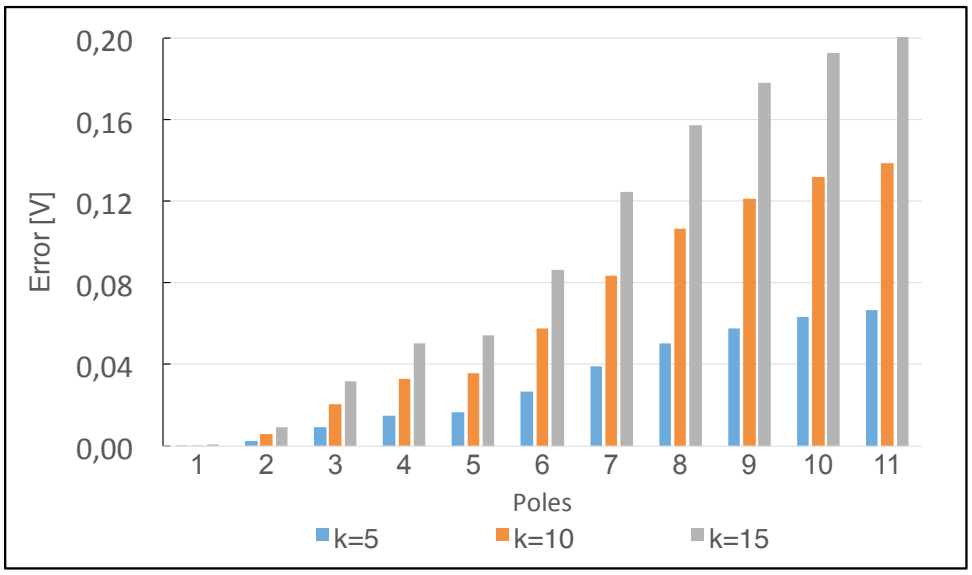


Figure 4.10: Maximum error found as a function of the number of poles in the slow part of the network and the ratio $k$

Table 4.1: Computation time (s)

| # of slow poles | k=5 | k=10 |
|---|---|---|
| 1 | 13.941769 | 13.796345 |
| 2 | 13.859429 | 13.510032 |
| 4 | 13.298749 | 13.152875 |
| 10 | 12.190794 | 11.803534 |
| 12 | 11.815353 | 11.455727 |
| 14 | 11.336278 | 10.957989 |
| 16 | 11.034261 | 10.452221 |
| 18 | 10.492678 | 10.154645 |
| 20 | 10.259190 | 9.584601 |

### 4.4.2 Case #2: LT 132 kV - 300m (MCNR)

This test case aims to demonstrate the applicability of the relaxed version of MCN approach, i.e, MCNR, for simulation of frequency dependent lines. The 132 kV overhead line to be considered here is depicted in Fig. 4.7b, the same configuration considered in [89].

The elements of the nodal admittance matrix $\mathbf{Y}_n$ are presented in Fig.4.11 and since this line length presents a natural resonance frequency around 250 kHz, the frequency sweep was in the range of 0.01 Hz to 1 MHz in order to obtain the data to be subjected to rational approximation with the *Vector Fitting* routine.

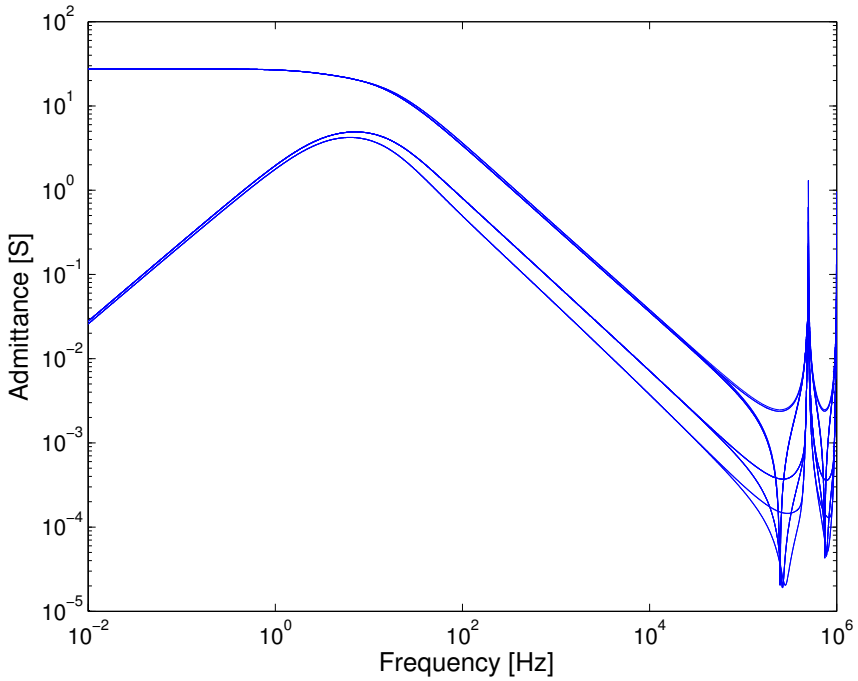


Figure 4.11: Case #2: Elements of $\mathbf{Y}_n$

As depicted in Section 2.3.3, $\mathbf{Y}_n$ is decomposed into an open-circuit and short-circuit counterparts, namely, $\mathbf{Y}_{oc}$ and $\mathbf{Y}_{sc}$, respectively, and Fig. 4.12a shows the fitting results for both. 16 poles were used for $\mathbf{Y}_{oc}$ and 20 poles for $\mathbf{Y}_{sc}$. A comparison between the fitted eigenvalues and the ones obtained directly from $\mathbf{Y}_n$ is depicted in Fig. 4.12b.

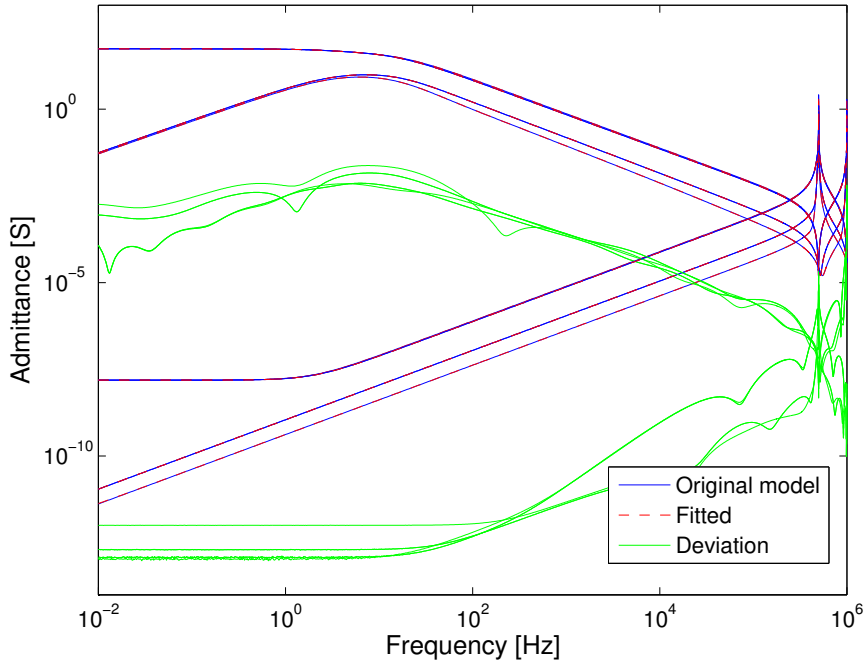


(a) Fitting of $\mathbf{Y}_{oc}$ and $\mathbf{Y}_{sc}$

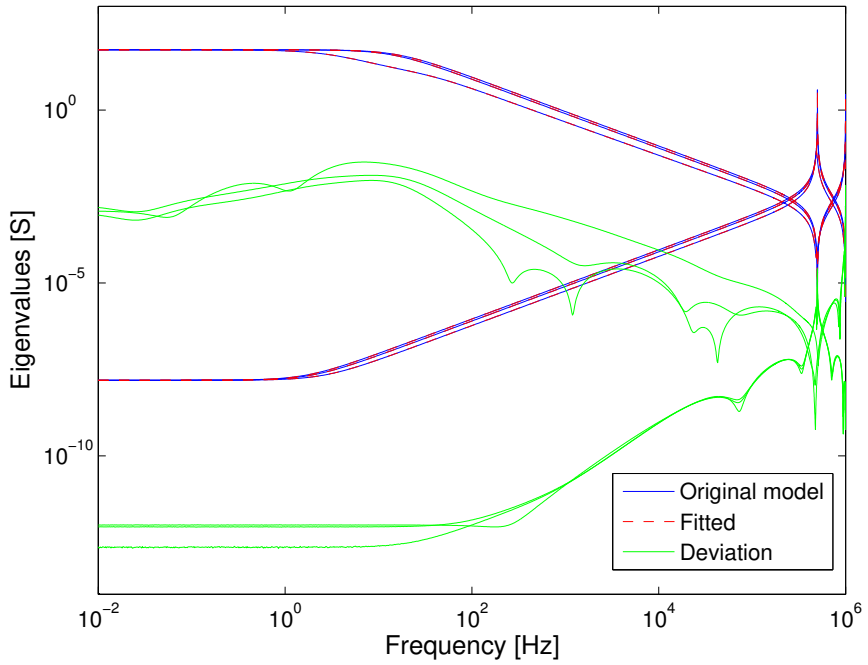


(b) Eigenvalues of $\mathbf{Y}_{oc}$, $\mathbf{Y}_{sc}$ and $\mathbf{Y}_{n}$

Figure 4.12: Case #2: Fitting results (300 m overhead line)

The choice of slow and fast poles were carried out as follows. First, only real poles in the rational approximation of $\mathbf{Y}_{oc}$ and $\mathbf{Y}_{sc}$ were allowed to be considered as slow. As the main goal is to speed up the overall simulation time, those poles that presented a discrete time counterpart close to one were considered to be slow, more precisely, $\alpha \geq 0.99$ was the threshold adopted in the sorting between fast and slow poles. At this time, all complex conjugate pairs of poles were treated as fast poles. This criterion led to the rational approximation of $\mathbf{Y}_{oc}$ presenting no slow poles while 10 poles out of the 16 poles used in the rational approximation of $\mathbf{Y}_{sc}$ can be treated as slow poles.

To illustrate the proposed formulation for the given rational model, this first test case aims to reproduce the results of the original FLE paper [89] and the circuit for this time-domain simulation is depicted in Fig. 4.13. In order to evaluate the multirate model, a three phase energization at $t_1 = 0$ is performed followed by a single phase fault at $t_2 = 0.5$ ms. The short-circuit reactance is considered by means of an inductance $L = 110$ mH and the adopted time-step is $\Delta t = 1$ $\mu$s.

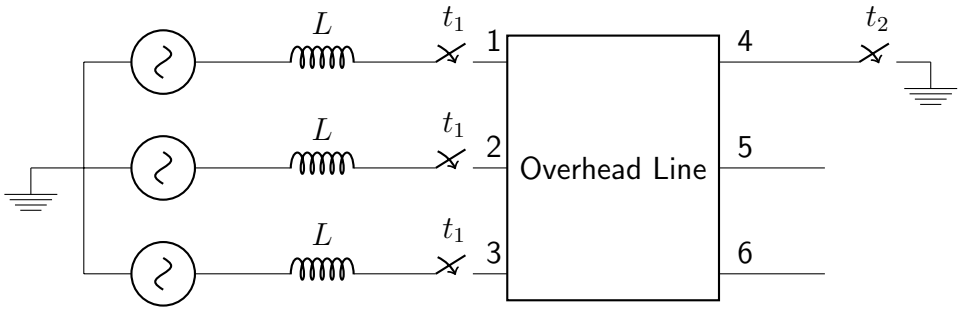


Figure 4.13: Case #2: Circuit for time-domain simulation

Fig. 4.14 shows the time response for voltage at the receiving end of the faulted and one unfaulted phases, i.e., terminals #4 and #5. It is noticeable that when the single phase fault occurs, it provokes a resonance that affects all the other phases. Even with the switching occurring when the voltage at terminal #4 is close to a peak value, the comparison with the results obtained with the FLE model highlights that a very accurate result is attained.

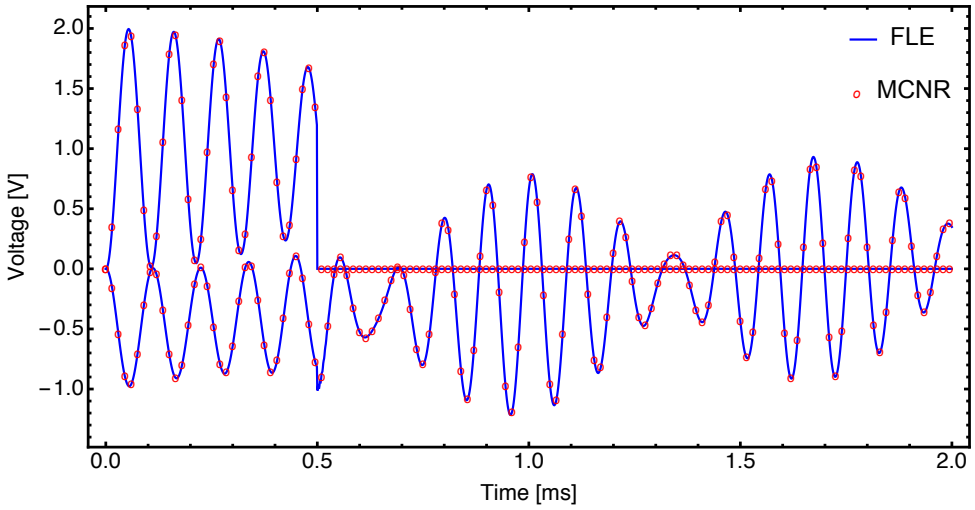


Figure 4.14: Case #2: Simulated voltage at terminals # 4 and # 5

To illustrate the simulated current profile, Fig. 4.15 presents the injected current at terminal #3. The results demonstrate a very close agreement between results obtained using the conventional FLE and MCNR. Besides providing a simulation without significant loss of accuracy, the proposed methodology reduces considerably the computational burden. The speed up of the simulation time due to using MCNR was close to 35 %.

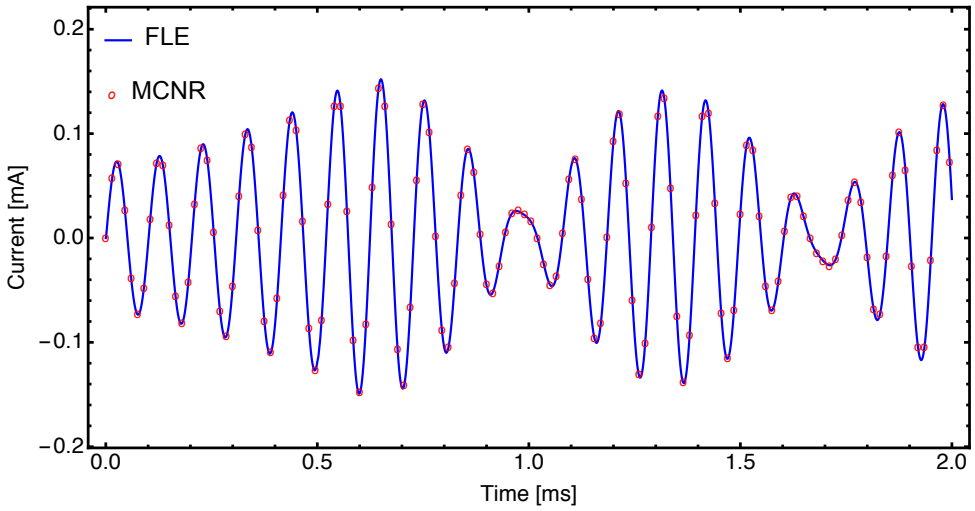


Figure 4.15: Case #2: Simulated current at terminal # 3

### 4.4.3 Case #3: LT 132 kV - 10 km (MCNR)

This test case aims to demonstrate the applicability of MCNR approach for the same overhead line geometry as before with a length of 10 km instead. For convenience, the configuration of this 132 kV overhead line is depicted in Fig. 4.7b.

The elements of the nodal admittance matrix $\mathbf{Y}_n$ are presented in Fig.4.16 and since this line length presents a natural resonance frequency around 7.5 kHz, the frequency sweep was in the range of 0.01 Hz to 150 kHz in order to obtain the data to be subjected to rational approximation with the *Vector Fitting* routine.

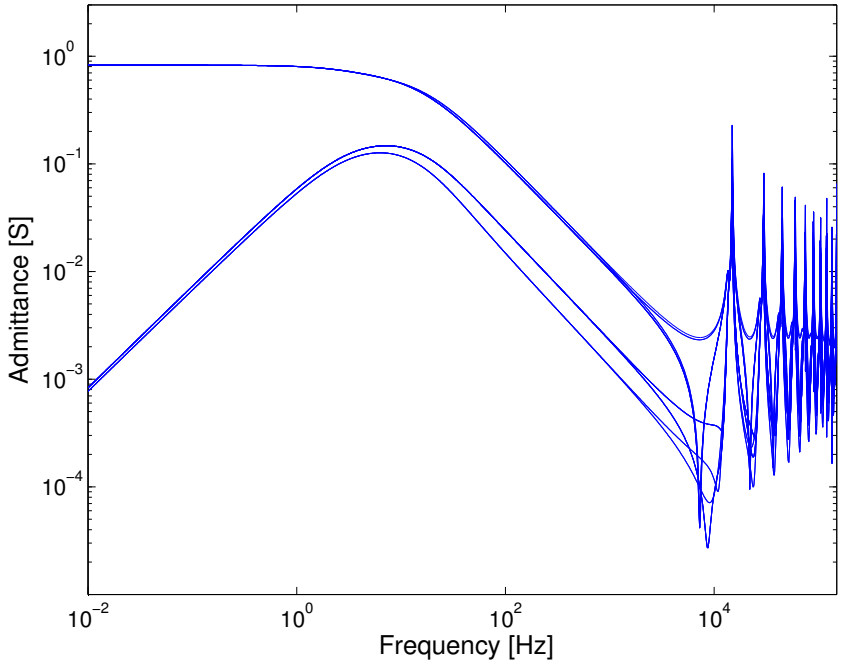


Figure 4.16: Case #3: Elements of $\mathbf{Y}_n$

The rational approximation of $\mathbf{Y}_{oc}$ and $\mathbf{Y}_{sc}$ is presented in Fig. 4.17a. The passive model was achieved using 38 poles for $\mathbf{Y}_{oc}$ and 50 poles for $\mathbf{Y}_{sc}$ with the corresponding eigenvalues depicted in Fig. 4.17b. It is noteworthy that despite the higher number of resonance peeks and valleys, a high accuracy is attained in all frequency range for this line configuration.

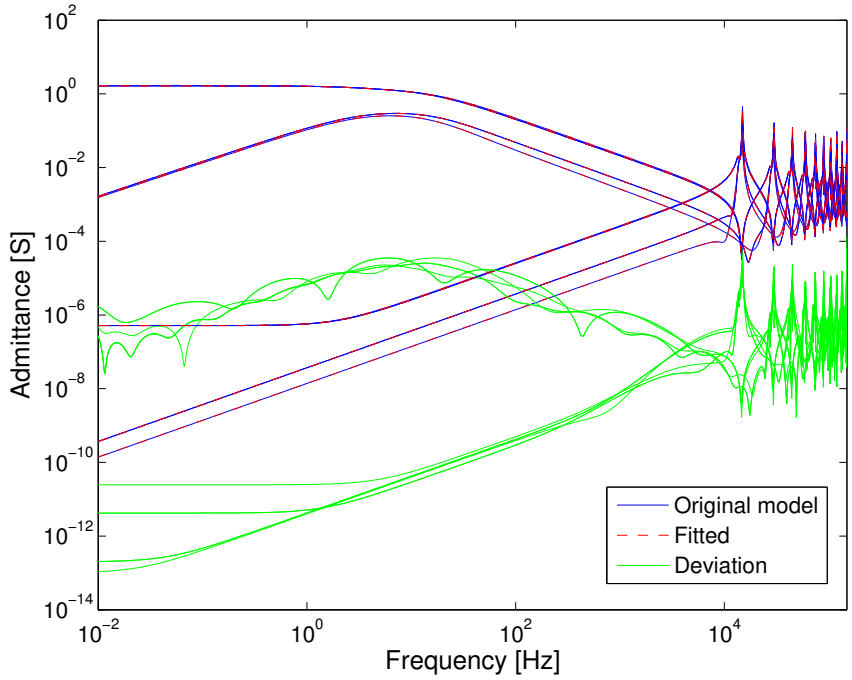


(a) Fitting of $\mathbf{Y}_{oc}$ and $\mathbf{Y}_{sc}$

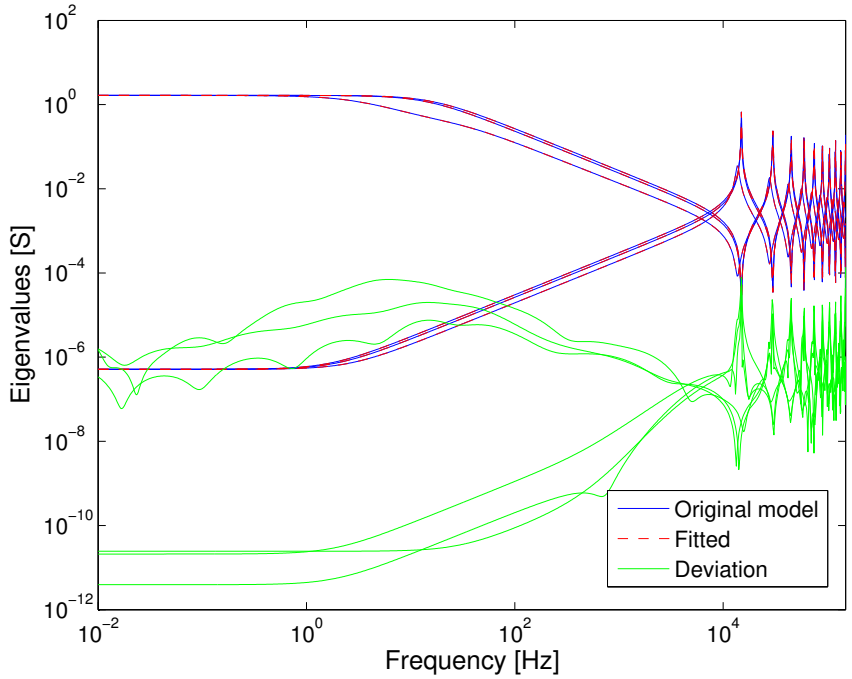


(b) Eigenvalues of $\mathbf{Y}_{oc}$, $\mathbf{Y}_{sc}$ and $\mathbf{Y}_n$

Figure 4.17: Case #3: Fitting results (10 km overhead line)

For the simulation using MCNR, the same criterion as in the previous test case, i.e., $\alpha \geq 0.99$ was adopted. Using this parameter, no slow poles in the rational approximation of $\mathbf{Y}_{oc}$ were found while in $\mathbf{Y}_{sc}$ 9 poles can be treated as slow with the other 24 poles treated as fast ones.

The circuit considered for the simulation of this test case is shown in Fig. 4.18. Now a single phase energization is performed followed by a single phase fault at $t_2 = 2.85$ ms. The short-circuit reactance is considered by means of an inductance $L = 110$ mH and the adopted time-step is $\Delta t = 30$ $\mu$s.

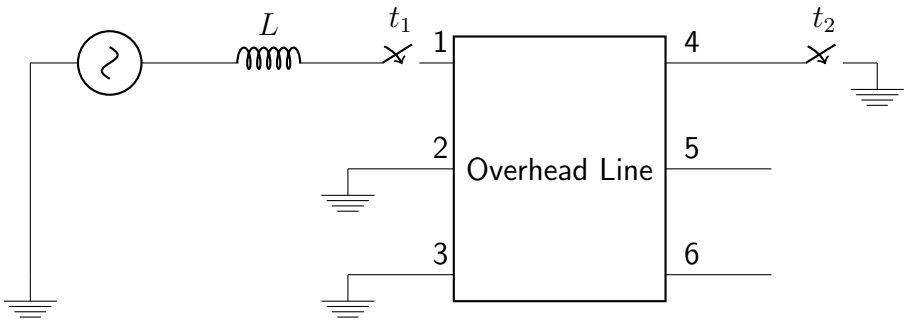


Figure 4.18: Case #3: Circuit for time-domain simulation

Fig. 4.19 shows the simulated voltage at the receiving end of the faulted and one unfaulted phases, i.e., terminals #4 and #5. It is noticeable that when the single phase fault occurs, it provokes a resonance that affects all the other phases. Even with the switching occurring when the voltage at terminal #4 is at its peak value, the comparison with the results obtained with the FLE model highlights that a very accurate result is attained.

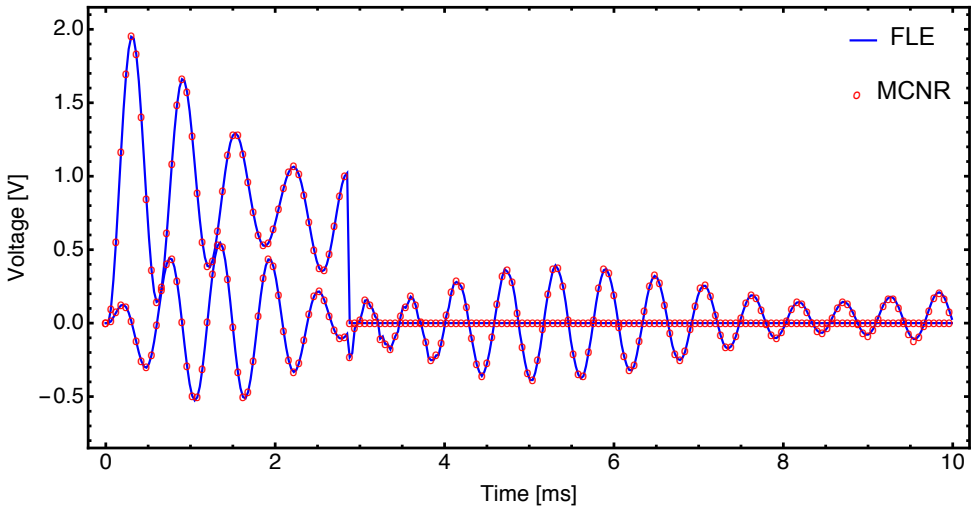


Figure 4.19: Case #3: Simulated voltage at terminals # 4 and # 5

To illustrate the simulated current profile, Fig. 4.20 presents the injected current at terminal #3. The results demonstrate a very close agreement between results obtained using the conventional FLE and MCNR. Besides providing a simulation without significant loss of accuracy, the proposed methodology reduces considerably the computational burden. As the number of poles involved in the rational

approximation is larger in this case, there is a decrease in the speed up gain. For this test the improvements are slightly higher than 30 %.

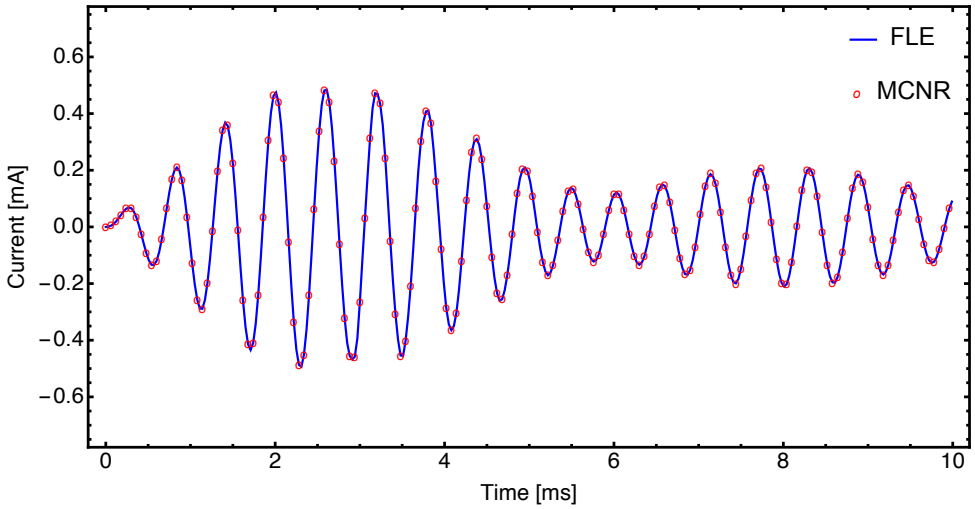


Figure 4.20: Case #3: Simulated current at terminal # 3

### 4.4.4 Case #4: LT 500 kV - 50 km (MCNR)

This test case aims to demonstrate the applicability of MCNR approach for a double-circuit overhead line with a length of 50 km. This kind of tower allows an evaluation taking into account a very asymmetric geometry which results in highly coupled circuits. The configuration of this 500 kV overhead line is depicted in Fig. 4.7c. It consists of an untransposed double-circuit configuration with ground wires continuously grounded.

The elements od the nodal admittance matrix $\mathbf{Y}_n$ are presented in Fig.4.21 and since this line length presents a natural resonance frequency around 1.5 kHz, the frequency sweep was in the range of 0.01 Hz to 20 kHz in order to obtain the data to be subjected to rational approximation with the *Vector Fitting* routine.

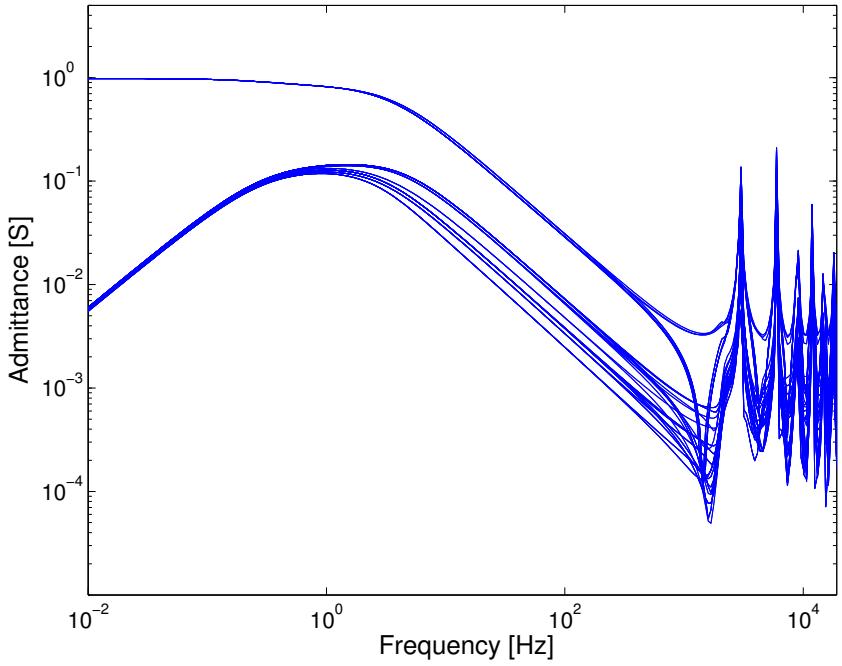


Figure 4.21: Case #4: Elements of $\mathbf{Y}_n$

The rational approximation of $\mathbf{Y}_{oc}$ and $\mathbf{Y}_{sc}$ is presented in Fig. 4.22a. The passive model was achieved using 38 poles for $\mathbf{Y}_{oc}$ and 60 poles for $\mathbf{Y}_{sc}$ with the corresponding eigenvalues depicted in Fig. 4.22b. Again a close agreement between the original and fitted data was achieved.

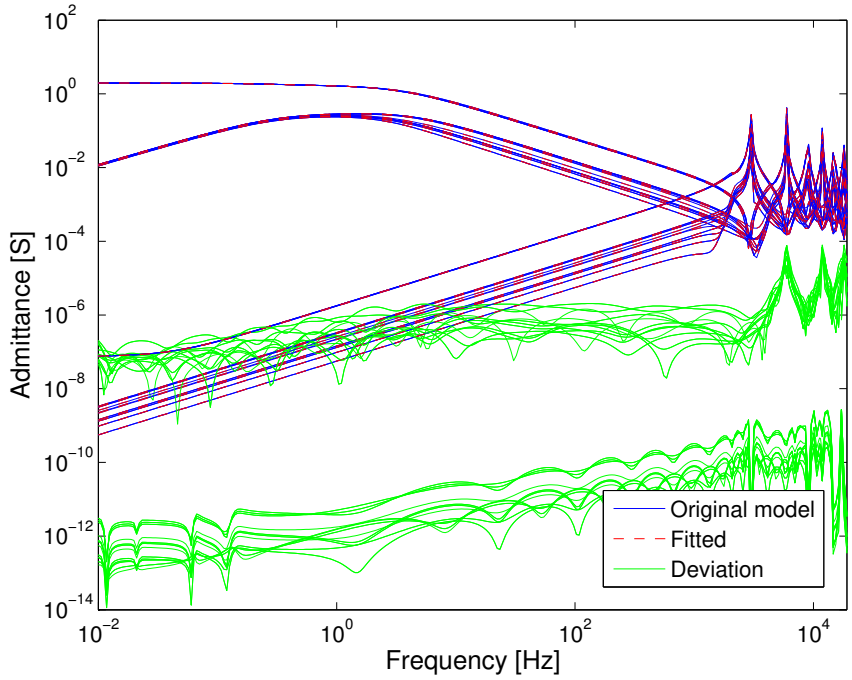


(a) Fitting of $\mathbf{Y}_{oc}$ and $\mathbf{Y}_{sc}$

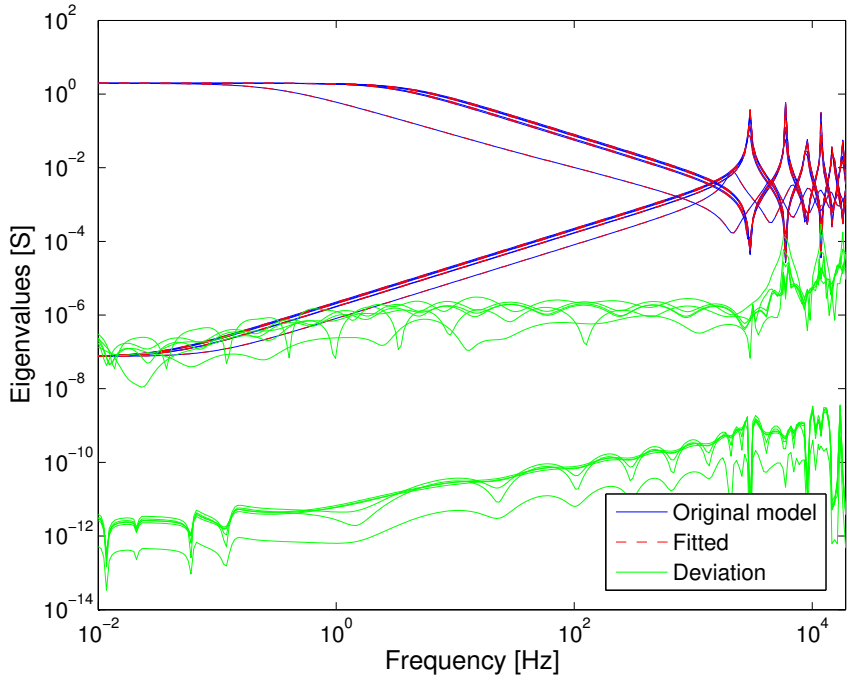


(b) Eigenvalues of $\mathbf{Y}_{oc}$ and $\mathbf{Y}_{sc}$

Figure 4.22: Case #4: Fitting results (500 kV overhead line)

This case addressed a special configuration with an inherent high coupling between phases. It was found that the value of alpha had to be greater than 0.9999 as the threshold adopted in the sorting between fast and slow poles. In this case, this criterion led to the rational approximation of $\mathbf{Y}_{oc}$ presenting no slow poles while

10 poles out of the 42 poles used in the rational approximation of $\mathbf{Y}_{sc}$ can be treated as slow poles. The former criteria would correspond to 18 slow poles.

In order to evaluate the multirate model, the configuration for this evaluation is presented in Fig. 4.23, i.e, a three phase energization with one phase short-circuited at the receiving end, similarly as performed in [82]. A time-step $\Delta t = 10$ $\mu$s is assumed.

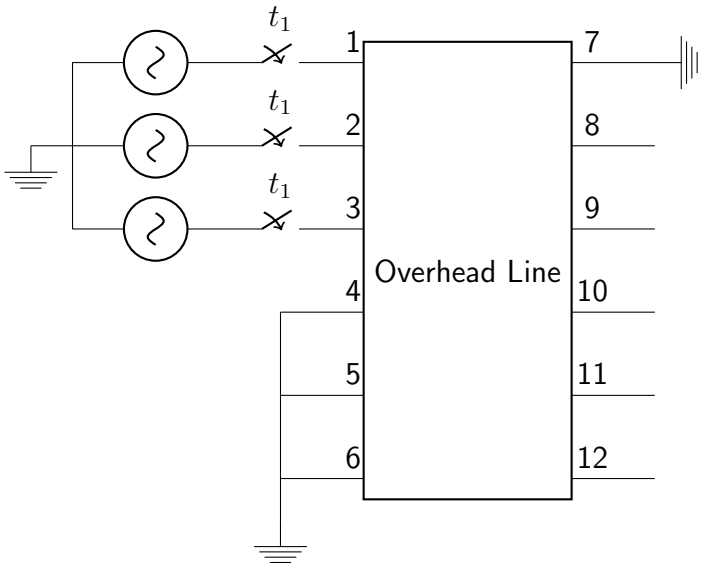


Figure 4.23: Case #4: Circuit for time-domain simulation

The simulated voltages at the unfaulted phases #9 and #12 are shown in Fig. 4.24. As expected, it is noticeable the agreement between the results obtained with the FLE model and MCNR.

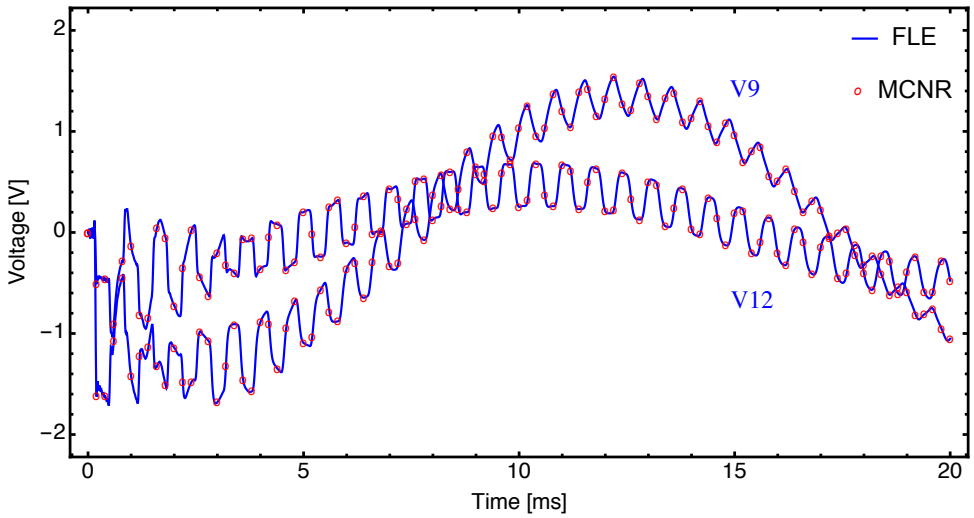


Figure 4.24: Case #4: Simulated voltage at terminals #9 and #12

Besides providing a simulation without significant loss of accuracy, the proposed methodology reduces considerably the computational burden. A reduction higher

than 10% was achieved when compared with the simulation when all poles were considered at each time-step. Otherwise, the reduction could be as high as 15%.

A double-circuit line would be a real challenge if the modeling was based on modal constant transformation matrix however a phase-coordinate model is adopted. To increase the difficulty in the fitting, a longer line with a 50 km length was considered without significant loss of accuracy. However, it should be pointed out that this last case stands for a scenario where the FLE is not so efficient since this type of modeling was developed to be used with overhead lines with shorter lengths [89].

## 4.5 Discussion

A novel multirate simulation scheme for time-domain simulations of full frequency dependent admittance-based models was introduced in this Chapter. Test cases comprising distinct line configurations were evaluated in order to evaluate the accuracy and range of validity of the MCN and MCNR formulations.

The evaluations on the original MCN formulation found that it was necessary to limit the time-step ratio $k$ to small values, typically $k \leq 10$, since as $k$ increases there is a significant increase in the maximum error. In addition, it was noticed that the error was basically monotonically increasing whenever the amount of poles considered as slow was changed.

Further investigations on a modified version of MCN formulation, namely, MCNM, achieved more accurate results for higher values of $k$ in the updating process of the fast and slow networks. It can be explained by the fact that the admittance matrix stands the same in comparison with the current EMTP modeling while in the original MCN formulation it slightly changes to accommodate the two different time-steps. This statement also stands for the relaxed version MCNR. The constraint imposed by the parameter $k$ does not hold for MCNR formulation as the overall algorithm excludes such time-step ratio and simplifies the computations to be performed by relaxing some of the coefficients used in the discrete time equivalent.

The employment of the FLE decomposition provides a kind of modeling which is already fast but with the improvements introduced by the MCNR it became even faster. It was found that only the poles associated with the short-circuit equivalent could be split into a fast and slow groups. As the open-circuit equivalent is associated with higher frequency phenomena, it lacks the presence of poles with larger time constants. It should be pointed out that the FLE is an alternative modeling suitable for short lines to improve the accuracy and to avoid numerical instabilities due to incorrect traveling time interpolation. The test case evaluating a double-circuit line stands for a scenario where the FLE is not so efficient and aims to increase the difficulty in the rational fitting a long line with a 50 km length was considered. It is noteworthy that even being a highly coupled configuration this line would be a real challenge if the modeling was based on modal constant transformation matrix. However, a phase-coordinate model was considered.

Future work is needed to investigate if the novel approach proposed here can be efficiently implemented using parallel computing and suitable for time-domain realization of FDNE.

# Chapter 5

# Conclusions

## 5.1 Final Conclusions

The preceding Chapters presented the research carried out during this doctorate project in the field of electromagnet transients (EMT). It focuses mainly on the development of frequency dependent admittance-based models to allow multiscale simulations of transmission lines and network equivalents. In addition, an investigation on the Latency concept was addressed aiming to introduce an alternative formulation to improve the numerical performance of a multirate simulation. The resulting models can be readily applied in a straightforward way in EMTP-like programs since they retain the same Norton-type structure. A more efficient realization of rational approximations of frequency dependent components is available through the proposed multiscale formulations. The employment of a single intermediate step is enough to allow the usage of multiple time-steps along the simulation run.

For all test cases comprising lumped elements, network equivalents, overhead lines and a subsea cable, an excellent match was attained when comparing the results achieved with the multiscale approach and the ones obtained considering a fixed time-step simulation. Besides keeping the accuracy of a fixed time-step simulation, the proposed methodologies provided a substantial gain in the overall computation time without a significant loss of accuracy. A smooth transition is achieved without numerical oscillations or discontinuities in the waveform regardless of the new time-step.

The modeling of overhead lines was addressed through three distinct admittance-based formulations as an alternative to the well-known MoC model, namely: direct fitting of the nodal admittance matrix ($\mathbf{Y}_n$–Line), Folded Line Equivalent (FLE–Line) and Idempotent Decomposition (Id–Line). The greatest advantage of these models is that no topological modification on the network matrix is required in

situations where the time-step is larger than the travel time since they feature a fully-coupled admittance matrix. This structure showed to be best suitable for multiscale simulations. The application of the FLE model proved to be very useful due to its numerical efficiency and high accuracy associated with a simple structure and, as in the case where a single time-step is considered, the FLE is a better alternative than the $\mathbf{Y}_n$ as it allows arbitrary terminal conditions, without the danger of large error magnifications. The renewed interest on Idempotent Decomposition for phase-coordinate modeling of transmission lines showed to be a feasible alternative to circumvent the poor rational fitting of the smallest eigenvalues of the nodal admittance matrix $\mathbf{Y}_n$ in the lower frequency range. The grouping routine of close eigenvalues succeeded with a reduced number of idempotent matrices, allowing a more compact realization. The results achieved with the new Id–Line model provided similar numerical performance in comparison with $Y_n$–Line and FLE–Line models. Thus, this finding encourages future investigation on Idempotent Decomposition in the rational modeling of frequency dependent network equivalent (FDNE).

A common procedure for representation of short lines is the replacement of a transmission line model by a frequency independent equivalent $\pi$–circuit whenever longer lines are presented. This procedure prevents the adoption of very small time-steps in evaluations of large systems resulting in time-consuming simulations. However, the drawback of such practice is that the $\pi$–circuit is accurate only at a single frequency. It is noteworthy that the FLE model is best suited for these situations in which the simulation time-step is larger than the travel time inasmuch as the frequency dependence can be taken into account. In addition, it is able to improve the numerical accuracy and to avoid numerical instabilities due to incorrect traveling time interpolation. Regarding real-time applications, looking for good precision and efficiency, the employment of the FLE model is recommended for transmission lines at a minimum shorter than 15 km ($\tau = 50$ $\mu$s) in substitution to $\pi$–sections as the time-step currently adopted by real-time simulators is 50 $\mu$s. From this length on, the travel time is smaller. Hence, the associated feature of fully-coupled matrices enables one to circumvent the constraints associated with traveling-wave models.

The major issue faced in this research was the passivity enforcement of the rational models. Even when the rational fitting presents a high accuracy, there is no guarantee that the overall model is passive. Furthermore, there is also no assurance whether the smallest eigenvalues are accurately represented in the lower frequency range or not. It was found that the passivity enforcement may not be possible even for very high order approximations. Due to the difficulty to find a passive model with acceptable precision, a case comprising a system of single core cables was not

presented.

The FAST concept has been revealed as a powerful modeling technique due to its versatility to cope either instantaneous or phasor-based representations. It has been taken to a new level of development because of the new class of components comprising frequency dependent admittance-based models designed to be applied in a unique algorithm for multiscale simulations of both electromagnetic and electromechanical transients. If the electromagnetic transients vanish and the system under evaluation reaches the steady state there is no constraint for a larger time-step. If one desires a time-step larger than, e.g., $\Delta t > 2$ ms, in order to accelerate the simulation run, a phasor-based mode must be employed. Although the computations performed with FAST process complex variables, the results attained the same accuracy as the MTS approach. The complex framework in conjunction with the frequency shifting enables the interface between the network and machine models in order to incorporate its dynamic behavior. Furthermore, the employment of dynamic phasors seems to provide a feasible mathematical or analytical description of power electronic converters. Contrary to the well-known averaging method [184], FAST can be used to provide a more precise solution instead of approximations based on time-varying windows.

A contribution to the multirate class of simulation techniques to approach latency was addressed using a novel formulation called Multiple Companion Networks (MCN) based on Norton-type companion networks. To improve the numerical efficiency of time-domain implementation of pole-residue models, different time-steps are considered for different poles in order to solve the slow and fast counterparts of a transmission line. A relaxed version was then introduced to face a limitation encountered in the original MCN algorithm to cope with a relative small ratio between the slow and fast time-steps. Gains in the overall computation time were achieved by relaxing some of the coefficients used in the discrete time equivalent model of frequency dependent transmission lines with different geometries.

## 5.2 Future Research

The field of electromagnet transients (EMT) focusing on the rational modeling of frequency dependent admittance-based models is a topic with multiple research possibilities. To continue the line of research pursued in the present work, the following topics are suggested:

- Employ the MTS and FAST approaches in the modeling of power transformers based on site frequency response measurements.
- Address further research on Idempotent Decomposition in the rational approximation of admittance-based models describing FDNE and cable systems.
- Implementation of the FLE model in real-time digital simulators in the modeling of transmission lines below 15 km as well as FDNE.
- Investigation on the MCNR approach if it can be efficiently implemented for time-domain realization of FDNE.
- Implementation of parallel computing for time-domain realization of frequency dependent admittance-based models.
- Address the modeling of power electronic devices with dynamic phasors by means of switching functions and further evaluation in multiscale simulations.
- Investigation of the influence of frequency dependence in ground parameters for time-domain simulations with FAST.

# Bibliography


[1] HEFFERNAN, M. D., TURNER, K. S., ARRILLAGA, J., et al. "Computation of A.C.-D.C. System Disturbances: Part I, II and III", *IEEE Transactions on Power Apparatus and Systems*, v. 100, n. 11, pp. 4341–4363, Nov. 1981.

[2] VENKATASUBRAMANIAN, V. "Tools for dynamic analysis of the general large power system using time-varying phasors", *International Journal on Electric Power and Energy Systems*, v. 16, n. 6, pp. 365–376, December 1994.

[3] HENSHEL, S. *Analysis of Electromagnetic and Electromechanical Power System Transients with Dynamic Phasors*. Ph.D. Thesis, The University of British Columbia, February 1999.

[4] ZHANG, P., MARTI, J., DOMMEL, H. "Synchronous Machine Modeling Based on Shifted Frequency Analysis", *IEEE Transactions on Power Systems*, v. 22, n. 03, pp. 1139–1147, August 2007.

[5] ZHANG, P., MARTI, J., DOMMEL, H. "Induction Machine Modeling Based on Shifted Frequency Analysis", *IEEE Transactions on Power Systems*, v. 24, n. 1, pp. 157–164, February 2009.

[6] ZHANG, P., MARTI, J., DOMMEL, H. "Shifted-Frequency Analysis for EMTP Simulation of Power-System Dynamics", *IEEE Transactions on Circuits and Systems - I: Regular Papers*, v. 57, n. 9, pp. 2564–2574, September 2010.

[7] HUANG, Y., CHAPARIHA, M., THERRIEN, F., et al. "A Constant-Parameter Voltage-Behind-Reactance Synchronous Machine Model Based on Shifted-Frequency Analysis", *IEEE Transactions on Energy Conversion*, v. 30, n. 02, pp. 761–771, 2015.

[8] GAO, F., STRUNZ, K. "Modeling of Constant Distributed Parameter Transmission Line for Simulation of Natural and Envelope Waveforms in Power Electric Networks", *Proceedings of the 37th Annual North American Power Symposium*, pp. 247–252, October 2005.

[9] STRUNZ, K., SHINTAKU, R., GAO, F. "Frequency-Adaptive Network Modeling for Integrative Simulation of Natural and Envelope Waveforms in Power Systems and Circuits", *IEEE Transactions on Circuits and Systems - I: Regular Papers*, v. 53, n. 12, pp. 2788–2803, December 2006.

[10] SHINTAKU, R., STRUNZ, K. "Branch companion modeling for diverse simulation of electromagnetic and electromechanical transients", *Electric Power Systems Research*, v. 77, n. 11, pp. 1501–1505, September 2007.

[11] GAO, F., STRUNZ, K. "Frequency-Adaptive Power System Modeling for Multiscale Simulation of Transients", *IEEE Transactions on Power Systems*, v. 24, n. 2, pp. 561–571, May 2009.

[12] GAO, F., STRUNZ, K. "Multi-Scale Simulation of Multi-Machine Power Systems", *International Journal of Electrical Power & Energy Systems*, v. 31, n. 9, pp. 538–545, October 2009.

[13] YE, H. *Multi-scale Frequency and Location Adaptive Simulation of Power System Transients*. Ph.D. Thesis, Technical University of Berlin, 2003.

[14] YE, H., STRUNZ, K. "Multi-Scale and Frequency-Depenent Modeling of Electric Power Transmission Lines", *IEEE Transactions Power Delivery*, v. 99, n. PP, 2017.

[15] DOMMEL, H. W. "Digital Computer Solution of Electromagnetic Transients in Single and Multiphase Networks", *IEEE Transactions on Power Apparatus and Systems*, v. 88, pp. 388–399, 1969.

[16] HO, C. W., RUEHLI, A. E. "The Modified Nodal Approach to Network Analysis", *IEEE Transactions on Circuits and Systems*, v. 22, n. 6, pp. 504–509, June 1975.

[17] MAHSEREDJIAN, J., DENNETIERE, S., DUBE, L., et al. "On a new approach for the simulation of transients in power systems", *Electric Power Systems Research*, v. 77, n. 11, pp. 1514—1520, September 2007.

[18] DUFOUR, C., MAHSEREDJIAN, J., BÉLANGER, J. "A combined state-space nodal method for the simulation of power system transients", *IEEE Transactions on Power Delivery*, v. 26, n. 2, pp. 928–935, 2011.

[19] DOMMEL, H. W. *Electromagnetic Transients Program (EMTP) Theory Book*. Portland, Oregon, Bonneville Power Administration, 1986.

[20] ALVARADO, F. "Parallel Solution of Transient Problems by Trapezoidal Integration", *IEEE Transactions on Power Apparatus and Systems*, v. 98, n. 3, pp. 1080–1090, May 1979.

[21] FALCAO, D. M., KASZKUREWICS, E. "Application of Parallel Processing Techniques to the Simulation of Power System Electromagnetic Transients", *IEEE Transactions on Power Systems*, v. 8, n. 1, pp. 90–96, February 1993.

[22] YUE, C., ZHOU, X., LI, R. "Node-splitting Approach Used for Network Partition and Parallel Processing in Electromagnetic Transient Simulation", *International Conference on Power System Technology*, November 2004.

[23] CROW, M., ILIC, M. "The Parallel Implementation of the Waveform Relaxation Method for Transient Stability Simulations", *IEEE Transactions on Power Systems*, v. 5, n. 3, pp. 922–932, 1990.

[24] SEMLYEN, A., DE LEON, F. "Computation of Electromagnetic Transients Using Dual or Multiple Time Steps", *IEEE Transactions on Power Systems*, v. 8, n. 3, pp. 1274–1281, August 1993.

[25] MARTI, J., LINARES, ROSALES, R., et al. "OVNI: A Full-Size Real-Time Power System Simulator", *Proceedings of the Second International Conference on Digital Power System Simulators (ICDS)*, 1997.

[26] MARTI, J., LINARES, L. R., CALVINO, J., et al. "OVNI: An Object Approach to Real-Time Power System Simulators", *International Conference on Power System Technology (Powercon)*, August 1998.

[27] MARTI, J., LINARES, L. R., HOLLMAN, J. A., et al. "OVNI: Integrated Software/Hardware Solution for Real-Time Simulation of Large Power Systems", *Proceedings of the Power Systems Computation Conference (PSSC)*, June 2002.

[28] MOREIRA, F. A., MARTÍ, J. R. "Latency Techniques for Time-Domain Power System Transients Simulation", *IEEE Transactions on Power Systems*, v. 20, n. 1, pp. 246–253, Feb. 2005.

[29] MOREIRA, F. A., MARTI, J., JR., L. C. Z., et al. "Multirate Simulations With Simultaneous-Solution Using Direct Integration Methods in a Partitioned Network Environment", *IEEE Transactions on Circuits and Systems I: Regular Papers*, v. 53, n. 12, pp. 2765–2778, 2006.

[30] ARMSTRONG, M. L. *Multilevel MATE Algorithm for Simulation of Power System Transients with the OVNI Simulator*. Ph.D. Thesis, University of British Columbia, December 2006.

[31] ARMSTRONG, M. L., MARTI, J., LINARES, L. R., et al. "Multilevel MATE for Efficient Simultaneous Solution of Control Systems and Nonlinearities in the OVNI Simulator", *IEEE Transactions Power Systems*, v. 21, n. 3, pp. 1250–1259, August 2006.

[32] TOMIM, M. A. *Parallel Computation of Large Power System Networks Using the Multi-Area Thévenin Equivalents*. Ph.D. Thesis, University of British Columbia, 2009.

[33] THERRIEN, F., JATSKEVICH, J. "Multirate EMTP-Type Induction Machine Models", *IEEE Transactions on Energy Conversion*, v. 31, n. 3, pp. 11142–1152, 2016.

[34] TOMIM, M. A., MARTI, J., FILHO, J. A. P. "Parallel Transient Stability Simulation Based on Multi-Area Thévenin Equivalents", *IEEE Transactions on Smart Grid*, v. 8, n. 3, pp. 1366–1377, May 2017.

[35] KRON, G. *Tensor Analysis of Networks*. London, Chapman & Hall, 1939.

[36] KRON, G. "Tensorial Analysis of Integrated Transmission Systems. Part III. The "Primitive" Division", *AIEE Transactions*, v. 71, n. 1, pp. 814–822, 1952.

[37] KRON, G. *Diakoptics: The Piecewise Solution of Large Scale Systems*. London, MacDonald, 1963.

[38] HAPP, H. H. "Diakoptics and Piecewise Methods", *IEEE Transactions on Power Apparatus and Systems*, v. 89, n. 7, pp. 1373–1382, September/October 1970.

[39] SU, H. T., CHAN, K. W., SNIDER, L. A., et al. "Recent Advancements in Electromagnetic and Electromechanical Hybrid Simulation", *International Conference on Power System Technology*, November 2004.

[40] JALILI-MARANDI, V., DINAVAHI, V., STRUNZ, K., et al. "Interfacing Techniques for Transient Stability and Electromagnetic Transient Programs (Task Force on Interfacing Techniques for Simulation Tools)", *IEEE Transactions on Power Delivery*, v. 24, n. 04, pp. 2385–2395, October 2009.

[41] ZHANG, Y., GOLE, A. M., WU, W., et al. "Development and Analysis of Applicability of a Hybrid Transient Simulation Platform Combining TSA and EMT Elements", *IEEE Transactions on Power Systems*, v. 28, n. 01, pp. 357 – 366, February 2013. doi: 10.1109/TPWRS.2012.2196450.

[42] PLUMIER, F., ARISTIDOU, P., GEUZAINE, C., et al. "Co-Simulation of Electromagnetic Transients and Phasor Models: A Relaxation Approach", *IEEE Transactions on Power Delivery*, v. 31, n. 5, pp. 2360 – 2369, October 2016. doi: 10.1109/TPWRD.2016.2537927.

[43] KASZTENNY, B., KEZUNOVIC, M. "A Method for Linking Different Modeling Techniques for Accurate and Efficient Simulation", *IEEE Transactions on Power Systems*, v. 15, n. 1, pp. 65–72, 2000.

[44] ABHYANKAR, S., FLUECK, A. J. "An Implicitly-Coupled Solution Approach for Combined Electromechanical and Electromagnetic Transients Simulation", *IEEE Power and Energy Society General Meeting*, pp. 1–8, July 2012.

[45] ZHANG, X., FLUECK, A., ABHYANKAR, S. "Implicitly-Coupled Electromechanical and Electromagnetic Transient Analysis using a Frequency Dependent Network Equivalent", *IEEE Transactions on Power Delivery*, v. 32, n. 3, pp. 1262–1269, June 2017. doi: 10.1109/TPWRD.2015.2501387.

[46] FAN, S., DING, H. "Time Domain Transformation Method for Accelerating EMTP Simulation of Power System Dynamics", *IEEE Transactions on Power Systems*, v. 27, n. 4, pp. 1778–1787, November 2012.

[47] HINGORANI, N. G., BURBERY, M. F. "Simulation of AC System Impedance in HVDC System Studies", *IEEE Transactions on Power Apparatus and Systems*, v. 89, n. 5, pp. 820–828, May 1970.

[48] CLERICI, A., MARZIO, L. "Coordinated Use of TNA and Digital Computer for Switching Surge Studies: Transient of a Complex Network", *IEEE Transactions on Power Apparatus and Systems*, v. 89, n. 8, pp. 1717–1726, November 1970.

[49] CIGRE. "The Calculation of Switching Surges. III - Transmission Line Representation for Energization Studies with Complex Feeding Networks (Working Group 05 of Study Committee 13)", *Electra*, v. 62, pp. 45–78, January 1979.

[50] MORCHED, A. S., BRANDWAJN, V. "Transmission Network Equivalents for Electromagnetic Transients Studies", *IEEE Transactions on Power Apparatus and Systems*, v. 102, n. 9, pp. 2984–2994, September 1983.

[51] DO, V. Q., GAVRILOVIC, M. M. "An Iterative Pole-Removal Method for Synthesis of Power System Equivalent Networks", *IEEE Transactions on Power Apparatus and Systems*, v. 103, n. 8, pp. 2065–2070, August 1984.

[52] DO, V. Q., GAVRILOVIC, M. M. "A Synthesis Method for One-Port and Multi-Port Equivalent Networks for Analysis of Power System Transients", *IEEE Transactions on Power Delivery*, v. 01, n. 02, pp. 103–113, April 1986.

[53] WATSON, N. *Frequency-Dependent AC System Equivalents for Harmonic Studies and Transient Convertor Simulation*. Ph.D. Thesis, University of Canterbury, 1987.

[54] WATSON, N. R., ARRILLAGA, J. "Frequency-Dependent AC System Equivalents for Harmonic Studies and Transient Convertor Simulation", *IEEE Transactions on Power Delivery*, v. 03, n. 03, pp. 1196 – 1203, July 1988.

[55] WATSON, N. R., ARRILLAGA, J., ARNOLD, C. P. "Simulation of HV DC System Disturbances with Reference to the Frequency Dependence of the AC System", *IEE Proceedings - Generation, Transmission and Distribution*, v. 136, n. 01, pp. 9 – 14, January 1989.

[56] MORCHED, A. S., OTTEVANGERS, J. H., MARTÍ, L. "Multi-Port Frequency Dependent Network Equivalents for the EMTP", *IEEE Transactions on Power Delivery*, v. 8, n. 3, pp. 1402–1412, July 1993.

[57] IBRAHIM, A., SALAMA, M. M. "Frequency Dependent Network Equivalent for AC Power Systems Using the QZ Algorithm". In: *Canadian Conference on Electrical and Computer Engineering*, v. 1, pp. 56–59, September 1995.

[58] IBRAHIM, A., SALAMA, M. M. "Frequency Dependent Network Equivalent Algorithm for AC Power Systems". In: *Canadian Conference on Electrical and Computer Engineering*, v. 2, pp. 639–642, May 1996.

[59] HOSSEINIAN, S. H., VAHIDI, B., BIEZA, J. "Frequency Dependent Network Equivalents for Harmonic and Transient Studies". In: *IEEE Region 10 Conference (TENCON)*, pp. 1–4, November 2006.

[60] WATSON, N., ARRILLAGA, J. *Power Systems Electromagnetic Transients Simulation*, v. 39, *IET Power and Energy Series*. London, Institution of Engineering and Technology, 2003.

[61] SEMLYEN, A., IRAVANI, M. R. "Frequency Domain Modeling of External Systems in an Electro-Magnetic Transients Program", *IEEE Transactions on Power System*, v. 8, n. 2, pp. 527–533, 1993.

[62] SEMLYEN, A., ABDEL-RAHMAN, M. H. "Transmission Line Modelling by Rational Transfer Functions", *IEEE Transactions on Power Apparatus and Systems*, v. 101, n. 9, pp. 3576–3584, September 1982.

[63] TODD, S., WOOD, A. R., BODGER, P., et al. "Rational Functions as Frequency Dependent Equivalents for Transient Studies". In: *International Conference on Power Systems Transients*, pp. 1032–1038, Seattle, USA, 1997.

[64] GUSTAVSEN, B., SEMLYEN, A. "Rational Approximation of Frequency Domain Responses by Vector Fitting", *IEEE Transactions on Power Delivery*, v. 14, n. 3, pp. 1052–1061, July 1999.

[65] GUSTAVSEN, B. "Improving the pole relocating properties of vector fitting", *IEEE Transactions on Power Delivery*, v. 21, n. 03, pp. 1587–1592, July 2006.

[66] DESCHRIJVER, D., GUSTAVSEN, B., DHAENE, T. "Advancements in Iterative Methods for Rational Approximation in the Frequency Domain", *IEEE Transactions on Power Delivery*, v. 22, n. 3, pp. 1633–1642, July 2007.

[67] DESCHRIJVER, D., MROZOWSKI, M., DHAENE, T., et al. "Macromodeling of Multiport Systems Using a Fast Implementation of the Vector Fitting Method", *IEEE Microwave and Wireless Components Letters*, v. 18, n. 6, pp. 383–385, June 2008.

[68] GUSTAVSEN, B. "Rational approximation of frequency dependent admittance matrices", *IEEE Transactions on Power Delivery*, v. 17, n. 4, pp. 1093–1098, 2002.

[69] GUSTAVSEN, B., SEMLYEN, A. "A Robust Approach for System Identification in the Frequency Domain", *IEEE Transactions on Power Delivery*, v. 19, n. 3, pp. 1167–1173, July 2004.

[70] RAMIREZ, A., SEMLYEN, A., IRAVANI, M. R. "Order Reduction of the Dynamic Model of a Linear Weakly Periodic System - Part II: Frequency-Dependent Lines", *IEEE Transactions on Power Systems*, v. 19, n. 2, pp. 866–871, May 2004.

[71] PORKAR, B., VAKILIAN, M., FEUILLET, R., et al. "Multi-Port Frequency-Dependent Network Equivalent for Electromagnetic Transient Studies", *Annual North American Power Symposium (NAPS)*, pp. 287–295, 2005.

[72] PORKAR, B., VAKILIAN, M., FEUILLET, R. "Frequency-Dependent Network Equivalent for Electromagnetic Transient Studies by Vector Fitting", *IEEE Transmission and Distribution Conference and Exhibition*, pp. 166–171, May 2006.

[73] LIN, X., GOLE, A. M., YU, M. "A Wide-Band Multi-Port System Equivalent for Real-Time Digital Power System Simulators", *IEEE Transactions on Power Systems*, v. 24, n. 1, pp. 237–249, February 2009.

[74] LIANG, Y., LIN, X., GOLE, A. M., et al. "Improved Coherency-Based Wide-Band Equivalents for Real-Time Digital Simulators", *IEEE Transactions on Power Systems*, v. 26, n. 3, pp. 1410–1417, August 2011.

[75] VERNAY, Y., GUSTAVSEN, B. "Application of Frequency-Dependent Network Equivalents for EMTP Simulation of Transformer Inrush Current in Large Networks", *International Conference on Power System Transients (IPST)*, July 2013.

[76] GUSTAVSEN, B. "Rational Modeling of Multiport Systems via a Symmetry and Passivity Preserving Mode-Revealing Transformation", *IEEE Transactions on Power Delivery*, v. 29, n. 1, pp. 199–206, February 2014.

[77] GUSTAVSEN, B., SEMLYEN, A. "Simulation of Transmission Line Transients using Vector Fitting and Modal Decomposition", *IEEE Transactions on Power Delivery*, 13(2):13pwrd02gust, April 1998.

[78] GUSTAVSEN, B., SEMLYEN, A. "Application of Vector Fitting to State Equation Representation of Transformers for Simulation of Electromagnetic Transients", *IEEE Transactions on Power Delivery*, v. 13, n. 3, pp. 834–842, July 1998.

[79] GUSTAVSEN, B., SEMLYEN, A. "Combined phase and modal domain calculation of transmission line transients based on vector fitting", *IEEE Transactions on Power Delivery*, v. 13, n. 2, pp. 596–604, April 1998.

[80] MORCHED, A., GUSTAVSEN, B., TARTIBI, M. "A Universal Model for Accurate Calculation of Electromagnetic Transients on Overhead Lines and Underground Cables", *IEEE Transactions on Power Delivery*, v. 14, n. 3, pp. 1032–1038, July 1999.

[81] GUSTAVSEN, B., IRWIN, G., MANGELROD, R., et al. "Transmission Line Models for the Simulation of Interaction Phenomena Between Parallel AC and DC Overhead Lines", *International Conference on Power System Transients (IPST)*, June 1999.

[82] GUSTAVSEN, B. "Frequency-Dependent Transmission Line Modeling Utilizing Transposed Conditions", *IEEE Transactions on Power Delivery*, v. 17, n. 3, pp. 834–839, JulyÍ 2002.

[83] GUSTAVSEN, B. "Wide Band Modeling of Power Transformers", *IEEE Transactions on Power Delivery*, v. 19, n. 1, pp. 414–422, Jan 2004.

[84] GUSTAVSEN, B. "Time Delay Identification for Transmission Line Modeling", *IEEE Workshop on Signal Propagation on Interconnects (SPI)*, pp. 103–106, May 2004.

[85] TOMMASI, L. D., GUSTAVSEN, B. "Accurate Transmission Line Modeling Through Optimal Time Delay Identification", *International Conference on Power System Transients (IPST)*, June 2007.

[86] GUSTAVSEN, B., MAHSEREDJIAN, J. "Simulation of Internal Overvoltages on Transmission Lines by an Extended Method of Characteristics Approach", *IEEE Transactions on Power Delivery*, v. 22, n. 3, pp. 1736–1742, July 2007.

[87] GUSTAVSEN, B., MO, O. "Interfacing Convolution Based Linear Models to an Electromagnetic Transients Program", *International Conference on Power System Transients (IPST)*, pp. 1–6, 2007.

[88] GUSTAVSEN, B., NORDSTROM, J. "Pole Identification for The Universal Line Model Based on Trace Fitting", *IEEE Transactions on Power Delivery*, v. 23, n. 1, pp. 472–479, January 2008.

[89] GUSTAVSEN, B., SEMLYEN, A. "Admittance-Based Modeling of Transmission Lines by a Folded Line Equivalent", *IEEE Transactions on Power Delivery*, v. 24, n. 1, pp. 231–239, January 2009.

[90] NODA, T. "Identification of a Multiphase Network Equivalent for Electromagnetic Transient Calculations Using Partitioned Frequency Response",

*IEEE Transactions on Power Delivery*, v. 20, n. 02, pp. 1134–1142, April 2005.

[91] NODA, T. "Application of Frequency-Partitioning Fitting to the Phase-Domain Frequency-Dependent Modeling of Overhead Transmission Lines", *IEEE Transactions on Power Delivery*, v. 30, n. 01, pp. 174–183, February 2015.

[92] NODA, T. "Application of Frequency-Partitioning Fitting to the Phase-Domain Frequency-Dependent Modeling of Underground Cables", *IEEE Transactions on Power Delivery*, v. 31, n. 4, pp. 1776–1777, August 2016.

[93] GOMES, S., MARTINS, N., PORTELA, C. "Sequential Computation of Transfer Function Dominant Poles of s-Domain System Models", *IEEE Transactions on Power Systems*, v. 24, n. 2, pp. 776–784, May 2009.

[94] VARRICCHIO, S. L., FREITAS, F. D., MARTINS, N., et al. "Computation of Dominant Poles and Residue Matrices for Multivariable Transfer Functions of Infinite Power System Models", *IEEE Transactions on Power Systems*, v. 30, n. 3, pp. 1131–1142, May 2015.

[95] ALMEIDA, C. F. M., KAGAN, N. "Determining Frequency Dependent Equivalents Through Evolutionary Algorithms", *International Conference on Harmonics and Quality of Power (ICHQP)*, pp. 403–408, June 2012.

[96] LEVENBERG, K. "A method for the solution of certain non-linear problems in least squares", *Quarterly Journal of Applied Mathematics*, v. 2, n. 2, pp. 164—168, July 1944.

[97] MARQUARDT, D. "An algorithm for least-squares estimation of nonlinear parameters", *Journal of the Society for Industrial and Applied Mathematics*, v. 11, n. 2, pp. 431–441, June 1963.

[98] MORÉ, J. J. *The Levenberg-Marquardt algorithm: implementation and theory*, v. 630, *Numerical Analysis, Lecture Notes in Mathematics*. Springer-Verlag, 1978.

[99] FERNANDES, A. *Modelo Otimizado para Estudos de Transitórios Eletromagnéticos (In Portuguese)*. Master Thesis, Universidade Federal da Paraíba (UFPB), 1996.

[100] FERNANDES, A. B., NEVES, W. L. A. "Transmission lines: Fitting technique optimization", *International Conference on Power System Transients (IPST)*, pp. 79–83, June 1997.

[101] NOCEDAL, J., WRIGHT, S. J. *Numerical Optimization*. Springer-Verlag, 1999.

[102] GRIVET-TALOCIA, S., GUSTAVSEN, B. *Passive Macromodeling: Theory and Applications*, v. 239, *Wiley Series in Microwave and Optical Engineering*. Hoboken, New Jersey, Wiley, December 2015.

[103] SINGH, H., ABUR, A. "Multi-Port Equivalencing of External Systems for Simulation of Switching Transients", *IEEE Transactions on Power Delivery*, v. 10, n. 1, pp. 374–382, January 1995.

[104] SANCHEZ-GASGA, J. J., CHOW, J. "Computation of Power System Low-Order Models from Time Domain Simulations Using a Hankel Matrix", *IEEE Transactions on Power Systems*, v. 12, n. 4, pp. 1461–1467, November 1997.

[105] WANG, Y. P., WATSON, N. R. "$z$-Domain Frequency-Dependent AC-System Equivalent for Electromagnetic Transient Simulation", *IEE Proceedings - Generation, Transmission and Distribution*, v. 150, n. 2, pp. 141–146, March 2003.

[106] WATSON, N. R., ARRILLAGA, J. "Harmonic Assessment Using Electromagnetic Transient Simulation and Frequency-Dependent Network Equivalents", *IEE Proceedings - Generation, Transmission and Distribution*, v. 150, n. 6, pp. 641–650, November 2003.

[107] WATSON, N. R. "Improved Fitting of $z$-Domain Frequency Dependent Network Equivalents for Electromagnetic Transient Simulation". In: *International Power Engineering Conference (IPEC)*, pp. 401–406, 2007.

[108] HENRIKSEN, T. "Including High Order Rational Functions in EMTP a Comparison Between Alternative Methods with Emphasis on Accuracy", *IEEE Trans. on Power Delivery*, v. 12, n. 1, pp. 372–379, Jan 1997.

[109] NODA, T., NAGAOKA, N., AMETANI, A. "Phase-domain modeling of frequency-dependent transmission lines by means of an ARMA model", *IEEE Transactions on Power Delivery*, v. 11, n. 1, pp. 401–411, Jan 1996.

[110] NODA, T., NAGAOKA, N., AMETANI, A. "Further Improvements to a Phase-Domain ARMA Line Model in Terms of Convolution, Steady-State Initialization, and Stability", *IEEE Transactions on Power Delivery*, v. 12, n. 3, pp. 1327–1334, July 1997.

[111] ANGELIDIS, G., SEMLYEN, A. "Direct phase-domain calculation of transmission line transients using two-sided recursions", *IEEE Trans. on Power Delivery*, v. 10, n. 2, pp. 941–949, April 1995.

[112] ABUR, A., SINGH, H. "Time Domain Modeling of External Systems for Electromagnetic Transients Programs", *IEEE Transactions on Power Systems*, v. 8, n. 2, pp. 671–679, May 1993.

[113] HONG, J.-H., PARK, J.-K. "A Time-Domain Approach to Transmission Network Equivalents via Prony Analysis for Electromagnetic Transients Analysis", *IEEE Transactions on Power Systems*, v. 10, n. 4, pp. 1789–1797, November 1995.

[114] DO COUTO BOAVENTURA, W., SEMLYEN, A., IRAVANI, R., et al. "Sparse Network Equivalent Based on Time-Domain Fitting", *IEEE Transactions on Power Delivery*, v. 17, n. 1, pp. 182–189, January 2002.

[115] NODA, T., SEMLYEN, A., IRAVANI, R. "Reduced-Order Realization of a Nonlinear Power Network Using Companion-Form State Equations with Periodic Coefficients", *IEEE Transactions on Power Delivery*, v. 18, n. 4, pp. 1478–1488, October 2003.

[116] NODA, T., SEMLYEN, A., IRAVANI, R. "Harmonic Domain Dynamic Transfer Function of a Nonlinear Time-Periodic Network", *IEEE Transactions on Power Delivery*, v. 18, n. 4, pp. 1433–1441, October 2003.

[117] GRIVET-TALOCIA, S. "Package Macromodeling via Time-Domain Vector Fitting", *IEEE Microwave and Wireless Components Letters*, v. 13, n. 11, pp. 472–474, November 2003.

[118] DO COUTO BOAVENTURA, W., SEMLYEN, A., IRAVANI, M. R., et al. "Robust Sparse Network Equivalent for Large Systems: Part I - Methodology", *IEEE Transactions on Power Systems*, v. 19, n. 1, pp. 157–163, February 2004.

[119] DO COUTO BOAVENTURA, W., SEMLYEN, A., IRAVANI, M. R., et al. "Robust Sparse Network Equivalent for Large Systems: Part I - Performance Evaluation", *IEEE Transactions on Power Systems*, v. 19, n. 1, pp. 293–299, February 2004.

[120] UBOLLI, A., GUSTAVSEN, B. "Comparison of Methods for Rational Approximation of Simulated Time-Domain Responses: ARMA, ZD-VF, and TD-VF", *IEEE Transactions on Power Delivery*, v. 26, n. 1, pp. 279–288, January 2011.

[121] UBOLLI, A., GUSTAVSEN, B. "Multiport Frequency-Dependent Network Equivalencing Based on Simulated Time-Domain Responses", *IEEE Transactions on Power Delivery*, v. 27, n. 2, pp. 648–657, April 2012.

[122] ABDEL-RAHMAN, M. *Frequency Dependent Hybrid Equivalents of Large Networks*. Ph.D. Thesis, University of Toronto, 2001.

[123] ABDEL-RAHMAN, M., SEMLYEN, A. "Two-Layer Network Equivalent for Electromagnetic Transients", *IEEE Transactions on Power Delivery*, v. 18, n. 4, pp. 1328–1335, October 2003.

[124] RAMIREZ, A. "Vector Fitting-Based Calculation of Frequency-Dependent Network Equivalents by Frequency Partitioning and Model-Order Reduction", *IEEE Transactions on Power Delivery*, v. 24, n. 1, pp. 410–415, January 2009.

[125] HUA, Y., SARKAR, T. K. "Matrix pencil method for estimating parameters of exponentially damped/undamped sinusoids in noise", *IEEE Transactions on Acoustics, Speech, and Signal Processing*, v. 38, n. 5, pp. 814–824, May 1990.

[126] SARKAR, T. K., PEREIRA, O. "Using the Matrix Pencil Method to Estimate the Parameters of a Sum of Complex Exponentials", *IEEE Antennas and Propagation Magazine*, v. 37, n. 1, pp. 48–55, February 1995.

[127] SHESHYEKANI, K., KARAMI, H. R., DEHKHODA, P., et al. "Application of the Matrix Pencil Method to Rational Fitting of Frequency-Domain Responses", *IEEE Transactions on Power Delivery*, v. 27, n. 4, pp. 2399–2408, October 2012.

[128] SHESHYEKANI, K., KARAMI, H. R., DEHKHODA, P., et al. "Application of the Matrix Pencil Method to Rational Fitting of Frequency-Domain Responses", *IEEE Transactions on Power Delivery*, v. 27, n. 04, pp. 2399–2408, October 2012.

[129] SHESHYEKANI, K., TABEI, B. "Multiport Frequency-Dependent Network Equivalent Using a Modified Matrix Pencil Method", *IEEE Transactions on Power Delivery*, v. 29, n. 5, pp. 2340–2348, June 2014.

[130] HU, Y., WU, W., ZHANG, B. "A Fast Method to Identify the Order of Frequency-Dependent Network Equivalents", *IEEE Transactions on Power Systems*, v. 31, n. 1, pp. 54–64, January 2016.

[131] BEWLEY, L. V. *Traveling Waves on Transmission Systems.* New York, Dover, 1963.

[132] LOWY, R. *Druckschwankungen in Druckrohrleitungen (Pressure Variations in Pressure Pipe Lines).* Viena, Austria, Springer, 1928.

[133] SCHNYDER, O. "Druckstosse in Pumpensteigleitungen (Pressure Impulses in Pumped Pipe Pines)", *Schweiz Bauztg*, v. 94, n. 22, pp. 271–286, 1929.

[134] BERGERON, L. *Du Coup De Belier En Hydraulique Au Coup De Foudre En Electricite (Water Hammer in Hydraulics and Wave Surges in Electricity).* Paris, France, Dunod, 1949.

[135] BARTHOLD, L. O., CARTER, G. K. "Digital Traveling-Wave Solutions. 1-Single Phase Equivalents", *Transactions of the American Institute of Electrical Engineers. Power Apparatus and Systems, Part III*, 1961.

[136] FREY, W., ALTHAMMER, P. "The Calculation of Transients on Lines by Means of a Digital Computer", *Brown Boveri Rev.*, v. 48, pp. 344–355, May/june 1961.

[137] MEYER, W. S., DOMMEL, H. "Numerical Modelling of Frequency-Dependent Transmission-Line Parameters in an Electromagnetic Transients Program", *IEEE Transactions on Power Apparatus and Systems*, v. 93, n. 5, pp. 1401–1409, September 1974.

[138] MARTI, J. "Accurate modelling of frequency-dependent transmission lines in EMTP simulation", *IEEE Transactions on Power Apparatus and Systems*, v. 101, n. 1, pp. 147–155, Jan 1982.

[139] SEMLYEN, A., DABULEANU, A. "Fast and accurate switching transient calculations on transmission lines with ground return using recursive convolutions", *IEEE Transactions on Power Apparatus and Systems*, v. 94, pp. 561–571, Mar./Apr. 1975.

[140] SEMLYEN, A., DABULEANU, A. "A system approach to accurate switching transient calculations based on state variable component modelling", *IEEE Transactions on Power Apparatus and Systems*, v. 94, n. 2, pp. 572–578, March 1975.

[141] AMETANI, A. "A Highly Efficient Method for Calculating Transmission Line Transients", *IEEE Trans. on Power Apparatus and Systems*, v. PAS-95, n. 5, pp. 1545–1550, September/October 1976.

[142] SEMLYEN, A. "Contributions to the Theory of Calculation of Electromagnetic Transients on Transmission Lines with Frequency Dependent Parameters", *IEEE Transactions on Power Apparatus and Systems*, v. 100, n. 2, pp. 848–856, February 1981.

[143] HAUER, J. F. "State-Space Modeling of Transmission Line Dynamics Via Nonlinear Optimization", *IEEE Transactions on Power Apparatus and Systems*, v. 100, n. 12, pp. 4918–4925, December 1981.

[144] TAVARES, M. C., PISSOLATO, J., PORTELA, C. M. "Mode domain multiphase transmission line model-use in transient studies", *IEEE Transactions on Power Delivery*, v. 14, n. 4, pp. 1533–1544, October 1999.

[145] MARTI, L. "Simulation of Transients in Underground Cables with Frequency-Dependent Modal Transformation Matrices", *IEEE Trans. on Power Delivery*, pp. 1099–1110, Jul. 1988.

[146] WEDEPOHL, L. M., NGUYEN, H. V., IRWIN, G. W. "Frequency-Dependent Transformation Matrices for Untransposed Transmission Line using a Newton-Raphson Method", *IEEE Transactions on Power Systems*, v. 11, n. 3, pp. 1538–1546, August 1996.

[147] NAKANISHI, H., AMETANI, A. "Transient calculation of a transmission line using superposition law", *IEE Proceedings C - Generation, Transmission and Distribution*, v. 133, n. 5, pp. 263–269, July 1986.

[148] MAHMUTCEHAJIC, R., BABIC, S., GARCANOVIC, R., et al. "Digital simulation of electromagnetic wave propagation in a multiconductor transmission system using the superposition principle and Hartley transform", *IEEE Transactions on Power Delivery*, v. 8, n. 3, pp. 1377–1385, July 1993.

[149] GUSTAVSEN, B., SLETBAK, J., HENRIKSEN, T. "Calculation of the electromagnetic transients in transmission cables and lines taking frequency dependent effects accurately account", *IEEE Trans. on Power Delivery*, v. 10, n. 2, pp. 1076–1084, April 1995.

[150] NGUYEN, H., DOMMEL, H., MARTI, J. "Direct Phase-Domain modelling of Frequency-Dependent Overhead Transmission Lines", *IEEE Transactions on Power Delivery*, v. 12, n. 3, pp. 916–921, July 1997.

[151] CASTELLANOS, F., MARTI, J. "Full Frequency-Dependent Phase-Domain Transmission Line Model", *IEEE Transactions on Power Systems*, v. 12, n. 3, pp. 1331–1339, August 1997.

[152] CASTELLANOS, F., MARTI, J., MARCANO, F. "Phase-Domain Multiphase Transmission Line Models", *Electrical Power & Energy Systems*, v. 19, n. 4, pp. 241–248, 1997. Elsevier Science Ltd.

[153] MARCANO, F., MARTI, J. "Idempotent Line Model: Case Studies". In: *Proceedings of IPST'97 - International Conference on Power Systems Transients*, pp. 67–72, 1997.

[154] GUSTAVSEN, B., SEMLYEN, A. "Calculation of Transmission Line Transients using Polar Decomposition", *IEEE Transactions on Power Delivery*, v. 13, n. 3, pp. 855–862, July 1998.

[155] YU, T. C., MARTI, J. "A robust phase-coordinates frequency-dependent underground cable model (zCable) for the EMTP", *IEEE Transactions on Power Delivery*, v. 18, n. 1, pp. 189–194, January 2003.

[156] FERNANDES, A. B., NEVES, W. L. A. "Phase-domain transmission line models considering frequency-dependent transformation matrices", *IEEE Transactions on Power Delivery*, v. 19, n. 2, pp. 708–714, April 2004.

[157] TOMASEVICH, M. Y., LIMA, A. C. "Some developments on phase coordinates line modeling based on Idempotent decomposition", *International Journal of Electrical Power & Energy Systems*, v. 74, pp. 410–419, 2016.

[158] SALEH, R. A., NEWTON, A. R. "The Exploitation of Latency and Multirate Behavior Using Nonlinear Relaxation for Circuit Simulation", *IEEE Transactions on Computer-Aided Design of Integrated Circuits and Systems*, v. 8, n. 12, pp. 1286–1298, 1989.

[159] Martinez, J. A. (Ed.). *Power System Transients: Parameter Determination*. CRC Press, 2010.

[160] GUSTAVSEN, B. "Passivity Enforcement for Transmission Line Models Based on the Method of Characteristics", *IEEE Transactions on Power Delivery*, v. 24, n. 3, pp. 2286–2293, October 2008.

[161] KOCAR, I., MAHSEREDJIAN, J., OLIVIER, G. "Improvement of Numerical Stability for the Computation of Transients in Lines and Cables", *IEEE Transactions on Power Delivery*, v. 25, n. 2, pp. 1104–1111, April 2010.

[162] GUSTAVSEN, B. "Avoiding Numerical Instabilities in the Universal Line Model by a Two-Segment Interpolation Scheme", *IEEE Transactions on Power Delivery*, v. 28, n. 3, pp. 1643–1651, July 2013.

[163] HENSCHEL, S., IBRAHIM, A., DOMMEL, H. "Transmission line model for variable step size simulation algorithms", *International Journal on Electric Power and Energy Systems*, v. 21, n. 03, pp. 191–198, March 1999.

[164] IBRAHIMA, A., HENSCHELB, S., LIMA, A. C. S., et al. "Applications of a new EMTP line model for short overhead lines and cables", *International Journal on Electric Power and Energy Systems*, v. 24, n. 08, pp. 639–645, October 2002.

[165] GUSTAVSEN, B., HEITZ, C. "Modal Vector Fitting: A Tool For Generating Rational Models of High Accuracy With Arbitrary Terminal Conditions", *IEEE Transactions on Advanced Packaging*, v. 31, n. 4, pp. 664–672, November 2008.

[166] TAVARES, M. C., PISSOLATO, J., PORTELA, C. "New multiphase mode domain transmission line model", *International Journal of Electrical Power and Energy Systems*, v. 21, n. 4, pp. 585–601, 1999.

[167] CASTELLANOS, F., MARTI, J. "Phase-Domain Multiphase Transmission Line Models", *International Conference on Power System Transients (IPST)*, pp. 17–22, September 1995.

[168] GUSTAVSEN, B. "Computer Code for Rational Approximation of Frequency Dependent Admittance Matrices", *IEEE Transactions on Power Delivery*, v. 17, n. 4, pp. 1093–1098, Oct. 2002.

[169] SEMLYEN, A. "Some Frequency Domain Aspects of Wave Propagation on Nonuniform Lines", *IEEE Transactions on Power Delivery*, v. 18, n. 1, pp. 315–322, January 2003.

[170] WEDEPOHL, L., INDULKAR, C. "Wave propagation in nonhomogeneous systems. Properties of the chain matrix", *Proceedings of the IEE*, v. 121, n. 9, pp. 997, September 1974.

[171] WILCOX, D. J. "Wave Propagation in Nonhomogeneous Multiconductor Transmission Systems: General Theory and Analysis", *Proceedings of the IEE*, v. 124, n. 05, pp. 459–462, May 1977.

[172] GUSTAVSEN, B., MARTINEZ, J. A. "Overview of Overhead Line Models and Their Representation in Digital Simulations". In: *IPST 2001 - International Conference of Power System Transients*, v. 1, 2001.

[173] LIMA, A. C. S. "Rational Modeling of Nonhomogeneous Systems", *Journal of Control, Automation and Electrical Systems*, v. 26, n. 02, pp. 180–189, April 2015.

[174] WILCOX, D. J. "Numerical Laplace Transformation and Inversion", *International Journal Elect. Eng.*, v. 15, pp. 247–265, 1978.

[175] URIBE, F. A., NAREDO, J. L., MORENO, P. "Electromagnetic transients in underground transmission systems through the numerical Laplace transform", *International Journal of Electrical Power & Energy Systems*, v. 24, n. 3, pp. 215–221, March 2002.

[176] MORENO, P., RAMIREZ, A. "Implementation of the Numerical Laplace Transform: A review (Task Force on frequency domain methods for EMT studies)", *IEEE Transactions on Power Delivery*, v. 23, n. 4, pp. 2599–2609, October 2008.

[177] "Wolfram Mathematica". Disponível em: <`https://www.wolfram.com/mathematica/`>.

[178] MAHSEREDJIAN, J., ALVARADO, F. "Creating an Electromagnetic Transients Program in MATLAB: MatEMTP", *Power Delivery, IEEE Transactions on*, v. 12, n. 1, pp. 380–388, jan. 1997.

[179] GUSTAVSEN, B., HEITZ, C. "Rational Modeling of Multiport Systems by Modal Vector Fitting", *IEEE Workshop on Signal Propagation on Interconnects*, pp. 49–52, 2007.

[180] GUSTAVSEN, B. "Validation of Frequency Dependent Transmission Line Models", *IEEE Transactions on Power Delivery*, v. 2, n. 2, pp. 925–933, April 2005.

[181] CHIEN, C. H., BUCKNALL, R. W. G. "Analysis of Harmonics in Subsea Power Transmission Cables Used in VSC–HVDC Transmission Systems Operating Under Steady-State Conditions", *IEEE Transactions on Power Delivery*, v. 22, n. 4, pp. 2489–2497, October 2007.

[182] SILVA, J. C. L. V., LIMA, A. C. S., MAGALHAES, A. P. C., et al. "Modelling seabed buried cables for electromagnetic transient analysis", *IET Generation, Transmission & Distribution*, v. 11, n. 6, pp. 1575–1582, May 2017.

[183] GUSTAVSEN, B. "Fast Passivity Enforcement for Pole-Residue Models by Perturbation of Residue Matrix Eigenvalues", *IEEE Transactions on Power Delivery*, v. 23, n. 4, pp. 2278–2285, October 2008.

[184] SANDERS, S. R., NOWOROLSKI, J. M., LIU, X. Z., et al. "Generalized averaging method for power conversion circuits", *IEEE Transactions on Power Electronics*, v. 6, n. 2, pp. 251–259, April 1991.

[185] GABOR, D. "Theory of Communication", *Journal of the Institution of Electrical Engineers - Part III: Radio and Communication Engineering*, v. 93, n. 26, pp. 429–457, November 1946.

[186] VAKMAN, D. E., VAINSHTEIN, L. A. "Amplitude, Phase, Frequency - Fundamental Concepts of Oscillation Theory", *Soviet Physics Uspekhi*, v. 20, n. 12, pp. 1002–1016, December 1977.

[187] COHEN, L. *Time-Frequency Analysis*. New Jersey, Prentice Hall PTR, 1995.

[188] DUNCAN, A. "The Analytic Impulse", *Journal of the Audio Engineering Society*, v. 36, n. 5, pp. 315–327, May 1988.

[189] HEYSER, R. C. "Determination of Loudspeaker Signal Arrival Times: Parts I, II and III", *Journal of the Audio Engineering Society*, v. 19, n. 9, 10, 11, pp. 734–743, 829–834, 902–905, October/November/December 1971.

[190] MARTI, L. *Simulation of Electromagnetic Transients in Underground Cables with Frequency-Dependent Modal Transformation Matrices*. Ph.D. Thesis, The University of British Columbia, November 1986.

[191] GUSTAVSEN, B., SILVA, H. M. J. D. "Inclusion of Rational Models in an Electromagnetic Transients Program: Y-Parameters, Z-Parameters, S-Parameters, Transfer Functions", *IEEE Transactions on Power Delivery*, v. 28, n. 2, pp. 1164–1174, April 2013.

[192] SEMLYEN, A., GUSTAVSEN, B. "Vector fitting by pole relocation for the state equation approximation of nonrational transfer matrices", *Circuits, Systems and Signal Processing*, v. 19, n. 6, pp. 549—566, 2000.

[193] GUSTAVSEN, B., SEMLYEN, A. "Enforcing Passivity for Admittance Matrices Approximated by Rational Functions", *IEEE Transactions on Power Systems*, v. 16, n. 1, pp. 97–104, February 2001.

[194] GUSTAVSEN, B. "Computer Code for Passivity Enforcement of Rational Macromodels by Residue Perturbation", *IEEE Transactions on Advanced Packaging*, v. 30, n. 2, pp. 209–215, 2007.

# Appendix A

# State-Space Realization

Consider a scalar element with the following transfer function in the frequency domain

$$I(s) = \left( \frac{r}{s-a} + d \right) V(s) \tag{A.1}$$

where $V(s)$ and $I(s)$ are the complex voltage and current, $r$, $d$ and $a$ are real. In the time-domain, it is possible to rewrite (A.1) as

$$\begin{aligned} \dot{x}(t) &= a\, x(t) + v(t) \\ i(t) &= r\, x(t) + d\, v(t) \end{aligned} \tag{A.2}$$

Using either the trapezoidal rule of integration or recursive convolution leads to the following discrete time equivalent

$$\begin{aligned} x(n) &= \alpha\, x(n-1) + (\alpha\lambda + \mu)\; v(n-1) \\ i(n) &= x(n) + (\lambda + d)\, v(n) \end{aligned} \tag{A.3}$$

The equation in (A.3) represents a companion network where $x(n)$ is the history current source and $g = \lambda + d$. If the trapezoidal integration rule is applied, the coefficients $\alpha$, $\lambda$ and $\mu$ are given by

$$\alpha = \frac{2 + a\,\Delta t}{2 - a\,\Delta t} \qquad \lambda = \mu = \frac{r\,\Delta t}{2 - a\,\Delta t} \tag{A.4}$$

and in the case recursive convolutions are considered

$$\alpha = \exp\left(a\,\Delta t\right) \qquad \lambda = -\frac{r}{a}\left(1 + \frac{1-\alpha}{a\,\Delta t}\right) \quad \mu = \frac{r}{a}\left(\alpha + \frac{1-\alpha}{a\,\Delta t}\right) \tag{A.5}$$

# Appendix B

# Vector Fitting

The *Vector Fitting* (VF) routine [64, 65, 67, 68] is a fast and robust method for the fitting of measured or calculated frequency-domain responses with rational function approximations. The objective is to estimate all coefficients in (B.1) over a given frequency interval. The difficulty in fitting $f(s)$ is due to the (unknown) poles $p_m$ which appear in the denominator, thus causing (B.1) to become a nonlinear problem in the unknowns. However, if the poles had been known, then (B.1) would have been linear in the unknowns $r_m$ and $d$, which could then have easily been calculated by solving a linear least-squares problem [192].

The methodology consists in relocate a set of initial poles in order to match a given frequency response $f(s)$ with a pole-residue model as an optimization problem in the least-squares sense. *Vector Fitting* is essentially a robust reformulation of the Sanathanan–Koerner iteration [65] and can be interpreted as a pole relocation process, that is, as an iterative refinement of a set of poles that quickly converge to the dominant poles of the system under modeling [102].

Consider the rational function approximation

$$f(s) \approx \sum_{m=1}^{N} \frac{r_m}{s - p_m} + d \tag{B.1}$$

where set of poles $p_m$ and residues $r_m$ are either real quantities or come in complex conjugate pairs while d is real. The summation limit $N$ is the order of the approximation, assumed to be known.

VF solves the problem (B.1) sequentially as a linear problem in two stages, both times with known poles.

## B.1 Pole Identification

Instead of fitting $f(s)$ directly, VF multiplies $f(s)$ with an unknown rational function $\sigma(s)$ of order $N$:

$$\sigma(s) = \sum_{m=1}^{N} \frac{\hat{r}_m}{s - \bar{p}_m} + 1 \tag{B.2}$$

and is postulated that the starting poles $\bar{p}_m$ of $\sigma(s)$ are the same as the approximation for $\sigma(s)f(s)$

$$f(s) \cdot \sigma(s) = \sum_{m=1}^{N} \frac{\tilde{r}_m}{s - \bar{p}_m} + \tilde{d} \tag{B.3}$$

Combining (B.2) and (B.3) yields

$$\left( \sum_{m=1}^{N} \frac{\hat{r}_m}{s - \bar{p}_m} + 1 \right) f(s) = \sum_{m=1}^{N} \frac{\tilde{r}_m}{s - \bar{p}_m} + \tilde{d} \tag{B.4}$$

After some manipulation, the sum of partial fractions in (B.2) can be written as a fraction

$$f(s) = \frac{f(s) \cdot \sigma(s)}{\sigma(s)} = \frac{\prod_{m=1}^{N} \frac{(s-\tilde{z}_m)}{(s-\bar{p}_m)}}{\prod_{m=1}^{N} \frac{(s-\hat{z}_m)}{(s-\bar{p}_m)}} = \frac{\prod_{m=1}^{N} (s - \tilde{z}_m)}{\prod_{m=1}^{N} (s - \hat{z}_m)} \tag{B.5}$$

It can be seen from (B.5) that the initial poles $\bar{p}_m$ cancel in the division process and that the zeros $\hat{z}_m$ of $\sigma(s)$ become equal to the poles of $f(s)$. Thus, calculating the zeros of $\sigma(s)$ gives an improved set of poles for fitting the original function $f(s)$. The zeros are calculated by solving the eigenvalue problem

$$\{p_m\} = \mathsf{eig}(\mathbf{A} - \mathbf{b} \cdot \mathbf{c}^T) \tag{B.6}$$

where $\mathbf{A}$ is a diagonal matrix holding the poles $\{p_m\}$, $\mathbf{b}$ is a column of ones and $\mathbf{c}$ holds the residues $\{\hat{r}_m\}$.

## B.2 Residue Identification

With the poles $p_m$ of $f(s)$ known from the pole identification step, (B.1) is solved with respect to the unknown residues $r_m$ and constant term $d$ by solving the corresponding least-square problem with known poles. Details regarding the implementation are given in [64].

## B.3 Passivity Enforcement

The inclusion of rational models in EMTP-like programs may result in unstable simulations if passivity is not enforced. The passivity requirement means that the model cannot generate energy when connected to an external network at any frequency [193], i.e., the eigenvalues of $\mathbf{Y}_n$ are positive for all frequencies

$$\mathsf{eig}(\mathrm{Re}\{\mathbf{Y}(s)\}) > 0 \quad \forall s, \quad s = j\omega \tag{B.7}$$

Even when only all poles are stable, i.e, lie in the left half plane, this stable poles requirement can usually be enforced without difficulty, e.g., by flipping unstable poles into the left half plane, followed by a refitting of the residues and constant term.

A much more challenging problem is the enforcement of passivity of the model, which is an additional requirement for guaranteeing a stable simulation [88, 194]. In general, the fitting is performed within a certain frequency range but there is no guarantee that $\mathbf{Y}_n$ is positive definite also outside this frequency range. In some cases, instability problems have been encountered due to large out-of-band passivity violations [160]. A robust enhancement provided in the VF package for passivity enforcement is able to cope out-of-band violations without corrupting the in-band behavior. The model is enforced to be passive by perturbing the eigenvalues of each residue matrix such that all eigenvalues become positive [183].

## B.4 Mode-Revealing Transformation

Admittance-based models describing terminal conditions in the frequency domain are usually adopted in the modeling of frequency dependent components since the interface with EMTP-like programs can be done in a straightforward way. The representation using rational functions or on pole-residue form presents a challenge by the fact that a large ratio between the large and small eigenvalues can result in error magnification when the model is to be applied in time-domain simulations. It occurs as a consequence of inaccurate representation of small eigenvalues of the admittance matrix $\mathbf{Y}_n$.

The introduction of a similarity transformation matrix called Mode-Revealing Transformation (MRT) [76] addressed this issue improving the observability of this small eigenvalues by choosing a suitable transformation matrix $\mathbf{Q}$ that preserves the physical properties of symmetry, realness, stability, causality and passivity. It can be understood as an alternative to the modal VF presented in [165, 179]. The procedure aims to find a proper choice of $\mathbf{Q}$ so that it is possible to achieve that the

small eigenvalues become more observable in the elements of $\tilde{\mathbf{Y}}_n$ than in $\mathbf{Y}_n$ by the similarity transformation

$$\tilde{\mathbf{Y}}_n = \mathbf{Q}^T \cdot \mathbf{Y}_n \cdot \mathbf{Q} \tag{B.8}$$

Subjecting $\tilde{\mathbf{Y}}_n$ to rational modeling (B.9) using VF and subsequent passivity enforcement, the model must be transformed back to the physical domain by applying the inverse transformation to give the original representation of $\mathbf{Y}_n$.

$$\tilde{\mathbf{Y}}_n \approx \sum_{m=1}^{N} \frac{\tilde{\mathbf{R}}_m}{s - p_m} + \tilde{\mathbf{D}} \tag{B.9}$$

# Appendix C

# Numerical Laplace Transform

During the development of the present research work, it was necessary to validate the time-domain results obtained using the fitting of the line parameters and either trapezoidal integration or recursive convolutions.

Therefore, a different modeling approach such as to solve all the equations in the frequency-domain, can be safely used to compare the results of the model tested. To convert the answer to the time-domain, a transformation routine such as the Fast Fourier Transform or the Numerical Laplace Transform is generally used, with the latter being preferred for its improved numerical stability and easiness of implementation.

For a causal function $f(t)$ and $F(s)$ its image in the Laplace domain, the analytical inverse of $F(s)$ is given by:

$$F(s) = \mathcal{L}\{f(t)\} = \int_0^{\infty} e^{-st}\, f(t)\, dt \tag{C.1}$$

$$f(t) = \frac{1}{2\pi j} \int_{\sigma-j\infty}^{\sigma+j\infty} F(s)\, e^{st}\, ds \tag{C.2}$$

Considering a finite integration range, we have:

$$F(c + j\omega) = \int_0^{T} [f(t)\, e^{-ct}]\, e^{-j\omega t}\, dt \tag{C.3}$$

$$f(t) = \mathrm{Re}\left[\frac{e^{ct}}{\pi} \int_0^{\Omega} f(c + j\omega)\, e^{j\omega t}\, d\omega\right] \tag{C.4}$$

where $\omega$ is the angular frequency, $c$ is the stability constant, $\sigma(j\omega)$ is a window function to reduce truncation errors, $T$ is the observation time and $\Omega$ is the maximum frequency.

The discretization of equations (C.3) and (C.4) that allows for the use of the Fast Fourier Transform (FFT) are as follows:

$$F_m = \Delta t \sum_{n=0}^{N-1} f_n \; D_n^{-1} \; e^{\frac{-2\pi mn}{N}} \tag{C.5}$$

$$f_n = \frac{2\Delta\omega}{\pi} \operatorname{Re}\left\{ D_n \sum_{n=0}^{N-1} f_m \; \sigma_m e^{\frac{2\pi mn}{N}} \right\} \tag{C.6}$$

where

$$\begin{aligned} F_m &= F[c + j(2m+1)\Delta\omega] \\ f_n &= f(n\Delta t) \\ D_n &= e^{cn\Delta t + \frac{j\pi n}{N}} \\ \sigma_m &= \sigma[(2m+1)\Delta\omega] \\ \Delta t &= T/N \\ \Delta\omega &= \frac{2\pi}{T} = \frac{2\pi}{N\Delta t} \\ \Omega &= \frac{2\pi}{\Delta t} \end{aligned} \tag{C.7}$$

being N the number of frequency samples.

To reduce the effect of Gibbs oscillations, there are different options for the window function, being the most common the Hanning and Blackman windows, which are respectively given by

$$\begin{aligned} \sigma(\omega) &= 0.5 - 0.5\cos(\pi\omega/\Omega) \\ \sigma(\omega) &= 0.42 - 0.5\cos(\pi\omega/\Omega) + 0.08\cos(2\pi\omega/\Omega) \end{aligned} \tag{C.8}$$

For the factor $c$, the most used approaches are the ones given by Wilcox and Wedepohl, which are respectively

$$\begin{aligned} c &= 2\Delta\omega \\ c &= \ln\left(N^2\right)/T \end{aligned} \tag{C.9}$$

Alternatively, another value of $c$ most frequently used is

$$c = -\ln(0.001)/T \tag{C.10}$$